Terms and Conditions of Use of Digitised Theses from Trinity College Library Dublin

Copyright statement

All material supplied by Trinity College Library is protected by copyright (under the Copyright and Related Rights Act, 2000 as amended) and other relevant Intellectual Property Rights. By accessing and using a Digitised Thesis from Trinity College Library you acknowledge that all Intellectual Property Rights in any Works supplied are the sole and exclusive property of the copyright and/or other IPR holder. Specific copyright holders may not be explicitly identified. Use of materials from other sources within a thesis should not be construed as a claim over them.

A non-exclusive, non-transferable licence is hereby granted to those using or reproducing, in whole or in part, the material for valid purposes, providing the copyright owners are acknowledged using the normal conventions. Where specific permission to use material is required, this is identified and such permission must be sought from the copyright holder or agency cited.

Liability statement

By using a Digitised Thesis, I accept that Trinity College Dublin bears no legal responsibility for the accuracy, legality or comprehensiveness of materials contained within the thesis, and that Trinity College Dublin accepts no liability for indirect, consequential, or incidental, damages or losses arising from use of the thesis for whatever reason. Information located in a thesis may be subject to specific use constraints, details of which may not be explicitly described. It is the responsibility of potential and actual users to be aware of such constraints and to abide by them. By making use of material from a digitised thesis, you accept these copyright and disclaimer provisions. Where it is brought to the attention of Trinity College Library that there may be a breach of copyright or other restraint, it is the policy to withdraw or take down access to a thesis while the issue is being resolved.

Access Agreement

By using a Digitised Thesis from Trinity College Library you are bound by the following Terms & Conditions. Please read them carefully.

I have read and I understand the following statement: All material supplied via a Digitised Thesis from Trinity College Library is protected by copyright and other intellectual property rights, and duplication or sale of all or part of any of a thesis is not permitted, except that material may be duplicated by you for your research use or for educational purposes in electronic or print form providing the copyright owners are acknowledged using the normal conventions. You must obtain permission for any other use. Electronic or print copies may not be offered, whether for sale or otherwise to anyone. This copy has been supplied on the understanding that it is copyright material and that no quotation from the thesis may be published without proper acknowledgement.

The silencing of HPV16 Oncogenes using E6siRNAs

By

Itunu Senami O. Soyingbe

Department of Histopathology and Morbid Anatomy

Trinity College Dublin

A thesis submitted to Trinity College,

University of Dublin,

For the degree of

Doctor of Philosophy

February 2014

Under the supervision of Prof John O'Leary & Dr Cara Martin

Declaration

I declare that this is my own work and has not been submitted previously for a PhD degree at this or any other university. I agree that the library may lend or copy this thesis on request.

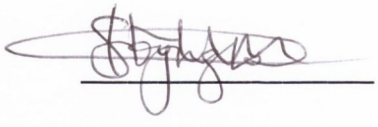

Itunu S.O. Soyingbe

Dedicated

to my quintessential Oluwatobilayemi Oke

Table of contents

List of tables

List of figures

Acknowledgements

I would like to take this opportunity to express my profound gratitude and thanks to my supervisors Professor John O'Leary and Dr Cara Martin for their exemplary support, guidance and continuous encouragement throughout the course of this thesis.

I would also like to convey my deep appreciation to Dr Cathy Spillane for her immense support, invaluable advice, guidance and encouragement throughout, it made the completion of this thesis possible. I would also like to say an enormous thank you to Dr Sharon O'Toole for her endless encouragement, support and belief throughout this thesis.

To everyone in the laboratory at the Coombe Women's hospital; Claudia, Gomaa, Katherine, Loretto, Mark, Mic, Nino, Padraig, and Victoria. I would like to extend my personal gratitude for their advice, support and encouragement. It has been a delight getting to know and work with each of you. I must especially thank Brendan, Christine, Helen, Lynne and Prerna for their inestimable support, it was greatly appreciated.

To those in the Laboratory at James' Hospital; Prof Orla Sheils, Dr Britta Stordal, Ms Jean Freeman, and Gordon for his statistical knowledge and expertise, a heartfelt thank you.

To my extended family and grandparents, your outstanding support and encouragement and prayers were and are truly invaluable.

To my parents and siblings(Ayo, Fikky, Dami); your exceptional encouragement, phenomenal and constant support and love were and are irreplaceable.

To 'Tobi; thank you for your understanding and bringing a smile to my face every day. You are my very own sunshine. I love you baby.

Finally to Mayowa, a better half no one could have, thank you for being there, loving and supporting me regardless. You mean the world to me. Thank you.

Summary

Cervical cancer is the fourth most common cancer worldwide and remains a rising cause of cancer deaths amongst women worldwide, particularly in low to mid-income countries. High risk HPV is the main etiological factor in cervical carcinogenesis. The overexpression of high risk HPV E6 and E7 due to viral genome integration and loss of high risk E2 is the key factor in this disease progression. These oncogenes subvert cellular tumour suppressor genes (p53 and unphosphorylated pRB) and create a neoplastic environment that facilitates increased cellular alterations that promote malignancy. The aim of this study was to elucidate novel pathways involved in this disease progression via the assessment of the effect of silencing these viral oncogenes. This was achieved by targeting HPV E6 and/or its splice forms using siRNAs and ascertaining downstream effects of this silencing via a genome-wide analysis and Raman spectroscopy.

HPV E6 targeting siRNAs were introduced into a HPV16 positive cervical cancer model system, which resulted in the simultaneous reduction in E6 and E7 expression. This reduction was confirmed at both mRNA and protein levels using TaqMan® RT-PCR and western blot analysis respectively. The silencing of these oncogenes resulted in distinct morphological phenotypes. E6#2 portrayed cellular shrinkage, membrane blebbing with no effect on cellular proliferation and indicative of the induction of apoptosis while E6#4, a G1 arrest in cell cycle accompanied by an enlarged flattened morphology of increased granularity and loss of contact inhibition, in addition to an increase in fluorescence, indicative of senescence.

The evaluation of downstream effects via transcriptome microarray analysis revealed 16 differentially expressed genes common to both siRNAs, with a FC >2 and FDR <0.05 which were representative of the overall differential gene pattern observed between these morphologies. An overrepresentation of innate immune response genes and pathways was observed in the apoptotic profile, particularly inducers of non-canonical

NF-κB signalling pathway. An overrepresentation of cell cycle arrest genes and pathways, particularly p53 signalling pathway, DNA repair genes and chromosomal maintenance genes were observed in the senescent profile. These responses were validated via the assessment of p21 surrogate biomarker expression. Hence, these results revealed how the silencing of E6 oncogene could result in the E7 becoming a cellular stressor and therefore causing cell death as in the case of E6#1, while the silencing of both oncogenes could result in a halt in DNA replication due to chromosomal instabilities leaving the cell in a senescent state.

A biochemical analysis study was then used to further evaluate cellular changes due to the induction of cell death. This study demonstrated vast changes in biochemical components (proteins and nucleotides) in the cytoplasm of these dead cells compared to scrambled control siRNA, further substantiating that the induction of apoptosis was inducing global cytoplasmic changes via cleavage of cellular proteins. These approaches reveal the potential of RNAi to provide gene specific therapies for all HPV-related diseases and the potential of Raman spectroscopy as a possible novel screening method for early detection of cervical neoplasia.

Abbreviations

2'OH	2 Hydroxyl
ACTB	Beta actin
ADA3	Adenosine Deaminase 3
ADP	Advanced Digital Processing
APC	Allophycocyanin
APE 1	apurinic/apyrimidinic endonuclease 1
APS	Ammonium Persulfate
ASCUS	Atypical Cells of Undetermined Significance
AS-ODN	Antisense Oligonucleotides
ATCC	American Type Culture Collection
ATP	Adenosine Triphosphate
AUC	Area under the curve
B2M	Beta-2- Microglobulin
B actin	Beta actin
BCA	Bicinchoninic Acid
BGP	Generic Background Probes
BLASTN	Basic Local Alignment Search Tool
BRCA	Breast Cancer Associated Gene
CaF_2	Calcium Fluoride
CCD	Crystallographic Construct Design
CDK	Cyclin-Dependent Kinases
cDNA	Complementary DNA
CIN	Cervical Intraepithelial Neoplasia
CIS	Carcinoma in situ
CKI	CDK-inhibitor
CR	Conserved Region

C_t	Threshold cycle
DAVID	Database for Annotation, Visualisation and Integrated
DDBJ	DNA Data Bank of Japan
DDR	DNA damage response
DEAE	Diethylaminoethyl
dH_2O	Deionised Water
DIT	Dublin Institute of Technology
DMSO	Dimethyl Sulfoxide
DNA	Deoxyribonucleic Acid
DPBS	Dulbecco's PBS
dsDNA	double stranded DNA
dUTP	Deoxyuridine Triphosphate
E6AP	E6-Associated Protein
EC	Expression Control Software
EBI	European Bioinformatics Institute
EDTA	Ethylenediamine Tetra Acetic Acid
EGF	Epidermal Growth Factor
EMBL	European Molecular Biology Laboratory
EMBOSS	European Molecular Biology Open Software Suite
FADD	Fas-Associated Protein with Death Domain
FBS	Fetal Bovine Serum
FCS	Flow Cytometry Standard
FDR	False discovery rate
FIGO	International Federation Gynaecology and Obstetrics
FITC	Fluorescein Isothiocyanate
FTP	Forward Transfection Protocol
GAPDH	Glyceraldehyde-3-phosphate dehydrogenase
GC	Human group-specific component

GFF	Glass Fibre Filter
GO	Gene ontology
HBVx	Hepatitis B virus X protein
HCL	Hydrochloric Acid
HDAC	Histone Deacetylases
HIV	Human Immunodeficiency Virus
HLA	Human Leukocyte Antigen
HPV	Human Papillomavirus
Hr-HPV	High-Risk Human Papillomaviruses
HRP	Horseradish Peroxidase
HSIL	High-grade Squamous Intraepithelial Lesion
HSV	Herpes Simplex Virus
hTERT	Human Telomerase Reverse Transcriptase
IARC	International Agency for Research on Cancer
IKK	Inhibitor of nuclear factor kappa-B kinase
INF-α	Interferon Alpha
IRF-3	Interferon Regulatory Ractor-3
IVT	in vitro Transcription
JAK-STAT	Janus Kinase- Signal Transducer and Activator of Transcription Signalling
KDa	kilo Dalton
KEGG	Kyoto Encyclopedia of Genes and Genomes
LBC	Liquid Based Cytology
LCR	Long Control Region
LNA	Locked Nucleic Acid modification
Lr-HPV	Low-Risk Human Papillomaviruses
LSIL	Low-grade Squamous Intraepithelial Lesion
MAP	Mitogen-Activated Protein
MAPK	Mitogen-Activated Protein Kinase

MCM	Minichromosome Maintenance Proteins
MEM	Modified Eagle Medium
MHC	Major Histocompatibility Complex
mRNA	messenger RNA
NCBI	National Centre for Biotechnology Information
NCR	Non-Coding Region
NEAA	Non-Essential Amino Acids
NF-κB	Nuclear factor kappa-light-chain-enhancer of activated B
NHEJ	Non-Homologous End Joining
NLS	Nuclear Locating Signal
NMR	Nuclear Magnetic Resonance
NMSC	Non-Melanoma Skin Cancer
NTC	No Template Control
ORF	Open Reading Frame
PANTHER	Protein Analysis through Evolutionary Relationships
PBS	Phosphate-Buffered Saline
PCA	Principal Component Analysis
PCR	Polymerase Chain Reaction
PE	Phycoerythrin
PI	Propidium Iodide
PM	Perfect Match
PMSF	Phenylmethanesulponylfluoride
PP2A	Protein Phosphatase 2A
pRB	Retinoblastoma Protein
ppRB	Phosphorylated Retinoblastoma Protein
rRNA	Ribosomal RNA
PPR	Pentatricopeptide repeat
PS	Phosphatidyl Serine

PV	Papillomaviruses
PVDF	Polyvinylidene Diflouride
qPCR	Quantitative PCR
RIN	RNA Integrity Number
RIPA	Radioimmunoprecipitation
RISC	RNA-Induced Silencing Complex
RLE	Absolute log expression
RMA	Robust Multiple chip Analysis
RNA	Ribonucleic Acid
RNAi	RNA interference
RSV	Rous Sarcoma Virus
RT-PCR	Real time PCR
RT	Reverse Transcription
RTP	Reverse Transfection Protocol
Rz	Ribozymes
SA β-gal	Senescence-Associated β-galactosidase
SA	Splice Acceptor
SD	Splice Donor
SDS-PAGE	Sodium Dodecyl-Sulfate Polyacrylamide Gel Electrophoresis
ShRNA	small hairpin RNA or short hairpin RNA
siRNA	small interfering RNA
SOP	Standard Operating Procedure
Sp1	Specificity Protein 1
STD	Sexual transmitted diseases
St Dev	Standard Deviation
STI	Sexually Transmitted Infection
SV40	Simian Virus 40
TBST	Tris-buffered Saline containing 1% Tween-20

TdT	Deoxynucleotidyl Transferase Dntp
TEMED	Tetramethylethylenediamine
TFO	Triple-Forming Oligonucleotides
TGF-ß	Transforming Growth Factor Beta
TLR	Toll-Like Receptors
T_m	Melting Temperature
TNA	Therapeutic Nucleic Acids
TNF	Tumour Necrosis Factor
TNFR	Tumour Necrosis Factor Receptor
TSC2	Tuberous Sclerosis 2
TYK2	Tyrosine Kinase 2
UDG	Uracil DNA Glycosylase
URR	Upstream Regulatory Region
WHO	World Health Organisation
β-gal	β-Galactosidase

Publications

Journal Articles

IS Soyingbe, CD Spillane, CM Martin, JJ O'Leary. Gene expression profiling of HPV16 E6/E7 silenced cervical cancer cells. *Manuscript in preparation*

IS Soyingbe, P Kearney, CD Spillane, CM Martin, JJ O'Leary. The effect of silencing HPV16 E6/E7 on Raman Spectra in a Cervical Cancer Cell Model. *Manuscript in preparation*

Presentations and Posters

Soyingbe I, Spillane C, Martin C, O'Leary J. Silencing HPV16 E6 Oncogene in a Cervical Cancer Cell Model. (Eurogin) 2013.

Soyingbe I, Spillane C, Martin C, O'Leary J. Silencing HPV16 E6 Oncogene in a Cervical Cancer Cell Model. (6th School of Medicine Postgraduate Research Day) October 2014.

Soyingbe I, Spillane C, Martin C, O'Leary J. Silencing HPV16 E6 Oncogene in a Cervical Cancer Cell Model. (United States & Canadian Academy of Pathology's 103rd Annual Meeting) March 2014.

***Note to readers:**

- Negative control and scrambled control used interchangeably throughout this thesis
- Extremely significant refers to P values< 0.001, while highly significant refers to P values between 0.001 and 0.01
- Unless otherwise stated, all figure created by author.

Chapter One

Introduction

1. Introduction

1.1. Cervical cancer overview

Cancer is a leading cause of death worldwide and accounted for 14.1 million new cases and 8.2 million deaths worldwide in 2012, representing an 11% and 16% rise respectively from 2008 figures according to recently published data from the International Agency for Research on Cancer (IARC), (Ferlay, et al., 2013) (Bray, et al., 2013). It is projected that by 2035, an estimated 24 million new cases and 15 million deaths per year will be attributed to cancer (Ferlay, et al., 2013). IARC 2012 statistics expose striking patterns of cancer in women with evident increases in breast and cervical cancers, demonstrating the need to prioritise prevention and control globally in these cancers (Ferlay, et al., 2013) (Bray, et al., 2013).

Cervical cancer is a malignant tumour that affects the lower portion of the female genital system, and starts as the gradual development of pre-cancerous changes in the cells lining the cervix. These pre-cancerous changes initially appear as lesions, which slowly progress into aggressive neoplastic and possibly metastatic cells. It is the fourth most commonly diagnosed female cancer and fourth leading cause of cancer death in the world causing over a quarter of a million deaths every year, 70% of which occur in developing countries as depicted in Figure 1-1. (Ferlay, et al., 2013) (Bray, et al., 2013). Annually, more than half a million women are diagnosed worldwide with cervical cancer (Ferlay, et al., 2013) (Bray, et al., 2013).

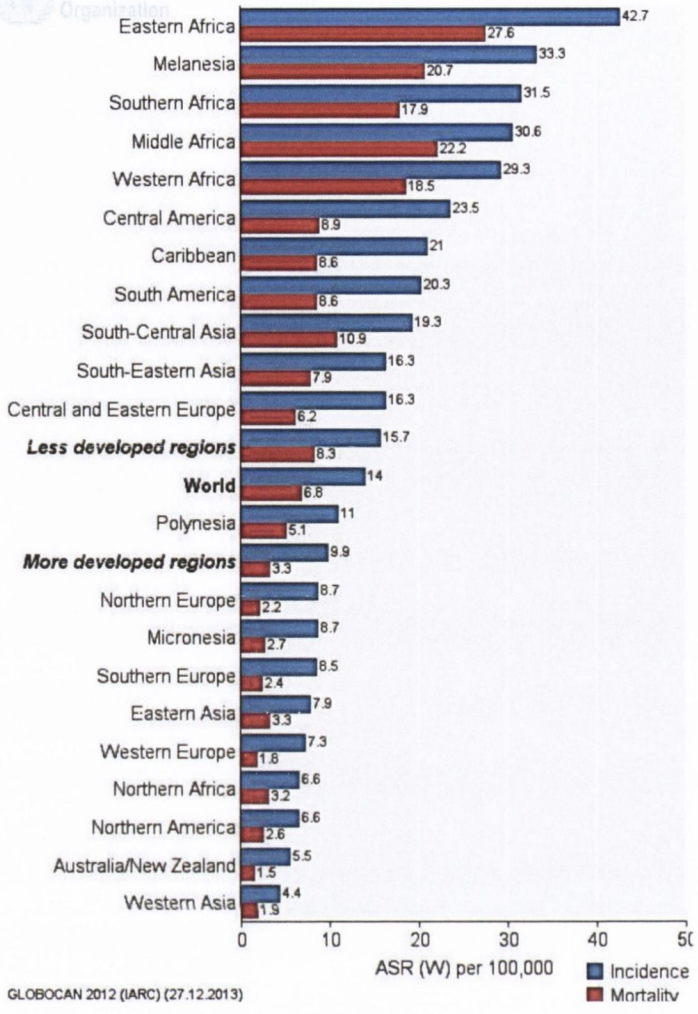

Figure 1-1: Worldwide Cervical Cancer rates. Age-standardised incidence and mortality rates of cervical cancer worldwide per 100,000 in the year 2012 **(Ferlay, et al., 2013) (Bray, et al., 2013)**.

1.2. Cervical cancer epidemiology

The disproportionate incidence of cervical cancer, with a higher burden in less developed regions, as shown in Figure 1-1, can also be seen across Europe. Cervical cancer is a common incident form and cause of cancer mortality in women in the western world; nevertheless rates vary widely across Europe with Central and Eastern Europe accounting for half of the 20 highest rates in Europe, as depicted in Figure 1-2. In the European Union (EU), cervical cancer accounted for 6% and 5% of the total new cancer cases and cancer deaths, respectively, amongst females in 2012 and it is

estimated that there will be 35,000 new cases by the year 2035 (Ferlay, et al., 2013) (Bray, et al., 2013).

This disproportionality can be explained by the lack of population-based screening programs which have had a remarkable effect on cervical cancer incidence across Nordic countries in Europe which by 2008 had age-standardised incidence rates of <14.5 per 100,000. However, not all European countries have implemented cervical screening (Albania, Azerbaijan, Cyprus and Malta) and some have only recently introduced population-based cervical screening programmes (Armenia 2007, Czech Republic 2008, Ireland 2008, Latvia 2009) and/or vaccination programmes.

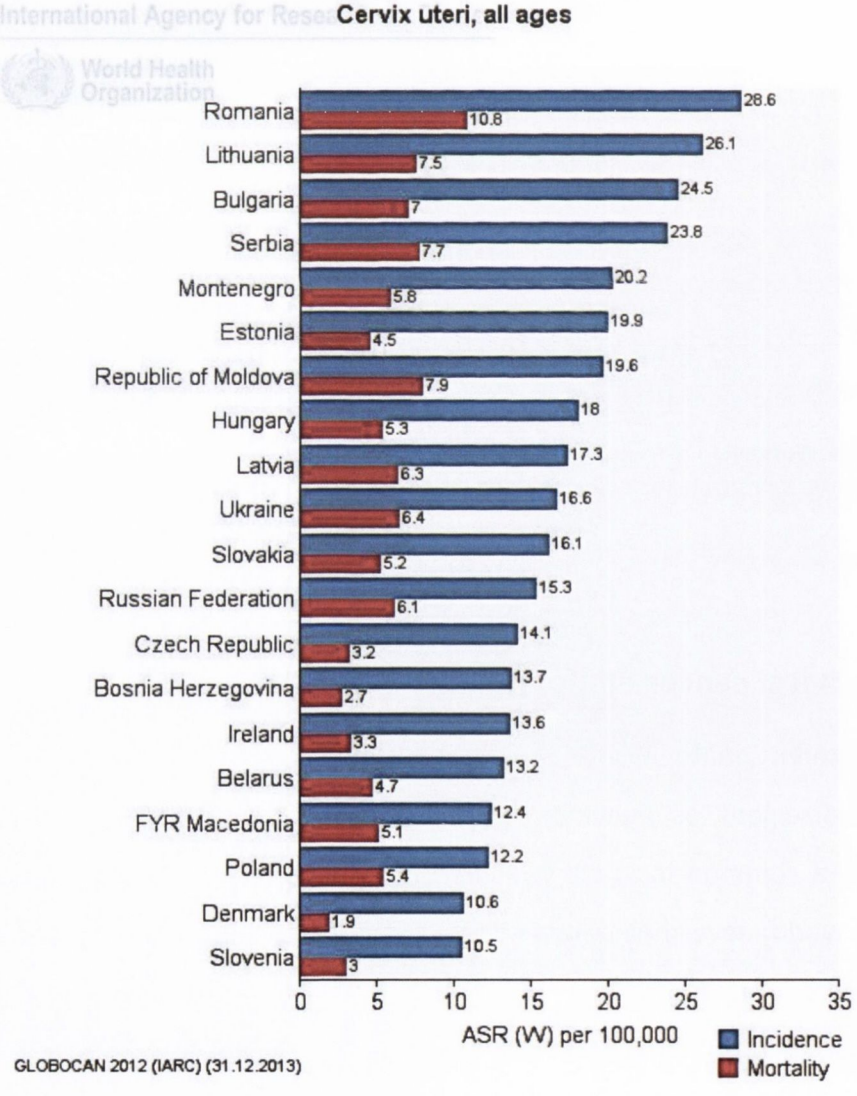

Figure 1-2: Cervical Cancer rates of 20 highest countries in Europe. Age-standardised incidence and mortality rates of Cervical Cancer per 100,000 in Europe in 2012 **(Ferlay, et al., 2013)**.

Cervical cancer is the second most common and second leading cause of cancer death in women under 44 in the Irish Republic. It is currently the 9th most common cancer in Irish women, with 357 new cases and 101 deaths reported due to cervical cancer in 2012, representing a 20% and 18% rise from 2007 figures (Ferlay, et al., 2013) (Bray, et al., 2013) (CervicalCheck-National Cancer Screening Service, 2012). Cervical cancer mortality in Ireland has steadily increased by an average of 1.5% since 1978, which is in contrast to neighbouring countries, such as Northern Ireland, England, Wales and Scotland, who have seen a steady decrease in the rates since the early 1970s, as illustrated in Figure 1-3 (Ferlay, et al., 2013) (Bray, et al., 2013) (Comber & Gavin, 2004).

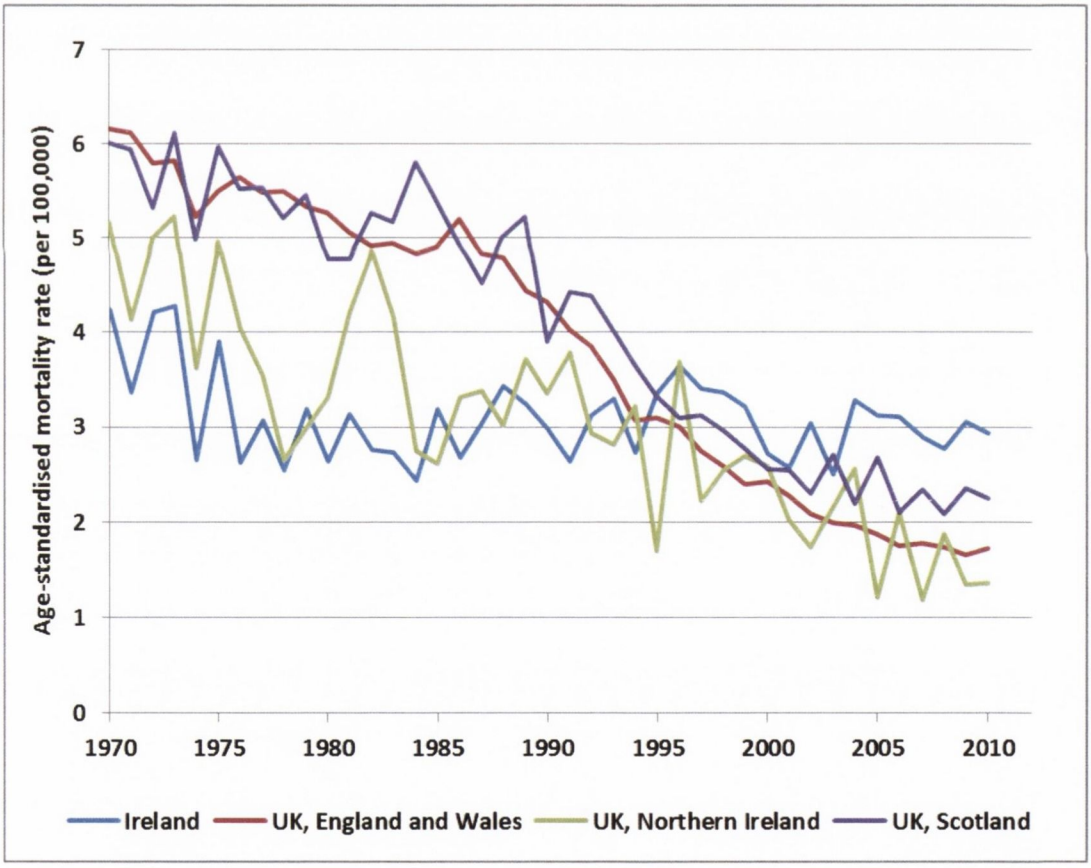

Figure 1-3: Britain & Ireland Cervical Cancer Mortality Rates. Graph of age-standardised mortality rates of cervical cancer per 100,000 in Ireland & United Kingdom from 1970-2010. (*Figure created by author from data* in **(Ferlay, et al., 2013) (Bray, et al., 2013)**)

Possible explanations for this trend, is the absence of comprehensive population-based screening in Ireland prior to 2008, which meant that screening was done in an opportunistic manner. In September 2008, Ireland implemented a free, quality assured, national cervical screening programme-CervicalCheck, modelled on the successful BreastCheck model, for 1.1 million women aged 25 to 60 years (National Cancer Screening Service, 2008). Also in September 2010, a free school-based national vaccination programme was launched to target 12-year-old girls in first year of secondary school and a one-off catch up HPV vaccine programme for 13-15 year old girls (National Immunisation Advisory Committee of the Royal College of Physicians of Ireland, 2011). The results of these implemented programmes, although yet to be seen, are expected to follow trends similar to other developed regions where screening programs have had a significant impact on cervical cancer incidence.

1.3. Human papillomavirus and cervical cancer

Several risk factors have been implicated in the aetiology of cervical cancer. Human papillomavirus (HPV) has been established as the main aetiological cause of cervical cancer with >99.7% of incidence occurring as a result of HPV infection. (Walboomers, et al., 1999) (Bosch, et al., 2002). The majority of HPV infections occur via sexual transmission but very rarely via fomites (inanimate objects) or perinatal transmission and will clear within 1 to 2 years. Approximately 50-80% of sexually active women contract some form of HPV at least once in their lifetime but only a small proportion will develop cervical cancer. Persistent unresolved infection by high risk oncogenic HPV types is an indispensable cause for premalignant and malignant lesions of the cervix. However, gaps in our understanding of HPV biology still remain.

1.3.1. HPV overview - a historical perspective

Since the start of the 1900s, varying indications of viral aetiology in the induction of oncogenesis have been made, with the first link, being the discovery that Rous sarcoma (retro) virus (RSV) caused tumours in cottontail rabbits in 1911 (Ullmann, 1923) (Kingerey, 1921) (Rous, 1911) (Rous & Beard, 1935) (Rous, et al., 1936). This laid a foundation for the premise by Harald zur Hausen in the 1980s that an oncogenic virus in cervical cancer biopsies induced chromosomal changes by DNA integration into their host genome, resulting in aberration of normal functioning and tumour growth (de Villiers, et al., 1981) (Dürst, et al., 1983) (Gissmann & zur Hausen, 1980). The recognition of this work however, did not come until the 1990s, when a number of epidemiological studies validated HPV as the causative agent for cervical cancer. This resulted in the classification of certain HPV types as carcinogenic to humans by International Agency for Research on Cancer (International Agency for Research on Cancer IARC, 2007). In October 2008, Harald zur Hausen was awarded one half of the Nobel Prize in Physiology or Medicine for his discovery of the role of HPV in cervical cancer.

1.3.2. HPV reservoir and transmission

PV types are generally ubiquitous, widely distributed and can affect species such as cows and rabbits. However, humans are the only natural reservoir of HPV. HPV infection is via direct skin-to-skin or skin-to-mucosa contact which requires micro-abrasions in the epithelium to access basement membrane cells, where primary human keratinocytes are natural host cells of the virus *in vivo*. HPV is transmissible during acute and persistent infection stages. Multiple HPVs types can exist in varying skin and mucosal epithelial sites in symbiosis with their host over long periods of time, where upon immune suppression or deficiency, latent infections become activated and give rise to benign tumours like warts and papillomas (de Villiers, et al., 2004).

1.3.3. Papillomavirus taxonomy

Papillomaviruses (PV) are a diverse group of viruses found in mammalian, reptile and bird species (Bernard, 2005). PVs can be categorised on the basis of genomic analysis into 118 PVs types and at evolutionary level into 16 genera, five of which infect humans; Alpha α-, Beta β-, Gamma γ-, Mu μ- and Nu ν-PVs, as illustrated in Figure 1-4 (Bernard, 2005) (de Villiers, et al., 2004). Alpha and Beta human PVs are the two main genera and account for 90% of all characterised HPV.

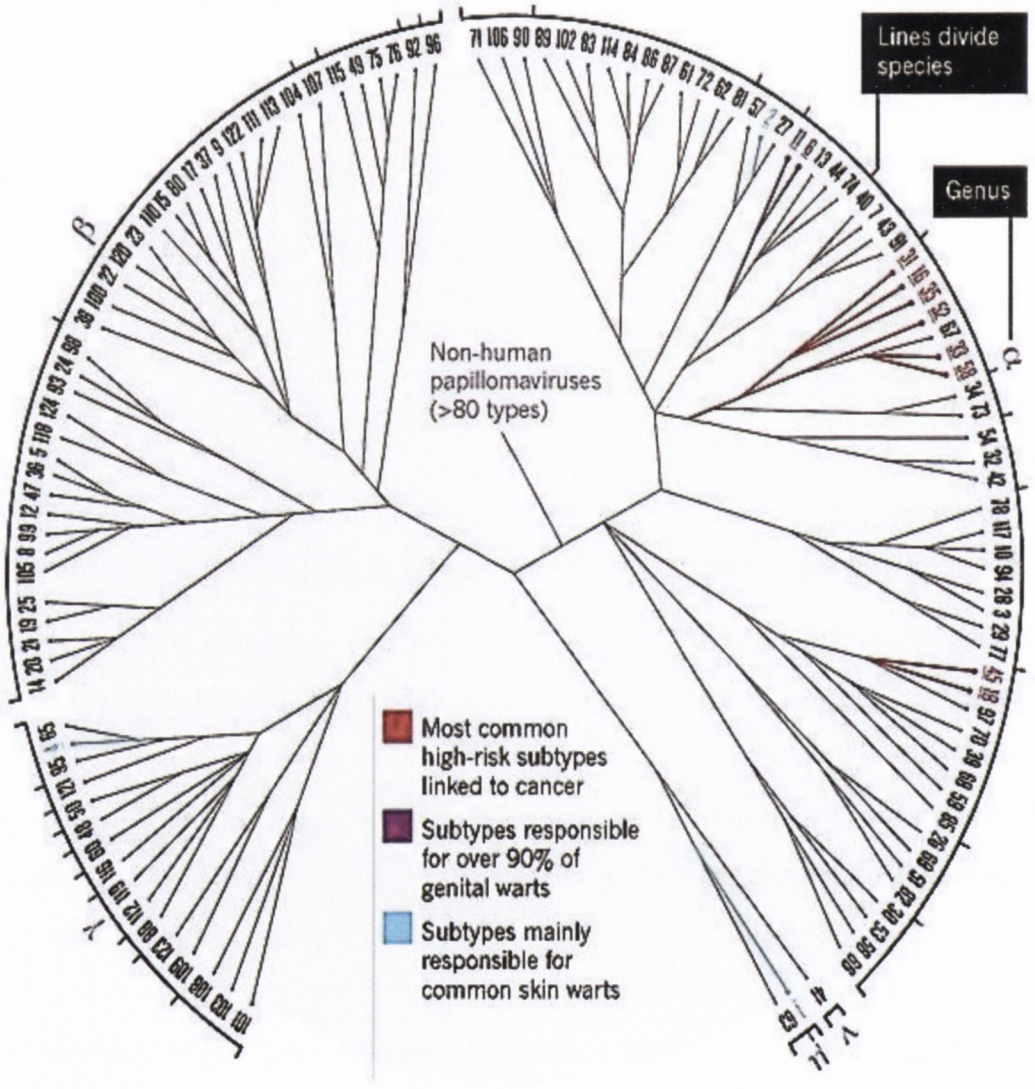

Figure 1-4: HPV genera showing α, β-, γ-, μ- and ν-papillomaviruses. α infects skin and mucosal surfaces while β-, γ-, μ- and ν-infect only skin. **(Crow, 2012)**

Alpha viruses (Super group A) viruses are characterised as genitally transmitted HPVs, as illustrated in Figure 1-5 and examples are HPV 6, 11, 16, 18, 2 and 10. Lr HPVs 6 and 11 infect oral sites in 1% of sexually active individuals and are often associated with benign papillomas. While HPV 2 and 10 infect cutaneous sites and cause warts (Brentjens, et al., 2002). Hr-HPV16 and 18 infect mucosal sites and cause lesions that can develop into cancer. Beta viruses (Super group B) cause cutaneous infections like warts (HPV4 in subgroup B2), non-melanoma skin cancer (NMSC) in immuno-compromised humans (HPV5 in subgroup B1) and latent infections in the normal population (Middleton, et al., 2003) (Peh, et al., 2002). Only three Mu and Nu HPVs are known and they cause warts verrucas and plantar warts (Doorbar, 2006) (Castellsagué, 2008).

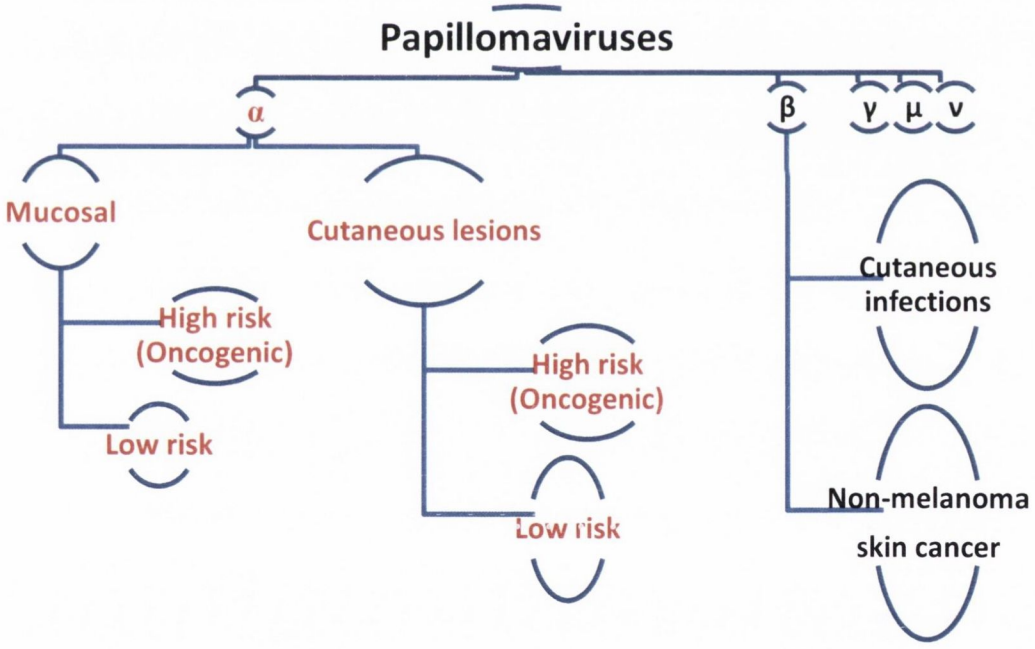

Figure 1-5: Classification of Human Papillomavirus. Diagram depicting the classification of mucosal and cutaneous infections into high risk and low risk HPVs. Genitally transmitted HPVs highlighted in red. *Figure created by author from data in* **(Brentjens, et al., 2002) (Middleton, et al., 2003) (Peh, et al., 2002) (Doorbar, 2006) (Castellsagué, 2008)**.

1.3.4. HPV classification

HPVs can be classified on the basis of oncogenic propensity (Table 1-1). High-risk Human Papillomaviruses (Hr-HPV) are usually associated with cervical cancer while low-risk Human Papillomaviruses (Lr-HPV) are associated with genital warts and papillomas. Probable high risk types may be associated with cervical cancer (Somsubhra & Sachchithanantham, 2010).

Table 1-1: HPV Risk Types. HPV16 and 18 are most commonly associated with cervical cancer, accounting for 70% of cases, while HPV 6 and 11 are associated with genital warts accounting for 90% of cases **(Somsubhra & Sachchithanantham, 2010)**.

Oncogenic Propensity	Risk Types
High-risk	16, 18, **31, 33, 35, 39, 45, 51, 52, 56, 58, 59, 68, 73 and 82**
Probable high-risk	**26, 53, and 66**
Low-risk types	6, 11, **40, 42, 43, 44, 54,61, 70, 72, 81 and CP6108**

1.4. HPV - molecular biology

HPV like other viruses has evolved unique mechanisms to adapt, maintain and regulate host cellular processes. HPV is a small non-enveloped icosahedral double stranded DNA virus (Castellsagué, 2008). The half-life of an HPV infection is usually 3-5 weeks for Lr-HPV, 8-10 weeks for Hr-HPV and 16 months for Hr-HPV16. Infection is usually overcome within two years in most women, but persistent unresolved Hr-HPV infection can lead to integration into host DNA, thereby causing cervical cancer in a small number of women.

1.4.1. HPV structure

HPVs share a common genetic structure of circular dsDNA genome that encodes approximately 8 open reading frames (ORFs) all transcribed from a single DNA strand. All genetic information is located on only 1 of 2 strands. This single stranded 8kbps viral HPV DNA molecule is bound to cellular histones and contained within a pentametric protein capsid. ORFs can be divided into 3 functional parts; Early region (early ORF), Late region (late ORF) and Upstream regulatory region (URR)/Non-coding region (NCR)/Long control region (Long coding region LCR), as portrayed in Figure 1-6. The LCR encodes an assortment of cis-elements required for replication and transcription of the viral DNA. These include the viral origin of replication responsible for regulation of replication, and the early promoter, p97, which can control transcription of some genes in the early region. Viral early genes are transcribed from either promoter, depending on environmental conditions, whereas the late genes are solely transcribed from the late promoter, p742/p670 (Fehrman, et al., 2003). The early ORF encodes non-structural proteins that can be divided into 6 coding regions (E1, E2, E4, E5, E6 and E7) responsible for maintaining high HPV numbers and immortalisation. E1, E2 and E6 give rise to more than one protein via differential splicing.

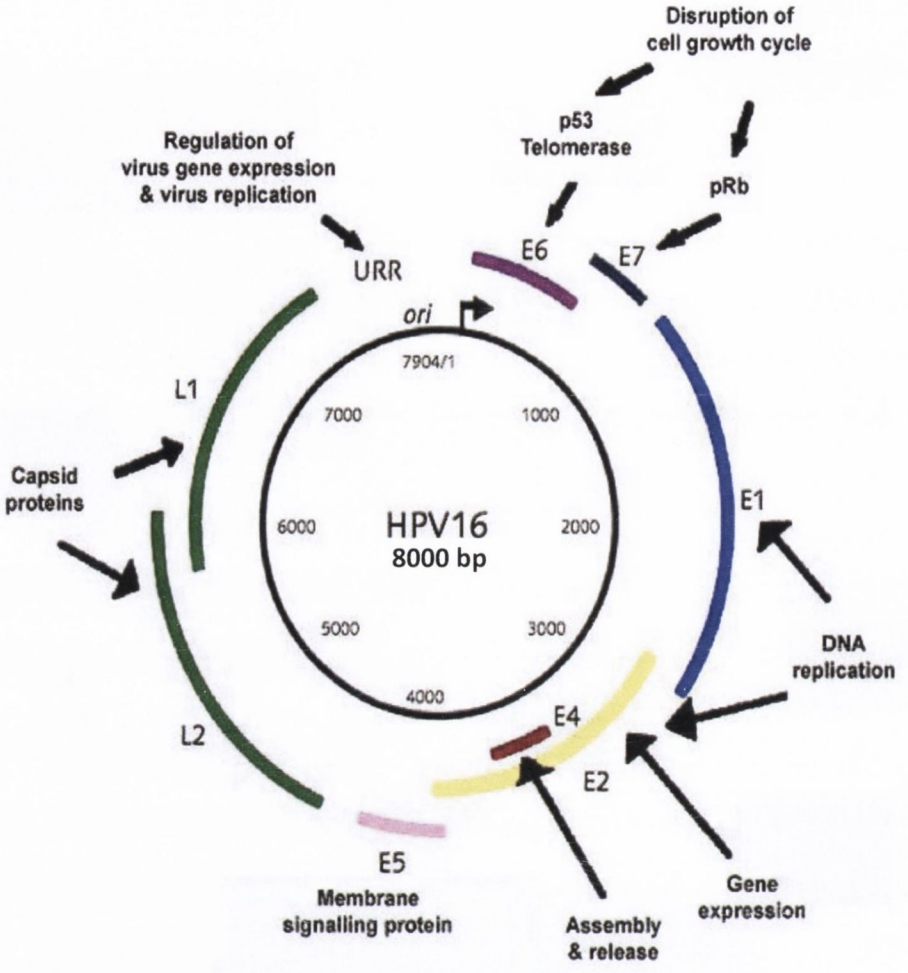

Figure 1-6: Diagram of HPV16 genome. ORFs responsible for transcription and regulation (E6, E7, E1, E2, E4 and E5) as well as structural ORFs L1 and L2 are highlighted in the arrangement. Viral gene transcription is controlled by URR within which enhancer sequences to which E2 and other cellular factors bind. The early p97 viral promoter responsible for E1 to E7 transcription and late p670 viral promoter responsible for L1 and L2 transcription are located at around 4000 and 7000bp respectively (not shown)**Invalid source specified.**.

1.4.2. HPV lifecycle

The E2 of human papillomaviruses is a DNA-binding protein necessary for the initiation of viral DNA replication and genome segregation. E2 protein mediates effects such as G1 arrest, abrogation of mitotic checkpoint control and initiation of apoptosis via p53 dependent and independent pathways. E2 protein acts as a transcription factor; functioning as an activator by regulating early promoter p97 in low levels and causing E6 and E7 transcriptional repression, via Specificity protein 1 transcription factor (Sp1)

displacement, in high levels (Massimi, et al., 1999). The E2 protein has an N-terminal transactivation domain, a flexible hinge region and a C-terminal region responsible for DNA binding and dimerisation. It loads E1 helicase to specific sites on the viral genome, which interacts using four specific palindromic recognition sites ($ACC_G(N_4)_CGGT$) on the HPV16 LCR to up regulate HPV oncogene expression (Massimi, et al., 1999). E1 and E2 act as co-factors in recognizing the origin of replication.

The E1 of human papillomaviruses is a 67.5-76.2kDa site specific hexametric helicase with the largest, most conserved open reading frame in PVs. E1 protein binds cellular proteins like replication protein A and DNA polymerase, α primase, essential for viral genomic replication. HPV E1 has an N-terminal region, a variable spacer and a large C-terminal region. Mucosal PVs have additional N-terminal residues hence are more varied in size than other PVs (Wilson, et al., 2002). N-terminal region activity is essential for replicative performance and phosphorylation. It is responsible for histone binding and alleviating chromatin condensation thereby promoting new viral DNA elongation and synthesis. The C-terminal region has a 3' to 5' ATPase/helicase-like activity where all essential replicative functions are located. Post transcriptional phosphorylation in E1 enables regulation of its activity in the cell cycle.

The E5 protein of human papillomaviruses is a short membrane-associated hydrophobic transforming protein expressed from the same polycistronic mRNA encoding E2. It is involved in both early and late stages of viral life cycle. It is located on the 3' end of the early region and influences the activity of cell signalling pathways and their growth factor receptors. For example, HPV E5, in conjunction with HPV E7, sensitises the response to epidermal growth factor (EGF) in the EGF receptor pathway, thereby maintaining the activation of the ras/mitogen-activated protein (MAP) kinase cascade and repressing expression of the cyclin-dependent kinase inhibitor, $p21^{WAF1/Cip1}$. The functional association between HPV E5 and 16 kDa V-ATPase is yet to be well established but may be involved in inhibiting acidification of endosomes and impaired cell-cell communication (DiMaio & Mattoon, 2001) (Conrad, et al., 1993).

The E4 of human papillomaviruses has been associated with the destabilisation of cytokeratins to aid viral progeny release, although the exact biological function in late phases of viral life cycle remains unclear. HPV E4 protein is encoded by a spliced E1^E4 mRNA transcribed on a single polypeptide and is expressed as a fusion protein with the N terminus of the E1 protein. E4 contributes to the mechanism of differentiation-dependent virus replication (Nakahara, et al., 2002) (Roberts, et al., 1997). The E6 and E7 proteins of human papillomaviruses will be discussed in detail in section 1.6.

The Late ORF encodes two structural proteins responsible for viral assembly; Late protein 1 (L1) and late protein 2 (L2). L1 is the major protein and makes up 80% of total viral protein, while the 70KDa L2 is the minor protein. Viral assembly and release is propagated by L1 and L2 proteins. L1 ORF is the most conserved within genome hence used in identifying new PVs types. Regions of L2 that interact with L1 are evolutionarily conserved (Lowe, et al., 2008). L2 protein has an N terminus shown to bind DNA in a sequence–dependent manner and a nuclear localisation sequence (NLS) confirming its role in packaging (Zhou, et al., 1994). L1 and L2 proteins are assembled as capsomeres which form an icosahedral viral capsid around viral genome during generation of viral progeny (Fehrman, et al., 2003). The 55nm diameter capsid consists of 72 capsomers arranged on an icosahedral surface lattice (Baker, et al., 1991). Capsids undergo a maturation process via disulphide cross-linking of the proteins to enable viral assembly and release.

1.4.2.1. Viral entry and mode of infection

The most susceptible regions of the cervix to neoplastic transformation by HPV are the cervical basal layer transformation zone at the squamous-columnar junction between the ecto- and endo-cervical epithelium and the pectineal line of the anal canal (Palefsky, 1999) (Poletti, et al., 1998) (Carter, et al., 2001) (Stanley, 2010). The cervical epithelium is composed of self-renewing progenitors-columnar basal cells attached to basal membrane that proliferate into daughter cells that separate from the membrane and migrate into the suprabasal layer. Under normal conditions, cells in the suprabasal

layer terminate cell cycle and initiate terminal differentiation (Jones, et al., 2007) (Madison, 2003). As these cells move upwards, they acquire protective characteristics such as cross linking with intermediate filaments, lipid emission and cornified envelop formation to make up the mucosal layer. Finally, the cells approach the surface and form the stratum corneum which is constantly sloughed off, as illustrated in Figure 1-7. This process is continuous to ensure structural integrity of the epithelium (Fehrman, et al., 2003).

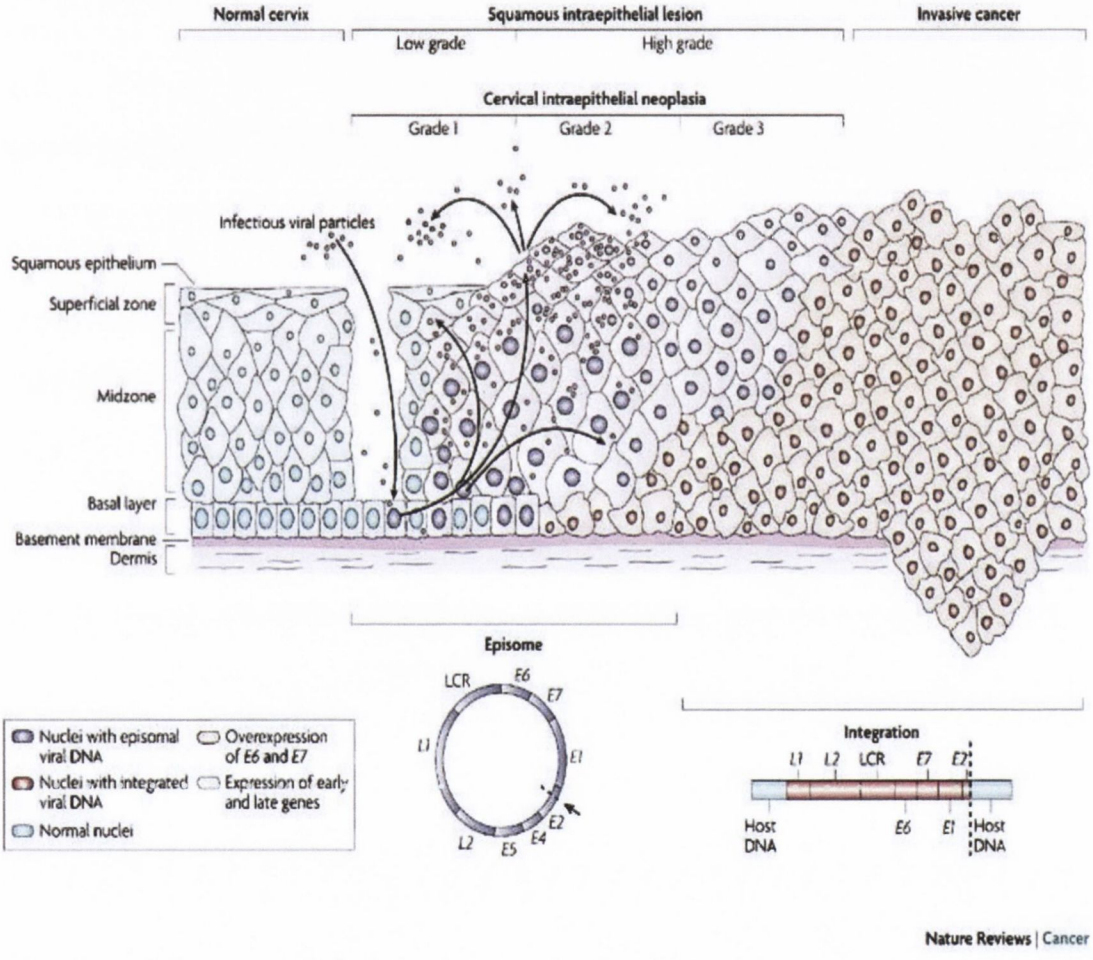

Figure 1-7: Progression of HPV infection in the cervical epithelium. Micro abrasions in the cervical epithelium enables HPV infect basal cells resulting in controlled expression of early genes (E1, E2, E4, E5, E6 and E7) which maintain the viral genome as an episome. As these cells move into upper layers, progeny assembly occurs due to expression of late genes (L1 and L2). Persistent unresolved infection advances into high grade and invasive cancer whereby viral genome is integrated into host DNA and oncogenes E6 and E7 are over expressed. **(Woodman, et al., 2007)** *Copyright Permission sought and reuse request is free of charge*

On infection with HPV, the virus requires access to the progenitor-columnar basal cells to initiate a successful infection (Boxman, et al., 2000) (Boxman, et al., 2001). Micro abrasions due to environmental trauma in the cervical epithelium, typically a consequence of sexual intercourse, facilitate viral access to columnar basal cells. The ability of HPV to successfully infect a host and establish their genome is dependent on induction and maintenance of viral DNA synthesis and cell proliferation in the suprabasal layer via E1, E2, E6 and E7. The exact mechanism of HPV entry into basal cells is yet to be fully elucidated. It is however, thought to occur via interaction with heparin sulphate proteoglycans, which results in conformational change in L1 and L2 capsid proteins. An additional secondary receptor protein is then required, such as cell adhesion receptor alpha 6-integrin, which promotes viral uptake by clathrin-dependent endocytosis (Giroglou, et al., 2001) (Culp & Christensen, 2004) (Johnson, et al., 2009). On viral entry, the acidic nature within the late endosome/lysosome offers a reducing surrounding and thereby assists in the uncoating of the viral genome. Transport then occurs of the HPV genome to the nucleus via the L2 protein (Day, et al., 2003) (Bousarghin, et al., 2003) (Smith, et al., 2007). Within the nucleus, HPV commences the 'productive' form of its life cycle (Figure 1-7) by establishing a stable episome of low copy number of between 10-200 per host cell, through the activity of early genes E1, E2, E4, E5 and in some cases E6 and E7 genes (International Agency for Research on Cancer IARC, 2007) (Moody & Laimins, 2010) (De Geest, et al., 1993) (Stanley, et al., 1989) (McBride, et al., 2006) (Middleton, et al., 2003).

HPVs can portray a unimodal, productive lifecycle, or bimodal, productive and non-productive lifecycle depending on the risk category and regulation by host differentiation. Specifically, low risk types portray a unimodal, productive lifecycle, and as previously stated are usually associated with genital warts and papillomas, whereby HPV viral proteins are expressed and viral progenies are generated (Figure 1-8). Whereas, high-risk types frequently associated premalignant lesions and cervical cancer, portray a bimodal, productive and non-productive lifecycle, whereby persistent unresolved infection leads to the non-productive phase, where no viral progeny are

generated (Figure 1-8). The ability to switch from the non-productive to productive cycle is due to the oncogenic potential of these HPVs.

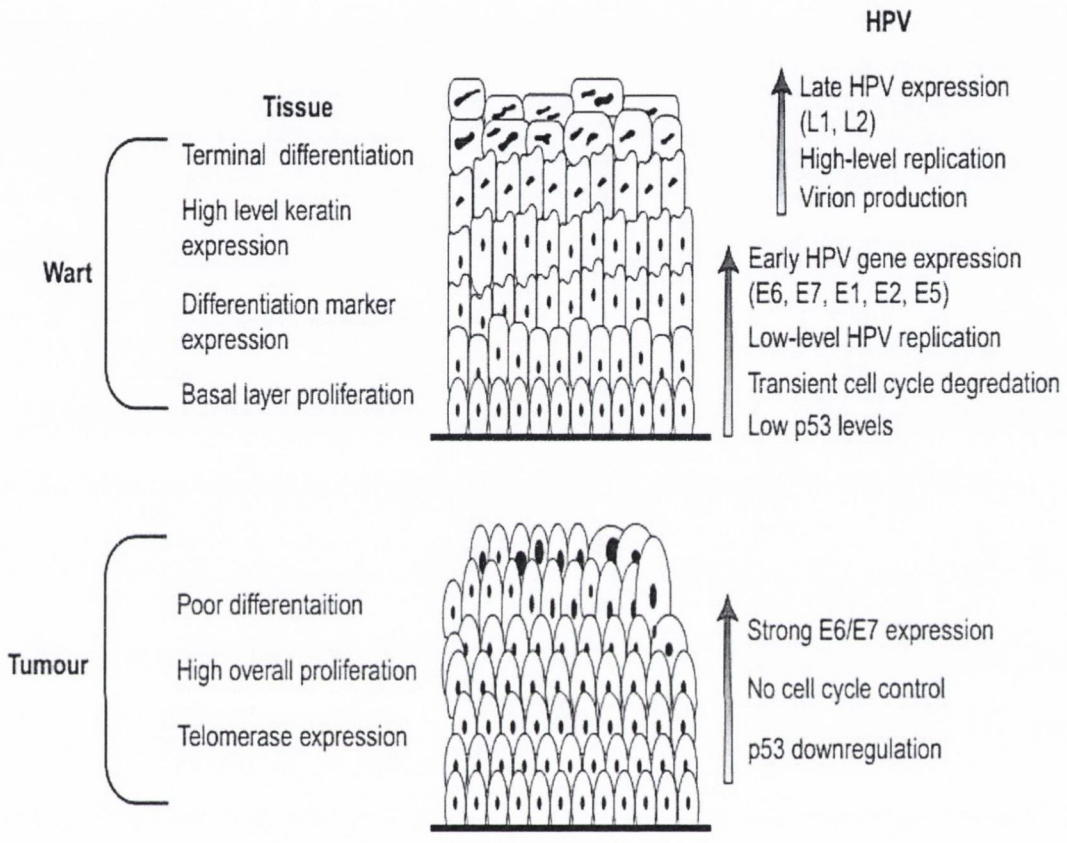

Figure 1-8: HPV lifecycle in cervical warts and tumours. Diagram showing cellular changes, viral proteins and cellular proteins expressed at different stages of the cycle **(DiPaolo & Alvarez-Salas, 2004)**. *Copyright Permission sought and payment required.*

1.4.2.2. Productive infection- episomal maintenance of viral genome

The establishment of the viral genome as a nuclear plasmid at low levels, which expresses early genes, indicates a successful infection (Frattini, et al., 1996). From studies on cottontail rabbit papillomavirus, it can be inferred that subsequent to a micro trauma in the cervical epithelium, most infected basal cells are induced to fill the wound giving rise to an active papillomavirus infection. However, a few infected basal cells with HPV episomes do not differentiate and thus remain undetectable until

triggered by an unknown stimulus, such as wound repair or hormonal regulation. (Gravitt, 2011).

The effective replication of the viral genome requires the activation of host cellular replication machinery such as DNA polymerase, which is absent in the viral genome, as well as the re-induction of cell division cycle, which is usually switched off in differentiated cells. The function of E6 and E7 is to facilitate cellular replication, by inhibiting p53 and unphosphorylated Retinoblastoma Protein (pRB) respectively (Munger, et al., 2004). In order to propagate virally infected cells, HPV up-regulates early gene expression to combat changes in the cellular environment that perturb the generation of new infectious virions via genome amplification, assembly and release in the suprabasal and protective layers. The early genes, particularly E6 and E7, cooperate to stimulate differentiating cells to re-enter S phase of the cell cycle, thereby inhibiting cell cycle arrest and activating host replication machinery. E6 and E7 are strongly regulated to prevent the progression into carcinogenesis. In the upper epithelial layers, amplification of the HPV genome occurs, thereby producing thousands of copies per cell (Figure 1-8) and instigating synthesis of capsid proteins. In the superficial layer viral assembly occurs with capsid proteins encapsulating viral genome. The final element of the productive infection is virion release with sloughed keratinocytes (Hummel, et al., 1992) (Ozubun & Meyers, 1997) (Bedell, et al., 1991).

1.4.2.3. Non-productive infection - viral genome integration

The switch from a productive to a non-productive infection is driven by persistent unresolved Hr-HPV infection, resulting in viral genome integration into the host genome. This process marks the end of HPV's productive life cycle, as large sections of the genome become inactivated. Integration is proposed to occur at fragile sites within host DNA, often near c-myc locus and genes involved in the non-homologous end joining (NHEJ) pathway (Dall, et al., 2008). NHEJ is an error prone pathway that repairs double stranded DNA breaks. It can take place at any stage of the cell cycle, overriding

any of the three checkpoints G1/S, intra-S and G2/M phase making it an advantageous avenue for viral subversity.

One major consequence of viral integration is the disruption of the regulatory viral E2 gene. This results in overexpression of viral E6 and E7 proteins, which are consistently expressed in HPV-positive cervical cancers. In Hr-HPV low grade lesions, where the episomal genomic state is predominant, HPV early gene expression occurs in non-differentiated replicating basal and parabasal cells. HPV genes alter normal cellular DNA replicative machinery thereby compromising chromosomal integrity, instigating DNA recombination and neoplastic transformation, as depicted in Figure 1-8 (Huang, et al., 2008).

However, in high grade lesions and invasive carcinomas where HPV genome integration is predominant and HPV oncogenes E6 and E7 are overexpressed, the cell's DNA replicative machinery is reactivated in terminally differentiated cells of the intermediate and upper epidemial layers to ensure viral replication and propagation (Vinokurova, et al., 2008). HPV abrogates the epithelium via neoplastic transformation resulting in abnormal cells that lose control of replication, thereby transforming the cervix.

1.4.3. Cervical cancer pathology

Cervical carcinoma develops by a progression of events initiated by viral infection of basal cells of the cervical mucosal epithelium, which results in subversion of normal cellular functioning, leading to easily detectable histological changes collectively known as Cervical Intraepithelial Neoplasia (CIN). These pre-cancerous abnormalities or cervical changes are histologically atypical and may revert to normal mucosa, persist as precancerous lesions or advance to invasive carcinoma. The extent of layering of dysplastic cells along the basal membrane of the transformation zone is used to grade CIN; from mild (1/3) to moderate (2/3) to severe (abnormal cells occupying the full or near full thickness of cervical epithelium) to Carcinoma in situ (cells metastasise into

underlying tissue) as outlined in Table 1-2. (Lyngea, et al., 2009). Pre-cancerous changes can also be detected by cytological screening via the Pap smear test, which may be classified by the Bethesda System (Table 1-2).

Table 1-2: Correlation between histology and cytology of cervical pre-cancer. This table shows the correlation between histology and cytology grades of cervical pre-cancer and on the rate of regression, persistence and development of cervical cancer for each disease grade. Women infected with HPV16 make up 50% of all cases

Dysplasia Classification	Mild	Moderate	Severe	CIS
Cervical Intraepithelial Neoplasia (CIN)	CIN 1	CIN 2	CIN 3	CIN 3
Bethesda Classification System	LSIL*	HSIL**	HSIL**	HSIL**
% Regression	70-90	43	30	
% Persistence	30	57	70	
% Cervical Cancer	1	5	>12	

*LSIL – Low-grade Squamous Intraepithelial Lesion, **HSIL – High-grade Squamous Intraepithelial Lesion

1.4.4. Cervical cancer staging

Staging is based on colposcopy inspection, palpation, curettage and biopsy, chest X-ray and intravenous urography. The clinical staging of cervical cancer is shown in Figure 1-9. Cervical cancer can be subtyped based on histological examination into squamous cell carcinoma, which accounts for 85% of all cases and depicted as abnormal tissue invading the cervical stroma, and adenocarinoma, which accounts for 5-15% and arises from the endocervical canal, and adenosquamous, also known as small cell carcinoma or neuroendocrine carcinoma, which are much rarer lesions including mixed adenosquamous tumours, adenocanthomas and sarcomas.

Screening for cervical cancer is recommended approximately 3 years after starting vaginal intercourse with many screening programs recommending the commencement of screening in women in their the mid-twenties. It normally involves either a conventional Pap smear test or liquid based cytology (LBC) Pap smear tests. In Ireland, LBC screening intervals range from every three years in women under 50 years to every five years in women over the age of 50. Cervical cancer prevention strategies include the use of prophylactic vaccines for girls ages 11-18.

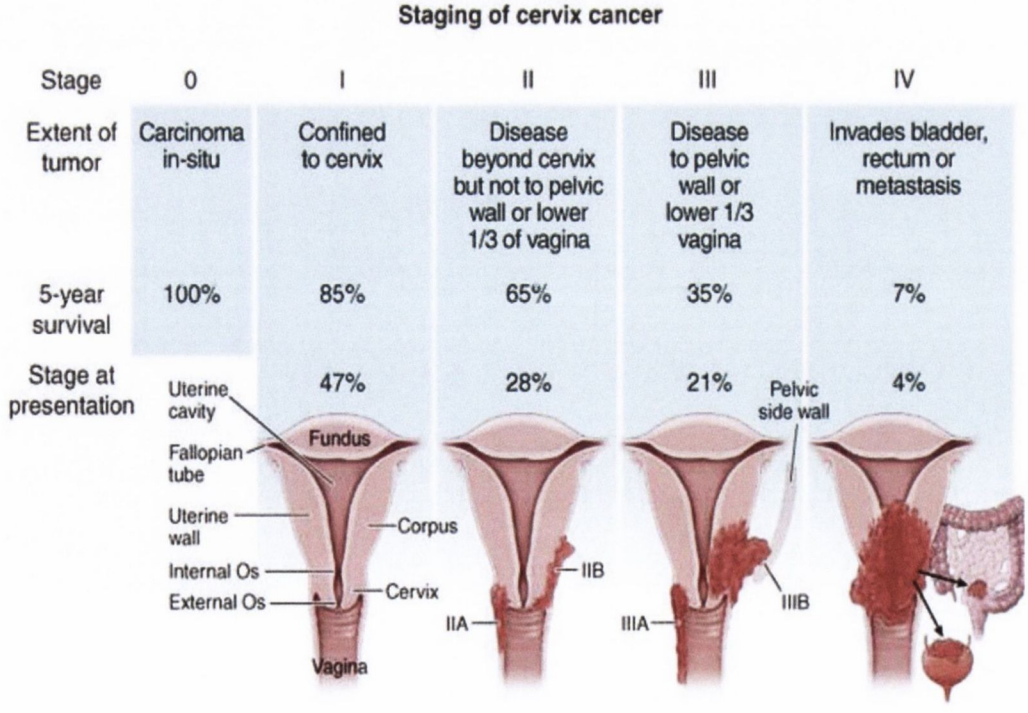

Figure 1-9: Clinical staging based on FIGO. Clinical staging in carcinoma of the cervix is based on the international federation of gynaecology and obstetrics (FIGO) system.**Invalid source specified.**

1.5. Other aetiology factors of cervical cancer

Other risk factors that have been associated with cervical cancer may be categorised either on the basis of pathogenesis (viral or environmental) or as genetic risk factors as illustrated in Figure 1-10. They may be directly linked with HPV infection or play a role independent of HPV. These factors include tobacco smoking, alcohol consumption, dietary factors, sexual behaviour, high parity, family history and prolonged use of oral contraceptives (Castellsagué & Muñoz, 2003) (Castellsagué, 2008).

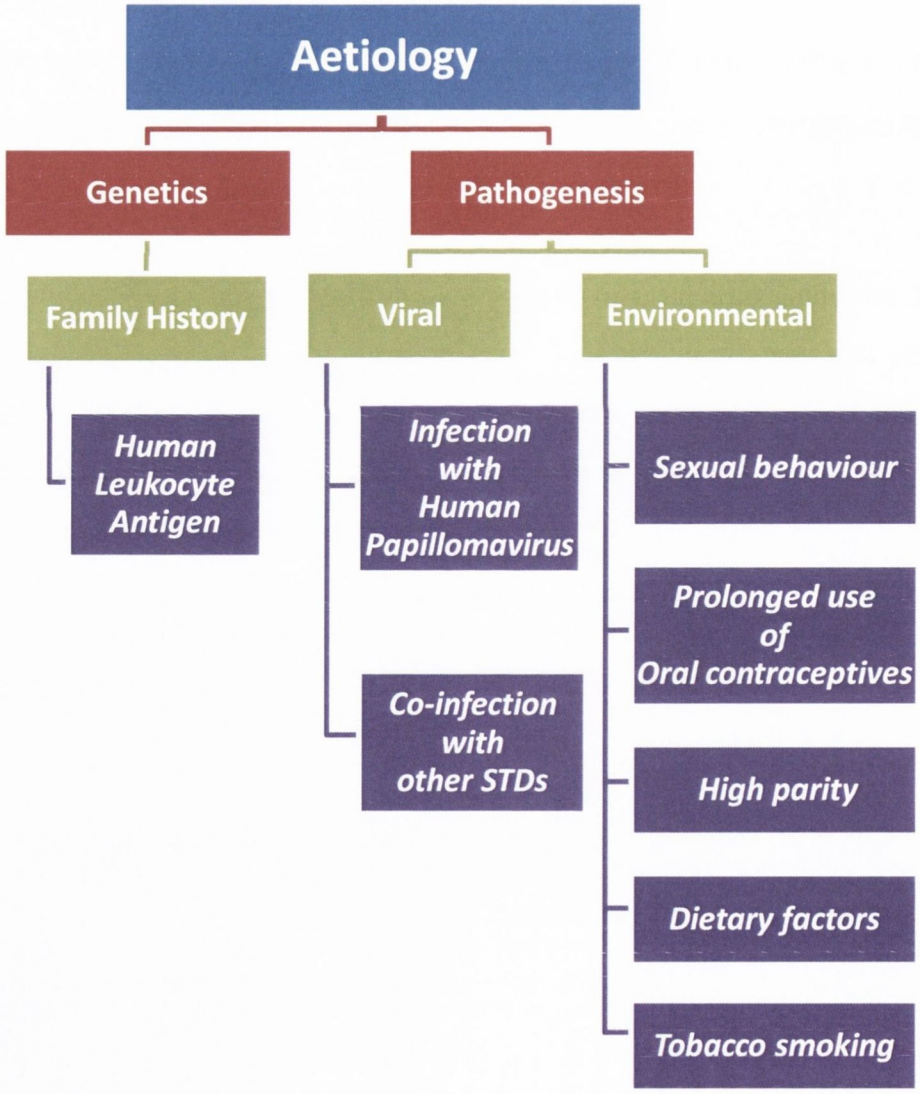

Figure 1-10: Classification of Cervical Cancer Risk factors. *Figure created by author.*

1.5.1. Pathogenesis

1.5.1.1. Viral risk factors

Most HPV infections are transient and resolve over time but persistence and progression into cervical dysplasia can be influenced by immunity. Sexual transmitted diseases (STDs) like Herpes Simplex Virus (HSV), *Chlamydia trachomatis* and Human Immunodeficiency Virus (HIV) weaken the immune system thereby exacerbating CIN progression into cervical cancer. Hence, STIs are regarded as HPV-dependent factors (Smith, et al., 2002) (Smith, et al., 2002) (Bosch & de Sanjosé, 2003). For example, the association between infection with HIV and CIN severity has been demonstrated by various studies, which suggest HIV-induced advanced immune suppression, declining $CD4^+$ count and high plasma HIV RNA levels as a basis for increased risk of developing cancer (Massad, et al., 1999) (Delmas, et al., 2000) (Moscicki, et al., 2001) (Luque, et al., 1999) (Nappi, et al., 2005) (Sellors, et al., 2003).

1.5.2. Environmental risk factors

1.5.2.1. Sexual Behaviour

Genital HPV infection is the most common sexually transmitted infection (STI) among young sexually active women, with more than 80% being infected by at least one HPV type in their lifetime (Baseman & Kotsky, 2005). Changes in sexual behaviour patterns aided HPV transmission in both younger and older women. Additional factors mediating HPV transmission include, but are not limited to, age at first sexual contact, number lifetime sexual partners, current HPV infection status, contact with high risk individuals (Winer, et al., 2003) (Winer, et al., 2012) (Andersson-Ellstrom, et al., 1996) (Rositch, et al., 2013).There is a direct relationship between the risk of CIN3/cervical cancer and age of first sexual intercourse and number of lifetime sexual partners (Wang, et al., 2003) (Burchell, et al., 2006) (Stone, et al., 2002) (Winer, et al., 2003).

1.5.2.1.1. Prolonged use of oral contraceptives

Studies have demonstrated that a linear dose-response relationship exists between cervical cancer and oral contraceptive use, which tends to wane or disappear on stopping oral contraceptives. It has been demonstrated that women who had used oral contraceptives for more than 10 years had the highest odds ratio of 4.48 of developing cervical cancer, with 95% confidence interval of 2.24-9.36, (Mitrani-Rosenbaum, et al., 1989) (Elson, et al., 2000) (Monreno, et al., 2002).

While epidemiological studies investigating associated risk of oral contraceptives with cervical cancer have consistently shown that long-term use increases the risk for carcinomas, confounding effects by HPV infection cannot be excluded (Mitrani-Rosenbaum, et al., 1989). Mitrani-Rosenbaum et al. (1989) examined the biological effect of oestrogen on the expression of HPV-16 viral oncogenes using estradiol. Estradiol was shown to stimulate the transcription of E6 and E7 known to be directly associated with alteration, immortalisation and oncogenic potential of HPV (Mitrani-Rosenbaum, et al., 1989). This effect was through the binding of specific oestrogen receptor complex to oestrogen-responsive element consensus sequence GGTCANNNTGACC located in the E2 ORF (Mitrani-Rosenbaum, et al., 1989). In 2000 Elson *et al.*, investigated the synergistic cooperation between HPV16 oncogenes and oestrogen receptor signalling using HPV16 infected transgenic mice. Experimental studies revealed a facilitation of carcinogenesis in the cervix when mice were continuously exposed to oestrogen (Elson, et al., 2000). Consistent with this finding, Moreno *et al.* (2002) performed a large pooled analysis, providing evidence for the association of oral contraceptives with HPV carcinogenesis. They concluded from this work that oral contraceptives, like estradiol, did not aid infection or persistence with HPV (HPV-independent), rather they contributed to the progression of cervical carcinogenesis (Monreno, et al., 2002).

1.5.2.1.2. High parity

High parity has also been shown to be associated with increased risk of cervical cancer in HPV positive women (Muñoz, et al., 2002). Pooled IARC analysis on multiparous women reported a 4-fold increased risk in women with 7 or more full term pregnancies compared with nulliparous women where both groups were HPV-positive. Results from studies also showed a 2-fold increase in risk in HPV-positive women with 7 or more pregnancies compared with women with 1 or 2 full term pregnancies (Castle, et al., 2002). Mode of childbirth also appeared to affect risk of cervical cancer; women who had given birth only by caesarean section and nulliparous had similar risks while women who had given birth only vaginally or vaginally and caesarean section had a much higher risks with odd ratios of 2.6 and 2.2 respectively (Muñoz, et al., 2002).

Interestingly, the combined effect of oral contraceptive and high parity had an overall increased risk compared to nulliparous women who had never used oral contraceptives. This suggest that the inducing effect of oestrogen may be of clinical significance in development of cervical cancer in the presence of HPV infection as it could act to enhance progression from dysplasia to Carcinoma in situ (Bosch, et al., 2006). Oral contraceptives and high parity, although HPV-independent, are factors that play similar roles by maintaining the transformation zone of the cervix. Thereby facilitating exposure to HPV and other cofactors by changing hormone levels which alter immune response to HPV infection and increase likelihood of cervical carcinoma (Castellsagué & Muñoz, 2003) (Hinkula, et al., 2004).

1.5.2.1.3. Dietary factors

Dietary factors account for 30% of cancers in industrialised countries and this proportion thought to be about 20% in developing countries and are the second to cigarette smoking as a preventable cause of cancer (WHO/FAO, 2003). The role of diet in the sustenance and promotion of good health, growth and development is unequivocal but this relationship is complicated by biological and social factors such as

sedentary lifestyles, genetic susceptibilities, socio-economic status and the progressive change from plant-based to high-fat, energy-dense animal-based diets in both developing and developed countries. Despite recognition by current literature of strong associations between dietary factors and cervical neoplasia, there has been inconsistent contradictory evidence of suspected dietary factors acting as independent risk factors/HPV cofactors or confounders of HPV-related factors (Garcıa-Closas, et al., 2005) (Tomita, et al., 2010) (González, et al., 2011) (Tomita, et al., 2009).

1.5.2.1.4. Tobacco smoking

Tobacco smoking has been linked with cancers such as lung, pancreas, kidney, penile, anal, liver bladder, laryngeal, head and neck as well as acute leukaemia (Harris, 1996). Tobacco is a free radical generating environmental toxin and therefore can be intuitively regarded as HPV independent. However, may potentially act as a contributory risk factor in HPV mediated cervical carcinogenesis. Nevertheless, most of the current literature available on the relationship between smoking and the incidence of HPV infection report conflicting results (Winer, et al., 2003) (Olsen, et al., 1998) (Matsumoto, et al., 2003). Many case control studies have demonstrated moderately and statistically significant associations with cervical cancer, even adjusting for HPV (Lacey, et al., 2001) (Deacon, et al., 2000) (Hildesheim, et al., 2001) (Castle, et al., 2002). This relationship also appears to correlate with dosage and lose correlation with termination of smoking. Studies have shown that smoking confers higher risk in HPV positive squamous-cell carcinoma than adenocarcinoma (Vaccarella, et al., 2008).

1.5.3. Genetics

A complex interaction between genes and environmental factors and varying epidemiological evidence suggests both host and viral genetic factors are vital determinants in a woman's susceptibility to cervical cancer development. However, the predisposition to such factors has only been consistent in studies of human leukocyte antigen (HLA) class I &II genes (Hildesheim & Wang, 2002). The highly polymorphic nature of HLA molecules determines peptide-binding affinity and dictates

differential risks for cervical cancer. Individuals that have HLA molecules that bind the HPV antigen with high affinity a decreased risk to developing cervical cancer is seen, while HLA molecules that do not recognise or bind HPV antigens an increased risk is seen, inferring HLA status is a contributory factor to HPV cervical carcinogenesis. The focal point of most studies on HLA and cervical cancer pathogenesis has moved on from HLA Class II to Class I genes as more HLA Class I genotyping methods become available. Conflicting reports regarding possible associations of HLA class I A-C and E-G in cervical neoplasia have been reported thus require further assessments studies to clarify their associations with cervical cancer (de Boer, et al., 2007) (Gonçalves, et al., 2008) (Hildesheim, et al., 1998) (Apple, et al., 1995) (Sanjeevi, et al., 1996) (Odunsi, et al., 1996). Protective alleles HLA class II DQB1 and DRB1 genes have been consistently associated with cervical neoplasia (Engelmark, et al., 2006) (Zoodsma, et al., 2005) (Madeleine, et al., 2008) (Engelmark, et al., 2004) (Schiffman & Kjaer, 2003).

1.6. HPV oncogenicity

A complex interplay exists between different proteins that control gene transcription to maintain a virally 'productive' phase. HPV can undergo changes like the loss of terminal differentiation, which attenuates full viral life cycle, and the integration of the viral nuclear plasmid into the host genome, which disrupts and renders its replication defective and results in up-regulation of E6 and E7 oncogene expression (Doorbar, 2006). Neoplastic progression in the cervical epithelium is as a consequence of an exponential increase in the expression of E6 and E7 from low grade CIN to carcinoma *in situ)* (Cattani, et al., 2009). The exploitation of cellular processes required for cell-cycle control and apoptosis by E6 and E7 endorses their potential to promote cellular transformation, induction and maintenance (Ghittoni, et al., 2009). Integration of the HPV genome with host DNA is, therefore, a key event in HPV induced carcinogenesis (Huang, et al., 2008). The molecular processes that are involved and drive this transformation are yet to be fully elucidated and the mechanism of transformation is the focus of this project. E6 promotes transformation by triggering cell cycle

deregulation and tumourigenesis. Therefore, a thorough understanding of its interactions is required for the development of therapeutic prospects that impede its activity and hereafter prevent future HPV induced cancers.

1.6.1. HPV E6

1.6.1.1. E6 structure

HPV E6 is a small basic cysteine rich protein of about 150-158 amino acids in length. HR-HPV E6 is the most potent and significant of the HPV primary oncoproteins responsible for promoting malignancy, as its functions involve cell transformation. It is a highly variable protein with conserved motifs and intragenic splicing (Nomine, et al., 2006). E6 is made up of atypical highly conserved N and C terminal zinc finger domains characterised by two cysteines motifs (Cys-X-X-Cys) separated by 30 amino acids and a C-terminal PDZ binding motif, as shown in Figure 1-11. Efforts in isolating and examining a native stable folded full length form have been hindered due to its tendency to form aggregates on synthesis, particularly HPV16 E6. Though, studies using varying spectroscopic methods such as NMR, circular dichroism, and fluorescence spectroscopy have proven insightful (Liu, et al., 2009) (Nominé, et al., 2006) (Zanier, et al., 2007).

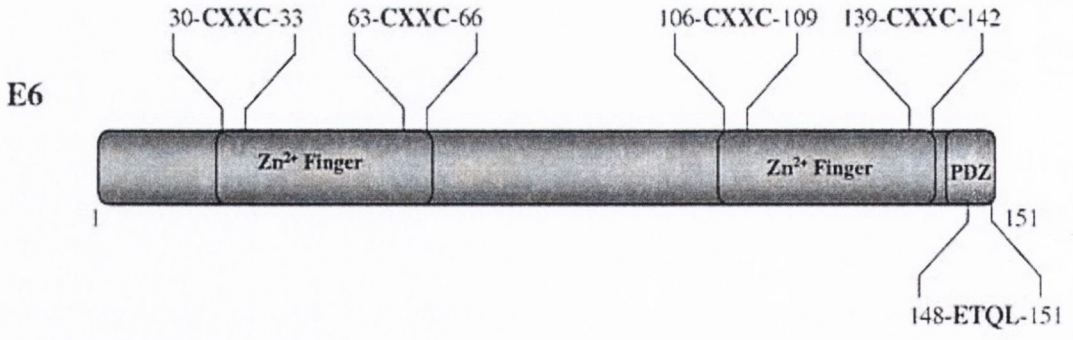

Figure 1-11: Schematic description of HPV16 E6 Structure. The amino terminal portion of E6 contains two cysteine-rich zinc-binding motifs. Similarly, the carboxyl terminal also consists of two cysteine-rich zinc-binding motifs in addition to a PDZ binding motif (present in only high risk types) **(Ghittoni, et al., 2009)**.

E6 is regulated by the upstream regulatory region (URR) via E2 over expression, which drives almost all early gene expression (Zhou, et al., 1994). E2 viral protein averts uncontrolled expression of transforming proteins E6 in HPV infected cells, by hindering their expression from the URR (Schmitt, et al., 1994) (Nomine, et al., 2006). In Hr-HPV16 and 18, E6 and E7 are expressed as a polycistronic pre-mRNA from a single promoter immediately upstream of E6 ORF, unlike Lr HPV6 and 11, where they are transcribed from two separate promoters individually (Zheng, 2010). A distinctive characteristic of oncogenic E6 is the presence of an intron which enables splicing in the E6 open reading frame (Zheng, 2010). Therefore, in Hr-HPV, the E6E7 cassette gives rise not only to full length E6E7 mRNA but also E6 splice variants, E6*I and E6*II (Figure 1-12). E6*II is the least abundant protein detected in transformed HPV cells and cell lines, followed by E6 and E6*I. The exact functions of the E6 splice variants are unclear at present. However, there is some evidence that they play a role in the transcription of E7, with unspliced transcripts encoding E6 primarily and splice transcripts encode both the splice E6 variants and E7.

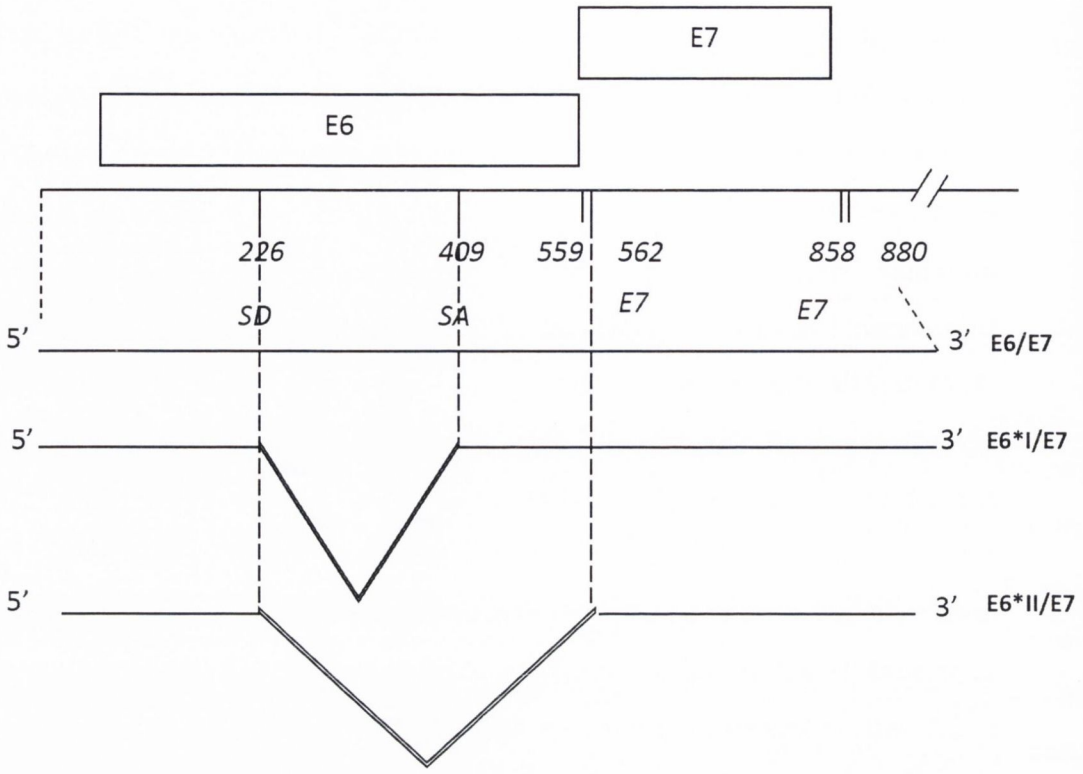

Figure 1-12: Schematic description and organisation of HPV16 E6 Open Reading Frame. E6E7 cassette is expressed as a bicistronic pre-mRNA from a single promoter p97 and gives rise to full length E6E7 mRNA, along with spliced E6*I/E7 and E6*II/E7 transcripts. The spliced transcript E6*I is generated by SD at position 226 and SA at position 409. The spliced transcript E6*II is generated by SD at position 226 and SA at position 560. Both the spliced (E6*I/E7 and E6*II/E7) and unspliced (E6/E7) transcripts are produced in high risk HPVs but no unspliced transcript is produced in low risk HPV. Numbering refers to transcript numbers, SA to splice acceptor; SD to splice donor Figure adapted by author from **(Venturini, et al., 1999)**. *Copyright Permission sought and reuse request is free of charge.*

E6 is an oncogenic multifunctional protein; it can act as a transcriptional transactivator and a weak transcriptional repressor. Its transcription activation domain can be used to transactivate the adenovirus E2 promoter, via zinc finger domain. It can also function as a weak transcriptional repressor of the immediate early promoter in the cytomegalovirus and the long terminal repeat in moloney murine leukaemia virus (Etscheid, et al., 1994). Both functions can be observed in Hr and Lr HPVs. In Hr-HPVs, the transcriptional transactivator function may be coupled to its transforming ability (Etscheid, et al., 1994).

1.6.1.2. Protein Interactions of E6

E6 has been identified to interact with and inactivate diverse proteins essential to cellular functioning, including tumour suppressor genes, genes involved in apoptosis, transcription, cell proliferation and epithelial function, as portrayed in Figure 1-13. On binding these proteins, E6 promotes transformation by triggering cell cycle deregulation, thus exerting its influence as an oncogenic protein. HPV E6 circumvents cellular response to viral infections by diverse methods, which could involve either E6 or E6-E6AP complex binding directly to pro-apoptotic proteins and/or manipulation at the transcriptional level, as is the case of Survivin whose promoter activity is appreciably up-regulated to cause apoptosis suppression. The most important effect of E6 expression in the Hr types is the loss of a multifunctional cellular regulatory protein p53, which has tumour suppressor properties (Figure 1-13).

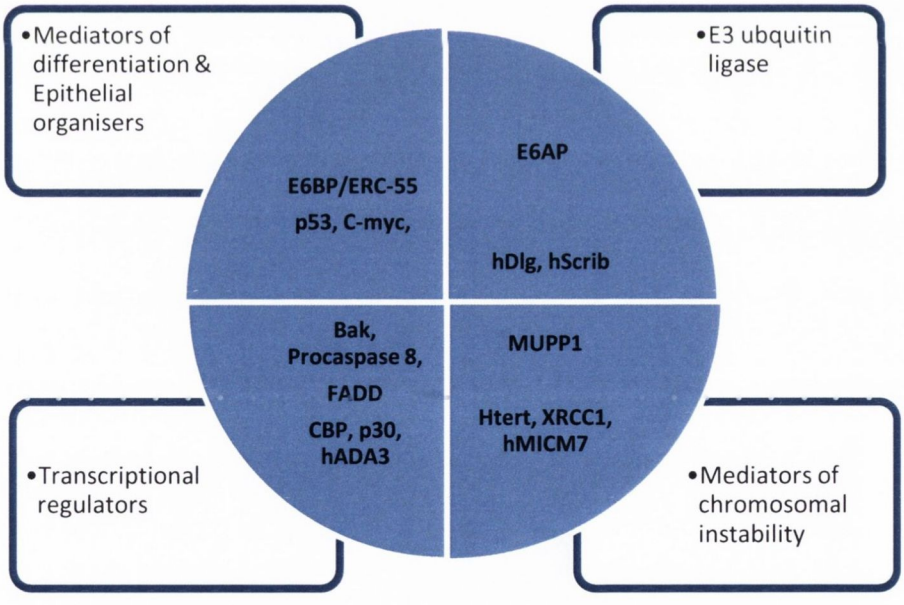

Figure 1-13: High risk HPV E6 interactions. HPV E6 interacts with diverse host proteins to mediate apoptosis, organise epithelium, suppress tumours, and regulate transcription and proliferation. The outer boxes represented circumvented functions while the quadrants of the circles represent the proteins Hr-HPV E6 interacts with in regards to each function. *Figure created by author.*

1.6.1.2.1. E6 and p53

p53 is the most important cellular target of E6. It is a tumour suppressor gene that encodes a 53-kilodalton (kDa) protein, which regulates the cell cycle by conserving genome stability and promoting apoptosis after irreparable DNA damage. This tumour suppressive activity requires p53 accumulation in the nucleus to proceed. p53 has seven domains: an acidic N-terminus activation domain 1, activation domain 2, an apoptotic proline rich domain, a central DNA-binding core domain, a nuclear localisation signalling (NLS) domain, homo-oligomerisation domain and a regulatory C-terminal. On transcription, p53 is imported into the nucleus using NLS via α-importin and transported into promyelocytic leukemia protein-nuclear bodies for further activation and biological functioning. Mdm2 regulates p53 by allowing its nuclear export for degradation by 26S proteasome. p53 is protected from Mdm2 byp14 ARF (alternate reading frame (ARF) product of the CDKN2A locus) and c-Abl. To overcome p53 function, most viruses directly target p53 or p53 target genes. For example, Hepatitis B virus X protein (HBVx) requisitions p53 in the cytoplasm (Wang, et al., 1994), while simian virus 40 (SV40) large T-antigen prevents transactivation of p53 target genes (Michalovitz, et al., 0986). Hr-HPV, however, abolishes p53 by inducing the ubiquitin-proteasome pathway, which normally controls p53 turnover rate.

HPV16 E6 abrogates p53-mediated transcriptional repression of target apoptosis inducing genes via complex formation with E6AP, leading to ubiquitin-dependent degradation of p53 (Ho & Benchimol, 2003). Hence, in conjunction with E6AP, E6 acts as an anti-apoptotic protein. E6AP is an E3 ubiquitin ligase that works in conjunction with E1 ubiquitin activating enzyme and E2 ubiquitin conjugating enzyme. All ubiquitin ligases share E1 ATPase enzyme, which activates ubiquitin for conjugation and transfers it to E2, an intermediary carrier for ubiquitin. E3 is a multi-protein complex enzyme that acts as a catalyst to facilitate E2 docking. It brings E2-ubiquitin in close proximity to target protein for tagging. HPV E6 modulates E6AP's affinity for p53, forms a ternary complex and promotes p53 ubiquitination. Lr-HPVs, such as HPV-6 and HPV-11, do not have the capacity to degrade p53. Other routes by which E6 overcomes p53 activities, include p53 destabilisation via binding to its C-terminus, interference

with its DNA binding ability, cytoplasmic sequestration and interaction with transcriptional co-activators such as adenosine deaminase 3 (ADA3), p300 and CBP (Ganguly & Parihar, 2009) (Kumar, et al., 2002) (Huang & McCance, 2002). The binding of E6 to CBP/p300, which are p53 co-activators, manipulates cell cycle progression by decreasing the affinity of p53 for its DNA binding site. Hence, E6 binding and interaction with both CBP/p300 and p53 respectively, promotes viral survival and enhances proliferation of infected cells, thus facilitating oncogenity (Schmitt, et al., 1994) (Narisawa-Saito & Tohru, 2007) (Zimmermann, et al., 1999).

1.6.1.2.2. E6-mediated hTERT induction

Human telomerase is another target of the E6-E6AP complex. Human telomerase is a ribonucleo enzyme complex that extends chromosomal end length, thereby suppressing senescence. It is made up of a catalytic transcriptase (hTERT) and an RNA component (hTR). The maintenance of telomere length plays a key role in immortalisation and tumourigenesis of varying human cancers cells (Horner, et al., 2004). HPV E6 induces hTERT expression via two E boxes at its promoter, by means of the transcriptional activator Myc (Wu, et al., 1999). This activity of E6 also requires alteration of the nuclear transcription factor, X-box binding 1 (NFX1) isoforms, which involves NFX1-91 degradation enabling NFX1-123 enhancement of the E6-E6AP effect on hTERT (Katzenellenbogen, et al., 2009).

1.6.1.2.3. E6 targeting of PDZ-domain proteins

Hr-HPV E6 proteins target certain cellular proteins containing a PSD95/Dlg/ZO-1 (PDZ) domain, such as mammalian homologs of discs large 1 (DLG1/hDLG) and Scribble (Scrib/Vartul). It degrades these proteins, which are important in cell signalling and adhesion, through its C-terminal motif. Consequently, E6 alters the physiological status of receptors linked or trafficked by PDZ proteins, such as β1-adrenergic receptor. This causes loss of cell–cell contacts mediated by tight junctions and lateral diffusion of integral membrane proteins between the apical and lateral/basal surfaces, thereby disrupting trans-cellular transport and promoting transformation and tumourigenesis.

Ultimately this leads to apical and baso-lateral surfaces no longer having specialised functions of receptor-mediated endocytosis and exocytosis and cells lose polarity as observed in HPV-associated cervical cancers (Ganguly & Parihar, 2009).

1.6.1.2.4. E6 and other proteins

The E6 protein also targets other molecules as outlined in Table 1-3. One group in particular is pro-apoptotic proteins, like Bak, FADD and procaspase 8. E6 modulates the activity of procaspase 8 and binds C-terminal end of tumour necrosis factor receptor (TNFR 1), thereby altering response of the tumour necrosis factor (TNF) family (Filippova, et al., 2004) (Tungteakkhun, et al., 2010) (Thomas, et al., 2002). The TNF family are a group of cytokines involved in regulation of systemic inflammation induction of apoptosis. Activation of TNF receptors triggers the binding of intracellular death domain with its adaptor protein, which forms a scaffold onto which other regulatory cellular proteins are recruited. These recruited proteins elicit the initiation of pathways NF-κB, MAPK and death signalling. TNF-R1 activation results in the binding of Fas-Associated protein with Death Domain (FADD) via its adaptor, which exacts the cleavage of downstream caspases and activation of NK-κB pathway resulting in apoptosis (Filippova, et al., 2007).

Although little is known about how squamous epithelial cells respond to a PVs infection, IFNs intrude on different aspects of the viral lifecycle and activate immune natural killer cells to stimulate the immune system. The absence of a strong immune response suggests viral interference with immune response. Some mechanisms involved include the disabling of IFN inhibitory effects; E6 inhibits transcription of toll-like receptors (TLRs), such as TLR9, Tyrosine kinase 2-mediated Janus Kinase- Signal Transducer and Activator of Transcription signalling pathway (JAK-STAT) activation via interferon alpha (INF-α) as well as transactivation of interferon regulatory factor-3 (IRF-3) which arbitrates apoptosis on viral detection. (Ronco, et al., 1998) Finally, E6 has been found to deregulate the p16/pRb pathway via a unique pathway involving activation of E2F-responsive genes, MCM7 and cyclin E (Malanchi, et al., 2002).

Table 1-3: Summary of Hr-HPV E6 functions. This table shows a list of observed biological effects of E6 targeting. (See Table 8-3 in the appendix for changes to these targets post silencing with E6 siRNAs).

Target molecules of E6	Implicated biological effect
E6AP/p53	Degradation of p53/suppression of apoptosis
PDZ-domain-containing proteins	Degradation of PDZ proteins/loss of cell polarity
CAL	Deregulation of the vesicular trafficking processes
NFX1-91	Degradation of NFX1-91/activation of hTERT, immortalisation
Paxillin	Interference in the association of paxillin and focal adhesion kinase
IRF3	Inhibition of IRF-3's transcriptional activity thereby inhibiting the IFN-induced signalling
Bak	Degradation of Bak/suppression of apoptosis
FADD	Degradation of FADD/suppression of apoptosis
Procaspase 8	Degradation of procaspase 8/suppression of apoptosis
GADD34/PP1	Suppression of apoptosis
Tyk2	Impairment of Tyk2 activation thereby inhibiting IFN-induced signalling
CBP/p300	Down-regulation of p53 activity by targeting the transcriptional coactivator
MCM7	Induction of chromosomal abnormalities
TSC2 (tubulin)	Activation of mTOR signalling
BRCA1	Release the inhibition of ER signalling

1.6.1.3. HPV E7

E7 of Hr-HPV (HPV16 and 18) is frequently associated with genital malignancies than Lr types (HPV6 and 11) as it has a higher affinity for tumour suppressor genes (Schmitt, et al., 1994). E7 is a highly conserved α-helical protein with extended strand and random coils, consisting of 98 amino acids with conserved regions known as conserved region 1, 2 and 3 (CR1,2,3) that represent 1–15, 16–37 and 38–98 amino acids respectively (Figure 1-14). CR2 and CR3 regions share sequence homology with corresponding regions in adenovirus E1A and SV40 large T antigens. It is a small 21kDa zinc-binding phosphor-protein that is located in the nucleus, where it executes its cell transforming and trans-activating functions. CR1 is thought to be involved in transformation and blocking TGF-ß and repression of c-myc, CR2 with pRb binding via the LXCXE motif and casein kinase II phosphorylation (residues 31 and 32) and CR3 has twin CXXC elements capable of zinc binding similar to HPV16 E6. The CR3/Carboxyl terminal zinc-binding domain also mediates dimeric and multimeric complexes formation *in vivo* (Liu, et al., 2006) (Narisawa-Saito & Tohru, 2007).

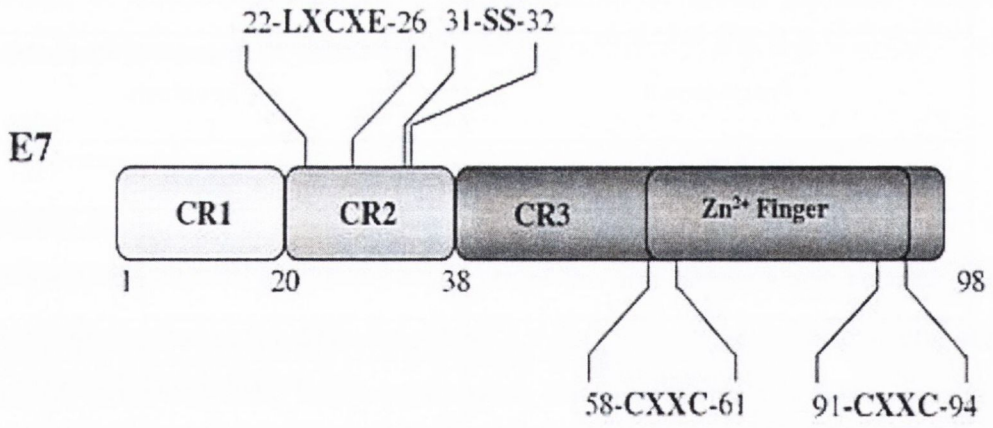

Figure 1-14: Schematic description of HPV16 E7 Structure. The amino terminal portion of E7 contains three conserved regions CR1, CR2 and CR3 (homologous to adenovirus E1A oncoprotein). CR2 contains a core LXCXE motif that binds pRB and pocket proteins. The carboxyl terminal also consists of two cysteine-rich zinc-binding motifs in addition to a PDZ binding motif. **(Ghittoni, et al., 2009)**.

1.6.1.3.1. E7 and its cellular targets

E7 can bind via LXCXE motif in its CR2 region and aberrantly inhibit retinoblastoma protein (pRb) and other "pocket proteins" family members, like p107 and p130 (Chakrabarti & Krishna, 2003), by itself or in collaboration with ras or HPV E6. p107, Rb/p105 and Rb2/p130 represent members of the Rb family of negative cell cycle regulators that function as tumour suppressors. They bind to the E2F family of DNA-binding transcription factors in a hypo-phosphorylated state and in so doing regulate proliferation and differentiation (Giacinti & Giordano, 2006) (Narisawa-Saito & Tohru, 2007). Progression into S phase of the cell cycle is preceded by E2F release, following pRb phosphorylation by G1 cyclin-dependent kinases (CDK), like p16INK4a, Cdk 2/Cyclin A and Cdk 2/Cyclin E. E7 exploits this by binding unphosphorylated pRb, preventing the anticipated pRb–E2F complex formation hence inducing cells to enter the S phase. E7 then ensures proteasomal degradation of pRb by its C-terminal cleavage via calcium-activated cysteine protease calpain and complete exit of the cell cycle which enables viral replication in the upper epithelial layers. E7 together with E6 causes genomic instability via p53 and pRb family members resulting in polyploidy. In addition, acute loss of pRb family members induces centrosome amplification and aneuploidy (Schmitt, et al., 1994) (Narisawa-Saito & Tohru, 2007) (Liu, et al., 2006). E7 can block transcriptional activation function of retinoblastoma protein family members (Rb).

Other proteins that E7 can complex with include; cyclin associated kinase p33cd 2, CDK-inhibitor (CKI) p27 and CKI p21 to abate cell-cycle inhibition, transcriptional co-repressors histone deacetylases (HDAC) to promote cellular growth, IRF1 and p48 to escape immune detection, cellular p600 for anchorage-independent growth and cellular transformation, both subunits of protein phosphatase 2A (PP2A) thereby hindering dephosphorylation and termination of PKB/Akt signalling pathway (Horner, et al., 2004).

1.6.1.3.2. E6 and E7

In summary, E6 and E7 are cooperative viral oncoproteins expressed in all HPV-cervical cancers and increased expression of both is observed in integrated viral forms. HPV infects and uses viral oncogenes E6 and E7 to subvert normal cellular function, thus maintaining an altered cell cycle state whereby viral genome replication and amplification is unhindered. This 'altered state' presents a challenge for the immune system, which often rapidly clears the infection, as it is unable to prevent cell growth and stimulate apoptosis due proteasomal degradation of p53 and displacement of retinoblastoma protein pRb. E6 complements E7's ability to immortalise human keratinocytes, therefore E6 is considered the more potent and significant of the two as its functions involve cellular transformation (Vinokurova, et al., 2008).

1.6.1.3.3. DNA methylation in Cervical Cancer

The progression from precancerous cervical lesions to cervical carcinogenesis is multifactorial process and mainly due to persistent unresolved Hr-HPV infection in addition to environmental, immunological, genetic and epigenetic factors (Section 1.5). The persistent unresolved Hr-HPV infection resulting in viral genome integration into the host genome whereby large sections of the genome become inactivated is proposed to occur at fragile sites within host DNA (Dall, et al., 2008). It has also been established that viral integration causes genetic alterations such as deletions, amplifications and DNA rearrangements as well as epigenetic modifications to the DNA methylation status resulting in the over expression of viral oncogenes E6 and E7 hence favouring tumour progression (Chaiwongkot, et al., 2013) (Saavedra, et al., 2012). While the link between HPV and aberrant methylation in cervical cancer remains unclear, it has been suggested as a means by which HPV conceals itself (Whiteside, et al., 2008) (Leonard, et al., 2012). That is, Hr-HPV E6 and E7 alter host DNA methylation status by increasing the expression and action of DNA methyltransferase (DNMT1) which preserves methylation pattern during each cellular division via p53 and pRb degradation (Figure 1-15).

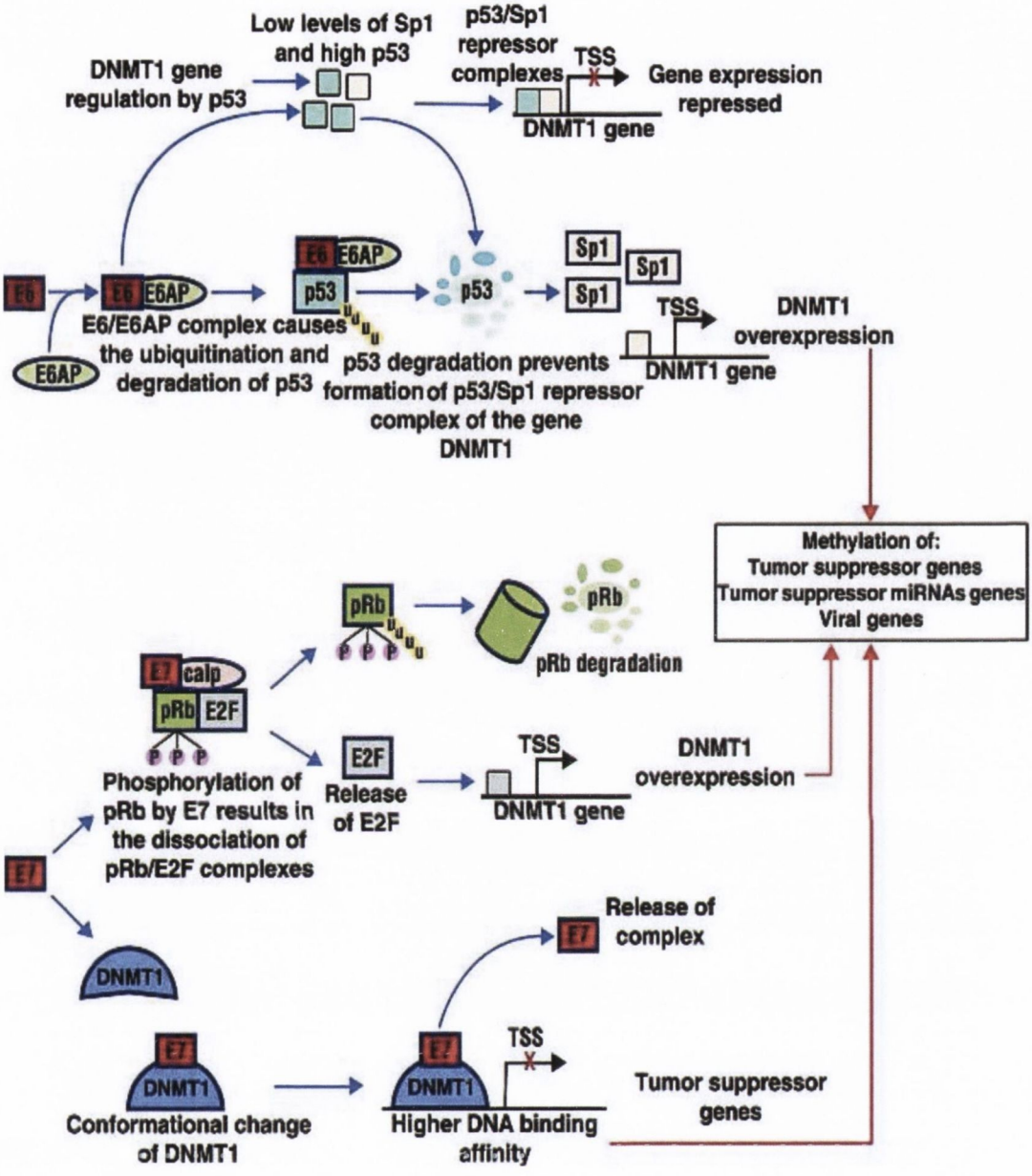

Figure 1-15: The regulation of host and HPV gene methylation by Hr-HPV E6 and E7. (A) in high concentrations, p53 forms a complex with specificity protein 1 (Sp1) and chromatin-remodelling proteins which subsequently binds to the DNMT1 promoter region. Therefore, Sp1 is inhibited from activating the transcription of DNMT1. However, the degradation of p53 due to E6 and E6AP binding releases Sp1 to activate DNMT1 transcription. (B) The binding and phosphorylation of pRb by E7 releases E2F which positively regulates the promoter activity of DNMT1. Hr-HPV E7 can also directly bind DNMT1, causing its conformational change and exposing its DNA binding site. This results in increased DNA binding affinity and the formation of a stable DNMT1/DNA interaction. The consequence of DNMT1 overexpression is cellular transformation and tumourigenesis via the hyper-methylation of tumour suppressor gene promoters **(Jimenez-Wences, et al., 2014)**.

1.7. Prevention of cervical cancer

The implication of HPV oncogenes as the main instigators of cervical dysplasia and the asymptomatic nature of the disease reiterate the paramount importance of early detection in halting and preventing the progress of cervical carcinogenesis. Prevention programs targeted against the disease comprise of two stages, primary prevention programs which involve the implementation of vaccination programs and secondary prevention programs which involve cervical screening programs (conventional Pap smear tests, liquid based cytology (LBC), visual inspection with acetic acid and HPV testing for high risk types), which are directed towards the detection and subsequent treatment of precancerous lesions amongst women aged 25 to 60 years (Figure 1-16).

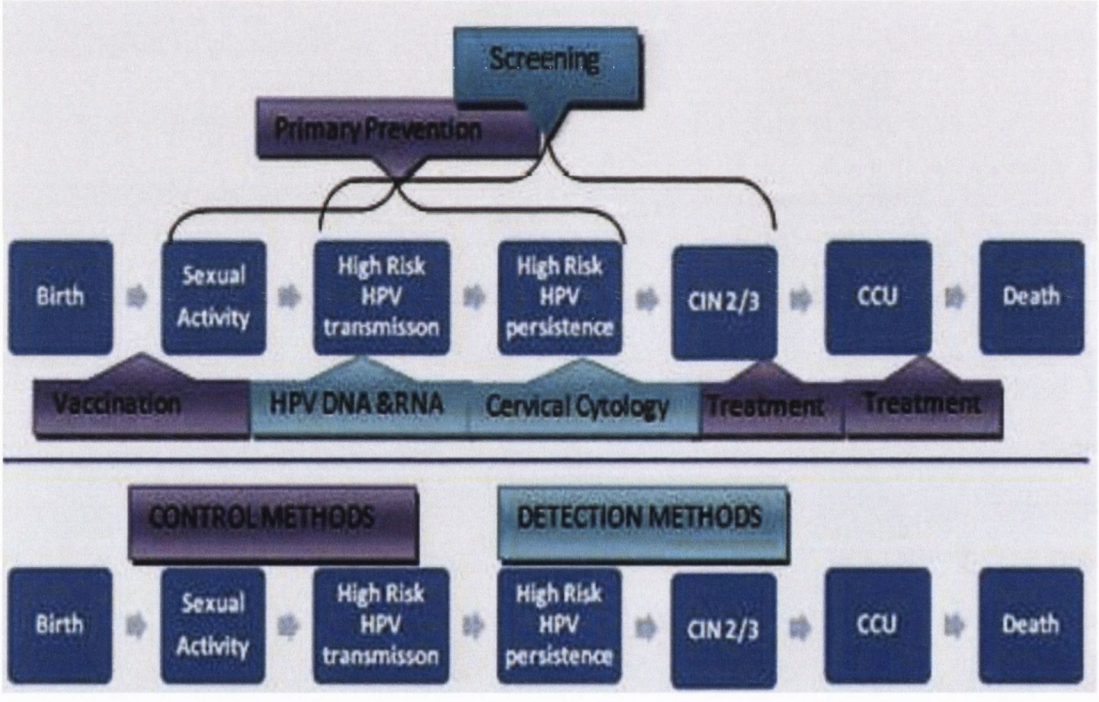

Figure 1-16: The course of HPV prevention. This diagram depicts primary and secondary HPV prevention programmes and their stages of intervention. *Figure created by author.*

Vaccine development is targeted at prevalent HPV types responsible for more than half the burden of cervical cancer (HPV16 and 18 which make up 50% and 20% respectively of all cases). These prophylactic vaccines target infectious agents to prevent development of diseases, unlike therapeutic vaccine treatments, which are used to treat existing conditions by strengthening body defences. Presently, two vaccines against cervical cancer are available. They are Merck's quadrivalent Gardasil vaccine (FDA approved in 2006) that offers protection against HPV16 and 18 as well as HPV6 and 11, which cause genital warts, and GlaxoSmithKline's bivalent Cervarix against HPV16 and 18. These vaccines are made up of HPV antigens comprising of different virus-like particles, which are not infectious but stimulate an antibody response. These vaccines have been shown to be safe and effective, as well as offering cross protection against less common HPV types that cause cervical cancer (Bonanni, et al., 2009). World Health Organisation (WHO) recommends 9-13 year old girls, who have not been exposed to HPV, will benefit most from vaccination (Parry, 2007). Post vaccination protection has been formally proven to be 7.3 years for Cervarix and 9 years for Gardasil with clinical trials showing at least five years protection post-vaccination. According to WHO, at the end of 2011, 40 countries had introduced vaccination programs as part of their national public health strategy (World Health Organisation, 2012). The increasing adoption of vaccine administration by developed countries is proposed to have a major impact in the elimination of cervical cancer, though a positive outcome is evident, it will only become apparent once vaccinated cohorts reach screening age.

Cervical screening involves a number of methods directed towards the detection and treatment of precancerous lesions. Detection of cervical pre-cancer facilitates treatment before lesions become invasive which improves prognosis (World Health Organisation, 2012). European guidelines for quality assurance in cervical cancer screening is one of the steps towards establishing appropriate standards or protocols for cervical screening. Currently the main form of cervical screening is the Pap smear test, of which there are two methods the conventional pap smear test and liquid based cytology (LBC). Pap smear test, while it has effectively reduced the incidence of

cervical cancer, exhibits a broad sensitivity range with high levels of inaccuracy when detecting particularly low-grade squamous intraepithelial lesions (LSIL) and equivocal lesions (ASCUS). The use of LBC which involves the processing of a sample in a preservative fluid is however, a more efficient method of cervical sampling for laboratory examination and has resulted reduction in the number of unsatisfactory smears (Gibb & Martens, 2011). A major shortcoming with cervical cytology is the fact that up to 80% of low grade abnormalities can spontaneously regress, resulting in an increased likelihood of over referrals, overtreatment and inappropriate follow ups. Nevertheless, Pap smear remains the most affordable test available, in spite of the varying levels of proficiency amongst these tests due to issues relating to sensitivity and specificity (Coste, et al., 2003) (Kulasingam, et al., 2002) (Cuzick, et al., 2003). Hence, research has focused on identifying new tests to use in conjunction with pap smears.

In spite of the efficacy of these prevention programs, neither are widely available to many at greatest risk of developing cervical cancer and this is reflected in the disease disproportionality between developed and developing countries. Disparities in the prevalence of risk factors (HPV), accessibility and use of medical practices, accessibility and quality of treatment facilities can dictate the differences in the likelihood of cervical cancer progression between developing and developed regions. Issues' relating to the adoption of primary or secondary prevention programs include lack of public health polices, general and professional HPV education, media awareness, clinical settings, financial resources.

1.8. Treatment of Cervical Cancer

Standard treatment options for cervical cancer include surgery, radiotherapy and chemotherapy or varying combinations thereof depending on the stage of disease and thus whether the treatment is in an effort to treat or avert metastasis and relieve symptoms, thereby improving quality of life and prognosis (Roque, et al., 2014). Surgery is the standard of care for the management and treatment for early-stage,

non-bulky cervical cancer (Roque, et al., 2014). It aims to surgically remove parts of the female reproductive system containing the tumour and can be described into types on the basis of which organs or tissues are removed such as hysterectomy (total, radical or modified radical) and bilateral salpingo-oophorectomy (Figure 1-17). Therefore, surgery offers an instant curative therapy while preserving ovarian and vaginal functions and though radical hysterectomy is the mainstay of surgical management of cervical cancer, less drastic measures provide small but significant role in CIN management. Such surgical procedures include loop electrosurgical excision procedure (LEEP), cold knife cone biopsy, cryotherapy, electrofulgaration, cold-coagulation and pelvic exenteration (Stern, et al., 2012). The LEEP is a relatively inexpensive procedure that can be performed in an outpatient setting. It involves the use of a thin, low-voltage electrified wire loop to cut out abnormal tissue. However, the cold knife cone biopsy is the standard procedure to excise deeply seated lesions in the endocervix and avoid diathermy artefacts at the margins which could obscure the extent to which the lesion or cancer has been removed (Stern, et al., 2012) (Roque, et al., 2014). Cryotherapy is a non-surgical procedure used to destroy abnormal cervical tissue using liquid carbon dioxide. A prior requirement of lesion diagnosis and visualization is essential as specimens for histopathology cannot be obtained subsequently (Stern, et al., 2012).

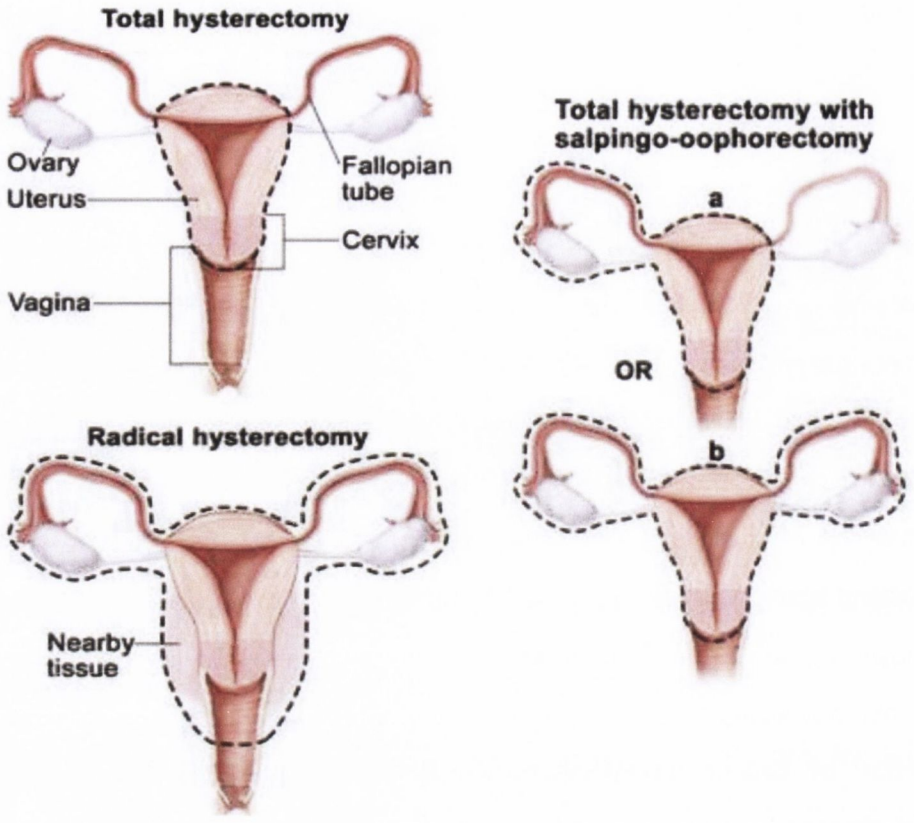

Figure 1-17: Types of Hysterectomy. Hysterectomy involving surgical removal of uterus with or without other tissues or organs. Total hysterectomy; uterus and cervix are removed. Total hysterectomy with salpingo-oophorectomy; a) uterus and one/unilateral ovary and fallopian tube are removed b) uterus and both/bilateral ovaries and fallopian tubes are removed. Radical hysterectomy; uterus, cervix, both ovaries, both fallopian tubes, and nearby tissue are removed **Invalid source specified.**.

Combinations of radiation therapy and chemotherapy are employed for the successful treatment of locally advanced disease. However, for women with advanced and recurrent cervical cancer, chemotherapy is the standard option for palliative treatment. Radiation therapy employs high-energy x-rays (external-beam high-energy to 18 MV) or other types of radiation such as implants loaded with Iridium-192 to kill cancer cells or prevent them from growing, via external radiation therapy or internal radiation therapy (Burd, 2003). Conversely, chemotherapy uses drugs to stop the growth of cancer cells, either by killing the cells or by stopping them from dividing. Chemotherapeutic drugs used in the treatment of cervical cancer can be classified into cytotoxic platinum-based anti-cancer drugs (Cisplatin and Carboplatin), alkylating agents (Ifosfamide), anti-metabolites (Fluorouracil, Gemcitabine), mitotic inhibitors

(Paclitaxel, Docetaxel) and inhibitors of transcription or replication (Topotecan, Irinotecan) (Allerton & Butler-Manuel, 2014). An example of such is Cidofovir, a broad spectrum acyclic nucleoside phosphonate derivative against DNA viruses like HPV that inhibits cellular proliferation (Yizhuo, et al., 209) (De Schutter, et al., 2013). Similarly, the combination of a cytotoxic chemotherapeutic agent, Podophyllin that arrests mitosis in metaphase and a DNA polymerase inhibitor, Vidarabine suppresses HPV gene expression and cell growth in addition to sensitizing cervical cancer cell lines to apoptosis. (Burd, 2003) These treatment options though very effective at treating CIN, are radical options with significant side effects, none of which target the cause of these lesions or cancer. In addition, they weaken cervical integrity and therefore all carry risks of increasing the risk of preterm birth hence alternative treatment modalities are being researched.

1.9. Therapeutic Nucleic Acids (TNAs)

An alternative approach to current treatment is the use of molecular therapeutic targeting techniques, such as therapeutic nucleic acids (TNAs), against HPV16 E6 and E7 (DiPaolo & Alvarez-Salas, 2004) (Jiang & Milner, 2005) (Alvarez-Salas & DiPaolo, 2007) (Yamato, et al., 2008) (Tan, et al., 2012). TNA technologies can be categorised into three approaches on the basis of their functions (Figure 1-18), antigene, antisense and aptamer approaches. The antigene approach involves triplex-forming oligonucleotides (TFOs), which block gene transcription. The antisense approach includes single stranded antisense oligonucleotides (AS-ODNs), ribozymes (Rz), which are catalytically active oligonucleotides that trigger RNA cleavage and inhibit mRNA translation, and RNA interference, which employs small interfering RNA molecules (siRNAs) that induce translational inhibition. Finally, the aptamer approach involves the use of RNA aptamers that inhibit protein function.

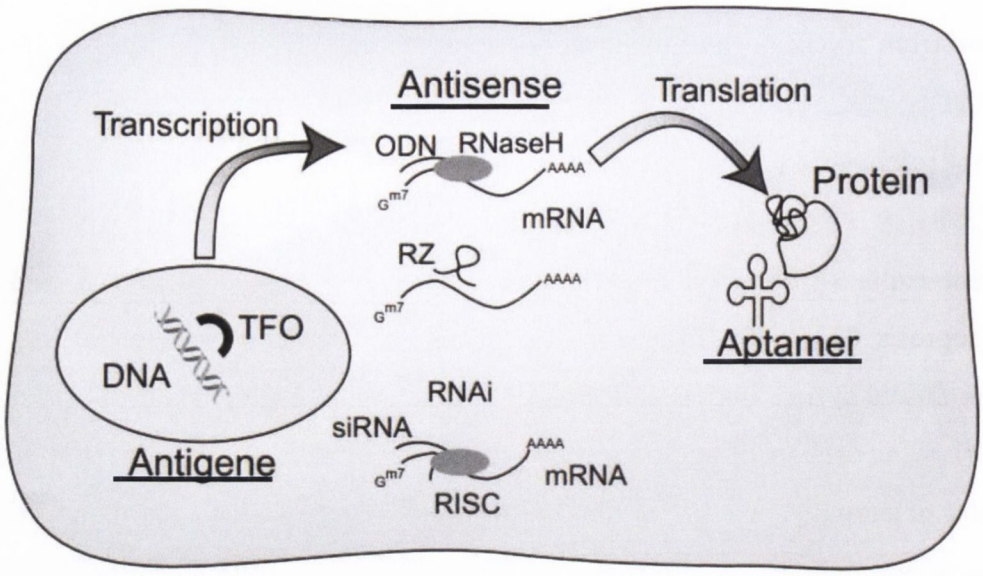

Figure 1-18: Modes of action of therapeutic nucleic acid technologies. In the antigene approach, TFOs bind DNA and block gene transcription. In the antisense approach, either mRNA cleavage may be triggered (ODNs or RZ) or translational inhibited (siRNAs). In the aptamer approach, RNA aptamers bind and inhibit protein function. TFOs: triplex-forming oligonucleotides; ODNs: Oligodeoxyribonucleotide; RZ: Ribozymes; RNAI; RNA interference; siRNAs: small interfering RNA molecules; RISC: RNA-induced silencing complex; TNA: of therapeutic nucleic acids **(DiPaolo & Alvarez-Salas, 2004)**.

TNA technologies are valuable application tools involving DNA/RNA manipulation and/or alterations to derive a complimentary mRNA which can be used to provide vital information on functional genomics and aid in the development of novel targeted anti-sense therapeutics for diseases in humans, plants and animals. The hybridisation of such complimentary antisense nucleotides to a specific target mRNA via varying mechanisms, results in the disruption of normal cellular processing of the genetic message of the gene in question thereby assisting in determination of the function of that gene. The degree to which the genetic message is disrupted can be termed as "knock-down" (partial elimination) or "knock-out" (completely elimination). These techniques may involve the reduction of one or more of an organism's genes via alteration in organism's chromosome or the binding of short complementary DNA or RNA oligonucleotide sequence to organism's mRNA transcript or a gene. The change in gene expression by an oligonucleotide sequence results in a transient knockdown whereby there is a temporary change in gene expression.

1.9.1. Antigene Technology- TFOs

Triplex-Forming Oligonucleotides (TFOs) are long stretches of DNA sequences that recognise and bind specific sequences in the major groove of homopurine stretches. Duplex double stranded DNAs (dsDNAs) are Watson-crick bonded and TFOs specifically form Hoogsteen or reverse Hoogsteen hydrogen bonds between the bases of the pyrimidine or purine TFO and the bases of the purine strand of the dsDNA helix; via T-A: T and C^{+}-G:C triplexes. Triplex formation results in blocking of mRNA elongation by polymerases or inhibition of transcription by interference with regulatory protein binding to dsDNA and has been reported to successfully inhibit transcription *in vitro* (Popa, et al., 1996). The level of control afforded by TFOs is advantageous in that it aids control and modification of cell functioning at genomic DNA level as only one or two targets are present per cell. However, TFOs require stringent conditions of targeting only purine-pyrimidine dsDNA and acidic conditions to ensure protonation of cytosines to form stable helix. Nucleotide modifications to TFOs have been reported by Sorensen *et al.* to alleviate problems relating to the formation of a stable triplex formation at physiological temperatures (Sørensen, et al., 2004).

1.9.2. Aptamers

Aptamers are single stranded nucleic acids that function by folding into specific globular structures and are often used in analytical chemistry to isolate high affinity ligands that bind to a wide variety of proteins and cell surface epitopes in picomolar to nanomolar affinities via SELEX procedure. They can be incorporated as modified nucleotides into RNA transcripts and used as probes to inhibit protein function. So far, no reports have established successful use of aptamers on HPV despite showing promise as efficient tools in viral detection and identification as single stranded DNA/RNA aptamers (Gopinath, et al., 2006) (Ramalingam, et al., 2011) Reviewed in (Sundarama, et al., 2013).

1.9.3. Antisense Technology

The overall aim of the antisense approach is to significantly decrease quantities of disease gene protein made in order to obviate or reverse disease progression. It involves the synthesis of a complementary molecule to disease gene mRNA using its DNA sequence to specifically obstruct translation which may result in gene silencing via degradation of target mRNA by RNAse H. The goal of introducing an antisense agent into a cell *in vivo* or *in vitro* is to supress or completely block production of a specific gene product which can be achieved at any point from DNA sequence to protein translation as illustrated in Figure 1-19.

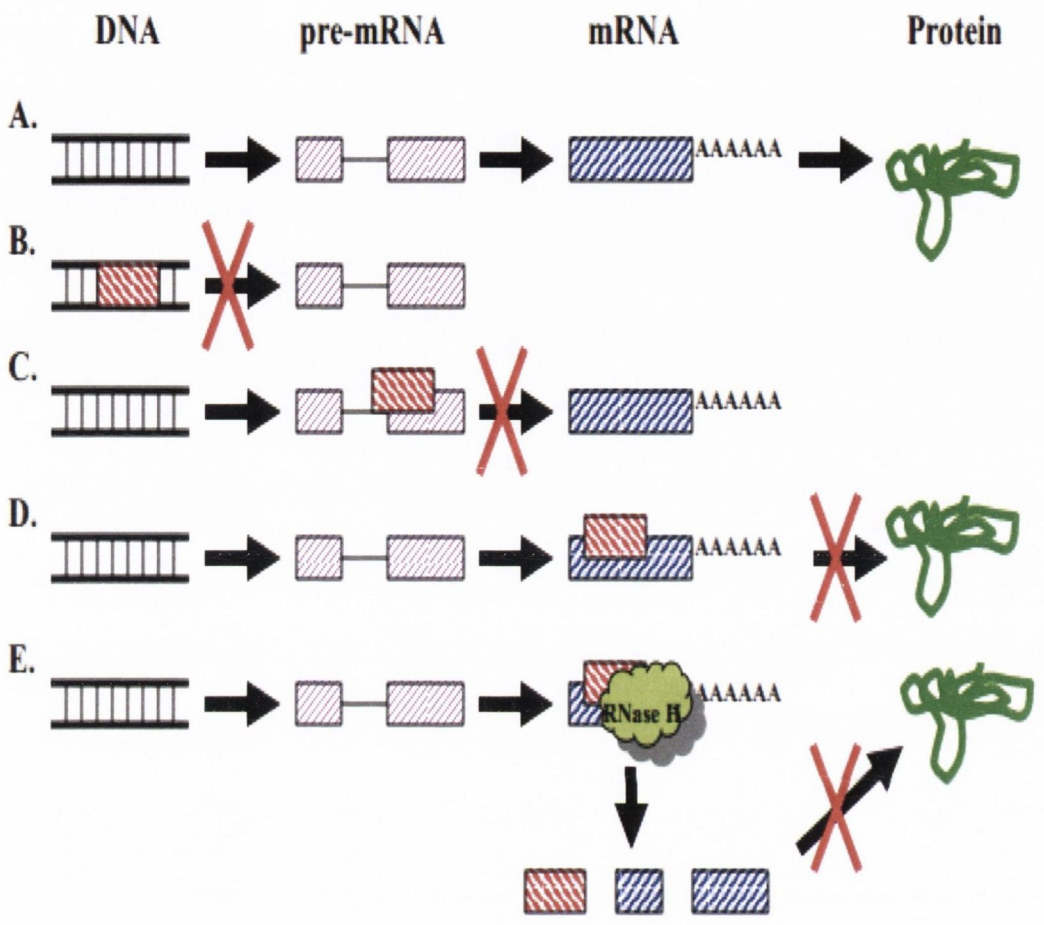

Figure 1-19: Diagram of available methods for antisense knock-down/knock-out. Diagrammatic representation of available methods for antisense knock-down or knock-out of a specific gene. A. The normal cellular process of transcription and translation. B. Prevention of transcription by DNA targeting agents. C. Prevention of mature mRNA formation by pre-mRNA targeting. D. Prevention of translation by disruption of the translational apparatus. E. Prevention of translation by RNase H digestion of mRNA **Invalid source specified.**.

1.9.3.1. Antisense Oligodeoxynucleotide (AS-ODNs)

AS-ODNs molecules are the first and most common approach to gene suppression or elimination. They involve the introduction of a synthetic oligonucleotide sequence complementary to mRNA transcribed from the gene of interest into a cell to ensure high specificity and affinity to target mRNA. These sequences bind their targets via Watson-crick bonding, significantly inhibit and interfere with genetic processes of the

normal or "sense" sequence such that the DNA:RNA heteroduplex formed causes translational arrest by physically blocking ribosomal binding and activating RNase H which cleaves the target mRNA. The initial use of AS-ODNs; which were unmodified, revealed they were highly unstable in biological fluids as they were being targeted by endogenous nucleases hence limiting their usage. This steered the development of several nucleotide analogues or modifications to increase stability. Three possible protective modifications which can be introduced on the nucleotide without changing hybridisation specificity or harming the cell include alteration of the phosphate backbone, alteration of the base and alteration of the 2'OH group in riboses as depicted in Figure 1-20.These antisense-motivated nucleotide modifications led to what has been termed as evolution of generations of AS-ODNs.

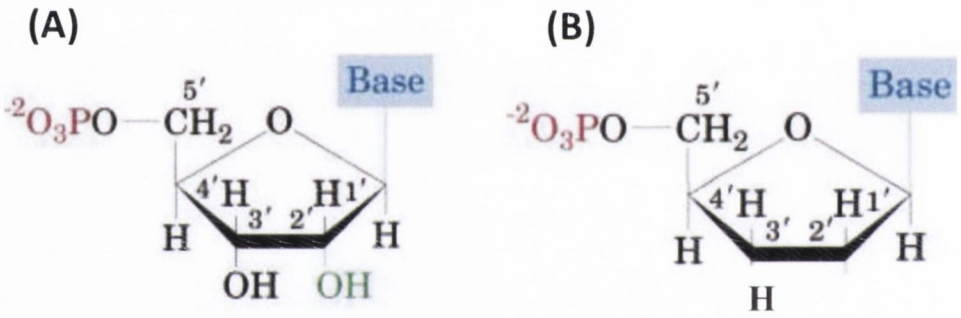

Figure 1-20: Nucleotide structure. The structure of Ribonucleotide (A) and Deoxyribonucleotide (B). Diagram showing three chemical modifications sites that confer protection against the action of endogenous nucleases, they include phosphate backbones highlighted in red for (A) and (B), bases highlighted in blue for (A) and (B) and 2'OH in ribonucleotides highlighted in green for (A) only. *Figure created by author's edits.*

1.9.3.1.1. Antisense oligonucleotide Technology in Cervical Cancer

E6 and E7 are stable oncogenic targets in cervical cancer that are advantageous to the use of antisense approach to degrading viral RNAs. Studies using antisense RNAs have showed inhibition, apoptosis, cell cycle arrest and reduction in E7 protein expression in cultured cell lines and confirm the validity of targeting high risk HPV E6 and E7 for cervical cancer therapy (Alvarez-Salas, et al., 2003) (DiPaolo & Alvarez-Salas, 2004)

(Sima, et al., 2007) (Reyes-Gutiérrez & Alvarez-Salas, 2009). However, difficulties have arisen as a result of an appropriate delivery method of large antisense RNA molecules to patients. This has propelled the alternate use of small antisense moieties such as AS-ODNs. Relative success has be reported with E6 and E7 targeting AS-ODNs and PS-ODNs, with growth inhibition in HPV16 cultured cell lines and inhibited tumours growth in nude mice models. Therefore the combination of AS-ODNs and PS-ODNs could result in a very efficient therapeutic tool against HPV variability.

1.9.3.2. Ribozymes

Another class of antisense molecules are small catalytic RNA molecules or enzymes called ribozymes (Rz) which cleave target RNA on hybridisation via Watson-crick bonding and are viewed as potential antisense agents due to their RNA processing capabilities (Kruger, et al., 1982) (James & Gibson, 1998) (Doudna & Cech, 2002) (Kurreck, 2003). The effectiveness of these traditional anti-sense oligonucleotides techniques has been limited due to undesirable side effects which ultimately hinder progression into viable therapies. Rzs possess both enzymatic cleavage and ligature properties hence do not require RNase H activity for cleavage like AS-ODNs. They can be characterised on the basis of their mode of action and catalysis for example Group I intron, Group II intron, RNase P, Hammer head Rz, Hairpin Rz, Twister, GIR1 branching and peptidyl transferases. Rzs can catalyse self-cleavage which is referred to as intramolecular or "in-cis" catalysis and cleavage of external substrates referred to as intermolecular or "in-trans" catalysis.

Rz engineering has focussed on altering native substrate recognition sequences to give rise to cis-cleaving Rz that cleave target RNAs in trans-orientations and trans-cleaving Rz that cleave any RNA in sequence specific manner. This theoretically ensures that any disease-associated target mRNA would be selectively cleaved before translation can occur. This makes Rzs a potentially valuable tool for viral replication inhibition, modulation of tumour progression and analysis of gene function. The most relevant catalytic Rz originating from plant viroids or virusoids are hammerhead and hairpin Rz

Therefore due to properties of relatively small size, inherent simplicity and ability to incorporate a wide variety of flanking motifs without altering site specific cleavage capacity.

1.9.3.2.1. Ribozymes therapeutics and HPV

The poor secondary structure of the mRNA translational start site makes it highly accessible to antisense molecules and has been exploited by Rzs. Synthesised hammerhead Rzs has displayed efficient catalytic activity against HPV16 E6 and E7 with target size and pre-denaturation step being crucial for activity. The cooperative effect of ionic strength, $Mg2^{+}$ concentration and temperature was also suggested to enhance disruption of E6/E7 gene expression. Hairpin Rzs have also been tested *in vitro* in-cis configuration downstream of HPV16 E6 and E7 and resulted in significant delay in growth rate of transfected cells. The greatest hindrance to the use of Rz is its dependence on Watson-crick bonding with target sequences hence specificity is dependent on target comprising of easily accessible sequences to interact with antisense Rz.

1.9.3.3. RNA Interference

RNA interference (RNAi) is one of the most powerful gene probing antisense tools that functions via a gene suppression strategy. It is an ancient protective mechanism that has been translated into an undoubtedly powerful molecular tool with profound applications as a means for gene manipulation (Fire, et al., 1998). RNA interference (RNAi) was initially observed and coined by Andrew Fire et al in 1998 and has potential therapeutic applications in a wide range of disorders such as Mendelian disorders, multi-factorial disorders, infectious diseases and modulation of normal physiological responses. In plants (petunias), this occurrence had evolved as an anti-viral defence mechanism and had been earlier termed co-suppression by Jorgensen and colleagues in 1990 (Napoli, et al., 1990). In recent years, intense activity has been focused in this area as it has also been established that a process similar to that found in nematodes can be stimulated in mammalian cells using small double stranded RNA molecules to achieve precise sequence gene suppression. It involves sequence-specific mRNA

degradation of viruses and rogue genetic elements on induction by double-stranded RNA (dsRNA) thereby regulating chromatin structure, gene transcription and translation and preserving genome integrity.

The RNAi mechanism in mammalian cells involves the cleavage of long dsRNA molecules into shorter 21-23 nucleotide long duplexes called small or short interfering RNAs (siRNAs) with 2 nucleotide overhangs at both 3' ends by an endogenous RNase II-Like enzyme, Dicer (Macrae, Li, Zhou, Cande, & Doudna, 2006) (Bernstein, Caudy, Hammond, & Hannon, 2001) (Hammond, Bernstein, Beach, & Hannon, 2000). In an ATP-dependent step, siRNA duplex unwinds and the antisense strand of the duplex becomes integrated into a multi-subunit protein complex known as the RNAi induced silencing complex (RISC) which guides and enables binding of the siRNA to the target RNA sequence. This results in the specific suppression of target gene or genomic region expression or function (Fire & Mello, 2006). On hybridisation, RISC directs the degradation of such complementary RNA sequences by activating its slicer activity (endo and exo-nuclease) hence preventing translation of that transcript as explained in Figure 1-21 (Elbashir, et al., 2001). Only the antisense siRNA strand interacts with the catalytic protein of RISC-Argonaute 2 which uses its catalytic domain to cleave target mRNA hence by repeating this process, RISC ensures no mRNA or protein of that sequence is made (Martin & Caplen, 2007).

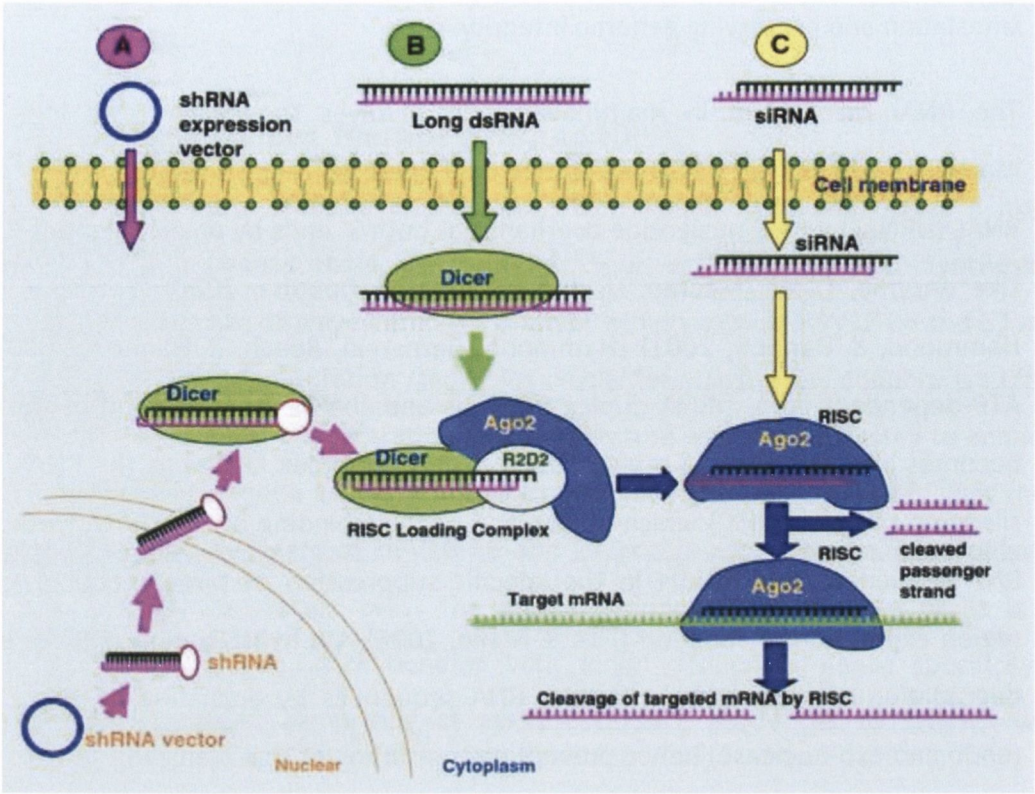

Figure 1-21: Schematic representation of RNAi mechanism. Long double-stranded RNA (dsRNA) or small hairpin RNA (shRNA) are processed by Dicer to form a small interfering RNA (siRNA), which associates with RNA-induced silencing protein complex (RISC) and mediates target sequence specificity for subsequent mRNA cleavage (Chen, Cheng, & Mahato, 2008). Copyright license permits non-commercial re-use as long as the original author and source are properly attributed.

1.9.3.3.1.RNAi and HPV

The complete reliance of Hr-HPV on E6 and E7 expression for malignancy (expression from the same promoter and same mRNA) make them highly attractive targets for RNAi therapeutics. Current therapies against cervical cancer attain a level of efficacy, but as no curative treatment exists, there is a need to improve overall survival rates. These therapies offer highly invasive physical interventions in their treatment of cervical cancer making RNAi, which offers direct antiviral intervention, a more attractive option. RNAi can be employed to specifically target of HPV oncogenes,

hence can be utilised via large-scale genome -wide screens to identify novel anti-viral drug targets, thereby contributing to potential therapies.

Most published works on siRNA-induced RNAi have focused on high risk HPV16 and 18 which account for 70% of all cases of cervical cancer. These studies have shown that siRNAs designed to selectively target either HPV16 E6 and/or E7 can cause extremely specific and highly potent HPV silencing, resulting in reduced cell growth or apoptosis in both cells and pre-clinical animal models (Jiang & Milner, 2005) (Butz, et al., 2003) (Khairuddin, et al., 2012) (Wu, et al., 2011) (Yoshinouchi, et al., 2003).

Although the efficacy of siRNAs like AS-ODNs and Rzs is limited due to its dependence on target site binding, overall its exceptional high activity at low concentrations without apparent toxicity makes it a more advantageous and compelling antisense therapy. In summary, the use of antisense RNAs against E6 and E7 mRNAs has shown Therapeutic Nucleic Acids (TNAs) to be quite useful and somewhat successful in *in-vitro* models, despite the limitation of transient knock-down of target (synthetic siRNAs) where by the re-expression of target mRNA can occur after a few days. Nevertheless, RNAi has opened up a potentially auspicious application of TNAs in cervical carcinogenesis and proposes to be the most effective cervical cancer therapy as its activity can be retained at concentrations of 100 fold lower than AS-ODNS and Rz.

1.10. Chapter summary

High-risk HPVs are the primary etiological factors in the development of cervical cancer. Cervical cancer remains a significant burden on the healthcare systems worldwide and particularly in low to mid income countries. The persistence and irresolution of this infection in a minority of women often results in the integration of the viral genome into hosts, causing abnormal changes to cervical cells that can progress into cervical cancer. The overexpression of E6 and E7 proteins are crucial in mediating HPV-induced carcinogenesis. These proteins work together to attain the

induction and maintenance of cellular transformation owing to their interference with cell-cycle control and apoptosis leading to uncontrolled cell proliferation and cervical cancer development.

Current therapeutics against HPV (such as vaccination), though effective are not curative. RNAi shows great potential in offering highly specific therapies for HPV diseases.

1.11. Hypothesis

The hypothetical basis for this study was that while high-risk HPV E6 and E7 are necessary but not sufficient to drive malignant progression in cervical cancer, these oncogenes provide environmental conditions that promote malignant transformation. Hence, it was hypothesised that

- Selective targeting of E6 in polycistronic E6/E7 mRNA species of an Hr-HPV cervical cell line model (SiHa) will highlight differences in the biological roles of E6 and E7oncogenes.
- Silencing of E6 in this model will result in a decline in replication, possibly via senescence or cell death (based known functions of E6) and therefore give a better insight into the role of E6 in impeding apoptosis in cervical carcinogenesis.
- Targeting of high risk HPV oncogenes (E6/E7) as a molecular therapeutic vaccine approach will potentially provide less invasive and drastic treatment for cervical cancer.

1.12. Project Aims

The premise for this study was that oncogenic proteins E6 and E7 drive malignancy by promoting a neoplastic atmosphere which aids and increases turnover of pro-oncogenic modifications. This study therefore aimed to

- Silence the expression of HPV oncogenes in a cervical cancer cell model using E6 targeting siRNAs and assess the effects of silencing endogenously expressed viral oncogenes via RNAi.
- Examine the downstream effects of silencing events using techniques such as gene expression microarray analyses and Raman spectroscopy.
- Investigate novel pathways implicated in these silencing events and ultimately in the pathogenesis of cervical cancer.

By identifying deregulated genes involved in cervical carcinogenesis and elucidating the effect of subsequent changes to their biochemical compositions, these technologies offer highly promising avenues and novel therapeutics in gene therapy development for HPV mediated cervical cancers.

Chapter Two

Materials and Methods

2. Materials & Methods

This chapter provides a full description of the methodologies employed in this thesis. For some of the more novel techniques some background information is also provided. Several of the techniques are used in a number of chapters. Where this occurs, the full description of the technique is restricted to this chapter, with specifics appearing in the relevant chapters only.

2.1. Preparation and Handling of Reagents

All laboratory reagents and chemicals were of analytical grade, purchased from Sigma-Aldrich Ireland Limited (Wicklow, Ireland) and stored according to the manufacturer's instructions unless otherwise stated. Solid chemicals were weighed using an electronic balance, Model Wa80 (Adam Equipment Co Ltd, UK) and prepared in deionised water (dH_2O). For transfer of liquid volumes up to 1 ml, Gilson pipettes were used (Gilson S.A, France). Volumes greater than 1 ml were measured using a motorised Fisherbrand pipette filler/dispenser (Thermo Fisher Scientific Inc., Ireland) and disposable plastic pipettes (Sarstedt Ltd, Ireland). The pH of all solutions was measured using a R720 pH meter (Reagecon Diagnostics Ltd, Ireland). Cell culture reagents were purchased from Lonza (Brennan & Company, Ireland) and Sigma-Aldrich Ireland Limited (Wicklow, Ireland), unless otherwise stated.

This chapter provides a full description of the methodologies employed in this thesis. For some of the more novel techniques some background information is also provided. Several of the techniques are used in a number of chapters. Where this occurs, the full description of the technique is restricted to this chapter, with specifics appearing in the relevant chapters only

2.2.Cell culture

2.2.1. Cell line

The SiHa cell line established from fragments of a primary tissue sample obtained after surgery from a 55 years old female Japanese patient of Asian descent was used throughout the course of these experiments. This HPV16 positive grade II squamous cell carcinoma was commercially obtained from the American Type Culture Collection (ATCC). It contains 1-2 copies of integrated HPV16 per cell and is p53 and Rb positive (Herrington, et al., 1992). SiHa cells were maintained in Modified Eagle Medium (MEM) supplemented with L-glutamine (2mmol/L), penicillin (200U), streptomycin (200µg), 10% non-essential amino acids (NEAA) and 10% heat-inactivated fetal bovine serum (FBS). All cell culture work was carried out aseptically in a BKF 4-RX laminar flow hood cabinet (Germfree Laboratories Inc., USA) and an Esco Airstream Class II Biological Safety Cabinet (Esco GB Ltd, UK).

.

2.2.2. Resuscitation of frozen cell line stocks

The cell line was quickly thawed from a 1ml $1x10^6$cells stock by gentle agitation in a 37°C water bath and split equally (500µL) into two T-25cm^2 sterile vented culture flasks (Sarstedt Ltd, Ireland) containing 5mls of complete growth media. The following day, media was changed and every 2-3 days thereafter. On attaining 80% confluence, cells were transferred to a T-75cm^2 sterile vented culture flask containing 14mls of complete media and then to a T-175cm^2 sterile vented culture flask containing 50ml of complete growth media. SiHa cells, which grow as attached monolayers (Figure 2-1), were cultured in T-175cm^2 sterile vented culture flasks at 37°C in a humidified 5% CO_2 atmosphere using a Forma Steri-Cycle CO_2 Incubator (Thermo Fisher Scientific Inc., Ireland).

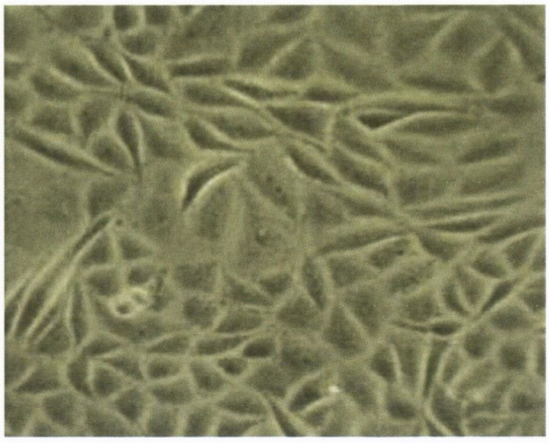

Figure 2-1: Light Microscopy image of SiHa Squamous Cell Carcinoma. (Magnification 200x)

2.2.3. Sub-culturing of SiHa cervical cell line

Cells were examined daily using an inverted phase contrast and Fluorescence Zeiss Axiovert 35 microscope (NY, USA). SiHa cells were passaged at 80% confluency by decanting the complete growth media and washing in 5ml of 0.01 M phosphate-buffered saline (PBS, without Ca and Mg) at 37°C to remove residual FBS. Cells were then detached from the bottom of the flask by using 1ml (T-25cm^2 flask), 2mls (T-75cm^2 flask) or 3mls (T-175cm^2 flask) of trypsin-ethylenediamine tetra acetic acid (0.05mg/ml Trypsin EDTA) (Sigma-Aldrich Ireland Limited, Wicklow, Ireland) and incubating the flask at 37°C for 5mins, until all cells were detached from the flask. Trypsin EDTA was neutralised by the addition of 3mls (T-25cm^2 flask), 5mls (T-75cm^2 flask) or 7mls (T-175cm^2 flask) of complete growth media. Cells were transferred into a sterile 15ml tube and pelleted by centrifugation in an IEC Centra centrifuge (Thermo Fisher Scientific Inc., MA, USA) at 1000rpm for 5mins. Following centrifugation, the supernatant was discarded and the cell pellet resuspended in 1ml complete growth media.

2.2.4. Cell counting

Cells were counted using a bright-line haemocytometer Hausser Scientific, PA, USA (Sigma-Aldrich Ireland Ltd, Ireland) and cover slips (VWR International Ltd, Ireland). Cells were cultured, harvested and resuspended in 1ml complete growth media as described above in section 2.2.2 and 2.2.3. Cell viability was assessed with the trypan blue exclusion assay using a 4 fold dilution factor of cell suspension with 0.4% (v/v) trypan blue (Invitrogen, Life Technologies, Maryland, USA, Gibco/Life Technologies Corporation, Ireland). Cells were added to the counting chamber of the slide and viewed using an inverted phase contrast microscope. Viable cells exclude trypan blue and appear colourless while dead cells are blue due to their disrupted cell membranes. The number of viable cells was counted in each of the four $1mm^2$ square corners of the grid and averaged (Figure 2-2). The total number of viable cells in 1ml was calculated using the equation; average number of cells per $1mm^2$ x dilution factor x conversion factor which corresponds to one $1mm^2$ haemocytometer square containing 10^4ml of solution. For example;

Total number of viable cells in 1ml = Average X 4 X 10^4

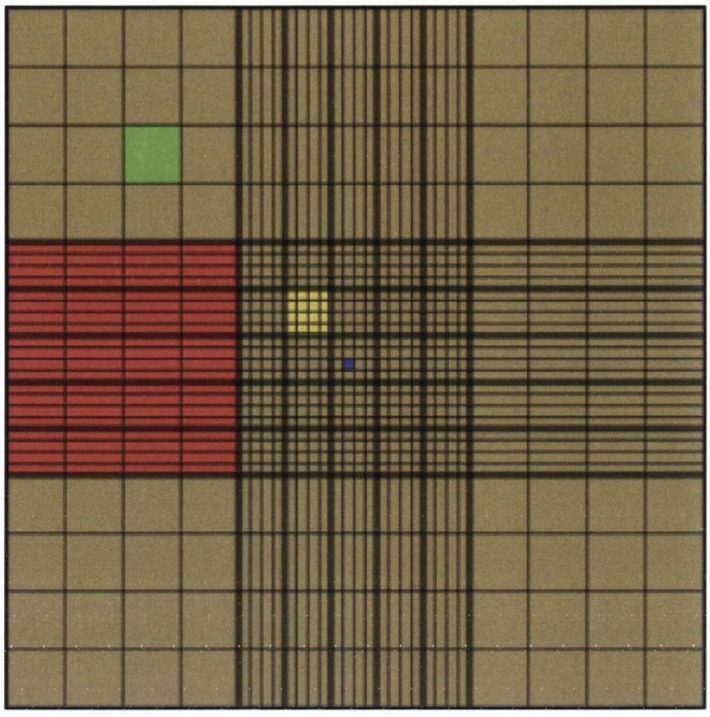

Figure 2-2: Schematic representation of a Haemocytometer. Haemocytometer showing side view and grid identifying different squares used in counting at a depth of 0.1 mm. Red square = 1.0 mm^2, green square = 0.0625 mm^2, yellow square = 0.040 mm^2, blue square = 0.0025 mm^2. (http://en.wikipedia.org/wiki/File:Haemocytometer_Grid.png)

2.2.5. Preparation of cell stocks

Cell stocks were prepared from 80% confluent cultures, harvested using trypsin EDTA and counted as per section 2.2.4. Cells were then aliquoted such that $2x10^6$ cells in 1ml was placed in each cryovial and pelleted at 1000rpm for 5mins. The supernatant was removed and 1ml of Recovery™ Cell Culture Freezing Media (Invitrogen, Life Technologies, Maryland, USA) was added to the cell pellet and mixed gently and stored for 24hrs at –80°C. The vials were then transferred to a liquid nitrogen tank (Thermo Fisher Scientific Inc., Ireland) for long-term storage.

2.3. siRNA transfection

Several techniques can be used to introduce nucleic acids into cells depending on the cell type. They can be categorised into chemically based, such as calcium phosphate, diethylaminoethyl (DEAE)-dextran and cationic lipid-based reagents, or by physical methods such as electroporation, sonoporation, particle based, nucleofection and viral transduction (Groskreutz & Schenborn, 1997) (McCutchan & Pagano, 1968) (Bennett, et al., 1998) (Loyter, et al., 1982) (Patil, et al., 2005).

In this study, a cationic lipid transfection was used to introduce nucleic acids into mammalian cells. It is based on the principle that neutral and cationic lipids with an overall net positive charge, at physiological pH, will form liposomes, which have an overall positive surface charge. This positive-charged head group allows for an interaction with the negatively charged cellular membrane and nucleic acids. That is, liposomes fuse with nucleic acids to form a transfection complex, which can then fuse with the cell membrane via endocytosis despite the negatively charged cell membrane surface (Felgner, et al., 1993) (Felgner, et al., 1994) (Gao & Huang, 1995). On internalisation through the plasma membrane, the membrane bound vesicle releases the nucleic acid, which then proceeds to target complementary sequences in the cytoplasm and nucleus.

Based on current literature, two types of cationic lipid transfection protocols may be used to ingress nucleic acids into mammalian cells that is forward and reverse transfection (Figure 2-3). The main difference between them is that the reverse is carried out as the cells are seeded and the forward after the cells have been seeded for a period of time. The Forward Transfection protocol (FTP) is the most consistently employed transfection protocol for adherent cell types. It involves seeding cells 24hrs before transfection. However, in the Reverse Transfection protocol (RTP), the cells lose a day of doubling their numbers as the freshly passaged cells are seeded and transfected on the same day. This protocol is therefore more suitable for suspension cells and high throughput applications with automated robotic systems and reduced

hands-on time. Similar volumes of the DNA, nucleic acid, cells and transfection reagent per well are required for both FTP and RTP. Both FTP and RTP methods were employed in this study.

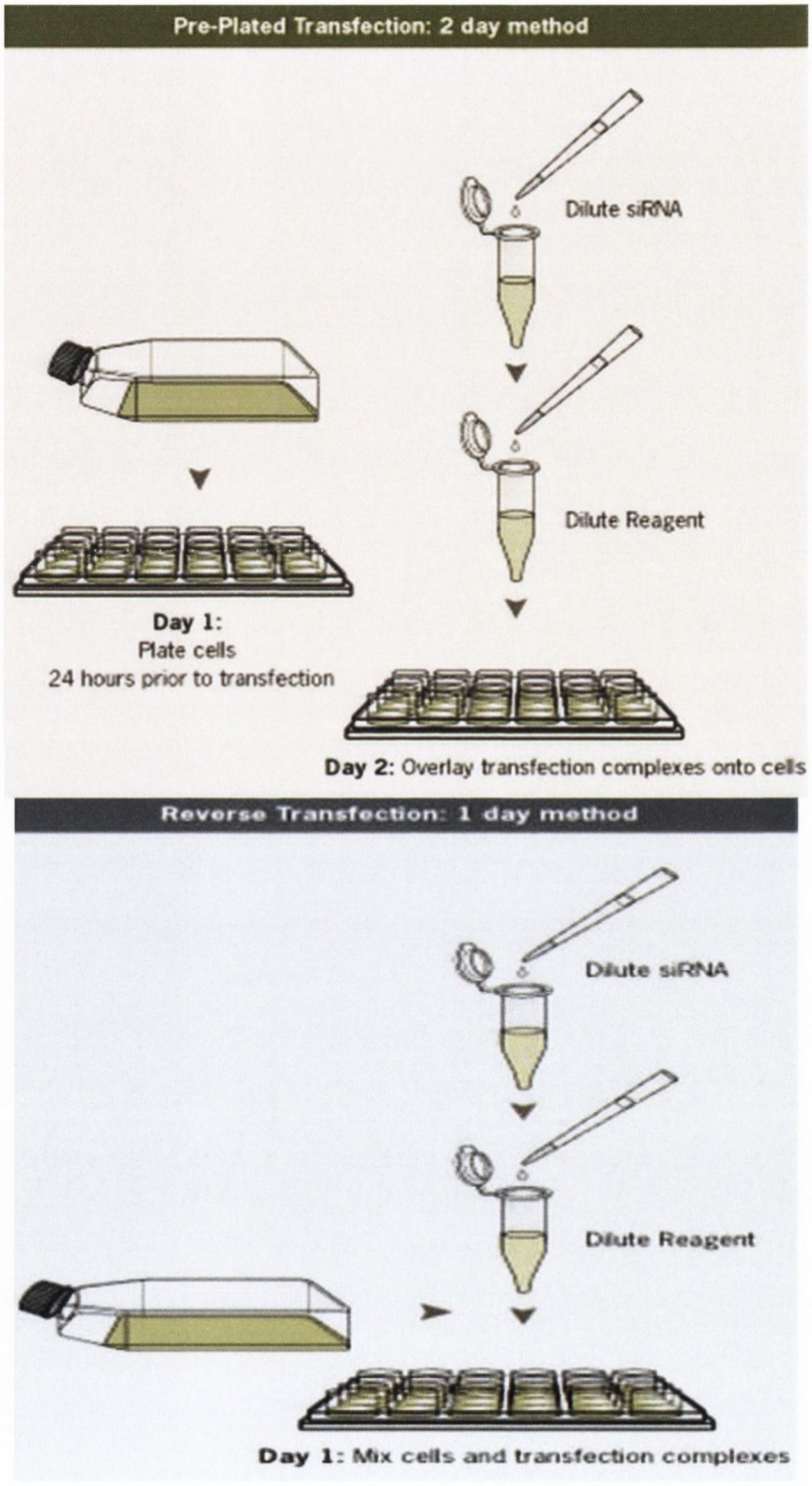

Figure 2-3: Schematic representations of forward and reverse transfection protocols. In the forward transfection (pre-plated Transfection: 2 day method), the cells are seeded on the first day and transfected on day2. In the reverse transfection (1 day method), cells are seeded and transfected on the same day. (www.ambion.com)

2.3.1. Transfection reagent selection

The choice of a suitable transfection reagent for FTP and RTP after selecting the appropriate gene transfer method is a crucial step in successful RNA interference (RNAi). Lipofectamine™ RNAiMAX (Invitrogen, Life Technologies, Maryland, USA) was the transfection reagent of choice, as it had previously been determined within our laboratory to be the most efficient reagent formulation for siRNA/miRNA delivery and gene knockdown in these SiHa cells. RNAi analysis showed this reagent to be suitable for both FTP and RTP in SiHa cells.

2.3.2. siRNA transfection using Lipofectamine™ RNAiMAX in 6well plate format

To determine the most proficient method of siRNA transfection into SiHa cells, both RTP and FTP were carried out. For each well to be transfected in the RTP method, 500µl Opti-MEM® I Reduced Serum Media was added with the appropriate amount of siRNA (final concentration of 10nM per well)) and gently mixed. *This is the standard siRNA concentration for all transfections carried in this laboratory.* Five µl Lipofectamine™ RNAiMAX was then added, mixed gently, and incubated at room temperature for 10-20mins to enable the formation of siRNA-Lipofectamine™ RNAiMAX complexes. Freshly passaged SiHa cells at 70-80% confluency were diluted in complete growth media without antibiotics (CWOA) such that 500µl contained $3x10^4$ cells. A 2.5ml aliquot of this medium containing cells was added to the wells to make a final volume of 3mls in each well. The cells were incubated for 24-72hrs at 37°C in a humidified 5% CO^2 atmosphere until required for experimental analysis.

In the FTP method, SiHa cells diluted in CWOA were seeded at $1.5x10^5$ per well in 6-well plates and incubated for 24hrs at 37°C in a humidified 5% CO_2 atmosphere. The following day, siRNAs (final concentration of 10nM per well) and 5µl Lipofectamine™ RNAiMAX were separately diluted in 250µl Opti-MEM® I Reduced Serum Media, combined, mixed gently and incubated at room temperature for 10-20mins to enable formation of siRNA-Lipofectamine™ RNAiMAX complexes. Fresh media of 2.5mls CWOA was added to the pre-plated cells after washing with PBS. The siRNA-

Lipofectamine™ RNAiMAX complexes in Opti-MEM® I Reduced Serum Media was added to appropriate wells to give a final siRNA concentration of 10nM in 3mls (as with RTP) and incubated for 24-72hrs at 37°C in a humidified 5% CO^2 atmosphere, until required for gene knockdown assay. Medium was not changed in either protocol after the addition of the transfection complexes.

For clarification purposes, the term 72hrs post transfection will imply the seventy-two hours immediately following the transfection of the cells with no regard to time points beforehand. That is, for the forward transfection protocol, this time point will commence on Day2 (24 hours after cells were seeded) of the experiment when transfection is carried out. While, for the reverse transfection protocol, this time point commences on Day1 wherein cells are seeded and transfected on the same day.

2.3.3. Cell harvesting protocol

Following the desired incubation time, media was aspirated from each well and cells washed with 1ml ice-cold PBS twice. To disaggregate the attached monolayer of cells, a 5mins incubation exposure to Trypsin EDTA at 37°C was carried out and complete media added to neutralise Trypsin EDTA. Disaggregates were transferred into sterile RNase/DNase-free eppendorf tubes on ice and pelleted by centrifugation at 1,200 rpm for 5mins. Following centrifugation, the supernatant was discarded and the cell pellet was washed with ice-cold PBS, re-pelleted and stored at-80°C until required for gene knockdown assays.

2.4. RNA isolation

Factors considered in selecting the right RNA preparation and purification technology were sample type, sample size and throughput. Technologies can be classified into magnetic particle methods, direct lysis methods, spin basket formats and organic extraction methods. Organic extraction involves sample homogenisation in a guanidinium thiocyanate phenol-containing solution, which on centrifugation, separates into a lower organic phase, a middle phase containing denatured proteins

and genomic DNA, and an upper aqueous phase that contains RNA. Alcohol precipitation and rehydration is then utilised for RNA recovery and collection. However, the spin basket format technology involves sample lysis in RNase inhibitory buffer, binding of nucleic acids to the membrane (glass fibre or derivitised silica or ion exchange membrane) via centrifugation, washing of the membranes and finally sample elution into a tube by centrifugation.

The isolation of high yields of high quality RNA, free from other nucleic acid and cellular component contamination, is important for molecular biology applications. Extracted RNA was purified intact from cells with the removal and prevention of inhibitory substances such as RNase contamination, which rapidly degrades RNA. RNases are ubiquitous enzymes released on cell lysis and can be difficult to inhibit. Therefore, precautions to ensure optimum RNA yield and RNA quality were taken. Maintenance of good laboratory hygiene and practice of clean microbiology techniques including the use of sterile powder free gloves, RNase-free tips, RNase-free tubes, RNase-free water, automated pipettes dedicated to RNA work (to prevent cross contamination with RNAses from shared equipment), proper storage of isolated RNA in RNase-free solution at -80°C for periods longer than 24hrs, and carrying out of procedures where possible in hoods.

2.4.1. mirVana™ miRNA isolation kit protocol

The mirVana™ miRNA Isolation Kit was selected and used to isolate total RNA (large mRNA and ribosomal RNA) ranging in size from Kilo-bases down to 10-mers from SiHa cell pellets. It is a hybrid method that combines the effectiveness of organic extraction (Guanidinium thiocyanate) with the ease of sample collection and purification on an efficient glass fibre filter (GFF), and washing and elution of the spin basket format. Total RNA was extracted from each SiHa pellet using the Ambion mirVana™ miRNA Isolation protocol (Ambion at Applied Biosystems, Foster City, CA, USA (Ambion)). The total RNA isolation protocol was performed according to the manufacturer's instructions and total RNA was eluted in 100µl of nuclease-free water.

2.4.2. DNase digestion protocol

DNase digestion and purification was performed on all mirVana™ miRNA Isolation Kit extracted RNA using TURBO DNA-free™ Kit (Invitrogen, Life Technologies, Maryland, USA) as per the manufacturer's instructions. This removed post digestion enzymes, divalent cations and further ensured efficient and complete DNA digestion. This protocol involved the use of incubating the RNA with 1X TURBO DNase buffer and 4 Units of TURBO DNase enzyme (more efficient recombinant engineered form of DNase I) at 37°C for 30mins. To inactivate the TURBO™ DNase Reaction and remove divalent cations, re-suspended DNase Inactivation Reagent was added to RNA samples at room temperature and mixed occasionally for 5mins. The samples were then centrifuged to pellet the DNase Inactivation Reagent. Purified RNA supernatants were transferred to fresh tubes and stored at -80°C until required.

2.5. Nucleic acid quantitation and quantification

Spectrophotometric quantification is the most widely used method to quantitate RNA in a sample. It operates on the principle that nucleic acids absorb ultraviolet light in a specific pattern and detection of such patterns can be quantified that is the more light absorbed by the sample, the higher the nucleic acid concentration in the sample

2.5.1. NanoDrop™ ND-2000

The Nucleic acid concentration and quality was determined using the NanoDrop™ ND-2000 spectrophotometer (Thermo Fisher Scientific Inc., Waltham, MA, USA). The NanoDrop™ ND-2000 Spectrophotometer is a full spectrum (190nm-840nm) spectrophotometer that measures 0.5-2ul nucleic acid samples with high accuracy and reproducibility. It uses a sample retention technology that employs surface tension alone to hold the sample in place. The ND-2000 can also measure highly concentrated samples (50X higher concentration than standard cuvette spectrophotometer) without dilution.

The ND-2000 consists of two measurement pedestals (upper and lower). It operates by the user pipetting the liquid sample onto the end of a receiving optic fibre cable (lower measurement pedestal) and bringing the source optic fibre cable in contact with the sample by closing the sampling arm. This causes the liquid sample to bridge the gap (1mm and 0.2 mm paths) between the fibre optic ends and automatically draw the sample column between the upper and lower measurement pedestals). The spectral measurement is initiated using the operating software on the computer and the data is logged in an archive file on the computer.

Nanodrop results were interpreted using 1) the A260/280 ratio of sample absorbance at 260 and 280nm. The ratio of absorbance at 260 and 280nm provides an estimate of the purity of RNA with respect to contaminants that absorb in the UV spectrum. A ratio of approximately 2.0 is generally accepted as "pure" for RNA. If the ratio is appreciably lower in either case, it may indicate the presence of protein, phenol or other contaminants that absorb strongly at or near 280nm. The A260/280 ratio is considerably influenced by pH; lower pH results in a lower ratio and reduced sensitivity to protein contamination. 2) A260/230: Ratio of sample absorbance at 260 and 230nm. This is a secondary measure of nucleic acid purity, being usually higher than the respective 260/280 values for "pure" nucleic acids. It is usually in a range of 1.8-2.2; if lower, it may indicate co-purified contamination. 3) Concentration (ng/µl): Sample concentration in ng/µl based on absorbance at 260nm minus the absorbance at 340nm (that is normalised at 340nm) and the selected analysis constant.

2.5.2. Agilent 2100 bioanalyser

The Agilent 2100 Bioanalyser (Santa Clara, CA, USA) is a chip-based microfluidics electrophoresis system used for sizing, quantitation and quality control of DNA, RNA, proteins and cells on a single platform. It is an efficient automated instrument that provides powerful data evaluation tools such as RNA Integrity Number (RIN) for unbiased total RNA quality control. Samples and a ladder (RNA reference standard) are loaded into designated wells on the RNA Lab Chip and placed into the Bioanalyser

where each sample is individually analysed and a gel-like image and an electropherogram generated by the software. The software automatically compares the peak areas from the unknown RNA samples to the combined area of the RNA Ladder RNA peaks to determine the concentration of unknown samples, Figure 2-4. The ratio of two major ribosomal RNA species (18S and 28S ribosomal RNA peaks) for each sample is also calculated and used as an indication of the degree of RNA degradation. The RNA Nano 6000 kit (Aglient, Santa Clara, CA, USA) was used, according to manufacturer's instructions, to assess RNA integrity of all samples prior to microarray analysis. This was achieved via visual evaluation of gel images and RIN values using the 2100 Bioanalyser Expert software.

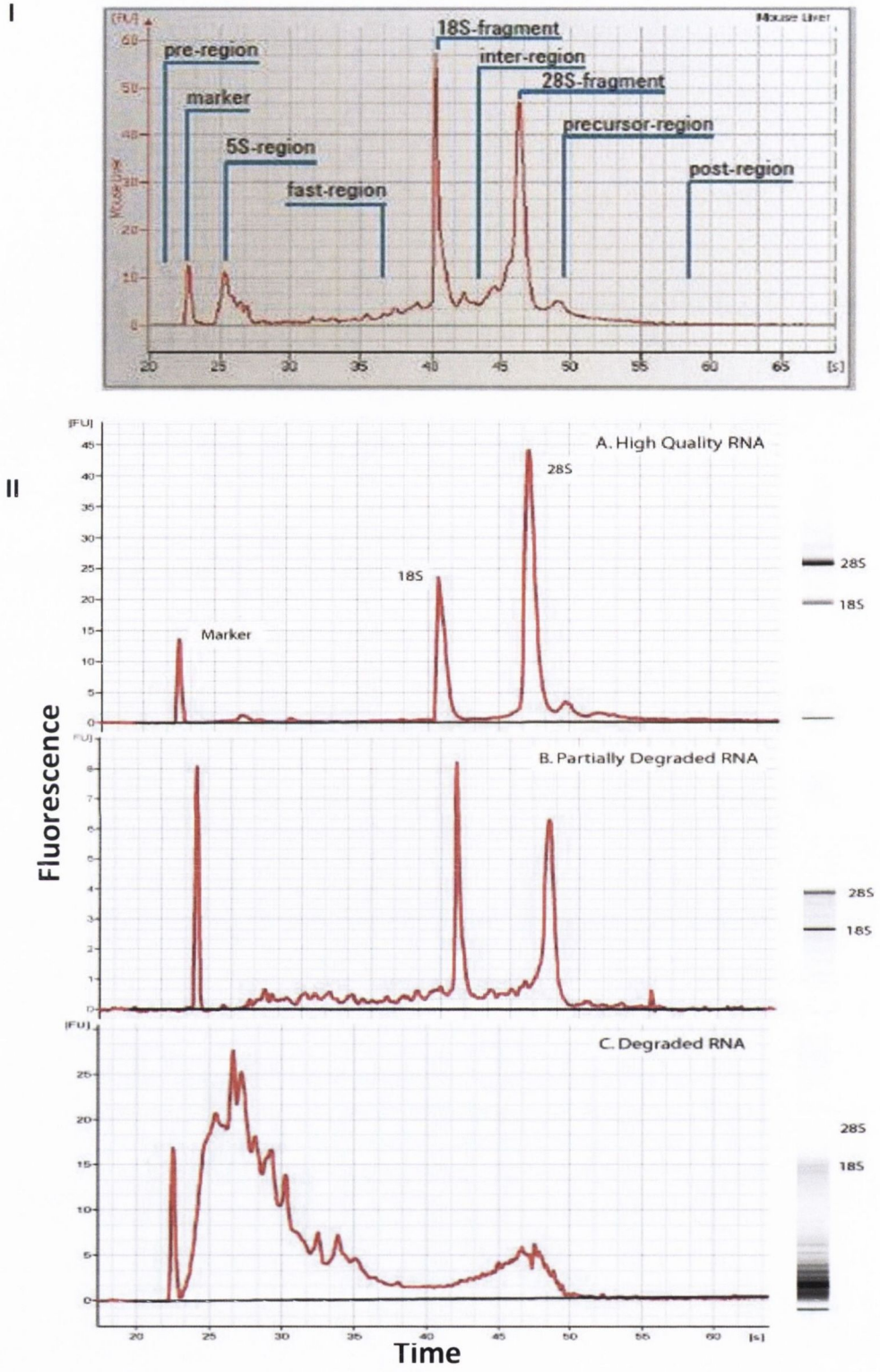

Figure 2-4: Schematic representations of RNA profile integrity. I) Electropherogram showing regions of RNA quality. II) Example of Agilent Bioanalyser electropherograms and gel-like images of varying RNA integrity. Panel [A] represents a highly intact RNA, panel [B] represents a moderately intact RNA and panel [C] represents a degraded RNA. RNAs of better quality have higher RNA Integrity Number (RIN).(http://genomics.nchresearch.org/submitting_RNA.html)
(http://cgs.hku.hk/portal/index.php/bioanalyser-analysis/data-collection)

2.6. TaqMan® RT-PCR

PCR is one of the most powerful technologies in molecular biology and involves the copying or amplification of specific sequences within a DNA or cDNA template to 10^3 or 10^6 folds. Real time PCR, of which Taqman® RT-PCR is an example of, in particular has become the foremost tool for DNA and RNA quantification and detection. In real time or quantitative PCR (qPCR), the amount of PCR product is measured after each cycle. Hence, it is possible to view the exponential doubling of the initial amount of target and correctly estimate the quantity of genetic material initially present, Figure 2-5.

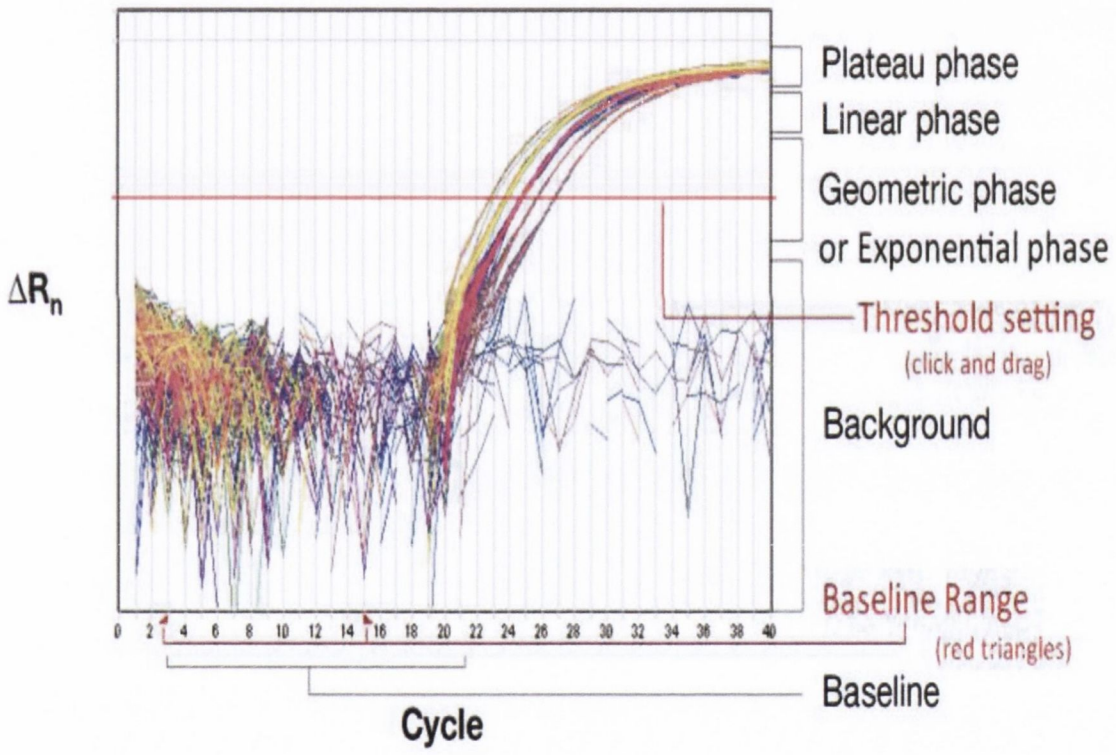

Figure 2-5: Schematic representations of end point vs real time PCR. (www.lifetechnologies/appliedbiosystems.com)

The PCR reaction exploits the 5′ nuclease activity of AmpliTaq Gold® DNA Polymerase to cleave a TaqMan® probe during PCR. The TaqMan® probe contains a reporter dye at the 5′ end of the probe and a quencher dye at the 3′ end of the probe. During the reaction, cleavage of the probe separates the reporter dye and the quencher dye,

which results in increased fluorescence of the reporter. Accumulation of PCR products is detected directly by monitoring the increase in fluorescence of the reporter dye.

The ABI Prism 7900 Sequence Detection System was used for fluorescence detection in qPCR (Applied Technologies, USA). qPCR reactions were run for 40 cycles, as per general standard, and were made up of 3 major steps; denaturation, annealing and extension. The denaturation temperature was determined by the DNA polymerase of choice, with time intervals increased to accommodate high GC content. Recommended annealing temperatures of 5-10°C below melting temperature (T_m) of selected primers were implemented and the extension step was carried out at temperatures for optimal DNA polymerase activity of 70-72°C (additional 60°C annealing step for small amplicons was also incorporated).

Gene expression was determined by two-step RT-PCR. TaqMan® Two-Step RT-PCR is a very specific and sensitive quantitative method designed for the reverse transcription (RT) and polymerase chain reaction (PCR) amplification of a specific target RNA from either total RNA, mRNA or poly $(A)^+$ RNA into cDNA. It is a highly proficient and convenient system that uses small inputs of RNA to execute RT, as well as PCR, in two distinct reaction-mixes, which enables the intermediate product cDNA to be archived or stored. Two-Step RT-PCR is thus versatile and cDNA synthesis can be primed using sequence specific primers, random hexamers/primers or oligod$(T)_{16}$. Template RNA, from which cDNA used for RT-PCR, that was isolated was devoid of RNase and genomic DNA contamination under aseptic conditions.

2.6.1. TaqMan® RT-PCR protocol

Step 1: cDNA synthesis

250ng of RNA was used a template in the first step of the PCR reaction. The cDNA reaction was performed using the Ambion High Capacity cDNA Archive kit (Invitrogen, Life Technologies, Maryland, USA) as per manufacturers protocol. The RT reaction was

carried out on the 9600 Thermal Cycler (ABI) at 25°C for 10mins, 37°C for 120mins, 85°C for 5mins to deactivate the enzyme, and cooling to 4°C. The generated cDNA was then stored at -80°C until required.

Step 2: PCR

Real time quantitative PCR was performed using optimally designed primer and probes sets and TaqMan® Universal PCR Master Mix following cDNA generation. Primer and probes sets used were either pre-formulated TaqMan gene expression assays or custom-designed TaqMan gene expression assays. For applications that involved viral detection, splice junction variants, detection of specific pathogens and species not available in the TaqMan® Gene Expression Assays, custom-designed assays were ordered. A cDNA scrambled control siRNA and no template control (NTC) were prepared for each primer and probe set.

Primer Design

Gene-specific primers were designed using a suitable primer design software program, considering general PCR primer design parameters of 18-24 nucleotides in length, compatible T_m, 50% GC content, GC rich 3' ends, devoid of polybase (poly(dG)) sequences or repeating motifs and no complementarity between primers. HPV16 full length E6, full length E6 and E6*I and E7 specific TaqMan® primers and probes were designed using Primer Express Software Version 3.0 and synthesised by Applied Biosystems (Applied Biosystems, Foster City, CA USA). Guidelines employed in primer design include; T_m of 58-60°C, 20–80% guanine and cytosine (GC) content, circumvention of identical nucleotide runs and 3' ends of ≤2GCs in the last five nucleotides. Probe guidelines were similar with exceptions of length of > 13 nucleotides, T_m of 68-70°C, 30-80% GC content and no Gs at the 5' end. NCBI program BLASTN (http://www.ncbi.nlm.nih.gov/blast/) was used to check specificity of the selected sequences.

PCR reactions were performed as 20 µl reactions in triplicates on the 7900HT (ABI) under the following thermal cycling conditions: 50°C for 1min (UNG activation), 95°C for 10mins (AmpliTaq Gold® activation) and 40 cycles of 95°C for 15secs and 1min at

60°C (melting and annealing/extension). An endogenous control was used to normalise differences in the amount of cDNA that is loaded into PCR reaction wells. FAM labelled Glyceraldehyde-3-phosphate dehydrogenase (GAPDH) positive control TaqMan® primers and probe and FAM labelled β-2- microglobulin (B2M) endogenous control TaqMan® primers and probe were included as endogenous controls. These controls were assayed separately from TaqMan® PCR reactions of the target gene and also in triplicates of 20 µl reactions using the same thermal cycling conditions on the 7900HT.

All cDNA and PCR reactions were prepared in a class II laminar flow hood. Maintenance of good laboratory hygiene and practice of clean microbiology techniques were used throughout for example using sterile powder free gloves, aerosol resistant RNase-free tips, RNase-free tubes and water and dedicated automated pipettes to RNA work to prevent cross contamination with RNAses from shared equipment.

2.6.2. TaqMan® RT-PCR analysis

2.6.2.1. Terminologies

Baseline is the background or "noise" of the reaction and refers to the signal level during the initial cycles of PCR wherein there is little change in fluorescence signal. It is manually or automatically determined for each reaction and often falls between cycles 3-15.

Threshold is the statistically significant level of increase in signal used to distinguish the amplification signal from the background over the calculated baseline. It is automatically set at 10 times the standard deviation of the fluorescence value of the baseline but can be manually set at any point in the exponential phase.

Threshold cycle (C_t) is the cycle number at which the reaction crosses the threshold. It is inversely proportional to the amount of starting genetic material hence can be used to determine initial cDNA copy number.

Standard curve is the graph of the log of each known concentration in the dilution series plotted against the C_t for that concentration. It is used to determine the starting

amount of the target template. Reaction parameters of slope, intercept and correlation coefficient can be obtained for absolute quantification.

Absolute quantification is a qPCR experiment in which samples of known concentrations are serially diluted and amplified to generate a standard curve from which an unknown sample can be quantified.

Relative quantification is a qPCR experiment in which the target of interest in one sample (treated) is compared against the same target of interest in another sample (untreated). Results are expressed as fold changes in the treated in relation to the untreated. House-keeping or endogenous gene (normaliser gene) is used as a control for experimental variability.

Reference gene is an internal control/house-keeping/endogenous gene for the normalisation of expression levels between experiments. It is expressed at the same level as the gene of interest and remains relatively constant at all points of the experiment. Examples include 18S ribosomal RNA subunit, Glyceraldehyde 3-phosphate dehydrogenase glycolysis enzyme, β-actin cytoskeletal gene.

2.6.2.2. Relative quantification

In this study, the Comparative CT Method (ΔΔCT) of relative quantification was employed for Taqman® RT-PCR. The data output is expressed as a fold-change of expression levels in a calibrator (normal sample) and one or more test samples. ΔΔCT uses arithmetic formulas to achieve the result for relative quantitation provided PCR efficiencies between the selected target and endogenous control(s) are relatively equivalent. It calculates the relative gene expression using the following equation:

$$\text{Relative Quantity OR Fold Difference} = 2^{-\Delta\Delta CT}$$

$$\Delta C_{t\ \text{sample}} - \Delta C_{t\ \text{calibrator}} = \Delta\Delta C_t \text{ ie}$$

$$C_{t\ (\text{gene of interest in sample})} - C_{t\ (\text{normaliser gene in sample})} = \Delta C_{t\ \text{sample}}$$

$$C_{t\ (\text{gene of interest in calibrator})} - C_{t\ (\text{normaliser gene in calibrator})} = \Delta C_{t\ \text{sample}}$$

ΔΔCT is calculated by adjusting the Cts for the gene of interest in both the calibrator (untreated) and test sample in relation to the Ct of a normaliser gene from the same two samples. The resultant ΔΔCT is expressed as fold difference or change in expression. The constraint of this method is that the efficiencies for both the target and normaliser genes are identical. Relative quantification was calculated using the analytical software (Applied Biosystems RQ Manager V1.2). Gene expressions of untreated cells were used as the calibrator sample in all calculations. To ensure the validity of this calculation, TaqMan®Gene Expression Assays guidelines recommend running at least three replicates for each sample, input of cDNA that span the expression levels of target genes, 900nM primer concentration, 250nM probe concentration and running of target and endogenous control reactions in separate wells.

2.7. Affymetrix microarray analysis.

Affymetrix microarray technology is a powerful tool used to investigate genome wide expression profiles. It provides exceptional and favourable circumstances to study interactions between pathways and genes, thereby enabling the identification of novel genes and the classification of regulatory pathways involved in disease pathogenesis. This study employed the use of Affymetrix Gene Chip® Gene 1.0 ST array system which is intended to quantify gene expression of well-annotated genes, using a single probe set per gene consisting of numerous probes that are distributed along the complete length of the genomic locus. Classical microarray design assumes that the 3'end of each gene is clearly distinct, each transcript has an intact poly-A tail and that the entire

length of the gene is expressed as a single unit (no alternative splicing). GeneChip Gene 1.0 ST Array however, offers whole–transcriptome coverage and its design is based on the most recent genomic content thereby offering the highest probe coverage (up to 26 probes across the full length of the gene). This enables accurate detection for whole-transcriptome microarray analysis and delivers higher resolution and accuracy than other classical 3'-biased microarray solutions. This approach therefore facilitates detection of multiple transcript isoforms, plus those that might be missed using a 3'-biased expression design, such as splice variants, non-polyadenylated transcripts, transcripts with alternative polyadenylation sites, and truncated transcripts. Hence, the whole-transcript coverage of this array provides the most accurate, sensitive, and comprehensive measurement of protein coding and long intergenic non-coding RNA transcripts.

2.7.1. Affymetrix GeneChip® Gene 1.0 ST array technology

These Affymetrix oligonucleotide arrays were synthesised using a process combining photolithography and combinatorial chemistry. The arrays are composed of a naturally hydroxylated quartz wafer. Photolithographic masks sets were contrived to allow the successive addition of specific nucleotides to particular locations on the chip. On exposing these masks to ultraviolet light, unprotected linkers become deprotected and accessible for nucleotide coupling. This occurs during the first step of synthesis. The single type nucleotide solution is then used to wash the wafer surface to enable attachment to the activated linkers. The following step involves the placement of another mask over the wafer for the next round of deprotection and coupling and this process is repeated until the probes reach their full length. The GeneChip® Human Gene 1.0 ST Array interrogates 28,869 well-annotated genes with 764,885 distinct probes. Each gene is denoted using a series of different 25-mer perfect match (PM) oligonucleotides. The probe sets are designed to be spread across the transcribed regions of each gene. The Gene 1.0 ST Array System uses a PM-only design with probes that hybridise to sense targets. Background is estimated using a set of ~17,000 generic background probes (BGP). This is a pool of probes that were designed based on the fact that they are not present in the human genome hence are not expected to cross-

hybridise to transcribed human sequences. Background is calculated by subtracting the mean BGP intensity of the BGP probes with the same GC content as the PM probe. For each of the possible 26 bins of varying GC count (from zero G/Cs out of a 25-mer sequence, to all 25 bases being G/Cs), there are approximately 1,000 25-mer probes representing each bin. Standard poly-A controls and hybridisation controls are also represented on the arrays to allow appropriate troubleshooting along the entire experimental process.

The Affymetrix WT assay was employed for sample preparation. It involves synthesis of double stranded cDNA (ds-cDNA) from mRNA by reverse transcription with random oligo d(T) primers manufactured to contain a T7 RNA promoter site. The ds-cDNA is then used as a template by T7 RNA polymerase to generate numerous copies of antisense cRNA. The second cycle of cDNA synthesis, involves the use of random primers in reverse transcription of generated cRNA to ssDNA in the sense orientation and dUTP is incorporated into the DNA. This ssDNA sample is then treated with a combination of uracil DNA glycosylase (UDG) and apurinic/apyrimidinic endonuclease 1 (APE 1) to specifically identify and cleave DNA strands with unnatural dUTP residues. Subsequently, DNA is terminally labelled with the Affymetrix® proprietary DNA Labelling Reagent (covalently linked to biotin) by deoxynucleotidyl transferase (TdT) and the fragmented labelled DNA sample is hybridised onto the GeneChip® Gene 1.0 ST array. The entire process is described in Figure 2-6.

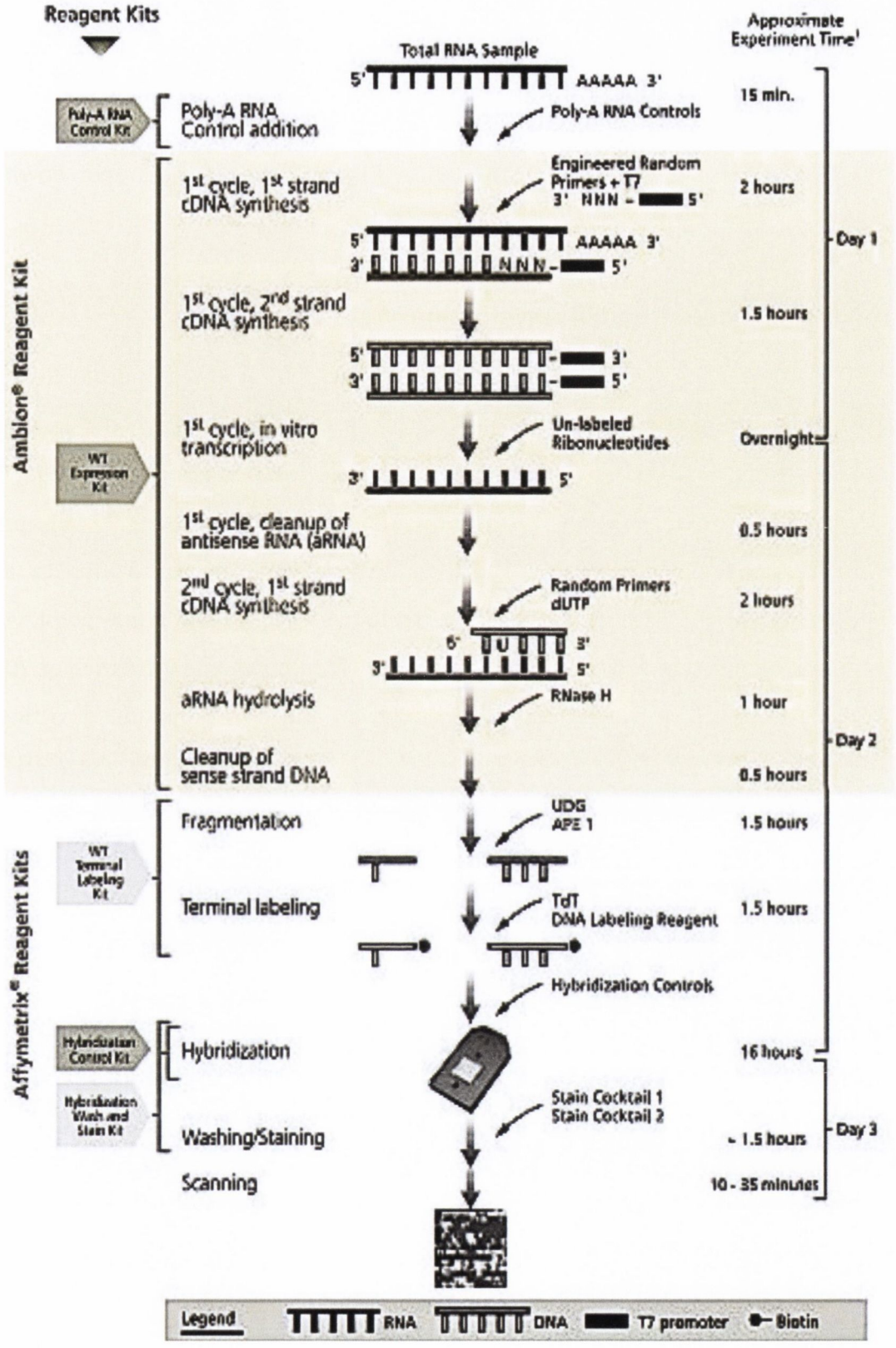

Figure 2-6: Schematic representation of Gene Expression analysis using Affymetrix microarrays. The above shows the synthesis of ds-cDNA from total extracted RNA from which antisense cRNA is generated. Subsequently, cRNA to ssDNA in the sense orientation and dUTP is incorporated into the DNA. This ssDNA sample is then fragmented, terminally labelled and hybridised onto the GeneChip® Gene 1.0 ST array. (www.affymetrix.com/index.affx)

2.7.2. Affymetrix GeneChip® analysis protocol

All thermal cycle reactions were performed on a 9600 Thermal Cycler (Applied Biosystems, Foster City, CA, USA) with a heated lid unless stated otherwise. Prior to the start of any thermal cycle reactions, samples were flick-mixed and spun down.

2.7.2.1. Double stranded cDNA synthesis

Double stranded cDNA was prepared from 150ng of total RNA using the GeneChip® WT cDNA synthesis kit (Affymetrix, Santa Clara, CA, USA). Initially, the Poly-A RNA controls were prepared as per the 1µg protocol in the GeneChip® WT Sense Target Labelling Assay Manual (Affymetrix, Santa Clara, CA, USA). Then, the T7-$(N)_6$ primers were prepared by dilution in the diluted Poly-A RNA controls solution to a final concentration of 2.5µg/µl as stated in protocol. The T7-$(N)_6$ primers/Poly-A RNA controls mix solution and total RNA were mixed, spun-down and incubated at 70°C for 5mins and cooled on ice for 2mins. The following reagents were added to the total RNA/ T7-$(N)_6$ primers/Poly-A RNA controls mix, 1X 1st strand buffer, 0.1M DTT, and 10mM dNTP mix, RNase inhibitor and SuperScript™ II reverse transcriptase for first strand cDNA synthesis reactions. This reaction was carried out under thermal cycling conditions of 25°C for 10mins, 42°C for 1hr, 70°C for 10mins and 4°C for 2mins.

For second strand cDNA synthesis reactions, the following reagents were added to the first stand synthesis reactions, RNase-free water, 17.5mM MgCl2, 10mM dNTP mix, DNA polymerase I and RNase H. The reaction was carried out under thermal cycling conditions: 16°C for 2hrs without a heated lid and then for at 75°C for 10mins and 4°C for 2mins with a heated lid.

2.7.2.2. cRNA synthesis and purification

The GeneChip® WT cDNA amplification kit (Affymetrix, Santa Clara, CA, USA) was employed for these reactions. For cRNA synthesis reactions, the following reagents were added to ds- cDNA synthesis reactions, 1X in vitro transcription (IVT) buffer, IVT NTP mix and IVT enzyme mix. The cRNA reaction then carried out under thermal cycling conditions of 37°C for 16hrs and cooling to 4°C. The purification step required the use of the GeneChip® sample clean up module (Affymetrix, Santa Clara, CA, USA).The protocol was performed as outlined in the GeneChip® WT Sense Target Labelling Assay Manual. The cRNA was eluted in RNase-free water and the final volume was approximately 13.5µl. The cRNA yield was determined on the NanoDrop ND-1000 spectrophotometer (section 2.5.1), using the RNA settings.

2.7.2.3. Single stranded DNA synthesis and purification

ss-cDNA was synthesised from cRNA using the GeneChip® WT cDNA synthesis kit (Affymetrix, Santa Clara, CA, USA). A cRNA/random primer mix was prepared; 10µg of cRNA was added to random primers (3µg/µl) and RNase-free water, final volume 8µl. The ssDNA reaction was the carried out under thermal cycling conditions of 70°C for 5mins, 25°C for 5mins and 4°C for 2mins. The purification procedure required the use of the GeneChip® sample clean up module (Affymetrix, Santa Clara, CA, USA). The protocol was carried out as outlined in the GeneChip® WT Sense Target Labelling Assay Manual. The ssDNA was eluted in RNase-free water and the final volume was approximately 28µl. The ssDNA yield was determined on the NanoDrop ND-1000 spectrophotometer (section 2.5.1), using the ssDNA setting.

2.7.2.4. Fragmentation and Labelling of Single stranded DNA

DNA fragmentation and labelling was performed using the GeneChip® WT Terminal Labelling Kit. For the DNA fragmentation reaction, single stranded DNA (5.5µg) was added to 16.8µL of fragmentation master mix (1X cDNA fragmentation buffer, 10U/µl UDG, 1000U/µl APE 1 and RNase-free water). The fragmentation reaction was then

carried out under thermal cycling conditions of 37°C for 1hr, 93°C for 2mins and 4°C for 2mins. The labelling reaction required addition of 15µL of fragmentation master mix (1X TdT buffer, TdT and 1mM DNA labelling reagent) to 45µl of fragmented single stranded DNA. The labelling reaction was carried out under thermal cycling conditions of 37°C for 1hr, 70°C for 10mins and 4°C for 2mins.

2.7.2.5. Hybridisation to GeneChip® Gene 1.0 ST arrays

Fragmented ssDNA (27µl) was added to 73µl of hybridisation cocktail (1X hybridisation mix, 1 X Eukaryotic hybridisation controls, 3nM control oligonucleotides, DMSO). The cocktail was heated to 99°C for 5mins, 45°C for 5mins and hybridised to GeneChip® Gene 1.0 ST arrays. 80µl of each specific sample was injected into the array cartridges and hybridisation was performed at 45°C for 18hrs in a GeneChip® Hybridisation Oven 640 (Affymetrix, Santa Clara, CA, USA).

2.7.2.6. GeneChip® washing, staining and scanning

Subsequent to hybridisation, each chip was washed and stained with streptavidin phycoerythrin, followed by a second cycle of washes and signal amplification using biotin labelled anti streptavidin phycoerythrin antibodies. The arrays were then re-stained with streptavidin phycoerythrin and a concluding cycle of washes carried out. The entire procedure was carried out using the GeneChip® Fluidics station 450 (Affymetrix, Santa Clara, CA, USA). Fluorescent signals were measured on the arrays using the GeneChip® Scanner 3000 7G (Affymetrix, Santa Clara, CA, USA). Images were analysed using the Expression Console™ software (Affymetrix, Santa Clara, CA, USA).

2.8. Senescence β-Galactosidase Staining

Cellular senescence is often associated with aging and age–related diseases like skin aging, osteoarthritis and cancer. It is characterised by decreased cell division, changes in cellular morphology, shape and physical appearance as well as changes in patterns of gene expression. Most dividing cells (with some exceptions) have limiting replicative capacity known as the Hayflick limit. Most cells on approaching this limit or on being challenged by oncogenic stimuli, move from actively dividing to a non-dividing (no DNA synthesis) yet metabolically active state. Common characteristics of senescent cells include increased number of polyploid cells, telomeric shortening, decreased expression of heat shock proteins, increased expression of pro-inflammatory proteins and metalloproteinases (Harley, et al., 1990) (Bonelli, et al., 1999) (de Magalhaes, et al., 2004)

The most defining characteristic of cellular senescence is β-Galactosidase (β-gal) activity. β -gal is a lysosomal hydrolase enzyme with an optimal activity at pH 4 in proliferating cells. In senescent cells, cellular changes such as an increase in size and an increase in accumulation of this enzyme results in an increase in lysosomal activity which can be detected at a pH of 6. Therefore, senescence-associated β-galactosidase (SA β-gal) activity is a commonly used biomarker for senescence. β-gal staining is used to test for β-gal enzyme activity at pH 6, a characteristic not found in pre-senescent, quiescent or immortal cells, using the artificial substrate 5-bromo-4-chloro-3-indolyl-β-D-galactopyranoside (X-gal) (Dimri, et al., 1995) (Itahana, et al., 2007). X-gal is cleaved by β-gal at pH 6.0 leading to a blue staining of cells.

2.8.1. Senescence Staining Protocol

A Senescence Cell Histochemical Staining Kit (Sigma-Aldrich Ireland Limited, Ireland) was used to detect any β-galactosidase associated senescence activity (SA-β-gal) in SiHa cells 72hrs post transfection as per the manufacturer's instructions. All kit components were thawed and thoroughly mixed. X-gal Solution was warmed at 37°C

for 1hr to avoid formation of aggregates that could interfere with the visualisation of the stained cells. All solutions were filter sterilised before use. SiHa cells at 72hrs post transfection had their growth media aspirated and all wells carefully washed twice with 1X PBS. Cells were then incubated in 1X Fixation Buffer for 7mins at room temperature and rinsed three times in 1X PBS. 1ml of staining mixture (1X Staining Solution, 125 ml of Reagent B, 125 ml of Reagent C and 0.25 ml of X-gal Solution in ultrapure water) was freshly prepared, added to all wells and incubated at 37°C without CO_2 overnight. As a precaution, plates were sealed with parafilm to avoid drying out and exclude CO_2 as senescent cells staining is pH dependent. The next day, blue-stained positive cells were counted by light microscopy at 200X magnification in four random fields. An average of 200 cells per sample was counted to determine the percent senescence. For long-term storage of the stained plate, staining mixture was aspirated; cells overlaid with a 70% glycerol solution and stored at 4°C.

2.9. Western Blot Analysis

Western blotting is a routinely used investigative technique for protein analysis that was devised by Tobin et al. (Towbin, et al., 1979). This technique employs the specificity of antibody-antigen interaction to detect and identify a target protein in the midst of a complex protein mixture. Blotting involves the detection of proteins on the surface of a membrane subsequent to electrophoretic transfer from a polyacrylamide gel. This method can produce qualitative and semi-quantitative data for the protein of interest.

2.9.1. Protein extraction

Cells were seeded and transfected (section 2.3.2) and following the desired experimental incubation time, media was aspirated from each well and the adherent cells were immediately placed on ice. The cells were washed with 1ml ice-cold PBS twice and disaggregated by a 5mins incubation exposure to Trypsin EDTA at 37°C. The

reaction was neutralised with complete media and contents transferred to sterile pre-chilled eppendorfs. Cells were pelleted by centrifugation at 1,200 rpm at 4°C for 5mins and the supernatant discarded. Cell pellets were washed with ice-cold PBS and centrifuged. Two methods of protein extraction were carried out to achieve ample protein concentration for electrophoretic separation.

2.9.1.1. Protein extraction using RIPA buffer

In this method, cell pellets were resuspended in 30µl ice cold radioimmunoprecipitation lysis buffer (RIPA buffer) ; 50mM Tris-HCl, 150mM NaCl, 1mM EDTA, 1.0% Nonidet P-40, 0.25% w/v deoxycholic acid, 1ul protease inhibitor cocktail (Sigma-Aldrich Ireland Limited, Ireland), 1µl of phosphatase inhibitor cocktail (Sigma-Aldrich Ireland Limited, Ireland), 2mM phenylmethanesulponylfluoride (PMSF), 1ml of 10X RIPA buffer (Upstate, CA, USA) and made up to 10ml with dH_2O. The samples were then incubated on ice with moderate vortexing every 10mins to disrupt cellular and nuclear membranes and spun at 10,000 rpm at 4°C for 15mins to collect debris. The supernatants were transferred to fresh pre-chilled eppendorfs and stored at -20°C until required for protein quantification.

2.9.1.2. Protein extraction using Sonication

Cell pellets were lysed via Soniprep 150 Sonicator in RIPA buffer solution (Santa Cruz Biotechnology, Inc. Heidelberg, Germany). RIPA buffer was made up directly prior to use as per the manufacturer's instructions. In brief, 10µl phenylmethanesulponylfluoride (PMSF) solution, 10µl sodium orthovanadate solution and 15µl protease inhibitor cocktail solution per ml of 1X RIPA buffer per $2.0x10^7$ cells in suspension. Sonication was carried out with samples on ice at 5microns (µm) amplitude for 10secs intervals for a total sonication time of 30secs, using general lab standard operating procedure (SOP). General precautions of ear protection, cleaning probe between samples and avoiding foam generation or scattering of droplets out of

the vessel were taken. As small sample volumes of less than 1ml were processed, samples were held in eppendorf tubes and treated with the exponential microprobe.

2.9.2. Protein quantification

Protein concentrations of cell extracts and BSA standards were determined using the Bicinchoninic Acid (BCA™) Protein Assay reagent Kit (Thermo Fisher Scientific, Rockford, IL, USA). The Thermo Scientific Pierce BCA Protein Assay Kit is a two component detergent-compatible preparation based on a modified biuret reaction to measure total protein concentration compared to a protein standard. In this reaction, peptide bonds are detected in the presence of a copper (II) ion ($Cu2^{+}$) that is $Cu2^{+}$ is reduced to Cu^{+} by proteins in an alkaline medium. BCA reacts with Cu^{+} and forms violet-coloured coordination complexes. This modified assay is highly sensitive and absorbs much more strongly than the classical peptide/copper complex. This allows total protein quantitation (0.0005 to 2 mg/mL) using the colorimetric detection of the copper cation Cu^{+} chelated to bicinchoninic acid. The water soluble BCA/copper complex exhibits a strong linear absorbance at 562 nm, producing the signature violet colour directly proportional to the protein concentrations analysed.

2.9.2.1. BCA™ assay protocol

Bovine Albumin Standard (BSA) standards of (0-1000ug/ml) were made as per the manufacturer's instructions. A 1:5 dilution with dH_2O of each protein sample was made and an additional diluted sample of RIPA buffer was used as a blank for the assay. The BCA™ working reagent (50:1 dilution of reagent A and B respectively) was made up as per kit instructions. 10µl of each protein standard or sample dilutions were added in triplicate to a 96-well plate and mixed with 200µl BCA™ working reagent. The plate was incubated at 37°C for 30mins and cooled to room temperature before measuring the optical density on the Sunrise TECAN microplate reader at 562nm. A standard curve was plotted using the values obtained from the protein standards and this curve was subsequently used to determine the concentration of the protein samples.

2.9.3. Electrophoretic Separation of Proteins

2.9.3.1. Sodium dodecyl sulphate Polyacrylamide gel electrophoresis (SDS-PAGE)

Sodium Dodecyl-Sulfate PolyAcrylamide Gel Electrophoresis (SDS-PAGE) is a common technique used to determine the apparent molecular weights of proteins in a sample by separation on the basis of their sizes or lengths of polypeptide chains. In this method, the protein samples to be analysed are mixed with an ionic detergent (SDS) which binds and breaks up non-covalent bonds in the proteins. This results in the linearisation or "smoothing" of proteins into negatively charged SDS-polypeptide micellular chains with roughly the same charge to mass ratio and therefore equal mobilities within an electric field. On the application of an electric field across the gel, from the top phase stacking gel to the bottom phase resolving gel, negatively charged anions migrate down through the gel toward the positive electrode. The mobility of each anion in the electric field is proportional to its charge to mass ratio. Therefore SDS-protein micelles with the same charge/mass ratio are separated according to size (molecular weight) in the resolving gel that is larger proteins move slower and remain closer to the top of the gel while smaller proteins move faster hence travel farther down the gel.

2.9.3.1.1. SDS-PAGE Protocol

SDS-PAGE was used to perform denaturing polyacrylamide gel electrophoresis of the protein samples obtained using the modified 1970 Laemmli method (Laemmli, 1970) (Studier, 1973). Before electrophoresis, 30µg of protein samples and biotinylated protein marker (Bio-Rad, Hercules, CA, USA/Fannin Ltd, Ireland) were mixed with 2X Lammeli buffer (Sigma-Aldrich Ireland Limited, Ireland) to a final concentration of 1X and boiled for 5mins. Pre-stained protein marker (Lonza Group Ltd, Switzerland) was warmed to 37°C. Each marker and sample was loaded into separate wells and gel electrophoresis was carried out at a constant current of 120mV on the Mini-PROTEAN® Tetra Cell (Bio-Rad, Hercules, CA, USA/Fannin Ltd, Ireland) as per the manufacturer's instructions. Samples were run through an upper stacking gel to condense the proteins into tight well defined bands < 1mm wide. Samples were then run through a lower

resolving gel to separate proteins according to molecular weights. The gels were made up as in Table 2-1 below and made up to 10mls with dH_2O.

Table 2-1: Stacking and resolving gel compositions. This table lists the components of the stacking and resolving gels made.

Stock Solutions	Resolving Gel (8-12%)	Stacking Gel (4%)
30% Bisacrylamide mix	1.3mls	1.3mls
*1.5M Tris-HCl buffer, pH8.8	2.5mls	-
*1M Tris-HCl buffer, pH6.8	-	1mls
*10% SDS	100ul	80ul
TEMED (N,N,N',N'-tetramethylethylenediamine)	6ul	8ul
***10% (w/v) APS (ammonium persulfate)	100ul	80ul
dH_2O	10ml	10mls

2.9.3.2. NuPAGE® Novex® 4-12% Bis-Tris Gels

NuPAGE® Novex® 4-12% Bis-Tris Gels (Invitrogen, Life Technologies, Maryland, USA, Gibco/Life Technologies Corporation, Ireland) are pre-cast polyacrylamide gels that separate proteins under denaturing conditions. It consists of a 4% stacking gel and a 4–12% separating gel (Bis-Tris-HCl buffer (pH 6.4), Acrylamide, Bis-acrylamide, APS, Ultrapure water at pH 7). It is more advantageous than SDS-PAGE as it maintains protein integrity, provides better band resolution and requires less preparation and running time (Moos, et al., 1998). NuPAGE® MOPS SDS running buffer was the running buffer of choice as it had a wider gel separation range of 15 kDa to 260kDa compared to NuPAGE® MES SDS running buffer of 3.5 kDa to 160kDa. The gels were run on the XCell SureLock™ Mini Cell and the XCell4 SureLock™ Midi Cell gel apparatuses.

2.9.3.2.1. NuPAGE® Novex® Protocol

Before electrophoresis, 30µg of protein samples was mixed with 2X Lammeli buffer (2 ml Tris HCl pH 6.8, 5 ml 10% (w/v) SDS, 1 ml 2-β-Mercaptoethanol, 2 ml glycerol, 0.05 g (w/v) bromophenol blue) (Sigma-Aldrich Ireland Limited, Ireland) to a final concentration of 1X and boiled for 5mins. MagicMark™ XP Western Protein Standard (Invitrogen, Life Technologies, Maryland, USA, Gibco/Life Technologies Corporation, Ireland) and SeeBlue®Plus2 Pre-Stained Standards were warmed up to room temperature. The XCell SureLock™ Mini Cell apparatus was assembled and set up with NuPAGE® MOPS SDS running buffer as per the manufacturer's instructions. Each marker and sample was loaded into a separate wells and gel electrophoresis was carried out at a constant current of 200mV for 50mins. Samples were run through an upper stacking gel to condense the proteins into tight well defined bands < 1mm wide and then a lower resolving gel to separate proteins according to molecular weights.

2.9.4. Wet Transfer of Proteins on PAGE gel to Membrane

Following electrophoresis run, gels were removed as per the manufacturer's instructions. The resolved proteins were transferred to Immobilon™ polyvinylidene diflouride (PVDF) membrane (Millipore, Billerica, USA/Millipore Ireland B.V., Cork, Ireland) using the wet transfer system (Mini Trans-Blot® Cell (Bio-Rad, Hercules, CA, USA/Fannin Ltd, Ireland) as per the manufacturer's instructions. All components were equilibrated in ice cold transfer buffer (25mM Tris-HCl pH8.0, 0.2M glycine, 20 % methanol) before being assembled with the orientation of the membrane noted. The transfer stack assembly was then placed in a cassette, the tank filled with ice cold transfer buffer and constant current of 100mV applied for 1hr.

2.9.5. Membrane Blocking and Probing

Subsequent to transfer, membranes were incubated in blocking solution 5% (w/v) non-fat dry milk (Marvel) in Tris-buffered saline (25mM Tris-HCl pH 7.6, 150mM NaCl) containing 1% Tween-20 (TBST) for 1hr at room temperature with constant gentle agitation to block non-specific binding sites. The membranes were washed in TBST for 5mins on a rocking platform at room temperature three times. Membranes were probed, using varying primary antibodies (dilution range 1: 0000 to 1: 0000) prepared in blocking buffer, at room temperature for 1hr or overnight at 4°C. The membranes were then washed in TBST for 5mins with gentle agitation at room temperature three times and incubated for 1hr at room temperature with the appropriate secondary antibodies prepared in blocking buffer using 1:1,000 dilutions. The membranes were then washed 3 times with TBST for 5mins with gentle agitation at room temperature.

2.9.6. Detection Methods

Blots were developed by enhanced chemiluminesence (ECL) which is based on classic chemiluminescence reaction where by a multi-step reaction of luminol oxidation results in light emission. In ECL, a horseradish peroxidase (HRP)-conjugated secondary antibody which is more sensitive is used and light emission is proportional to protein quantity.

2.9.7. Imaging

Bound antibody complexes were detected using the Amersham™ ECL™ Select Western Blotting Detection Reagent (GE Healthcare Life Sciences, Buckinghamshire, UK) as per the manufacturer's instructions and imaged on the LAS-3000 Imaging System (Fuji Photo Film Co. Ltd, Tokyo, Japan).

2.9.8. Stripping and Re-probing Membranes

To re-probe membranes with a different antibody, the membrane was stripped of antibody complexes and re-probed by covering the membrane in Restore buffer™ PLUS Western Blot Stripping Buffer (Thermo Scientific) and incubating for 15mins at room temperature with constant gentle agitation. The membrane was washed three times in TBST for 5mins each at room temperature. The membrane was re-blocked by incubating in blocking solution for 1hr at room temperature with agitation and repeating primary and HRP labelled secondary antibody incubation steps as earlier mentioned.

2.10. Flow cytometry Analysis

Flow cytometry is a laser-based, biophysical technology employed to analyse and quantitate optical properties of microscopic particles (usually cells), by suspending them in a stream of fluid and passing them through a focused laser beam. Applications include: cell counting, cell sorting, biomarker detection, cell cycle, kinetics, fluorescent protein work, apoptosis/necrosis, ploidy determination, multi-colour immunophenotyping, $Ca2^{+}$ concentration and protein engineering. In addition to measuring fluorescence emission of cells, physical characteristics relating to how light signals interact with the cell, such as: forward scatter and side scatter are quantified (Figure 2-7).

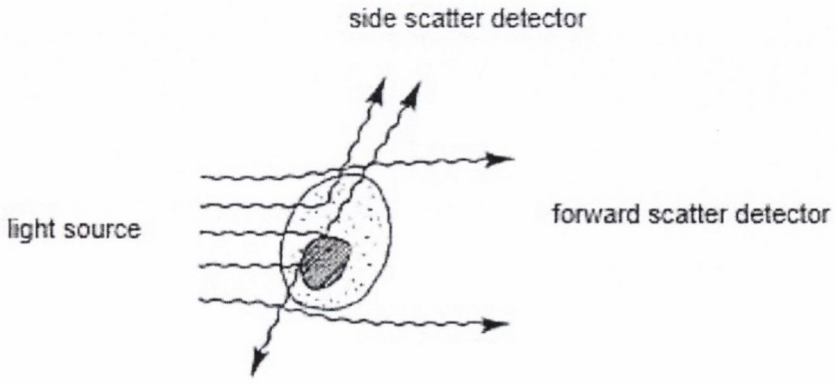

Figure 2-7: Light scattering properties of a cell.

Biological characteristics are assessed via the use of fluorescent molecules, such as fluorophore-labelled antibodies, which bind to proteins of interest and the higher the levels of protein expression the more the binding of fluorescent antibodies. Thus, protein expression is reported by relative fluorescent intensity, on a cell by cell basis. Multiple fluorescent labels can be analysed simultaneously via multiple fluorescent channels. Auto-fluorescence is based on the intrinsic nature of certain normal cellular components, such as riboflavin, flavoproteins and nucleotides, which fluoresce in the absence of a fluorescent tag or stain. Auto-fluorescence is observed in all fluorescence channels but decreases at longer wavelengths (>600nm). Thus, to accurately determine fluorescence intensity due to a tag or stain, auto-fluorescence must be subtracted from the total fluorescence intensity measured. The Beckman Coulter CyAn Advanced Digital Processing (ADP) was the flow cytometer used in this study. It uses three excitation sources 405 nm (UV), 488nm (blue) and 635nm (red) and simultaneously detects up to 11 parameters at 50,000events/second. CyAn ADP uses Summit Data Acquisition and Analysis Software (Summit) for instrument control, parameter adjustments (threshold, photo-multiplying tubes, voltage and gain), data acquisition and subsequent data analysis.

2.10.1. Flow cytometry Analysis Apoptosis detection analysis: FITC Annexin V / PI analysis

Apoptosis is a characteristically and morphologically distinct type of "programmed" cell death. Externalisation of the cell membrane phospholipid: phosphatidyl serine (PS) is one of the early regulatory events in apoptotic cells (Figure 2-8). When on the outer lipid bilayer, it functions as a recognition ligand for phagocytes and prompts the down-regulation of the inflammatory response (Bratton, et al., 1997). Annexins are calcium dependent proteins located in several membranous surfaces within a cell that bind negatively charged phospholipids. Annexin V is a 35-36 kDa Ca^{2+} dependant recombinant protein with high PS affinity. It can be used as a sensitive apoptosis probe via conjugation to various fluorochromes such as Fluorescein isothiocyanate (FITC). Propidium Iodide (PI) is a membrane-impermeable, DNA intercalating dye that binds

every 4th or 5th nucleic acid base pair of both DNA and RNA. It undergoes conformational change to become 40 times brighter on binding. PI serves as a useful viability marker for viability measurements in apoptosis experiments when paired with Annexin V. PS externalisation is an indicator of early to intermediate stages of apoptosis and precedes loss of membrane integrity and cytoskeletal collapse.

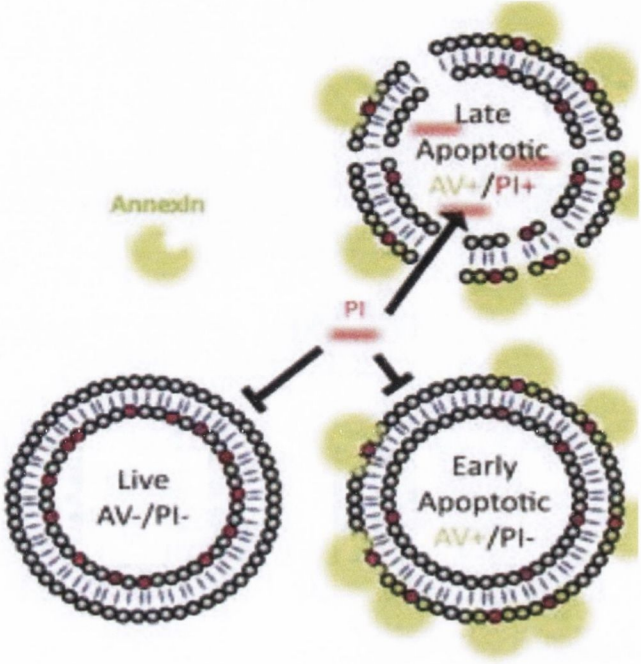

Figure 2-8: Externalisation of phosphatidylserine in cells undergoing apoptosis. In live cells, phosphatidylserine is present on the inner membrane of the lipid bilayer and therefore, excludes Annexin and Propidium Iodide binding to phosphatidylserine and nucleic acids respectively. During early apoptosis, phosphatidylserine becomes externalised (moves to the outer membrane of the lipid bilayer) with the lipid bilayer remaining intact therefore only Annexin binding can occur and Propidium Iodide is excluded. In late apoptosis, phosphatidylserine is externalised and the lipid bilayer is no longer intact hence Annexin binding to phosphatidylserine and Propidium Iodide binding to nucleic acids can occur.

Therefore, FITC Annexin V staining identifies apoptosis at earlier stages before PI permeability. Viable cells with intact membranes exclude PI and are FITC Annexin V and PI negative. Early apoptotic cells with externalised PS are FITC Annexin V positive and PI negative. Whereas late apoptotic, dead cells are permeable to PI and stain FITC Annexin V and PI positive. Distinctions between late stage apoptosis and necrosis cannot be made via this assay, as both will stain FITC Annexin V and PI positive. However, apoptosis may be inferred if cells are tracked through 3 stages of i) FITC Annexin V and PI negative, ii) FITC Annexin V positive and PI negative and iii) FITC

Annexin V and PI positive (Figure 2-9). Conversely, single movement of cells to FITC Annexin V and PI positive is less informative about the demise pathway.

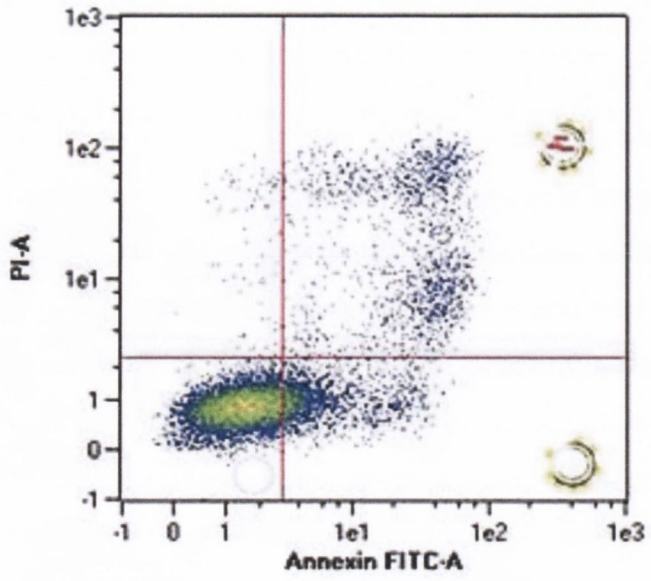

Figure 2-9: Dot plot depicting the process of apoptosis. Cell populations are grouped according to their surface marker expression.

2.10.1.1. Assay protocol

SiHa cells were seeded and transfected as per experimental conditions (section 2.3.2). At 72hrs post transfection, all cells (adherent and non-adherent) were harvested and collected using 10mM EDTA to ensure minimal membrane damage during cell detachment. The solution was neutralised using PBS and pelleted by centrifugation at 1200 rpm for 5mins.

Cells were then washed twice in ice cold PBS and an aliquot counted to determine the number of cells in each pellet (section 2.2.4). Subsequent to PBS washes, the cells were resuspeneded in 1X binding buffer (BD Biosciences, California, USA) at a concentration of 1 x 10^5 cells per 100 µl. 5 µl of FITC Annexin V (BD Biosciences, California, USA) was added to 100 µl aliquots of cells and incubated at room temperature for 15mins. A 400 µl aliquot of 1X binding buffer and 5 µl of PI (BD Biosciences, California, USA) was then added to these cells and incubated for a further 5mins on ice and analysed by flow cytometry. Staining controls of unstained cells, cells stained with FITC Annexin V (no

PI) and cells stained with PI (no FITC Annexin V) were also included to set up compensation and quadrants.

2.10.1.2. Flow cytometry analysis

Each sample is analysed for four parameters (FSC, SSC, FITC, and PI fluorescence). FSC and SSC are used to gate cells from subcellular debris. A gate is a graphical boundary used to define the characteristics of cells to include for further analysis. In this assay, a gate is set to allow for analysis of cells and eliminate data from subcellular debris, based on the FSC vs. SSC plot.

The argon ion laser emits light at 488nm which excites FITC and PI, which are detected at 530 and 620nm respectively. As shown in figure 2-9, a FITC vs PI plot was used to quantify viable (low FITC and PI), early apoptotic (high FITC, low PI), and late apoptotic/dead (high FITC and PI) cells.

To determine the actual intensities from each antibody conjugate in a multi-coloured sample, a compensation process must be carried out. This is used to define the relative amount of light that 'spills over' into another detector using the single colour staining controls (as described in Section 2.8.1.1). This effect is known as compensation. Compensation is used to determine how much light from FITC ends up in the fluorescence parameter FL2 detector and how much light from PI ends up in the fluorescence parameter FL1 detector.

2.10.2. Cell Cycle Analysis: BrdU/PI Analysis

A commonly used procedure to analyse cell cycle by flow cytometry is DNA quantitation. It is based upon the univariate analysis of DNA content of cells following staining with a dye that binds to the DNA, such as PI. The fluorescence level of the bound dye is proportional to the amount of DNA in the cells. This method distributes cells into the three major phases of the cycle (G1 vs S vs G2/M). Cells in S phase have more DNA than cells in the G1 phase and therefore, proportionally bind more dye and fluoresce with greater intensity. Cells in G2 fluoresce more intensely again than those

is S phase. With G2 phase cells being approximately twice as bright as G1 phase, as they contain a cell population with twice the amount of DNA as G1. To prevent active pumping out of PI and enable its entry to bind DNA in live cells, cells are fixed or permeabilised using formaldehyde or ethanol. PI also stains double-stranded RNA; hence RNase A is added to the staining solution to remove all traces of RNA. G1 and G2/M cell populations are represented on frequency histograms by peaks of various widths with S phase cells appearing in between these two peaks (Figure 2-10). However, standard PI cell cycle technique does not distinguish cells in early S phase from those in G1 phase; neither does it distinguish cells in late S phase from those in G2. BrdU staining is used to distinguish early and late S phase from G1 and G2 respectively.

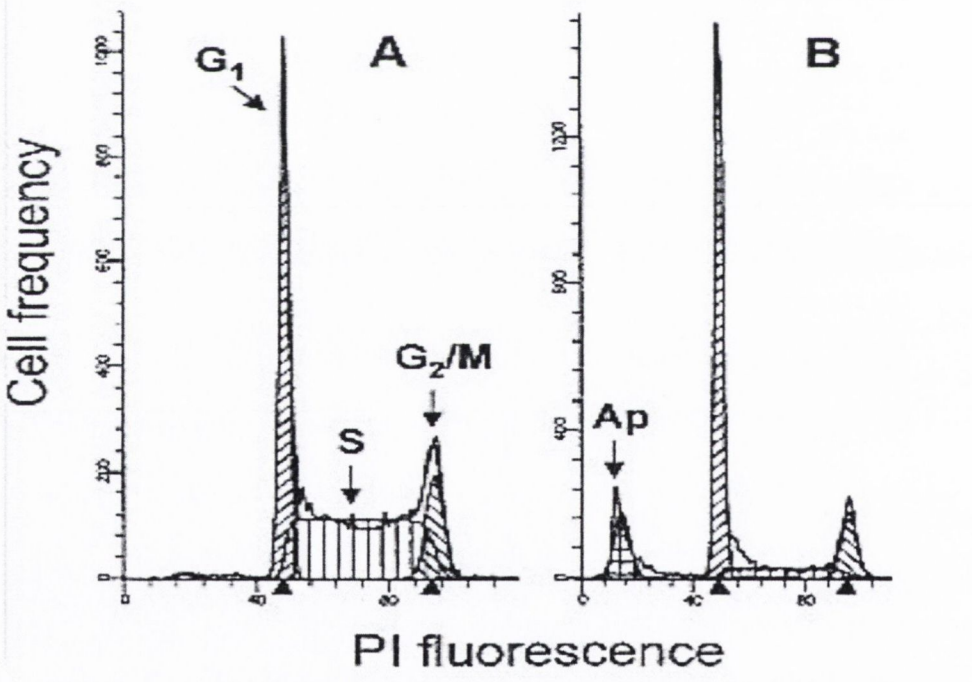

Figure 2-10: Frequency histograms of cells undergoing a G1 arrest representing cells from the untreated cultures stained with PI showing estimate of percentage of cells with fractional DNA content (apoptotic cells: Ap) and cells in G1, S, and G2/M phases of the cycle.

2.10.2.1. Cell cycle Assay protocol

SiHa cells were seeded and transfected as per experimental conditions (section 2.3.2). At 72hrs post transfection, all cells (adherent and non-adherent) were harvested and collected as per section 2.3.3. Cells were fixed and permeabilised using BD Cytofix/Cytoperm™ Buffer and BD Cytoperm™ Permeabilisation Buffer Plus (BD Biosciences, California, USA) on ice as per the manufacturer's instructions. The cells were subsequently treated with 10µg PI and 100µg RNase A in 1X Dulbecco's PBS (DPBS) overnight at 4°C. The following day, 400 µl of BD Pharmingen™ Stain Buffer (BD Biosciences, California, USA) was added to these cells and analysed by flow cytometry. Unstained cells (no PI) were used as controls to set up compensation and quadrants.

2.10.2.2. Flow cytometry analysis

As described in Section 2.10.1.2, FS and SS measurements were used to gate cells and pulse processing (pulse area vs. pulse width) used to exclude cell doublets. A PI frequency histogram (as seen in Figure 2-10) was set up to quantitate the percentage of cells in each cell cycle.

2.11. Raman Spectroscopy

Prior to transfection, calcium fluoride chips (CaF_2) were obtained from Dublin Institute of Technology ((DIT) Dublin, Ireland) and disinfected overnight in 12 well plates (Sarstedt Ltd, Ireland) using Penicillin-Streptomycin solution (Sigma-Aldrich Ireland Limited (Wicklow, Ireland). The following day, the CaF_2 chips were washed and SiHa cells were then transfected via forward transfection protocol technique on the chips using E6#2 designed siRNAs as described in section 2.3.2. A negative siRNA was also included as scrambled control siRNA. All experiments were carried out under aseptic conditions in biological duplicates. Seventy-two hours post forward transfection, CaF_2 chips were washed in PBS and fixed in 10% filtered formalin solution at -20°C for 15mins. The CaF_2 chips were then washed in PBS and moved to the Focas Research

Institute, where Raman studies were performed using a HORIBA Jobin Yvon XploRA^{TM} system (Villeneuve d'Ascq, France) (Figure 2-11).

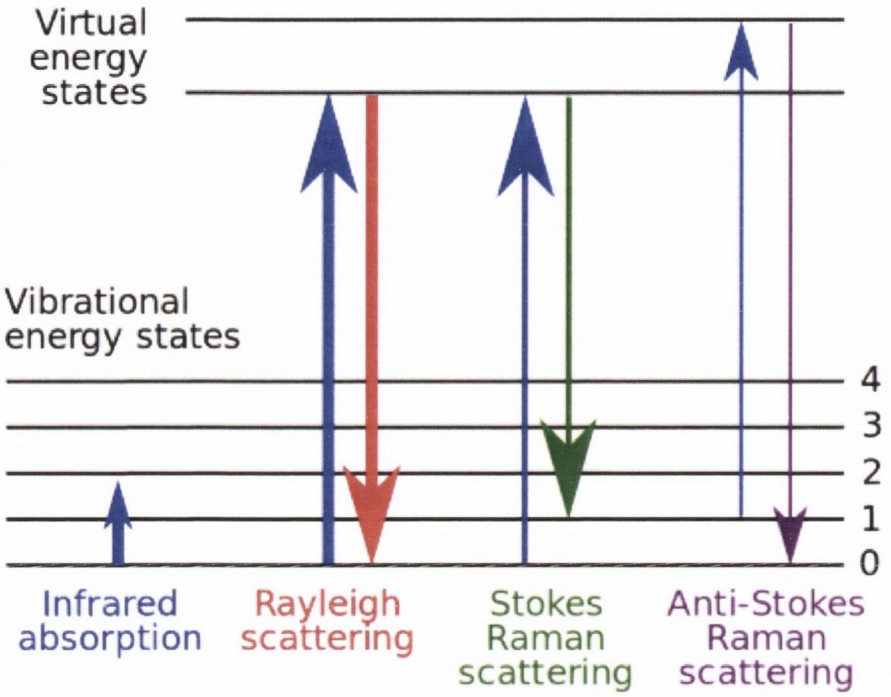

Figure 2-11: Raman spectroscopy profile showing energy-level diagram of the different states involved in Raman signalling. The line thickness is roughly proportional to the signal strength from the different transitions. **(Moxfyre, 2009)**

2.12. Statistical Analysis

In order to determine the significance of the results obtained in these experiments, a Student's t test was carried using the GraphPad Prim version5 software (GraphPad Software, USA) with a null hypothesis that "there is no significant difference between the untreated or scrambled control SiHa cells and SiHa cells transfected with E6 siRNAs". The p-values obtained from these analyses were used to weigh the strength of the evidence. Statistical significance was accepted at $P < 0.05$ that is small p-values of ≤ 0.05 indicated strong evidence against the null hypothesis (null hypothesis rejected) and large p-values of > 0.05 indicated weak evidence against the null hypothesis (null hypothesis accepted).

Chapter Three

Gene silencing of HPV16 Oncogenes

3. Silencing HPV16 oncogenes

3.1. Introduction

The relationship between human papillomavirus (HPV) infection and the progression of cervical cancer has been well established. There is overwhelming evidence to support the causal role of high risk types in the development of cervical cancer (Bosch, et al., 2002) (Moody & Laimins, 2010) with the most prominent oncogenic high risk HPV types, HPV16 and HPV18 associated with approximately 70% of cervical cancers (HPV16 accounts for 50-60% and HPV18 for 10-12%) (Bosch & de Sanjosé, 2003). Infection with a high risk HPV type is considered a necessity for the development of cervical cancer, with the expression of the HPV oncogenes E6 and E7 a crucial requirement for the development and maintenance of malignancy. In the majority of cervical cancers, the HPV genome becomes integrated into the host cell genome, causing disruption of the E2 ORF. This loss of E2 and its inhibitory activity results in overexpression of viral oncogenes E6 and E7 and thus, allows uncontrolled host cellular proliferation to occur. HPV E6 and E7 play distinct but cooperating roles in the oncogenic process by driving to stimulate squamous epithelial cells in the mid and superficial zones to re-enter the cell cycle. This is achieved by targeting different pathways leading to the activation of cellular oncogenes and the neutralisation of tumour suppressor proteins. HPV E6 promotes genetic instability and contributes to tumour progression primarily by targeting the tumour suppressor and cell cycle checkpoint protein, p53 for degradation via the ubiquitin/proteasome pathway (Reviewed in (Howie, et al., 2009). HPV E7 is an efficient cell cycle promoter and deregulator that subvert host cell genome integrity via binding and inactivating the pRB tumour suppressor protein (Reviewed in (McLaughlin-Drubin & Münger, 2009)). A more comprehensive overview of HPV E6 and E7, their characteristics and their interactions can be found in Chapter 1.

The complete reliance of HPV on E6 and E7 overexpression for malignancy, their transcription from the same promoter and their expression from the same mRNA make them highly attractive targets for RNAi therapeutics. RNAi is a highly conserved, naturally occurring post transcription phenomenon of effectively silencing gene

expression in a sequence specific manner that can be manipulated via the introduction of double stranded DNA (dsRNA) or short interfering RNAs (siRNA). This occurrence was initially observed in plants and Caenorhabditis elegans worms where it was thought to serve a protective role (Horvitz, 1999) (Fire, et al., 1998). It has also been found to occur in numerous multicellular organisms and is proposed to play a role in chromosomal formation and maintenance during cell division (Volpe, et al., 2002) (Allshire, 2002). Presently, RNAi is a powerful standard technology used in a wide range of disciplines to assess gene function and is instigated by the introduction of dsRNA molecules that induce degradation of complementary target RNA in a sequence specific manner (Elbashir, et al., 2001).

The RNAi pathway is initiated in most eukaryotes by an endogenous RNase II-Like enzyme, Dicer, which cleaves long double stranded RNA (dsRNA) molecules into shorter 21-23 nucleotide long duplexes called small or short interfering RNAs (siRNAs) (Macrae, et al., 2006) (Bernstein, et al., 2001) (Hammond, et al., 2000). These siRNA duplexes have 2 nucleotide overhangs at both 3' ends and in an ATP-dependent step, are unwound and the antisense strand of the duplex incorporated into a multi-subunit protein complex known as the RNAi induced silencing complex (RISC). RISC guides the incorporated siRNA strand to the target RNA sequence. On hybridisation, RISC directs the degradation of complementary RNA sequences by activating its slicer nuclease activity hence preventing translation of that transcript (Elbashir, et al., 2001) .

The manipulation of this mechanism in cell culture by the exogenous introduction of dsRNA or siRNAs into cells can facilitate the impediment of specific gene expression. This can be achieved via binding to the active gene or its transcripts, thereby causing decreased expression through a variety of processes and thus, knocking-down and reducing the activity of such a gene. Although the mechanisms by which these processes occur are yet to be fully elucidated, they are however, considered diverse and multi-factorial. Transient and stable knockdown of a target gene can be attained using either synthesised siRNAs or vector expressing small hairpin RNAs (shRNAs)

respectively. As a better understanding of the functions of HPV oncogenes were desired in this study, reverse genetics using transient knockdowns was utilised to facilitate the elucidation of their roles in cervical carcinogenesis. Efficient gene suppression using siRNA has been demonstrated *in vivo,* hence there are vast potential applications for such effective suppression agents, as research tool(s) or as therapeutic molecules (Elbashir, et al., 2001) (Bartlett & Davis, 2006).

3.2. Chapter aim

The aim of this work was to establish a system for the suppression of HPV E6 oncogenes in an *in vitro* cervical cancer cell line model using RNA interference (RNAi). This technique was achieved using short interfering RNAs (siRNAs) to specifically target the E6 coding region of the E6/E7 bicistonic mRNA. Due to the production of alternatively spliced E6 mRNAs from this region, a key aspect of this work was the validation of highly effective siRNAs towards the E6 mRNA transcript. This refined system was proposed to become a building block for future investigations within this laboratory, as the evaluation of new and unique functions of the E6 protein (via assessment of three species; full length E6, spliced E6 and E7) and how their actions contribute to the oncogenic process would considerably expand our knowledge of cervical carcinogenesis.

3.3. Materials and Methods

3.3.1. Cell culture

The HPV16 positive SiHa cervical cancer cell line was employed in this chapter and cultured at 37°C in a humidified 5% CO_2 atmosphere (section 2.2)

3.3.2. siRNA design

An ideal algorithm for siRNA design has not yet been developed. However, a number of guidelines and criteria for designing siRNA have been validated by a number of studies (Reynolds, et al., 2004) (Ui-Tei, et al., 2004). Using suggested guidelines, companies like Ambion and Sigma-Aldrich supply predesigned and validated siRNAs that primarily target rat, mouse and human genomes. In this study, two different approaches were used to design siRNAs towards HPV16 E6 mRNA and its splice forms using one in-house approach based on criteria from the literature and a second an Ambion designed machine learning methods.

Before either design process was undertaken, a preliminary query was entered into BLASTN, an online sequence alignment tool provided by the National Centre for Biotechnology Information (NCBI). BLASTN searches all publicly available nucleotide sequences and protein translations complied as a database by NCBI in collaboration with the European Molecular Biology Laboratory (EMBL), the European Bioinformatics Institute (EBI) and the DNA Data Bank of Japan (DDBJ). The initial query was for HPV16 complete genome sequence between nucleotides 83 to 559 representing the coding region for HPV16 E6. The output yielded variants with identical and divergent sequences which were identified and extrapolated. These variants were then used to identify further variants through BLASTN and a total of 80 variants were identified, 70 of which were determined to be representative of the entire divergence amongst the 80. These 70 sequences were aligned using CLUSTALW, a multiple sequence alignment program for DNA or proteins. On the basis of this alignment, conserved and divergent regions within the sequences were identified. Five regions of homology within HPV16

E6 coding sequence were determined and siRNAs targeting these regions designed to ensure that any variant form of HPV16 would be targeted by these siRNAs.

3.3.3. In-house designed HPV16 E6 siRNA

Using literature defined conditions; the maximum possible numbers of crucial parameters were included in the design of in-house siRNAs. HPV16 E6 coding sequence was inputted into each of these online siRNA design algorithm tools; Whitehead Institute, EMBOSS, Hannon Laboratory and MWG. A list of the criteria used in the selection of in-house designed HPV16 E6 targeting siRNA is outlined in Table 3-1. The number of siRNAs identified by these prediction tools varied and information such as secondary structure of the target mRNA and thermodynamic stability of the siRNA ends (supplied by MWG and Whitehead Institute respectively) were considered as additional parameters. Also, siRNAs common to at least 2 of the 4 design algorithms used were selected for extra consideration.

Table 3-1: Criteria used in the selection of in-house designed HPV16 E6 targeting siRNA.

Criterion	Description (Criterion based on sense strand)
I	G/C content of 30 -52%.
II	Low internal stability at the 3' end,
III	that is A/U rich between point 1 to 7
IV	U or A at point 1
V	G or C (more often C) at point 19 on the siRNA sequence
VI	A or U (more often A) at point 10 on the siRNA sequence
VII	Avoid extended run of alternating GC, more than 7
VIII	Avoid runs of greater than 3 G's. VIII U at point 17 on the siRNA sequence

siRNA sequences identified by these prediction tools were then compared with the conserved five E6 regions to determine if any sequence homology existed with human genes using BLASTN which could alter the proposed effect of siRNA and possibly cause toxicity. Only siRNAs within these conserved coding regions of HPV16 E6 were considered for further analysis. The siRNAs were then ranked as per Ui-Tei, et al and Reynold et al as well as on thermodynamic properties and secondary structure of target mRNA sequence (Ui-Tei, et al., 2004) (Reynolds, et al., 2004).

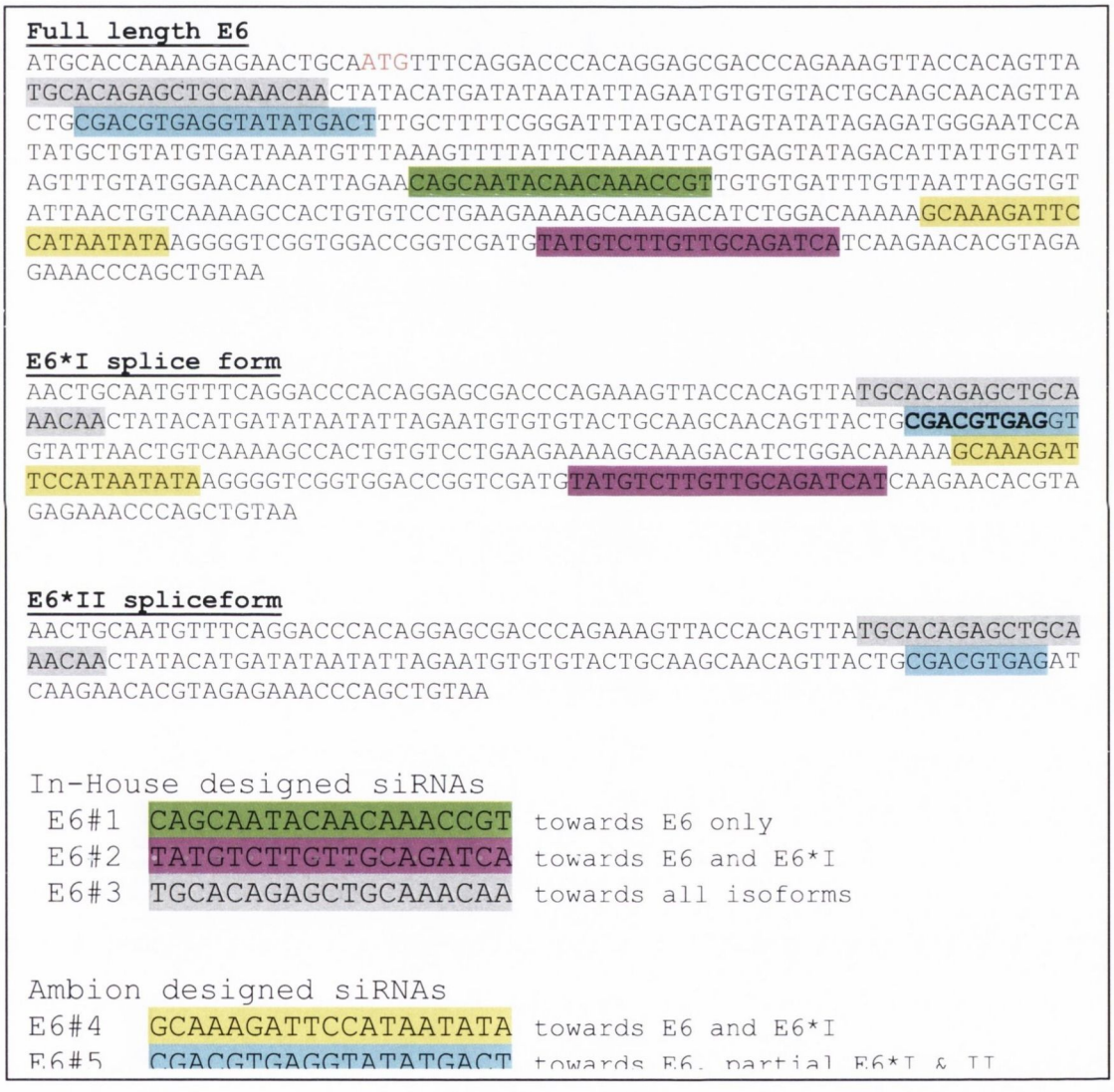

Figure 3-1: The representation of designed siRNA targets against E6 and its isoforms. This figures shows full length HPV16 E6 and two of its splice forms E6*I and E6*II and the five siRNAs employed in targeting HPV16 E6. In-house designed E6#1 (green) towards full length E6 only, E6#2 (purple) towards full length E6 and E6*I, E6#3 (grey) towards all isoforms (full length E6, E6*I, E6*II) Ambion designed E6#4 (yellow) towards full length E6 and E6*I and E6#5 (turquoise) towards E6, 11 nucleotides of E6*I and 9 nucleotides of E6*II. Start site indicated as ATG and highlighted in red.

On these bases, 3 siRNAs sequences were selected and provided to Ambion for synthesis with no chemical modifications. One to target the 5'end another the 3'end and the last to target the centre of full length HPV16 E6 as illustrated in Figure 3-1 and Figure 3-2.

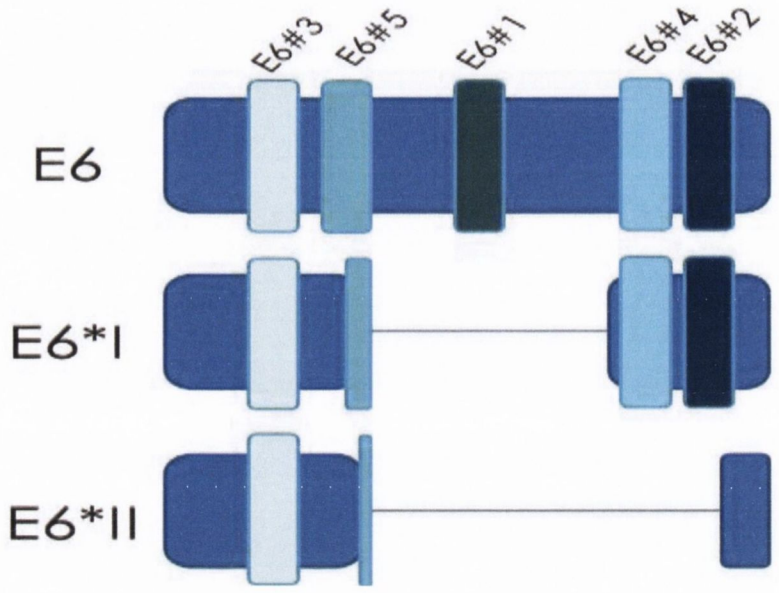

Figure 3-2: Diagrammatic representations of designed siRNA targets against E6 and its isoforms. The above diagram depicts the three isoforms of E6; full length E6 (full rectangle), E6*I (rectangle missing central portion) and E6*II (rectangle missing a larger central portion). The five siRNAs employed in targeting these isoforms are represented by smaller rectangles and labelled E6#1, 2, 3, 4 and 5. These rectangles are placed at targeted regions (N terminal, C terminal or centre) of each isoforms.

3.3.4. Ambion designed HPV16 E6 siRNA

HPV16 E6 coding region was supplied to Ambion to design siRNAs for this project with conserved regions within the sequence highlighted. Ambion, using the latest technology available at the time designed silencer select siRNAs based on machine learning methods and produced siRNAs with 5 to 20 fold less concentration to stimulate potent silencing event compared to available siRNAs. A 5-step bioinformatics filtering procedure as detailed in Table 3-2 was also used to incorporate chemical modifications to ensure elimination of off target effects. Locked Nucleic Acid modification (LNA) of siRNAs was employed to reduce off target effects by 90%. Using these parameters and those outlined by Ui-Tei et al and Reynolds et al. (Ui-Tei, et al.,

2004) (Reynolds, et al., 2004), 2 additional siRNAs specific for HPV16 E6 were identified and synthesised by Ambion. One to target the 5' end another the 3' end as illustrated in Figure 3-2.

Table 3-2: Criteria used in the selection of Ambion designed HPV16 E6 targeting siRNA.

Bioinformatics filtering used
Mismatch filter
Silencer select toxicity classifier
Natural miRNA seed region filter
Antiviral response motif filter
siRNA seed region ranking

3.3.5. Transfections

Forward and Reverse transfections were carried out on SiHa cells using 5uM Lipofectamine™ RNAiMAX (Invitrogen, Life Technologies, USA) in 6 well plates at a seeding concentration of $1.5X10^5$ cells per well and containing a GAPDH positive control and a universal scrambled control siRNA at a concentration of 10nM as described in section 2.3.1.2.

3.3.6. TaqMan® RT-PCR

The mRNA expression of GAPDH, full length HPV16 E6 , full length HPV16 E6 and E6*I splice form and E7 for both transfection methods was determined by TaqMan® RT-PCR on SiHa cells left untreated, treated with transfection agent, transfected with 10nM of scrambled control siRNA or experimental siRNA. Total RNA was extracted from these cells following a 24-72hrs post transfection incubation using the Ambion MirVana kit (section 2.3.3.1). The RNAs were DNase digested, their concentration and 260/280 nm

ratio then determined using the NanoDrop® ND-1000 (section 2.3.3.2). TaqMan® two-step RT-PCR was subsequently carried out as per section 2.3.4 using primer and probe sets listed in Table 3-3 and the relative quantity of gene expression calculated using the $2^{-\Delta\Delta Ct}$ comparative CT method whereby mRNA expression was normalised to B2M and calibrated to untransfected control.

3.3.6.1. Primers and Probes

PCR primers and probes towards HPV16 E6 and E7 were designed in-house using Primer Express Software Version 3.0. Two sets of primers and probes were designed towards E6, one targeting E6 and its splice form E6*I and the second targeting full-length E6 only while one set was designed for E7. These primer and probe sets were used at a concentration of 300nM for each primer set and 250nM for each probe. Pre-designed primers and probe sets specific for controls (GAPDH and B2M) were commercially obtained in 20X mixes from Applied Biosystems (Invitrogen, USA) and used at a 1X concentration as per the manufacturer's instructions.

Table 3-3: Representation of designed HPV16 E6 and E7 Primers and Probes. HPV16E6-344F, HPV16E6-415R and HPV16E6-372T are primer and probe set towards E6 and E6*I. HPV16E6-133F, HPV16E6-218R and HPV16E6-158T are primer and probe set towards E6. HPV16 E7-140F, HPV16 E7-205R and HPV16 E7-164T are primer and probe set towards E7.

	Name	Sequence
Forward	HPV16E6-344F	AGC CAC TGT GTC CTG AAG AAA AG
Reverse	HPV16E6-415R	ACC GAC CCC TTA TAT TAT GGA ATC T
Probe	HPV16E6-372T	6-FAM-ACA TCT GGA CAA AAA G-MGB
Forward	HPV16E6-133F	CTG CGA CGT GAG GTA TAT GAC TTT
Reverse	HPV16E6-218R	CAT TTA TCA CAT ACA GCA TAT GGA TTC C
Probe	HPV16E6-158T	6-FAM-CTT TTC GGG ATT TAT GC-MGB
Forward	HPV16 E7-140F	CGG ACA GAG CCC ATT ACA ATA TT
Reverse	HPV16 E7-205R	CGC ACA ACC GAA GCG TAG A
Probe	HPV16 E7-164T	6-FAM-TAA CCT TTT GTT GCA AGT GTG A-MGB

3.3.7. Senescencent β-Galactosidase Staining

The β-galactosidase activity of cells was determined by histochemical staining of cleaved chromogenic substrate X-gal post transfection. Only adherent cells were employed in this analysis and the overexpression and accumulation of the endogenous lysosomal beta-galactosidase was specifically assessed in all samples via observation of positively stained blue cells.

3.3.8. Western Blot Analysis

72hrs post transfection, protein extracts were recovered by sonicating cells in 30µl of RIPA buffer using Soniprep 150 as detailed in section 2.7.3 and their concentrations determined using the Pierce BCA™ protein assay kit (section 2.7.4.2). Thirty µgs of protein per lane for each sample was resolved using Invitrogen NuPage Novex 4-12% Bis Tris MiniGels and electrotransferred to PVDF membranes. The membranes were blocked in bovine serum albumin, incubated overnight with anti-p53, anti-p21 and anti-GAPDH antibodies, washed and subsequently incubated with the appropriate peroxidise-conjugated secondary antibody. Chemiluminescent detection was then carried out according to the manufacturer instruction using ECL Plus western blotting detection reagents (GE Healthcare, Dublin Ireland). GAPDH or β-actin was used to assess protein loading controls.

Table 3-4: Table of antibodies and their dilutions. This table lists antibodies used, their suppliers, types, species raised in and dilution factors.

Primary Antibodies	Supplied by	Antibody Type	Species Raised	Dilution factor
GAPDH	Abcam UK	Monoclonal	Mouse	1/250000
β-actin	Abcam UK	Monoclonal	Mouse	1/1000
p53	BD Pharmigen™ (BD Biosciences, USA)	Monoclonal	Mouse	1/1000
P21	BD Pharmigen™ (BD Biosciences, USA)	Monoclonal	Mouse	1/500

Secondary Antibody	Supplied by	Species Raised	Dilution factor
	Jackson Immuno Research, USA	Goat	1/1000

3.3.9. Apoptosis Analysis

Flow cytometry was used to determine and differentiate the apoptotic profile of cells using Annexin V-FITC and Pi staining 48 and 72hrs post transfection. All cells (adherent and non-adherent) were collected for this analysis (section 2.8.1.1.).

3.3.10. Cell cycle Analysis

Flow cytometry was used to determine the cell cycle state of cells 72hrs post transfection using PI staining as described in section 2.8.2.1. All cells (adherent and non-adherent) were collected for this analysis.

3.3.11. Statistical Analysis

A Student's t test using the GraphPad Prim version5 software (GraphPad Software, USA) was used to evaluate the statistical significance of data from three biological replicates of treated groups versus control groups. Statistical significance was accepted at $P < 0.05$

3.4. Results

3.4.1. Optimisation conditions for HPV16 E6 knockdown

The SiHa cell line was the *in vitro* model system of choice for HPV16 positive cervical cancer. In this study, initial optimisations were performed for the most suitable transfection technique and endogenous control. In-house designed E6#1 and Ambion designed E6#5 siRNAs were used to silence endogenous HPV16 E6 expression in the SiHa cells. Scrambled control siRNA and GAPDH targeting siRNA were also included as negative and positive controls respectively. All experiments were carried out and repeated in triplicate.

3.4.1.1. GAPDH Knockdown

Prior to transfecting SiHa cells with designed E6 siRNAs, optimal conditions for forward and reverse transfection protocols were considered in terms of cell seeding concentration and the duration of transfection to determine if there was any effect on the efficiency of transfection. This preliminary experiment was carried out to eliminate systematic error by using a cheaper positively-responding siRNA (also from Ambion), targeted against a gene whose expression remains constant in SiHa cells and proven to be accurate at silencing. This was determined by using an Ambion validated siRNA towards GAPDH, using a seeding concentration of $1.5x10^5$ and transfection duration of 48hrs, as previously validated by this laboratory for the reverse transfection protocol. 48hrs post transfection, the efficiency of the knockdown was assessed at the RNA and protein level via TaqMan® RT-PCR and western blotting respectively (Figure 3-3 A and B). There were no significant differences in mRNA expression levels between SiHa cells left untreated, mock-transfected and transfected with scrambled control siRNA and all expression values were within biological variation limits between 50% and 200% (Figure 3-3A). Positive control siRNA GAPDH attained an average knockdown of 93% at the RNA level both with the reverse and forward transfection techniques (Figure 3-3A). Ninety-three percent was calculated by determining ΔΔCT using the relative quantification method (section 2.3.6.2.2), calculating fold change ($2^{(-\Delta\Delta CT)}$) and multiplying it by 100. Also substantial decrease in GAPDH expression in the GAPDH

positive control siRNA at the protein level compared to the scrambled, untreated and mock (Figure 3-3B)

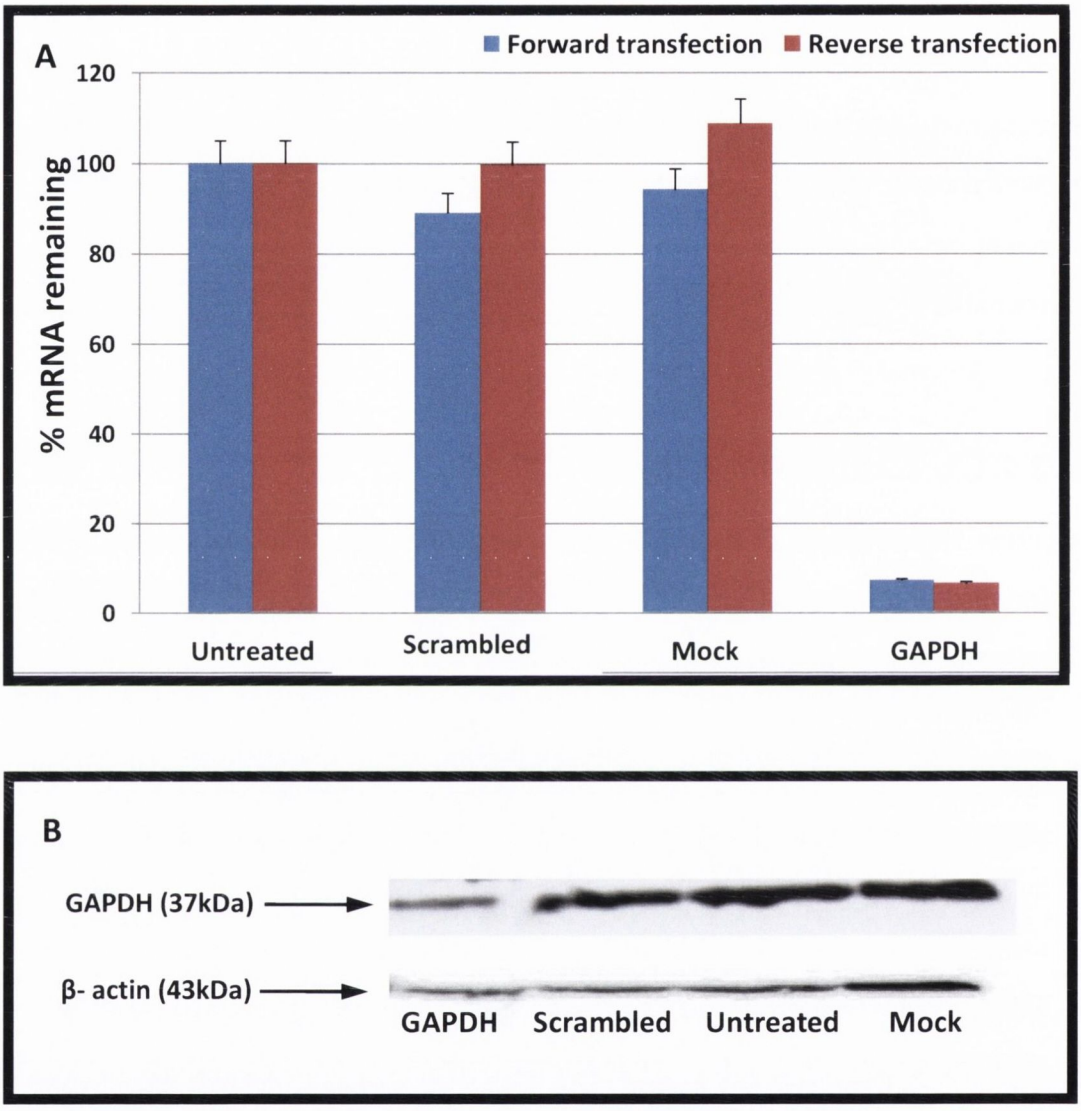

Figure 3-3: GAPDH silencing in SiHa cell line 48hrs post transfection. SiHa cells seeded at 1.5x 10^5 were left untreated, mock-transfected, transfected with scrambled control siRNA (10nM) and transfected with GAPDH targeting siRNA (10nM) in three biological replicates for 48hrs using the reverse transfection protocol (blue) and forward transfection protocol (red) techniques. (A) The total RNA was extracted and mRNA expression levels were assessed via TaqMan RT-PCR using primers and probes selective for GAPDH mRNA. GAPDH mRNA expression was normalised to B2M and calibrated to untransfected control to establish the relative level of mRNA expression and these values are expressed in percentages. (B) Cells were lysed in RIPA buffer and 30µg of lysate samples was resolved using 4-12% SDS-PAGE gels and wet transferred to PVDF membranes. The membrane was blocked in 5% non-fat dry milk in TBST and then immunoblotted for β-actin (lower). The membrane was then stripped and re-immunoblotted for GAPDH (upper). β-actin was used as loading control. As a result of the constant expression of GAPDH (hence longer half-life) in SiHa cells and supplier recommendation, data was only obtained 48hrs post transfection as to allow sufficient time for significant knockdown to occur both at mRNA and protein levels.

Similarly, no significant differences were observed morphologically between cells that were left untreated, mock-transfected and transfected with scrambled control siRNA controls at 24 and 48hrs in both reverse and forward techniques (Figure 3-4 and Figure 3-5 respectively). This result confirmed optimal transfection conditions and also showed no impact of scrambled control siRNA on transfection in the SiHa cell line.

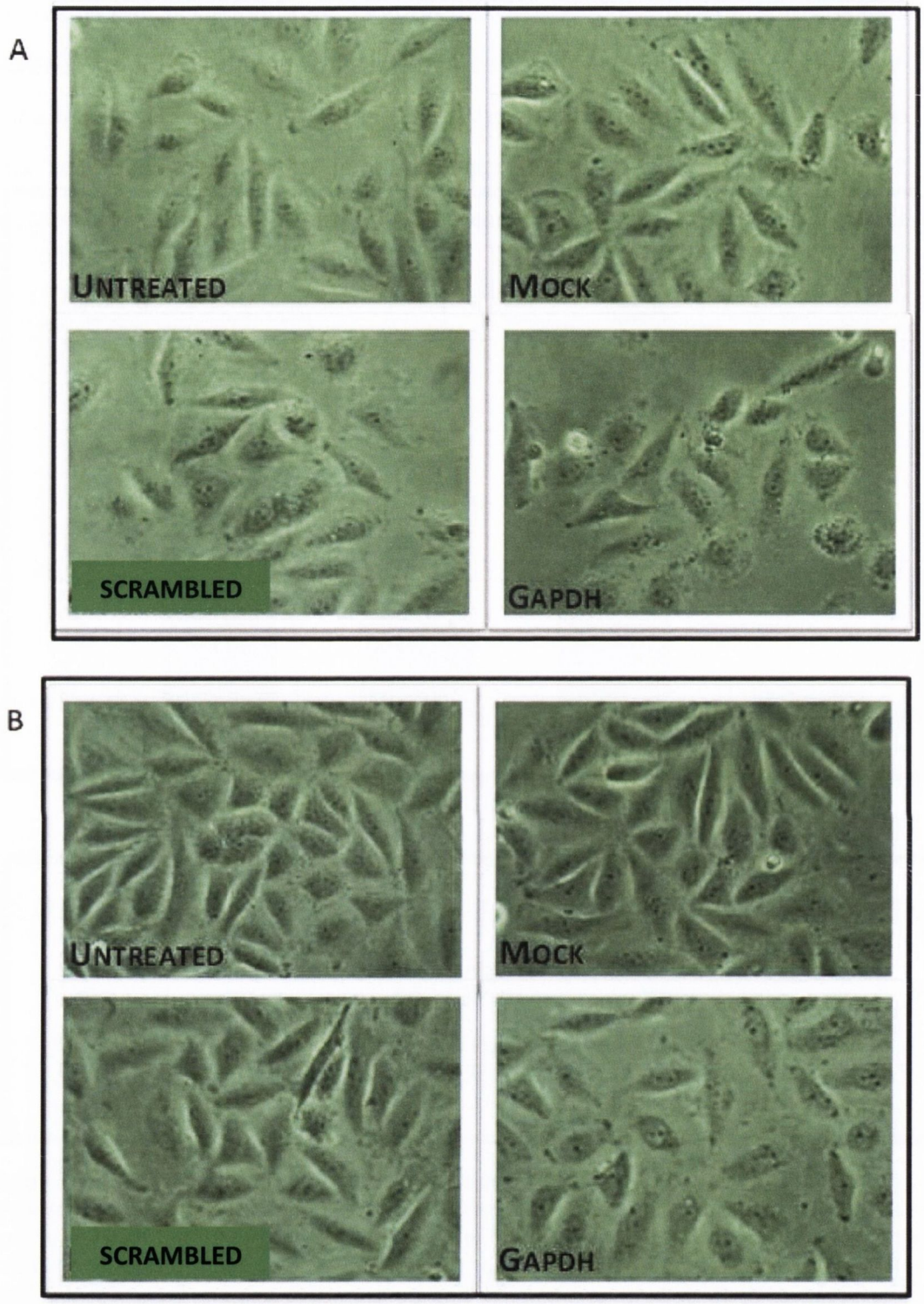

Figure 3-4: Light microscopy using the Reverse transfection protocol technique. SiHa cells seeded at $1.5x10^5$ cells were left untreated, mock-transfected, transfected with scrambled control siRNA (10nM) and transfected with GAPDH targeting siRNA (10nM) in three biological replicates and examined by light microscopy at 24hrs post transfection (panel A) and 48hrs post transfection (panel B). No morphological differences were observed between the untreated, mock-transfected, transfected with scrambled control siRNA at 24 and 48 hour time points. However, at 24hrs, cells transfected with GAPDH siRNA appear to have slightly altered morphology of less regular polygonal shape and at 48hrs cells appear to be more granular and rounding up. (Magnification 200X).

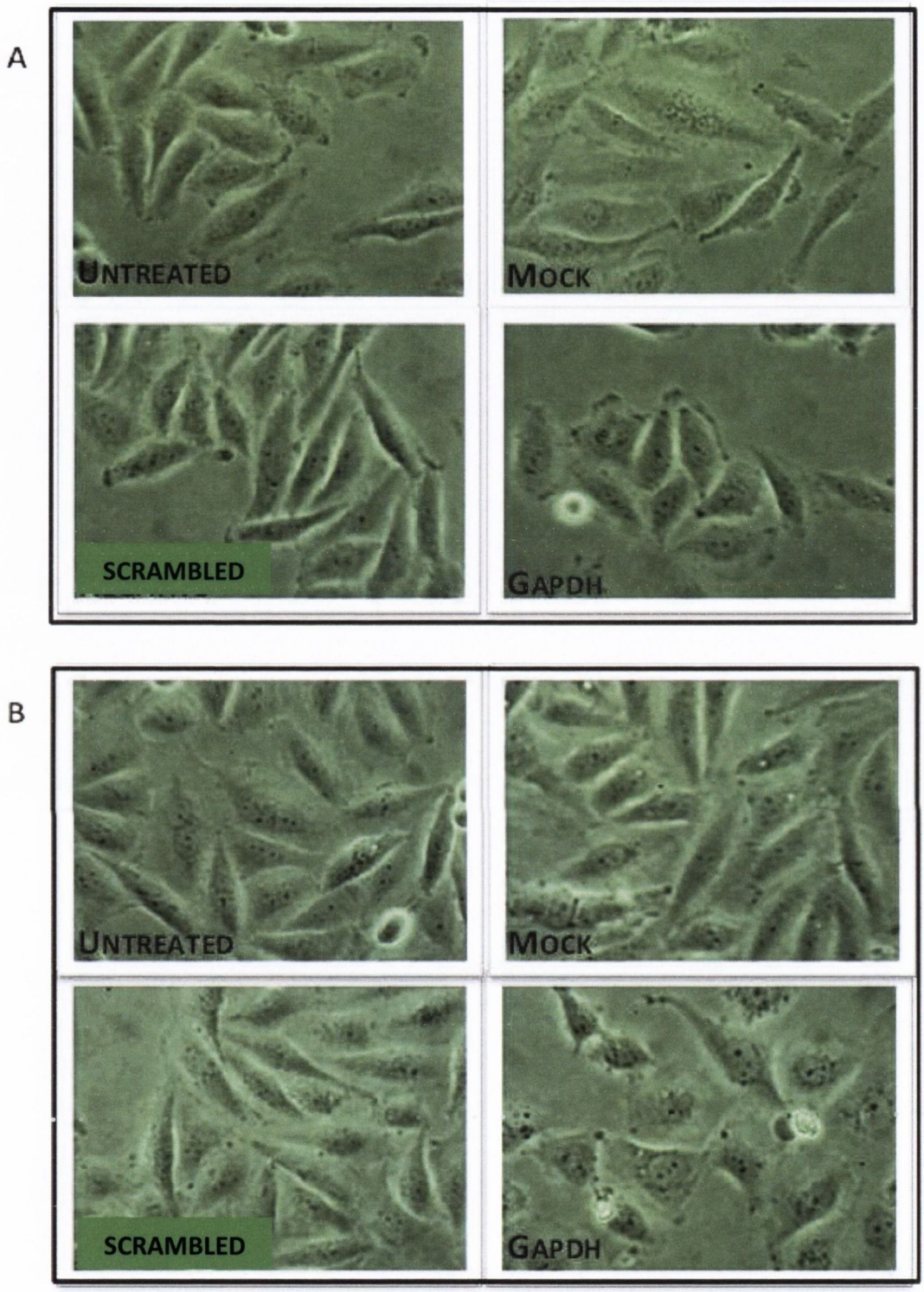

Figure 3-5: Light microscopy using the Forward transfection protocol technique. SiHa cells seeded at $1.5x10^5$ cells were left untreated, mock-transfected, transfected with scrambled control siRNA (10nM) and transfected with GAPDH targeting siRNA (10nM) in three biological replicates and examined by light microscopy at 24 hours post transfection (panel A) and 48 hours post transfection (panel B). No morphological differences were observed between the untreated, mock-transfected, transfected with scrambled control siRNA at 24 and 48 hour time points. However, at 24 hours, cells transfected with GAPDH siRNA appear to have slightly altered morphology of less regular polygonal shape and at 48 hours have fewer cells are forming tight junctions; appear to round up with more granular and shrunken cytoplasm (Magnification 200x).

3.4.1.2. Reverse transfection of HPV16 E6 siRNA

Following the positive control, GAPDH targeting siRNA optimisations, two HPV16 E6 specific siRNAs were selected, in-house designed E6#1 and Ambion designed E6#5 siRNAs initial knockdown analysis. Since no difference was observed between the forward and reverse protocols during the initial optimisation work with GAPDH, the reverse transfection protocol for 48hrs was chosen. These conditions were chosen to enable direct comparisons with previous work carried out in this lab, where under the same conditions, HPV16 oncogenes were silenced using Ambion designed HPV16 E7 siRNAs. In addition, these conditions (transfection at 37°C using Lipofectamine) were standard laboratory protocols of this group for the SiHa cell line. 48hrs post transfection, total RNA was extracted and the level of E6 expression was assessed using E6 specific TaqMan® RT-PCR primers and probes. Using these conditions, neither of the two siRNAs induced consistently significant silencing of E6. The duration of the reverse transfection protocol was then increased to 72hrs but neither E6#1 or E6#5 siRNAs resulted in significant silencing of E6 despite the consistency in expression levels (significant reductions in mRNA levels) of GAPDH positive control siRNA Figure 3-6.

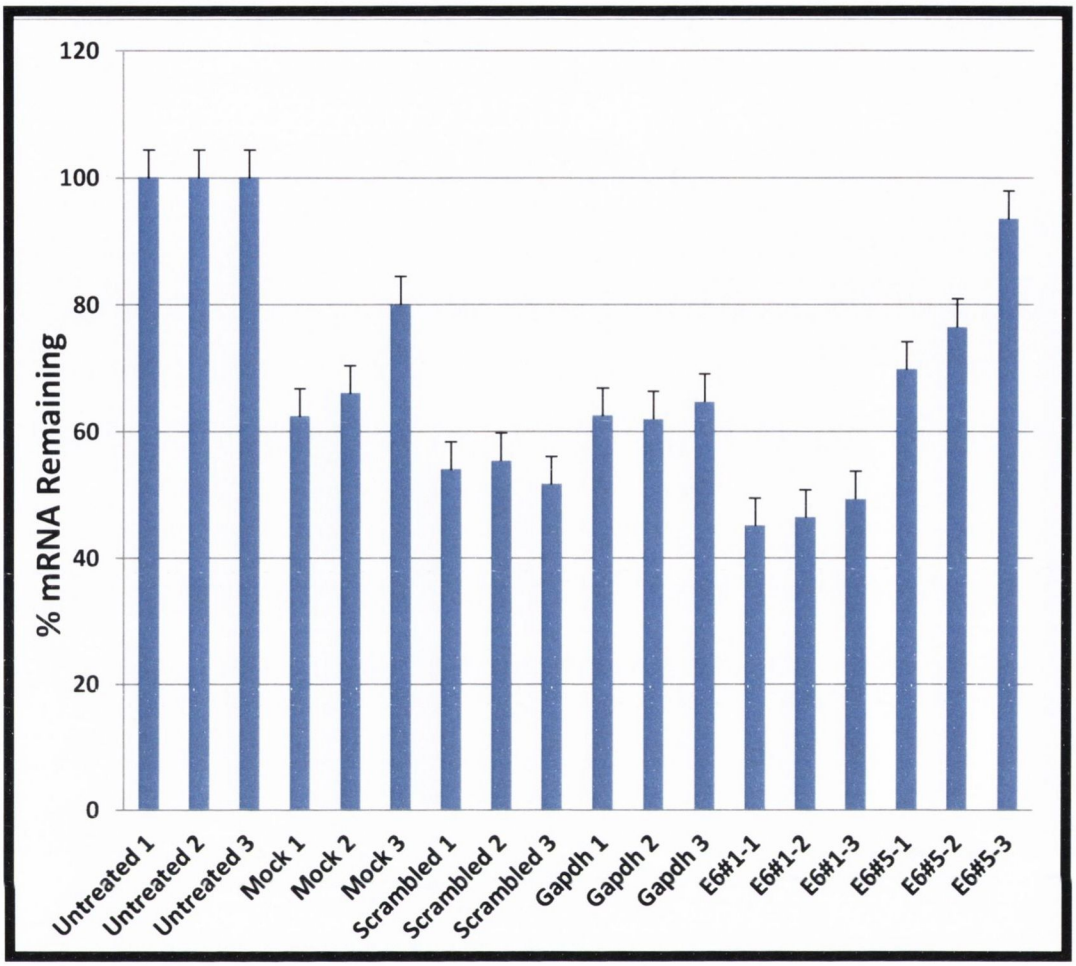

Figure 3-6: E6 mRNA silencing using the reverse transfection protocol technique at 72 hours. SiHa cells seeded at 1.5x 10^5 concentrations were left untreated, mock-transfected, transfected with scrambled control siRNA, transfected with GAPDH targeting siRNA (10nM), transfected with E6#1 and E6#5 (10nM) targeting siRNA in three technical replicates (E6#1-1 represents technical replicate 1, E6#1-2 represents technical replicate 2 and so on). Total RNA was extracted 72 hours post transfection and mRNA expression levels were assessed via TaqMan RT-PCR using primers and probes selective for E6. Each mRNA expression was normalised to B2M and calibrated to untransfected control to establish the relative level of mRNA expression

3.4.1.3. Forward transfection of HPV16 E6 siRNA

As a result of issues encountered with the use of the reverse transfection protocol, the forward transfection protocol was selected as it had worked efficiently with GAPDH siRNA during validation. Optimisation conditions involving varying seeding concentrations for SiHa cells were assessed and the forward transfection protocol

technique using seeding concentration of $1.5x10^5$ cells per well and transfection durations of 24, 48 and 72hrs was carried out. Following each time point, total RNA was extracted and the level of E6 and E7 expression was assessed using TaqMan® RT-PCR primers and probes specific for each Figure 3-7. However, there was no substantial knockdown with E6#1 and E6#5 siRNAs in SiHa cells. The percentage mRNA levels obtained were borderline values of between 40 and 50% as shown in Figure 3-7. Nevertheless, significant morphological changes were observed in both E6#1 and E6#5 siRNAs (Figure 3-8, Figure 3-9 and Figure 3-10). The high and variable Ct values obtained for E6#1 led to the evaluation of the endogenous control employed (B2M) using a panel of endogenous controls.

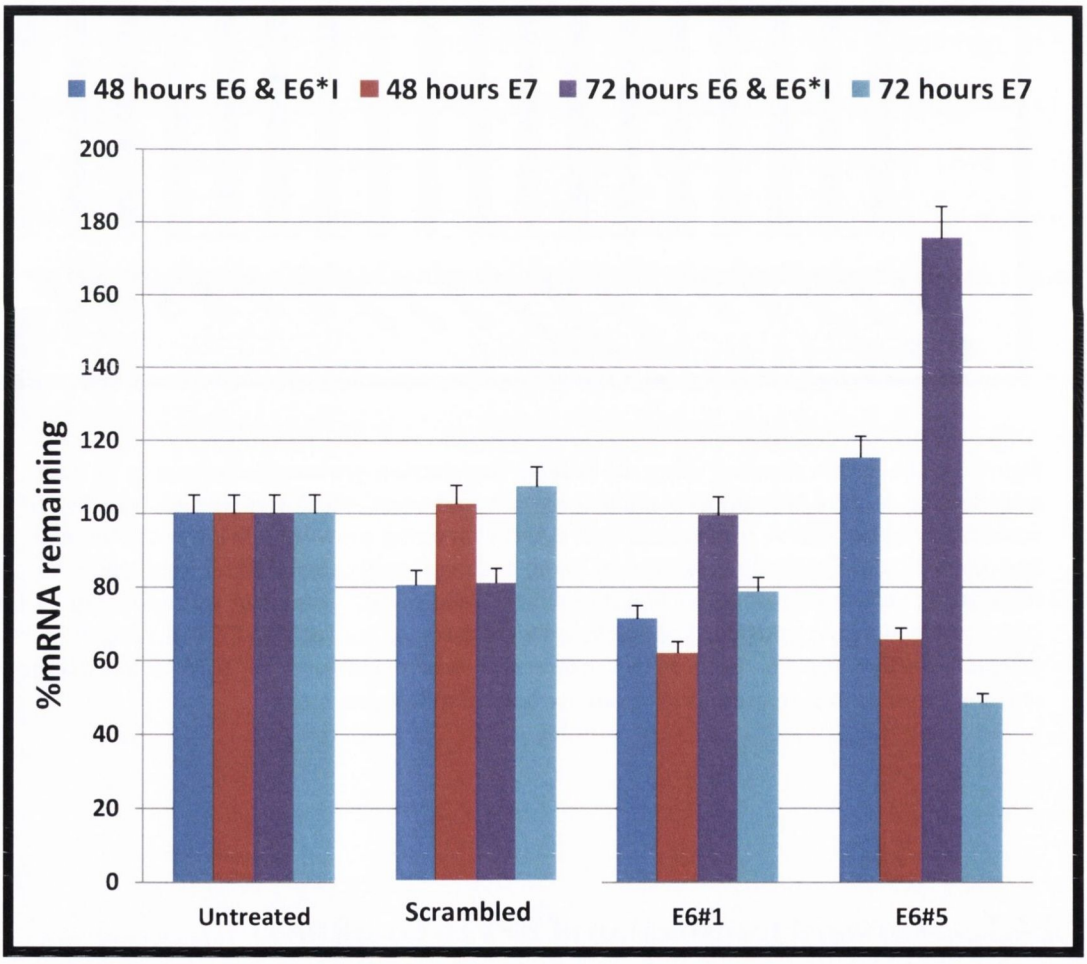

Figure 3-7: E6 mRNA silencing using the forward transfection protocol technique at 48 and 72 hour time points. SiHa cells seeded at $1.5x\ 10^5$ concentrations were left untreated, mock-transfected, transfected with scrambled control siRNA, transfected with E6#1 and E6#5 targeting siRNA in three biological replicates. After 48 and 72hour time point incubations, total RNA was extracted and mRNA expression levels were assessed using E6 and E7 specific TaqMan® RT-PCR primers and probes. Each mRNA expression was normalised to B2M and calibrated to untransfected control to establish the relative level of mRNA expression.

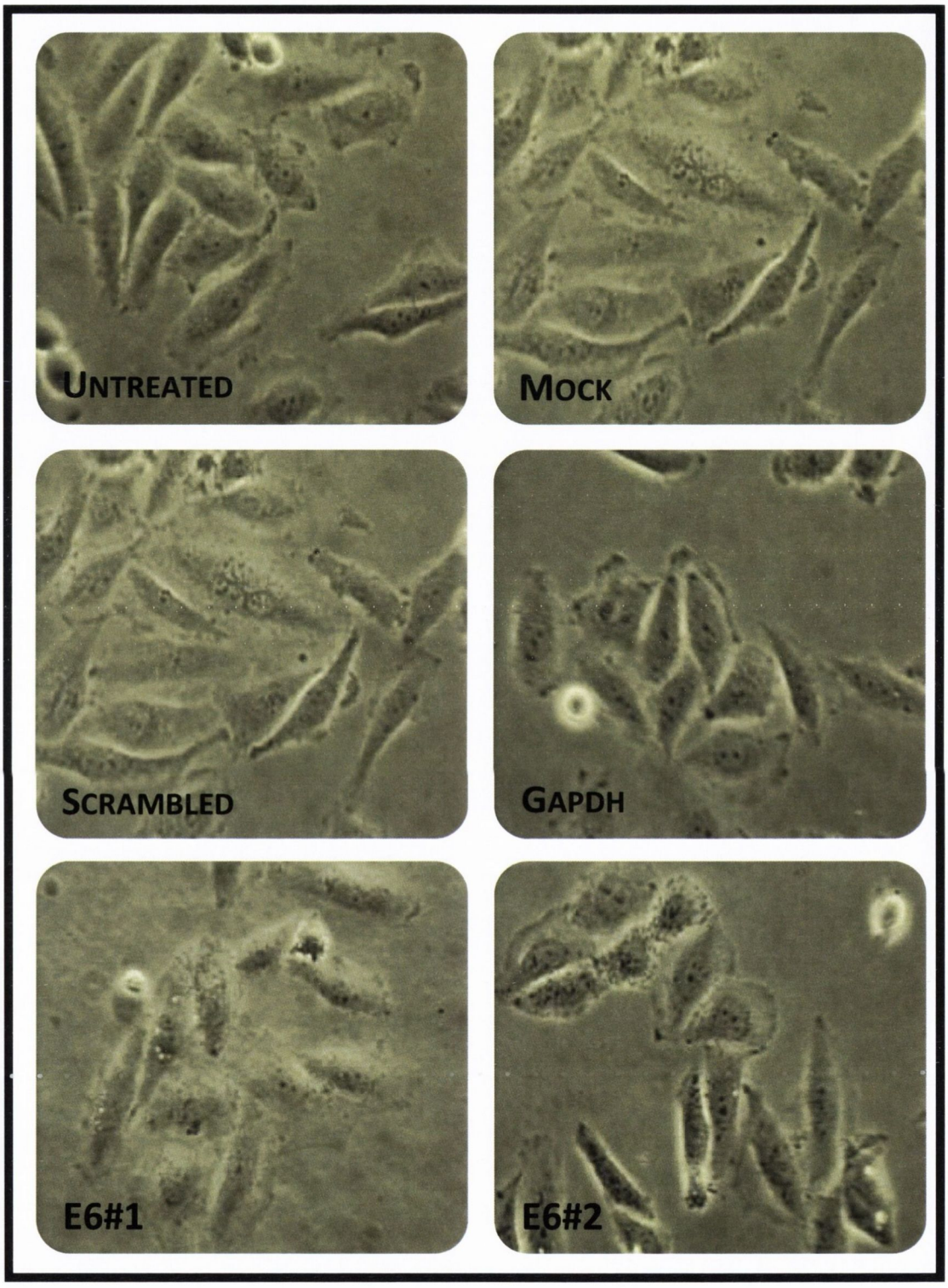

Figure 3-8: Light microscopy 24hrs post forward transfection technique. SiHa cells seeded at $1.5x10^5$ cells were left untreated, mock-transfected, transfected with scrambled control siRNA and transfected with GAPDH targeting siRNA, E6#1 and E#5 siRNAs in three biological replicates. After 24 hours, cells were examined by light microscopy. No morphological differences were observed between the untreated, mock-transfected and transfected with scrambled control siRNA while cells transfected with GAPDH, E6#1 and E6#5 transfected cells display slightly altered morphology of less regular polygonal shape (Magnification 200x).

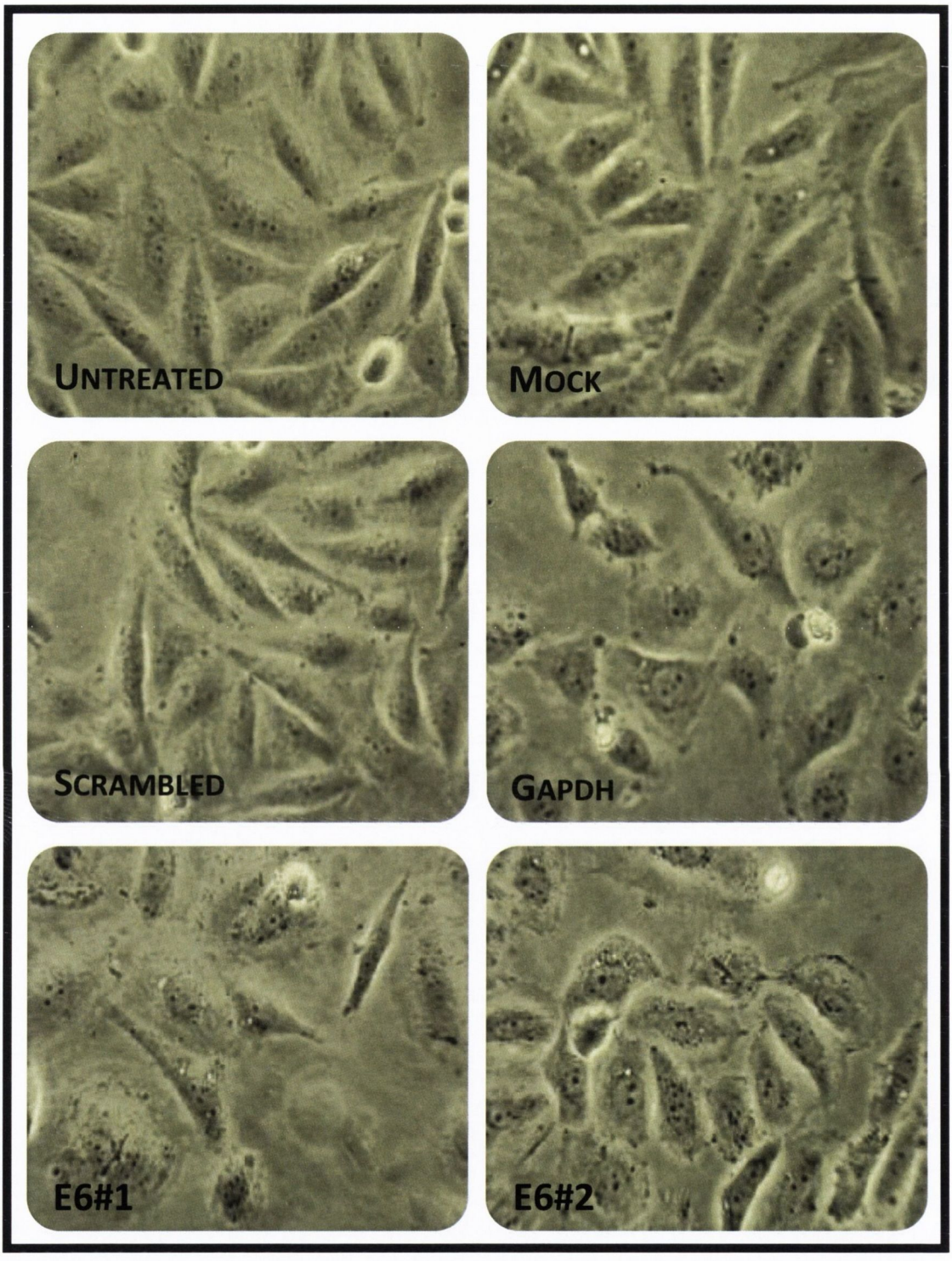

Figure 3-9: Light microscopy of SiHa cells 48hrs post forward transfection technique. SiHa cells seeded at $1.5x10^5$ cells were left untreated, mock-transfected, transfected with scrambled control siRNA and transfected with GAPDH targeting siRNA, E6#1 and E6#5 siRNAs in three biological replicates. After 48 hours, cells were examined by light microscopy. No morphological differences were observed between the untreated, mock-transfected, transfected with scrambled control siRNA while the cells transfected with GAPDH siRNA alter their morphological phenotype forming less tight junctions; appear round up with granular and shrunken cytoplasm. E6 #1 transfected cells appear to have condensed in cell size and cytoplasm while E6#5 transfected cells displayed a flattened appearance (Magnification 200x).

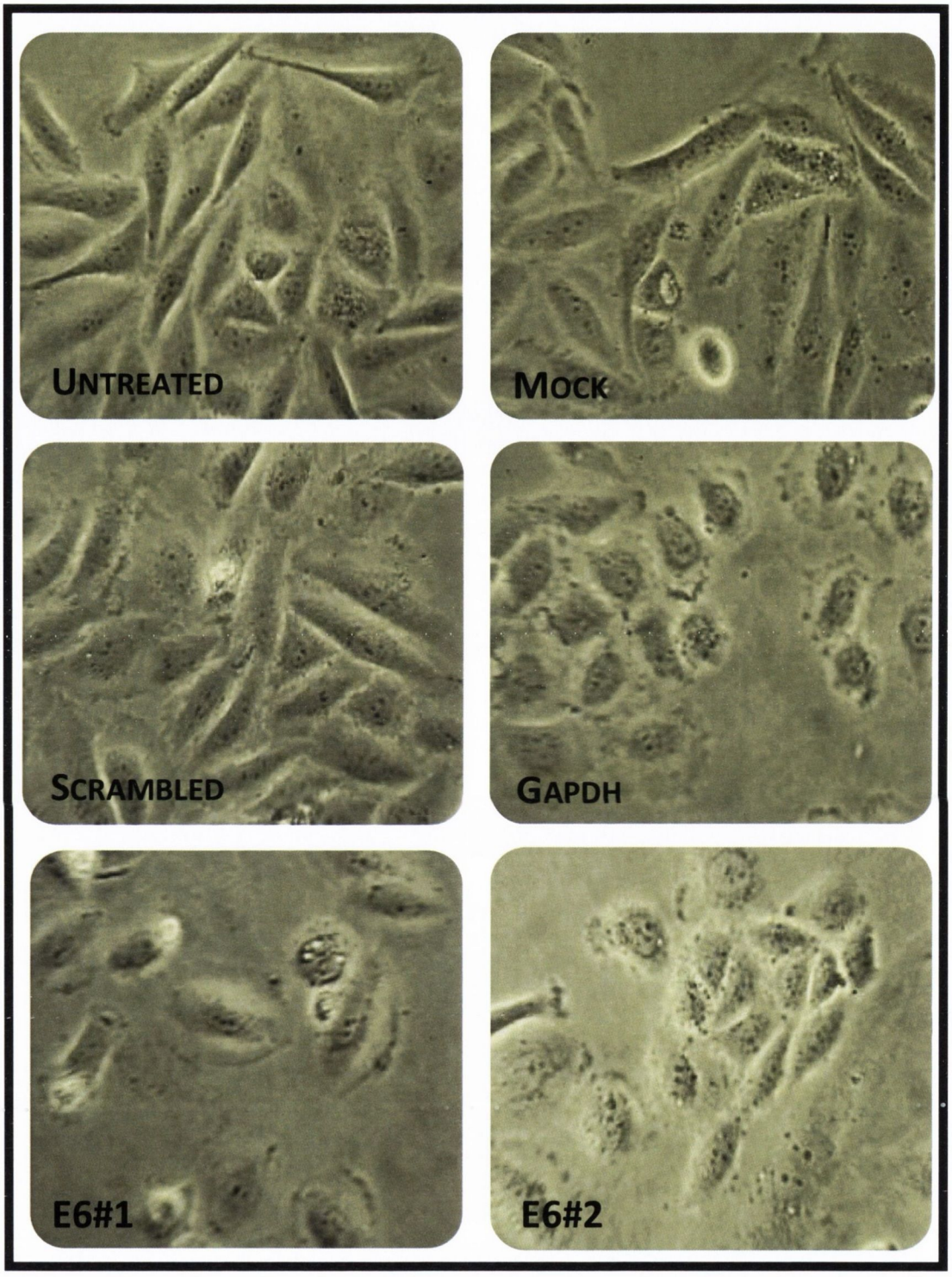

Figure 3-10: Light microscopy of SiHa cells 72hrs post forward transfection technique. SiHa cells seeded at $1.5x10^5$ cells were left untreated, mock-transfected, transfected with scrambled control siRNA (and transfected with GAPDH targeting siRNA, E6#1 and E6#5 siRNAs in three biological replicates. After 72 hours, cells were examined by light microscopy. No morphological differences were observed between the untreated, mock-transfected, transfected with scrambled control siRNA while cells transfected with GAPDH siRNA show more pronounced rounded morphological phenotype with more granular and shrunken cytoplasm. E6#1 transfected cells appear to have condensed cytoplasm, cell shrinkage and membrane blebbing while E6#5 transfected cells displayed growth arrest and flattened appearance (Magnification 200x).

3.4.1.4. A panel of endogenous controls

A panel of four endogenous controls were assessed for their suitability as endogenous controls for PCR reactions in SiHa cells post transfection with siRNA. This was as a result of the observed variations in Ct values of the endogenous control (Beta-2-microglobulin (B2M)), employed in the validation of the forward transfection protocol technique by TaqMan® RT-PCR with E6#1 and E6#5 siRNAs in section 3.3.1.3 (Beta-2-microglobulin (B2M)). These were 18S ribosomal RNA subunit (18S rRNA), Beta-actin (ACTB_AB) cytoskeletal gene, Glyceraldehyde 3-phosphate dehydrogenase glycolytic enzyme (GAPDH) along with B2M, which is a major histocompatibility complex (MHC). These three controls have been widely used in knockdown experiments (Palanichamy, et al., 2010) (Rho, et al., 2010) and were compared to B2M to assess if lack of an observed substantial knockdown in these cells was due to the siRNAs having an effect on the endogenous control (Table 3-5).

Table 3-5: Assessment of a panel of four endogenous controls. SiHa cells seeded at 1.5x 10^5 were left untreated, mock-transfected, forward transfected with scrambled control siRNA in two biological replicates for 72hrs. After 72 hours incubation, total RNA was extracted and mRNA expression levels were assessed via TaqMan RT-PCR using primers and probes selective for 18S rRNA, ACTB_AB, B2M and GAPDH mRNA from same cDNA. The table below shows the average Ct value and standard deviation for each sample in each control. Values above normal standard deviation (St Dev.) of ≤0.3 are highlighted in red.

	18S rRNA		ACTB_AB		B2M		GAPDH	
	Average Ct	St Dev.	Average Ct	St Dev.	Average Ct	St Dev.	Average Ct	St Dev.
Untreated 1	10.95	0.57	18.76	0.72	19.50	0.10	20.45	0.36
Untreated 2	10.90	0.34	19.01	0.47	19.44	0.05	20.39	0.14
Mock 1	10.12	0.29	18.66	0.60	19.23	0.18	19.60	0.27
Mock 2	10.33	0.56	18.53	0.32	18.75	0.06	20.18	0.12
Scrambled 1	14.37	0.84	22.44	0.50	21.35	0.06	24.25	0.49
Scrambled 2	13.56	1.20	24.03	1.27	21.71	0.20	23.76	0.33

Table 3-5 is a representation of average Ct values of four technical replicates of each sample for the panel of four endogenous controls examined and their standard deviations. The Ct standard deviation value obtained for 18S rRNA was the second highest of all four endogenous controls despite its average Ct values being the lowest of all four which correlates with its amplification plots in Figure 3-11A and B. In qPCR experiments, the baseline (cycles 3 to 16) refers to the signal level during the initial cycles, in which there is little or no change in fluorescent signal. This low level signal is equated to noise or background of the reaction and facilitates accurate determination of the Ct. Hence, the baseline determination of a reaction must take into consideration enough cycles to disregard the background found in the early cycles of amplification but should not include the cycles in which the amplification signal begins to rise above the background. In 18S rRNA, its initial cycles are too close to the start of the PCR run (Figure 3-11B, hence results in short and narrow baseline which makes it difficult to determine an accurate Ct or the RNA concentration at which 18S rRNA would provide a wide enough baseline and also generate target gene Cts within 40 cycles.

For the ACTB_AB control, its initial cycles are at a sufficient distance from the start of the PCR run and the baseline calculated is within normal acceptable range of 3-16 (Figure 3-11C and D). However, ACTB_AB has the highest Ct standard deviation amongst all four endogenous controls. All of its Ct standard deviation values highlighted in red in Table 3-5 as a result of them being above the acceptable standard deviation range of 0-0.3. Hence, ACTB_AB yields large variability and lowers the confidence in distinguishing between small differences in target concentration. The early cycles of GAPDH are also at a sufficient distance from the start of the PCR run and the baseline calculated is within normal range of 3-16 (Figure 3-11 G and H). It also has the second lowest standard deviation of the four controls, with three out of six standard deviation values within the acceptable standard deviation Ct range of 0-0.3. However, the amplifications plots for GAPDH are too close to the end of the PCR run hence its curves are plateauing beyond 40 cycles where the reaction should be ending.

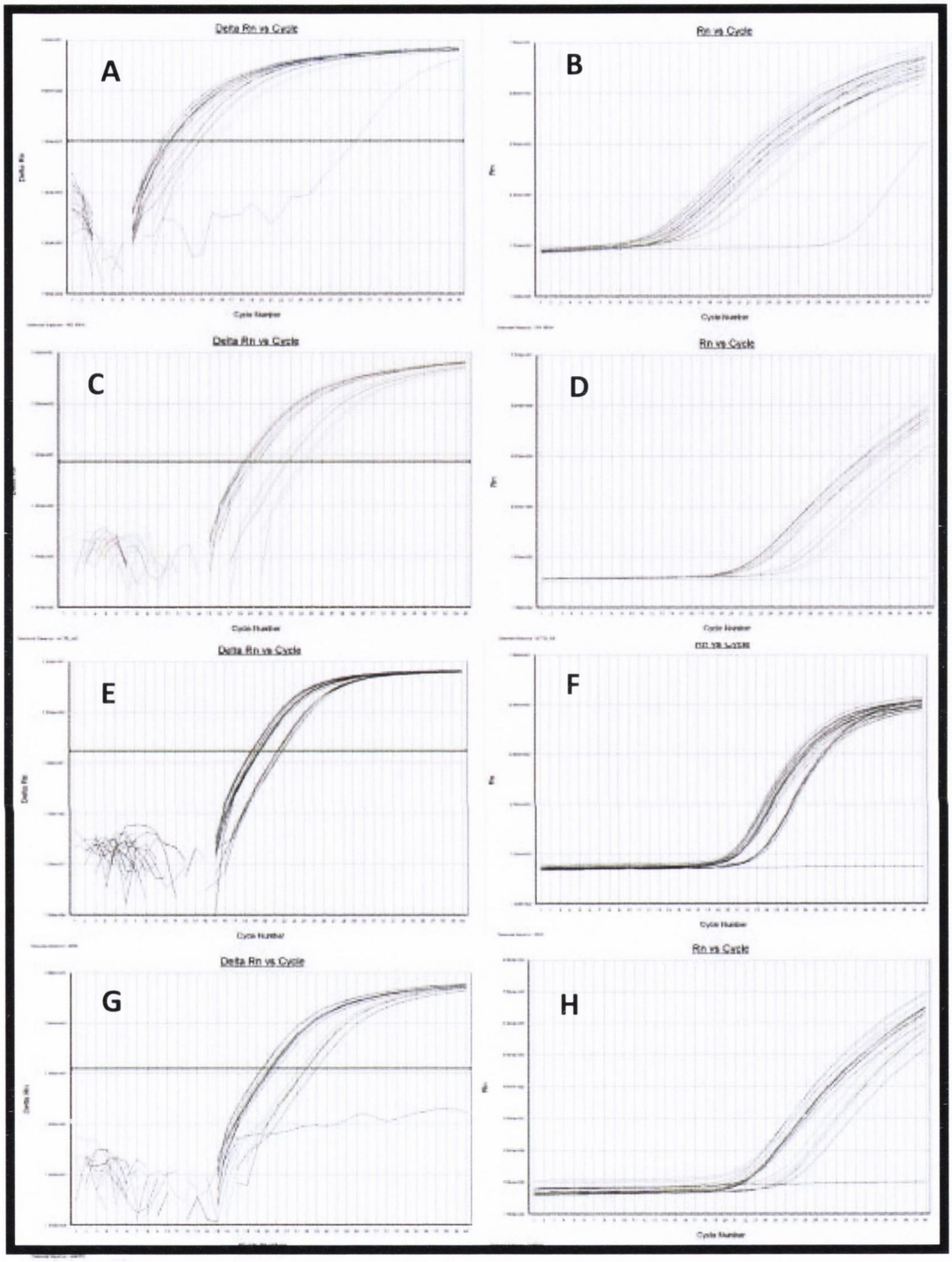

Figure 3-11: Amplification plots of a panel of endogenous controls in SiHa cell line using the forward transfection technique. SiHa cells seeded at 1.5x 10^5 were left untreated, mock-transfected, transfected with scrambled control siRNA in two biological replicates for 72hrs. After 72 hours incubation, total RNA was extracted and mRNA expression levels were assessed via TaqMan RT-PCR using primers and probes selective for (A&B) 18S rRNA, (C&D) ACTB_AB, (E&F) B2M and (G&H) GAPDH mRNA from same cDNA. The left hand side graphs (A, C, E, G) depict an amplification plot of ΔRn against PCR cycle number with the green line representing the threshold. The Ct is the intersection between an amplification curve and a threshold line and represents the relative measure of the concentration of target in the PCR reaction. The right hand side graphs (B, D, F, H) depict amplification plots of Rn against PCR cycle number which aid the baseline determination of each control PCR run.

Finally, of all four controls, B2M had its early cycles at a sufficient distance from the start of the PCR run and its calculated baseline within the normal range, in addition to having its amplification plots within 40 cycles (Figure 3-11E and F). The amplification plots for B2M are also tighter, compact and clustered together compared (Figure 3-11 E and F) to other control (Figure 3-11 A, B, C, D, G and F) which is represented in Table 3-5. Its standard deviation values fall within the acceptable standard deviation Ct range of 0-0.3 (Table 3-5). As B2M was the closest in exhibiting characteristics desired of our endogenous control using the untreated mock and control samples, a surrogate biomarker (used and taken as a measure of the effects of a specific treatment) was used to further assess its appropriateness for this RNAi experiment due to consistency issues when assessing mRNA expression levels post transfection with E6#1 and E6#5 siRNAs using E6 and E7 specific TaqMan® RT-PCR primers and probes.

3.4.1.5. Assessing the expression a surrogate biomarker in HPV16 E6 siRNAs

The lack of a consistent knockdown with E6#1 and E6#5 siRNAs prompted the use of p21 as an indirect biomarker for E6 expression. p21 is known to mediate anti-proliferative effects of p53 (which is targeted by E6), via cell-cycle arrest at G1 phase and repression of DNA replication. TaqMan RT-PCR analysis on the same cDNA used for E6 mRNA expression showed a highly significant 30 fold increase ($p<0.001$) in p21 expression in E6#5 siRNA targeted SiHa cells (Figure 3-12). This elevation in p21 levels suggests that p53 is functional which a transcriptional target of p21 is thus confirming the efficacy of these siRNAs.

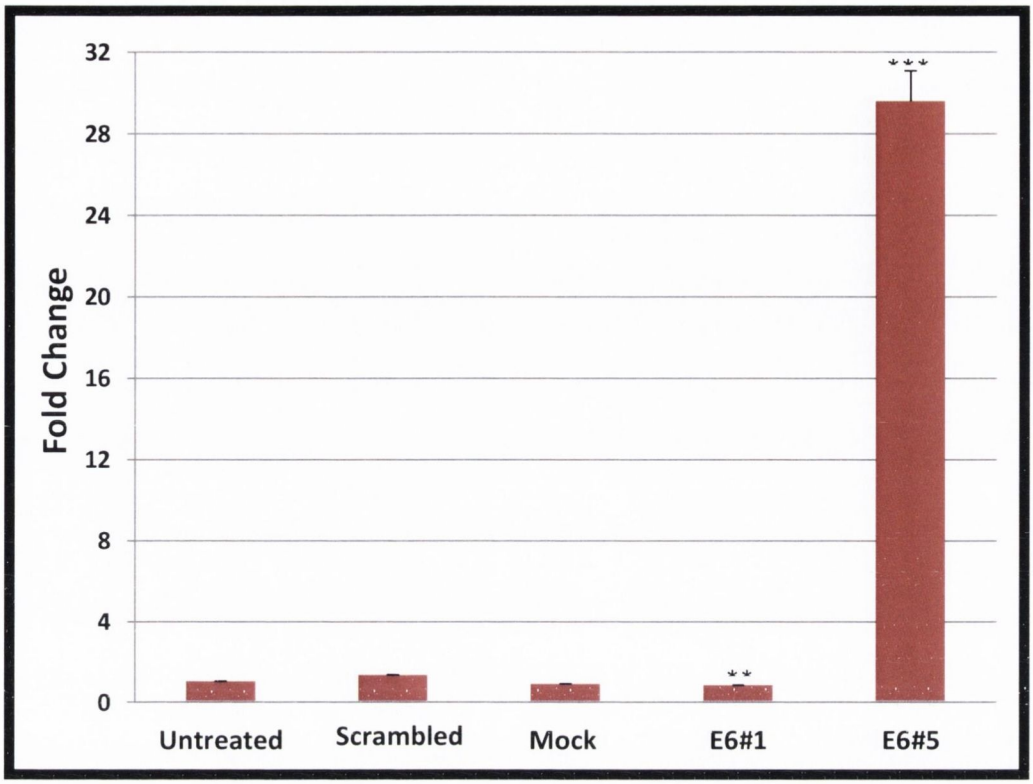

Figure 3-12: Assessing p21 expression in previous E6 mRNA. Si Ha cells seeded at 1.5x 10^5 were left untreated, mock-transfected, transfected with scrambled control siRNA, transfected with GAPDH targeting siRNA (10nM) – not shown, transfected with E6#1 and E6#5 targeting siRNA in three biological replicates for 72hrs. After 72 hours incubation, total RNA was extracted and mRNA expression levels were assessed via TaqMan RT-PCR using primers and probes selective for p21 mRNA from the same cDNA used to assess E6 and E7 mRNA levels. p21 mRNA expression was normalised to B2M and calibrated to untransfected control establish the relative level of mRNA expression. A paired T-test via graph pad prism was carried out and values calculated were compared to scrambled control; **p<0.1 ***p<0.001

3.4.2. Silencing of HPV16 E6 and E7 using a panel of 5 siRNAs

Five HPV16 E6 siRNAs (E6#1, E6#2, E6#3, E6#4 and E6#5) were designed to silence endogenous E6 expression in the SiHa cell line. E6#1, E6#2 and E6#3 were designed in-house and E6#4 and E6#5 were designed by Ambion. In order to assess the potency of E6#1, E6#2, E6#3, E6#4 and E6#5 in silencing HPV16 E6 and/or E7 expression in SiHa cells, TaqMan® RT-PCR primers and probes sets were designed to detect E6 mRNA (full length E6 and its splice form E6*I), E7 mRNA as well as full length E6 mRNA only. SiHa cells were independently transfected with five siRNAs E6#1, E6#2, E6#3 E6#4 and E6#5 for 72hrs using the forward transfection technique. 72hrs post transfection, total RNA was extracted and the levels of expression of E6, E7 and full-length E6 mRNA only were assessed using TaqMan® RT-PCR (Figure 3-13). There were no significant differences in mRNA expression levels between SiHa cells left untreated, mock-transfected and transfected with scrambled control siRNA and all expression values were within biological variation of between 50% and 200%. E6#2, E6#3 and E6#4 siRNAs resulted in simultaneous reduction of E6 and E7 expression as well as full-length E6 mRNA expression; E6#3 siRNA had the greatest effect on the expression of all three with average mRNA percentage of 3.9, 5.1 and 13.2, followed by E6#4 siRNA with 14.3%, 16.1% and 34%, and E6#2 siRNA with 25.9%, 17.6% and 20.6% respectively (Figure 3-13). E6#5 siRNA also had a simultaneous reduction of E6 and E7 expression but no significant effect on full-length E6 mRNA expression (Figure 3-13) while E6#1 siRNA resulted in reduction of full-length E6 mRNA only expression but had no significant effect on of E6 and E7 expression (Figure 3-13).

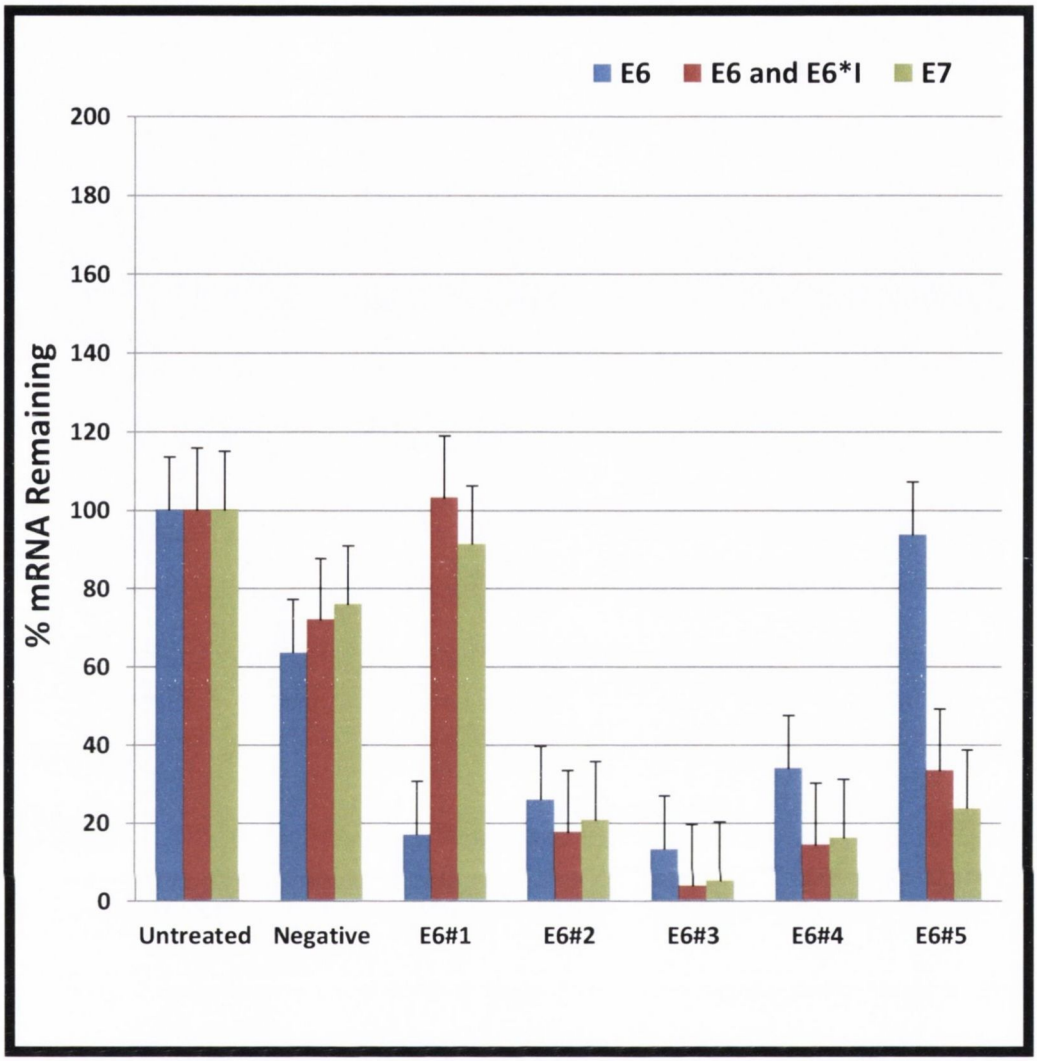

Figure 3-13: E6 and E7 mRNA silencing in SiHa cells using the forward transfection technique at 72 hours. SiHa cell line seeded at 1.5x 10^5 were left untreated, mock-transfected, transfected with scrambled control siRNA, transfected with E6#1, E6#2, E6#3, E6#4 and E6#5 targeting siRNA in three biological replicates for 72hrs. After 72 hours incubation, total RNA was extracted and mRNA expression levels were assessed using E6 and E7 specific TaqMan® RT-PCR primers and probes (panel A). Primers and probes selective for p21 mRNA were also assessed from same cDNA (panel B). Each mRNA expression was normalised to B2M and calibrated to untransfected control to establish the relative level of mRNA expression.

In spite of the apparent null effect of E6#1 siRNA on E6 and E7 expression as well as E6#5 siRNA on full length E6 only expression, considerable morphological differences were observed for these two siRNAs as depicted in Figure 3-14, Figure 3-15 and Figure 3-16. Morphological differences observed for E6#1 siRNA transfected cells revealed a condensed cytoplasm and cell shrinkage, with blebbing and apoptotic bodies which progressively became more pronounced as the time point post transfection increased from 24 to 48 to 72hrs (Figure 3-14, Figure 3-15 and Figure 3-16).

E6#2 siRNA transfected cells are also exhibited a similar profile of condensed cytoplasm and cell shrinkage, with blebbing and apoptotic bodies but to a lesser extent (Figure 3-14, Figure 3-15 and Figure 3-16). E6#3 siRNA transfected cells exhibited a rounded, refractile morphology with no tight cell-cell contacts and some cell floating dead cells (Figure 3-14, Figure 3-15 and Figure 3-16). E6#4 and E6#5 siRNA transfected cells had increased size and volume with a larger and flattened elongated morphology more evident in E6#4 than E6#5 siRNA compared to the controls (Figure 3-14, Figure 3-15 and Figure 3-16). However, no significant morphological differences were observed between the untreated, mock-transfected and scrambled control siRNA transfected cells in Figure 3-14, Figure 3-15 and Figure 3-16.

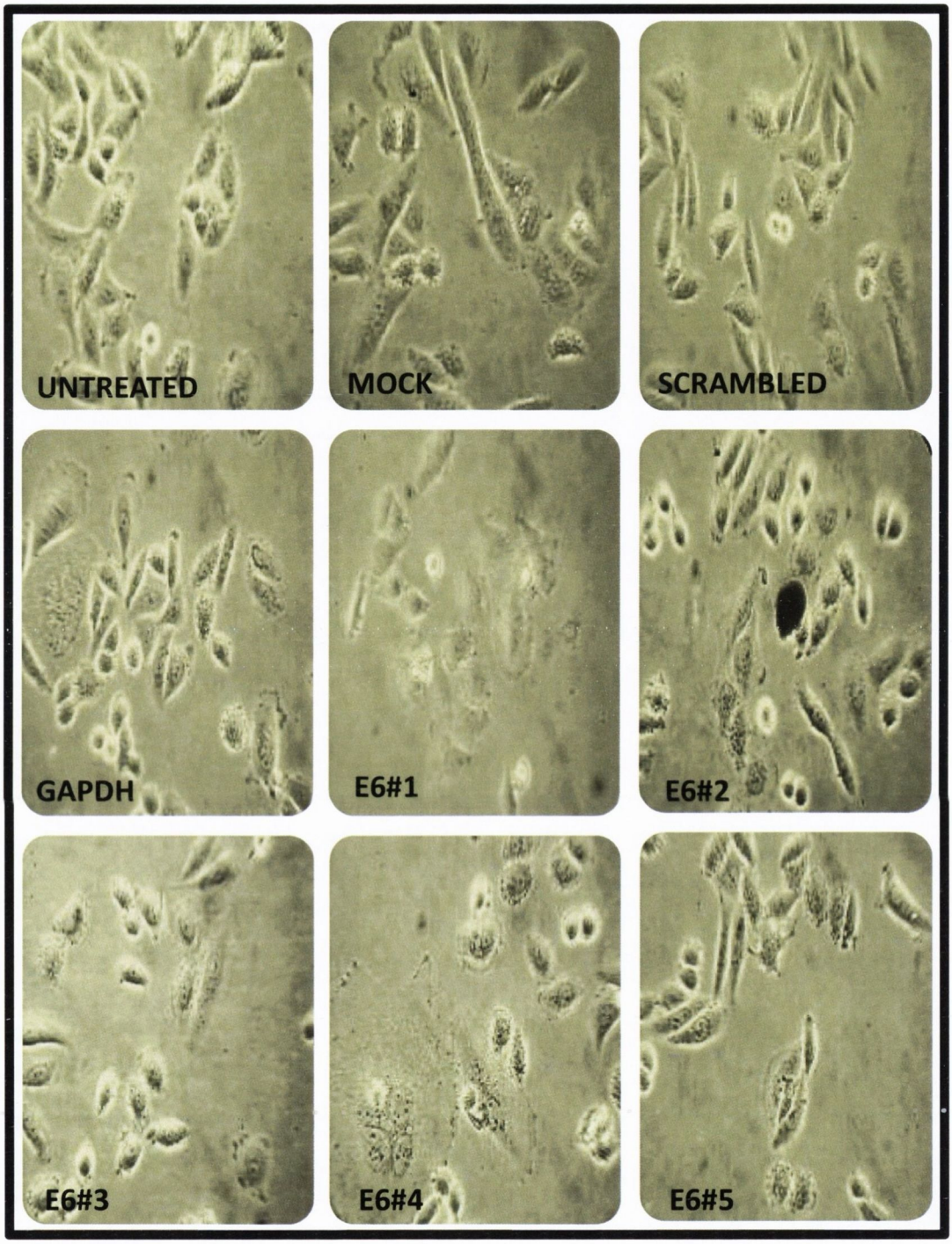

Figure 3-14: Light microscopy of SiHa cells 24hrs post forward transfection technique. SiHa cells seeded at $1.5x10^5$ cells were left untreated, mock-transfected, transfected with scrambled control siRNA and transfected with GAPDH targeting siRNA or E6 targeting siRNA (E6#1-E6#5)in three biological replicates. After 24 hours, cells were examined by light microscopy. No morphological differences were observed between the untreated, mock-transfected, transfected with scrambled control siRNA and cells transfected with GAPDH siRNA, E6 #1, E6#2, E6#3, E6#4 and E6#5 transfected cells show slightly altered morphologies (Magnification 200x).

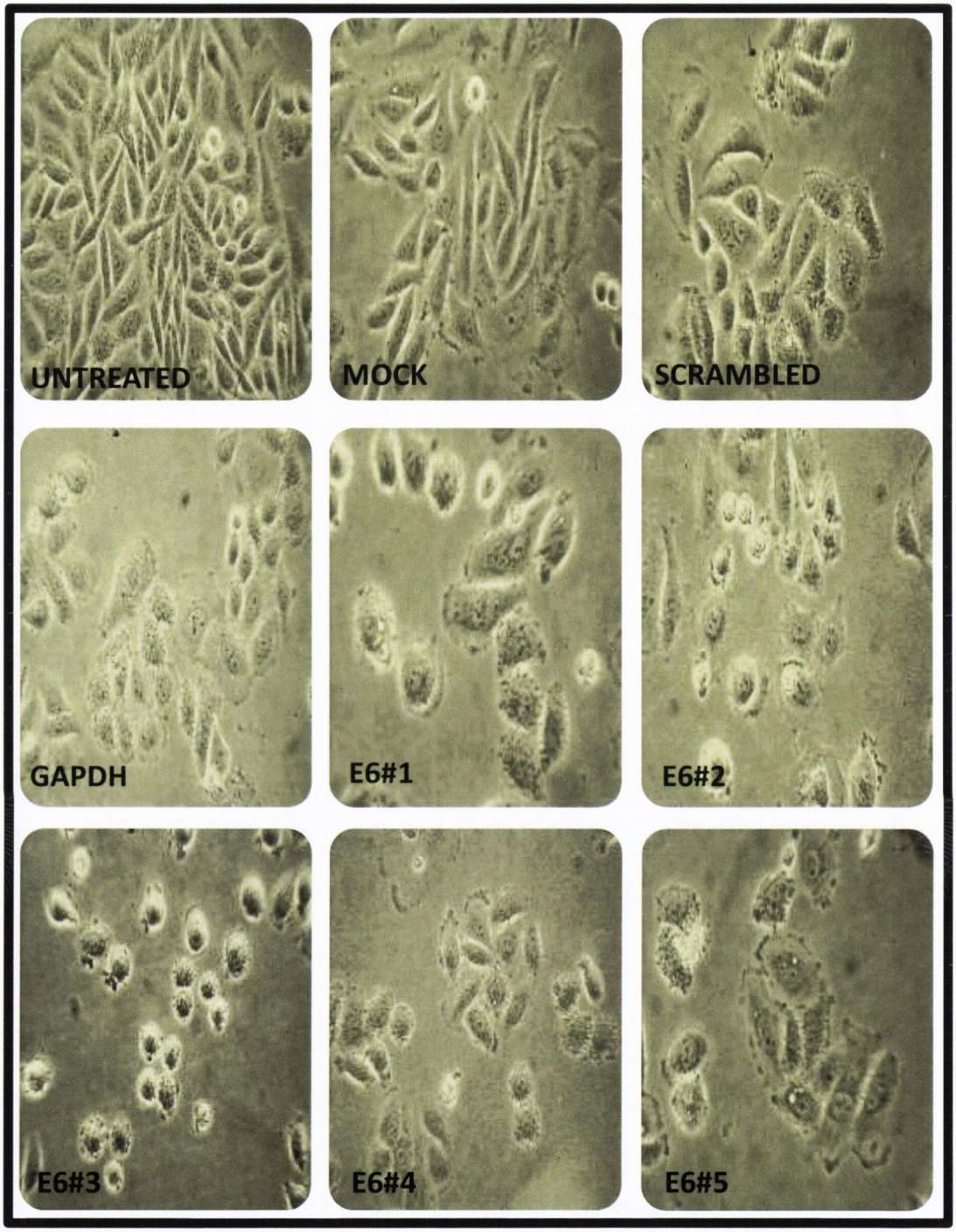

Figure 3-15: Light microscopy of SiHa cells 48hrs post forward transfection technique. SiHa cells seeded at $1.5x10^5$ cells were left untreated, mock-transfected, transfected with scrambled control siRNA and transfected with GAPDH targeting siRNA or E6 targeting siRNA (E6#1-E6#5)in three biological replicates. After 48 hours, cells were examined by light microscopy. No morphological differences were observed between the untreated, mock-transfected, transfected with scrambled control siRNA and cells transfected with GAPDH siRNA show similar morphology as previously stated. E6#1 and E6#2 transfected cells appear to have condensed cytoplasm and cellular shrinkage. E6#3 transfected cells appear to be rounding up while E6#4 and E6#5 siRNA show slower growth, flattened appearance (Magnification 200x).

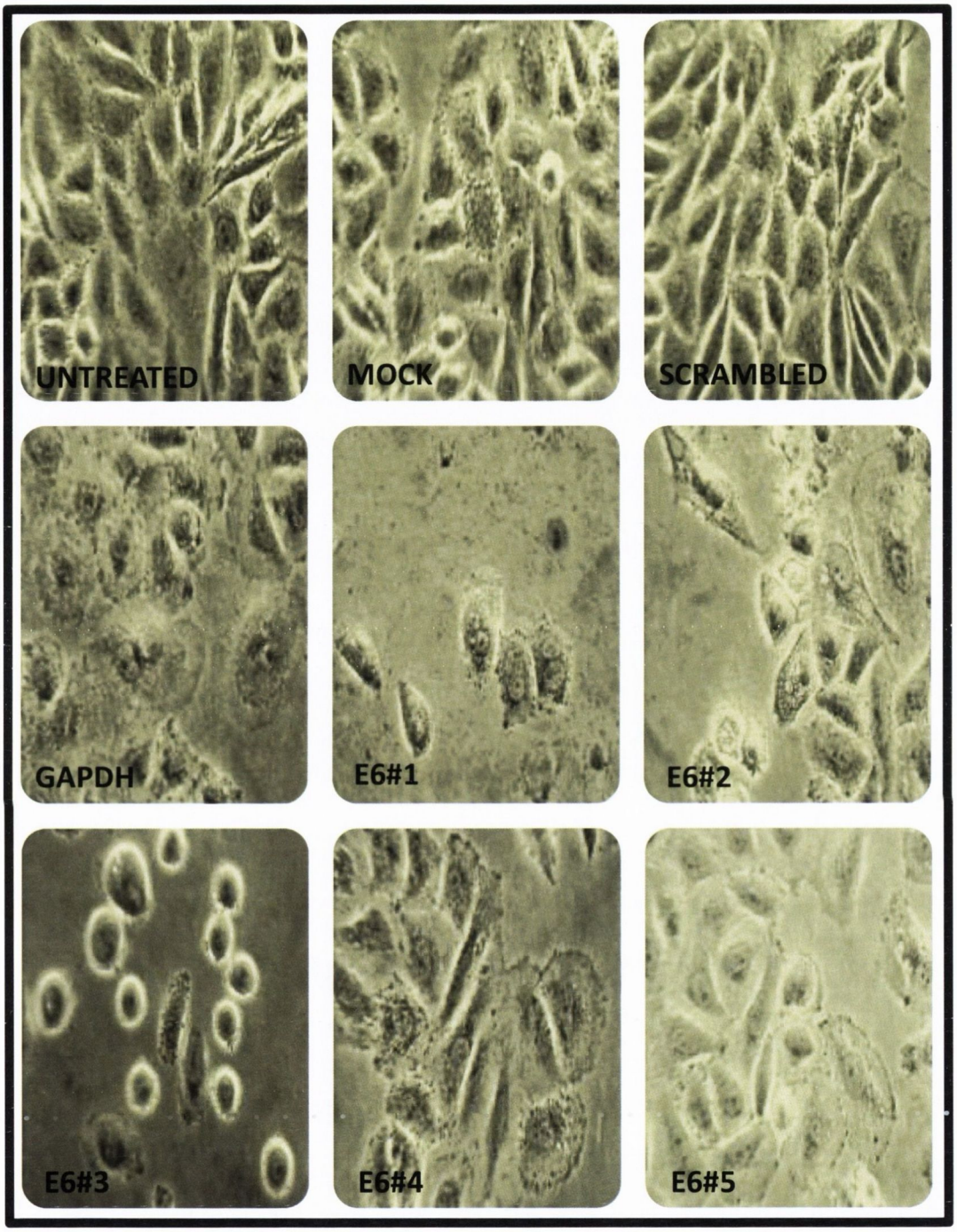

Figure 3-16: Light microscopy of SiHa cells 72hrs post forward transfection technique. SiHa cells seeded at $1.5x10^5$ cells were left untreated, mock-transfected, transfected with scrambled control siRNA and transfected with GAPDH targeting siRNA or E6 targeting siRNA (E6#1-E6#5)in three biological replicates. After 72 hours, cells were examined by light microscopy. No morphological differences were observed between the untreated, mock-transfected, transfected with scrambled control siRNA and cells transfected with GAPDH siRNA show similar morphology as previously stated. E6#1 and E6#2 transfected show condensed cytoplasm, membrane blebbing and cellular shrinkage and cell death with E6#2 siRNA having less cell death than E6#1 cells. E6#3 transfected cells appeared rounded up with a refractile appearance with some cell death. E6#4 and E6#5 transfected cells were spread out with fewer tight cell junctions, slower growth and flattened appearance (Magnification 200x).

Consequently, to correlate alterations in E6 expression in these knockdowns, p21, expression levels were assessed to indirectly quantitate E6 expression. TaqMan RT-PCR analysis was performed on the same cDNA used for E6 and E7 mRNA expression using p21 specific TaqMan® RT-PCR primers and probes and expression levels were assessed as fold changes as depicted in Figure 3-17. There were no significant fold changes in p21 mRNA expression levels between SiHa cells left untreated, mock-transfected and scrambled control siRNA transfected and all expression values were within biological variation of between 0 and 2. E6#1, E6#2, E6#3 showed a statistically significant ($p<0.05$) fold increase in p21 expression with values of 2.2, 2.6 and 2.7 respectively, however, E6#4 and E#5 siRNAs showed highly significant fold ($p<0.001$) changes 9.9 and 9.5 respectively (Figure 3-17).

Subsequently, protein extracted from all adherent cells 72hrs post transfection was used to assess the levels of functional inhibition of E6 and E7 expression via antibodies against their targeted proteins p53. p21 levels were also assessed and GAPDH antibody was used as loading control in these experiments (Figure 3-17). A highly substantial increase in p53 protein levels was observed in E6#4 and E6#5 siRNAs compared to negative siRNA transfected or untreated cells (Figure 3-17A) with a concomitant rise in p21 levels in both siRNAs (Figure 3-17 B). These results correlate with highly significant fold increase observed in p21 mRNA expression at TaqMan® RT-PCR levels (Figure 3-17). E6#2 siRNAs exhibited a considerable rise in p53 and p21 protein levels compared to the controls (negative siRNA transfected or untreated cells) (Figure 3-18 A and B respectively). This was also observed at TaqMan® RT-PCR levels as a significant fold change of 2.6 in p21 expression levels in Figure 3-17. E6#3 siRNAs also exhibited a considerable rise in p53 protein level with no increase in p21 protein level compared to the controls (negative siRNA transfected or untreated cells) (Figure 3-18 A and B respectively) although a significant fold change of 2.7 in p21 expression levels was observed at TaqMan® RT-PCR levels as in Figure 3-17.

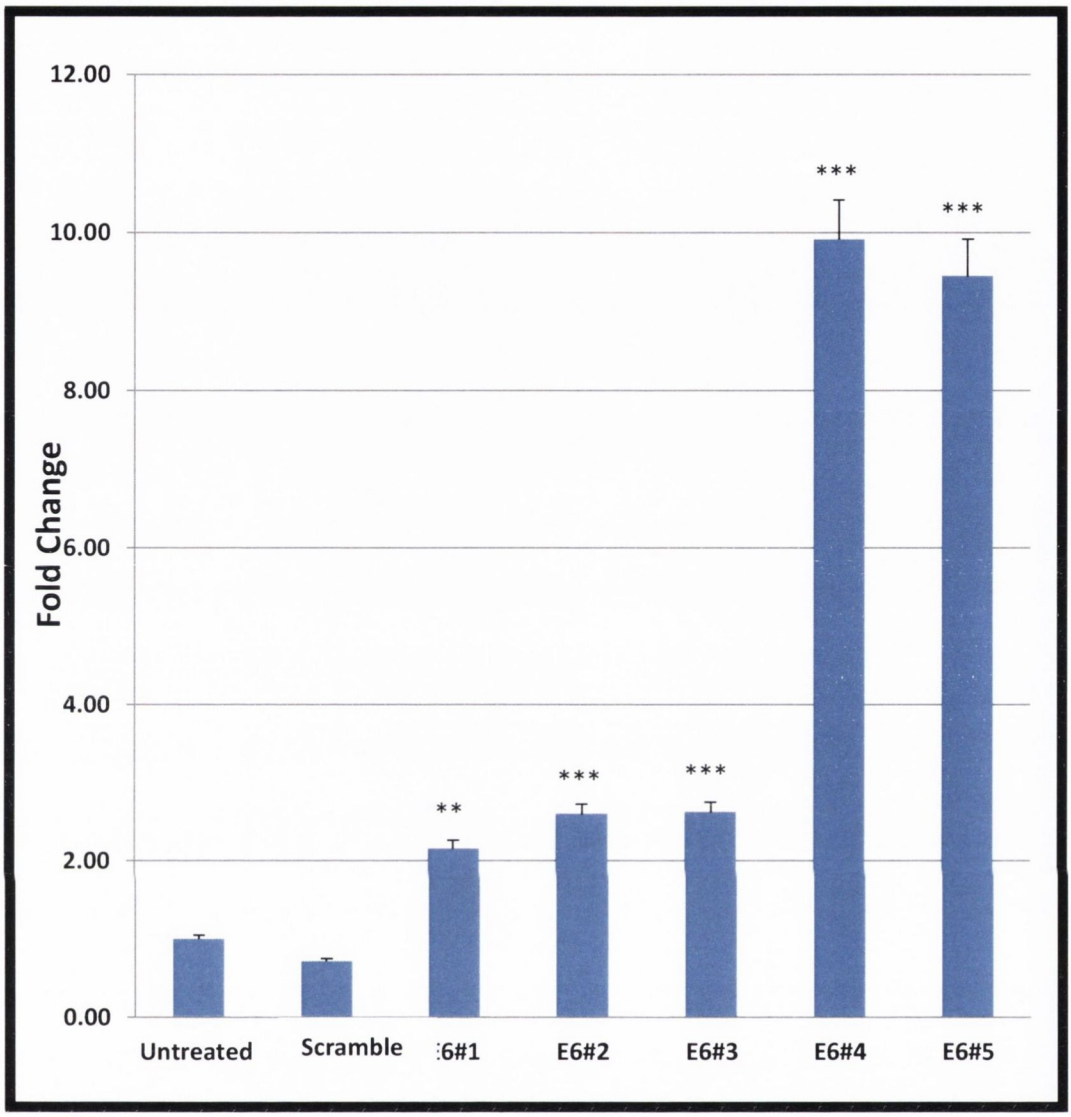

Figure 3-17: Assessing p21 expression in SiHa cell line using forward transfection technique at 72 hours. SiHa cells seeded at 1.5x 10^5 were left untreated, mock-transfected, transfected with scrambled control siRNA, transfected with E6#1, E6#2, E6#3, E6#4 and E6#5 targeting siRNA in three biological replicates for 72hrs. After 72 hours incubation, total RNA was extracted and mRNA expression levels were assessed using primers and probes selective for p21 mRNA were also assessed from same cDNA. Each mRNA expression was normalised to B2M and calibrated to untransfected control to establish the relative level of mRNA expression. . A paired T-test via graph pad prism was carried out and values calculated were compared to scrambled control; **p<0.1 p***p≤0.05.

E6#1 siRNA, however, showed no increase in p53 or p21 levels (Figure 3-18A and B) despite a slight fold increase of 2.2 in p21 mRNA expression at TaqMan® RT-PCR level in Figure 3-17. The result of the western blot analysis correlates with that of RNA analysis in relation to biomarker assessment of E6 expression. However, a direct correlation in the magnitude of the efficiency of these siRNAs at knocking down E6 and E7 expression do not correspond with observed western blot analysis. E6#3 siRNA induced the most potent knockdown of E6 and E7 at RNA level via TaqMan® RT-PCR (Figure 3-17) yet its protein analysis depicts that it is not as efficient as E6#4 or E6#5 as there are far more abundant levels of p53 and p21 (Figure 3-18A and B respectively) in E6#4 and E6#5 than E6#3 or even E6#2 siRNAs. The potency of E6#1 siRNA could not be efficiently assessed at protein level (Figure 3-18A and B) as TaqMan RT-PCR analysis suggested silencing of E6 and not E7 by E6#1 siRNA (Figure 3-13 and 3-17) which should correlate in a rise in p53 and p21 protein levels (Figure 3-18A and B).

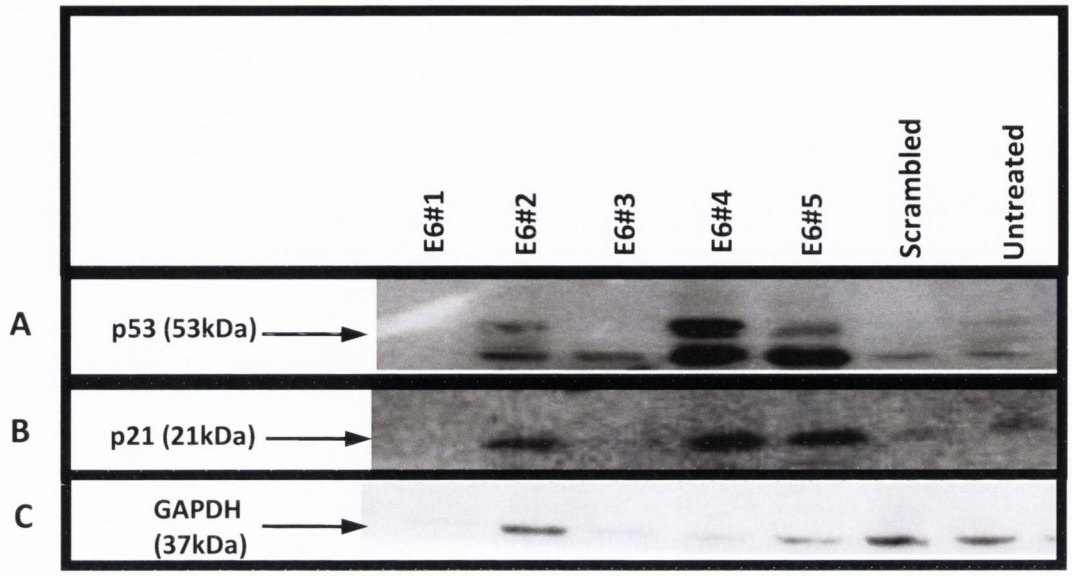

Figure 3-18: Silencing of HPV16 E6 protein in the SiHa cell line 72hrs post forward transfection technique. SiHa cells seeded at $1.5x10^5$ cells were left untreated, mock-transfected, transfected with scrambled control siRNA or E6 targeting siRNAs (E6#1, E6#2, E6#3, E6#4 and E6#5). Cells were lysed by sonication and 30ug of lysate proteins resolved on NuPage Novex 4-12% Bis Tris MiniGels and electrotransferred to PVDF membranes. The membranes were blocked in 5% non-fat dry milk and immunoblotted for p53 (panel A), p21 (panel B). All membranes were stripped and re-immunoblotted for GAPDH (panel C), which was used as a loading control. This figure shows of E6#1-E6#5 siRNA immunoblotted with p53 antibody in the top panel labelled A, p21 antibody in the middle panel labelled B and GAPDH antibody as loading control in the bottom panel labelled C. No bands appear for E6#1 siRNA when probed with any of the three antibodies. E6#2, E6#4 and E6#5 siRNA have bands for p53 and p21 antibodies, although its loading control appears slightly more. E6#3 siRNA has bands for p53 and GAPDH loading control antibody. The double banding of p53 in the above blot reflects differential phosphorylation status of p53 or different p53 isoforms resulting from differential splicing, polymorphisms or alternative promoter usage often seen.

3.4.3. HPV16 E6 siRNAs drive cellular senescence

In order to further examine the potency of E6 siRNAs at silencing E6 and E7, a senescent cell histochemical staining was carried out 72hrs post independent transfection of SiHa cells with all 5 siRNAs (E6#1, E6#2, E6#3 E6#4 and E6#5).

The results demonstrated that there was no statistically significant increase in the levels of β-galactosidase activity in E6#1 and E6#2 transfected cells (Figure 3-19). However, an extremely statistically significant ($p<0.0001$) increase in β-galactosidase activity was observed with E6#3 E6#4 and E6#5 (See Figure 8-1 in the appendix) compared to the untreated or scrambled control siRNA transfected cells (Figure 3-19). The level of significance was based at their two-tailed P value being ≤ 0.0001. The degree of β-galactosidase activity observed with the E6#1, E6#3, E6#4 and E6#5 siRNAs correlates with earlier mRNA and protein analysis on p21 levels Figure 3-17 and Figure 3-18B. Protein analysis of cells transfected with E6#4 and E6#5 siRNAs show that they have the greatest accumulation of p53 and p21 (Figure 3-18 A and B) which is translated in this experiment by their high significance in comparison to the scrambled control siRNA and untreated cells (Figure 3-19). Although E6#2 β-galactosidase activity does not seem to correlate with TaqMan RT-PCR analysis (Figure 3-17) and protein p21 (Figure 3-18 B) levels, the level of β-galactosidase activity is nonetheless insignificant.

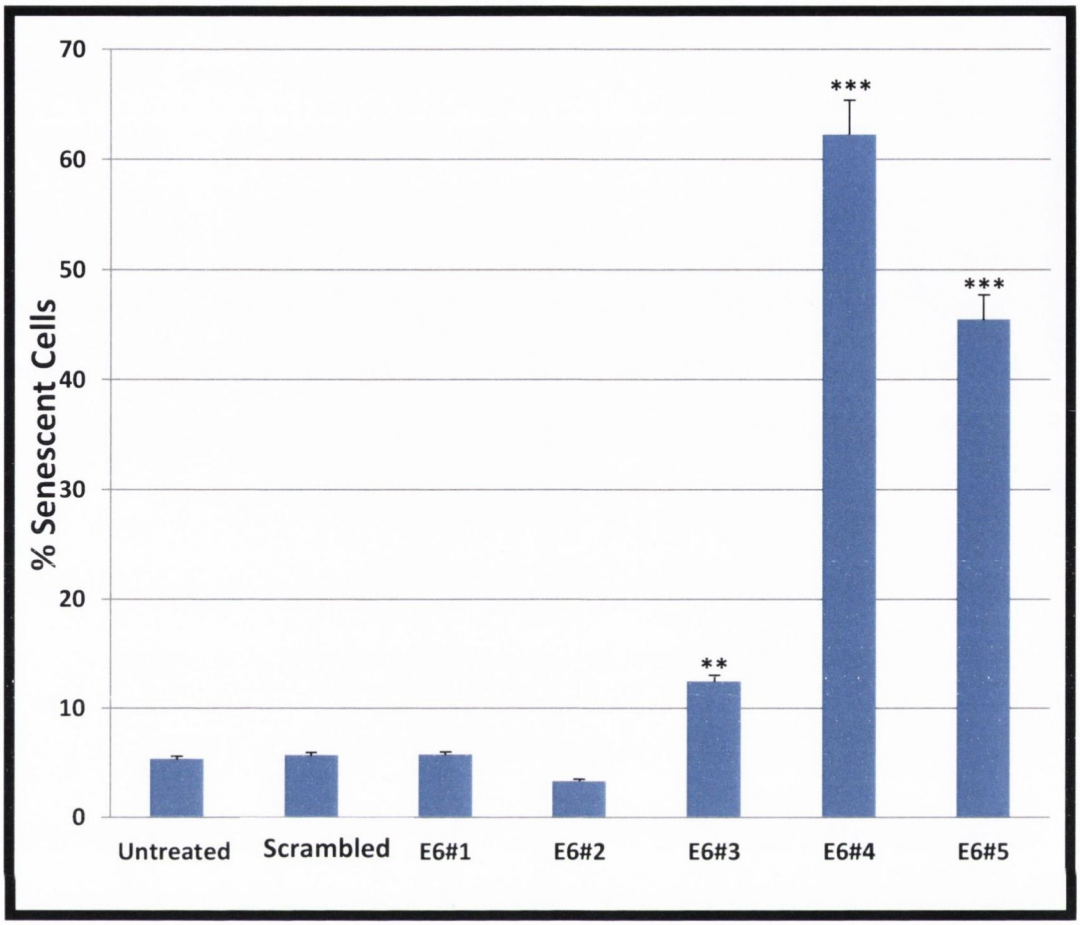

Figure 3-19: E6 siRNAs induce cellular senescence in the SiHa cell line 72hrs post forward transfection technique. SiHa cells seeded at $1.5x10^5$ cells were left untreated, mock-transfected (not shown), transfected with scrambled control siRNA (10nM) or E6 targeting siRNAs (E6#1, E6#2, E6#3, E6#4 and E6#5). 72hours post transfection; cells were fixed and stained with a mixture containing X-gal solution as substrate and incubated overnight in a CO_2 deprived atmosphere. The following day, the number of blue-stained cells was counted in four fields and analysed using a paired T-test via graph pad prism. The histograms represent the percentage of blue-stained cells post transfection for each siRNA. Results are representative of three biological replicates. Values calculated were compared to scrambled control; **p=0.0001 ***p<0.0001

3.4.4. HPV16 E6 siRNAs inhibit cell proliferation

Due to the role of HPV E6 in inhibiting p21 transcription and E7 in promoting cell cycling, the effect of silencing of E6 and E7 by the E6 siRNAs was examined to determine if the morphological phenotypes observed were in any relation to a decrease in cellular proliferation. SiHa cells were transfected independently with all 5 siRNAs (E6#1, E6#2, E6#3 E6#4 and E6#5) and 72hrs post transfection, all adherent and non-adherent cells were harvested and stained with propidium iodide (PI). Figure 3-20 and Figure 3-21 show that though no significant changes in the cell cycle were induced by the controls, three of the five siRNAs (E6#3, E6#4 and E6#5) had significantly varying effects on the progression through the phases of the cell cycle.

Comparing the controls in Figure 3-20A-C, (untreated, mock transfected and negative siRNA transfected cells respectively) with E6#1 siRNA (Figure 3-20D), these cells have a G1 positive cell population, a slightly larger S phase population and G2/M positive cell population. A sharp peak in the histogram representative of a distinct sub-population of debris/dead cells highlighted in green is also observed. This peak appears to be the highest in E6#1 siRNA compared to other controls and other siRNAs analysed. In addition, E6#1 siRNA cells show no increase in forward scattering profile that is light scattered by cells in the forward direction or straight through (Figure 3-21D).

Likewise, E6#2 siRNA exhibits a histogram profile (Figure 3-20E) very similar to the controls (Figure 3-20A-C) with a portion of G1 positive cells and a proportion of S phase and G2/M phase positive cells. A significant broad peak representative of a proportion of debris/dead cells is also present in Figure 3-20E. The light scattering profile of E6#2 siRNA portrays no cells with an increase in forward scattering (Figure 3-21E) like E6#1 siRNA.

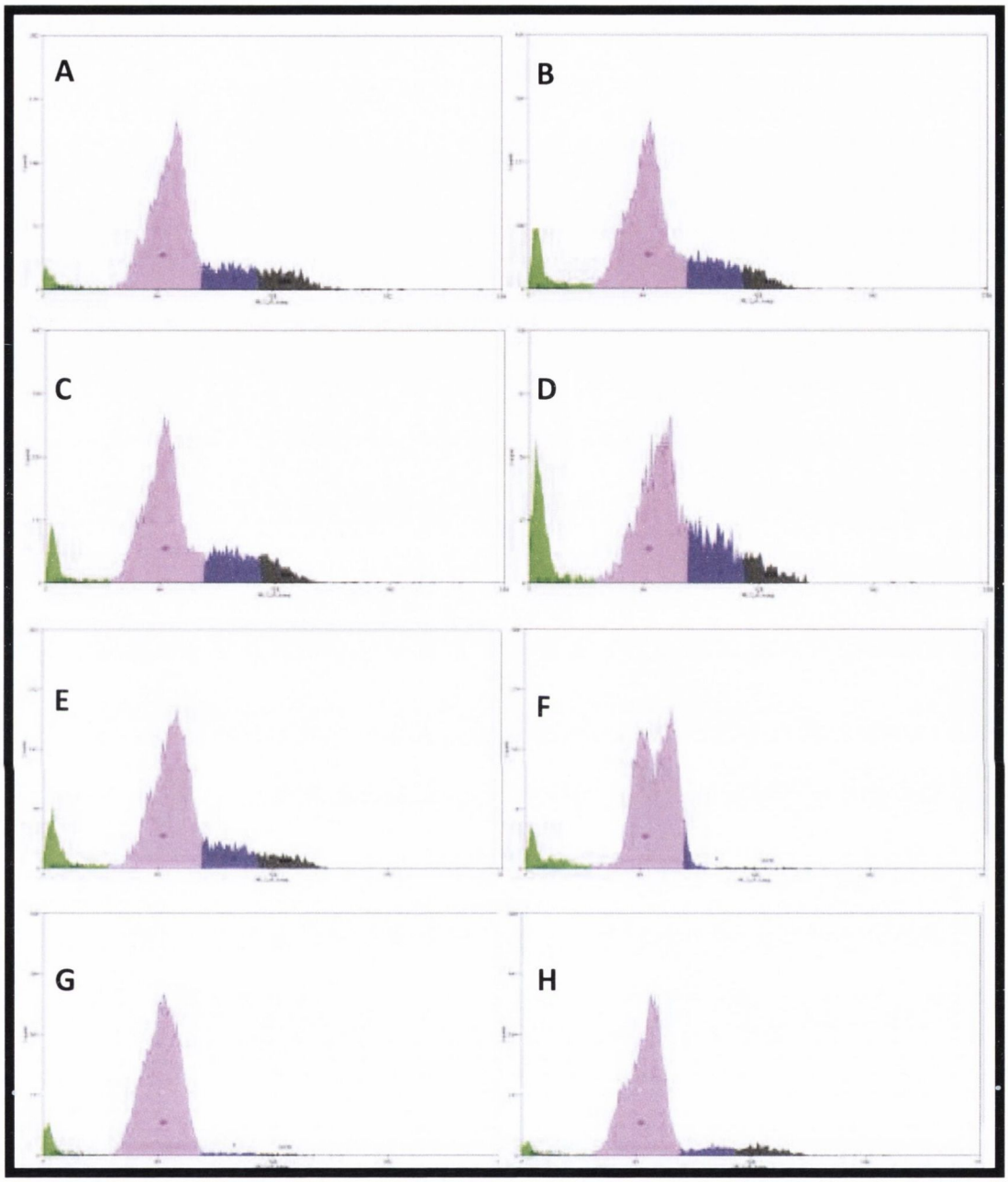

Figure 3-20: Descriptive histogram of cell cycle analysis on SiHa cells 72hrs post E6 siRNA transfection. SiHa cells seeded at $1.5x10^5$ cells were left (A) untreated, (B) mock-transfected, (C) transfected with scrambled control siRNA (10nM) or E6 targeting siRNAs (E6#1 (D), E6#2 (E), E6#3 (F), E6#4 (G) and E6#5(H)). 72 hours post transfection, all cells were collected (adherent and non-adherent), stained with PI and analysed by flow cytometry. The histograms show apoptotic cells (*green*), G1 phase *(pink)*, S phase *(purple)* and the G2/M phase *(black)* of the cell cycle. The data presented is from one complete experiment and representative of three biological replicates. Values were calculated compared to scrambled control; **p=0.0001 ***p<0.0001

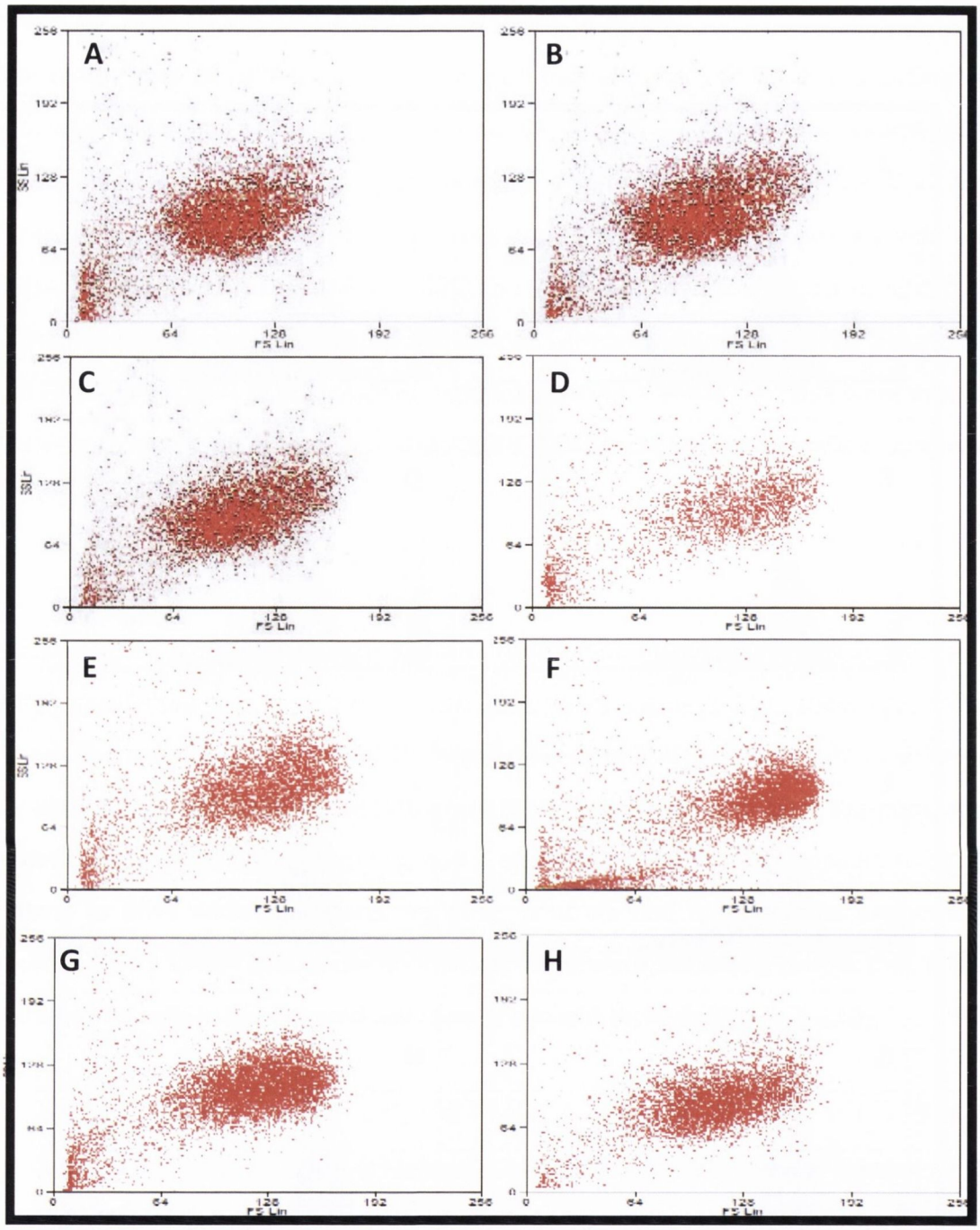

Figure 3-21: Light scatter plot of SiHa cell line 72hrs post forward transfection technique. SiHa cells seeded at $1.5x10^5$ cells were left (A) untreated, (B) mock-transfected, (C) transfected with scrambled control siRNA (10nM) or E6 targeting siRNAs (E6#1 (D), E6#2 (E), E6#3 (F), E6#4 (G) and E6#5(H). 72 hours post transfection, all cells were collected (adherent and non-adherent), stained with PI and analysed by flow cytometry. The dual parametric dot plots combine side and forward scatter profiles of the cells. The side scatter on the vertical axis is proportional to cellular granularity that is the more granular a cell, the greater the light scatters and the higher the signal detected. The forward scatter on horizontal axis is proportional to cell size that is the larger the cell the greater the light scatter and the higher the signal detected. The data presented is from one complete experiment and representative of three biological replicates. E6#3 depicts a highly compact cell population at the mid-centre right of the plot compared to the controls. E6#3, E6#4 and E6#5 portray profiles indicative of senescence.

E6#3 siRNA displayed the most dramatic change in the histogram profile of cell populations at different stages of the cycle with a double peak of G1 positive cell population, a corresponding complete loss of S phase and G2/M phase positive cell population in Figure 3-20F. This dramatic shift was also correlated on the light scattering profile of E6#3 siRNA (Figure 3-21F) compared to the controls (Figure 3-21A-C). In other words, there is an increase in forward and side scattering (Figure 3-21F) compared to the untreated, mock transfected and negative siRNA transfected cells (Figure 3-21A, B and C respectively) suggestive of senescence. E6#4 siRNA exhibits a similar pattern to E6#3 siRNA, with a single population of G1 phase positive cell population, a complete loss of S and G2/M phase positive cells in Figure 3-20G). The light scattering profile of E6#4 siRNA demonstrates the greatest increase in forward and side scattering (Figure 3-21H) compared to other siRNAs and to the untreated, mock transfected and negative siRNA transfected cells (Figure 3-21A, B and C respectively) and also suggestive of senescence. E6#5 siRNA also shows a similar profile to E6#3 and E6#4 siRNA, with a single population of G1 phase positive cell population and a complete loss of S and G2/M phase positive cells (Figure 3-20H), although there is less of a G1 cell population than E6#3 andE6#4. The light scattering profile of E6#5 siRNA also demonstrates an increase in forward and side scattering (Figure 3-21H) similar to E6#4 (Figure 3-21G) compared to the untreated, mock transfected and negative siRNA transfected cells (Figure 3-21A, B and C respectively) similarly suggestive of senescence.

In summary, E6#1 and E6#2 displayed no inhibiting impact on cell cycle progression, although a significant of amount of dead cells was observed in histogram profiles for both. E6#2 however, displayed significant oncogene suppression at RNA level as well as a rise in the level of p53 and p21 proteins with no significant increase in the levels neither of β-galactosidase activity nor in the number of cells at different stages of the cell cycle. While E6#1 portrayed only a significant E6 oncogene suppression at RNA level with no increase in p53 and p21 protein nor β-galactosidase activity nor change number of cells at different stages of the cell cycle. As a result, further analysis was

required to ascertain the cause of the dramatic morphological changes observed in E6#1 and E6#2 siRNAs.

However, E6#3, E6#4 and E6#5 had highly substantial effects on cell cycle progression with a rise in G1phase positive cell population and a complete loss of S and G2/M phase positive cells. E6#3 cells displayed the greatest oncogene suppression at the RNA level as well as a rise in the level of p53 protein; yet, there was no concurrent increase in p21 protein levels. However, an extremely statistically significant ($p=0.0001$) increase in the levels of β-galactosidase activity was detected with an increase in forward and side light scattering. Conversely, E6#4 and E6#5 also exhibited oncogene suppression at RNA level, though to a lesser degree but with the highest rise in p53 and p21 expression levels, an extremely statistically significant ($p<0.0001$) increase in the levels of β-galactosidase activity and an increased forward and side light scattering profiles. These results for E6#3, E6#4 and E#5 siRNAs are suggestive of their inhibition of cell proliferation via G1 arrest/ senescence in the SiHa cell line.

3.4.5. HPV16 E6 siRNAs induce cellular apoptosis in SiHa cells

3.4.5.1. Apoptosis analysis using FITC/PI DNA staining

To assess the ability of E6 siRNAs to induce apoptosis post transfection, flow cytometry analysis was carried out 72hrs post transfection on all siRNAs (E6#1, E6#2, E6#3, E6#4 and E6#5) using Annexin V-FITC and propidium iodide (PI) dual staining. The fluorocytograms obtained in this part of the study were quite unusual as, no Annexin positive PI negative cell population was observed, this could infer to cellular dead occurring in these cells via process other than apoptosis (autophagy, associated with mitotic catastrophe, enzymatic or immunological involvement). Hence, a two quadrant analysis approach was employed to enable isolation of positive and negative cells. The cells at the bottom left hand side were representative of live cells (Annexin and PI negative) while cells at the upper right hand were representative of dead cells (no Annexin and Pi positive) (Figure 3-22).

No significant change in apoptotic profile amongst the untreated, mock-transfected and transfected with scrambled control siRNA controls (Figure 3-22A-C, Figure 3-23, Figure 3-24 A-D) was observed. In Figure 3-22, most cells are congregated at the lower left hand corner of the plot signifying live cells, with minor populations of dying cells spreading across the top half from left to right (Figure 3-22 A, B and C). In Figure 3-23, the bar chart demonstrates very similar percentages controls amongst the controls, with values of 79%, 72% and 75% live cells and 24%, 28% and 28% apoptosed cells in untreated, mock-transfected and transfected with scrambled control siRNA cells respectively. The single parameter histogram of untreated cells overlaid with mock-transfected (Figure 3-24A and B) and scrambled control siRNA (Figure 3-24C and D) show the absence of a positive dataset of cells stained with Annexin V-FITC (Figure 3-24A and C) and PI (Figure 3-24 C and D).

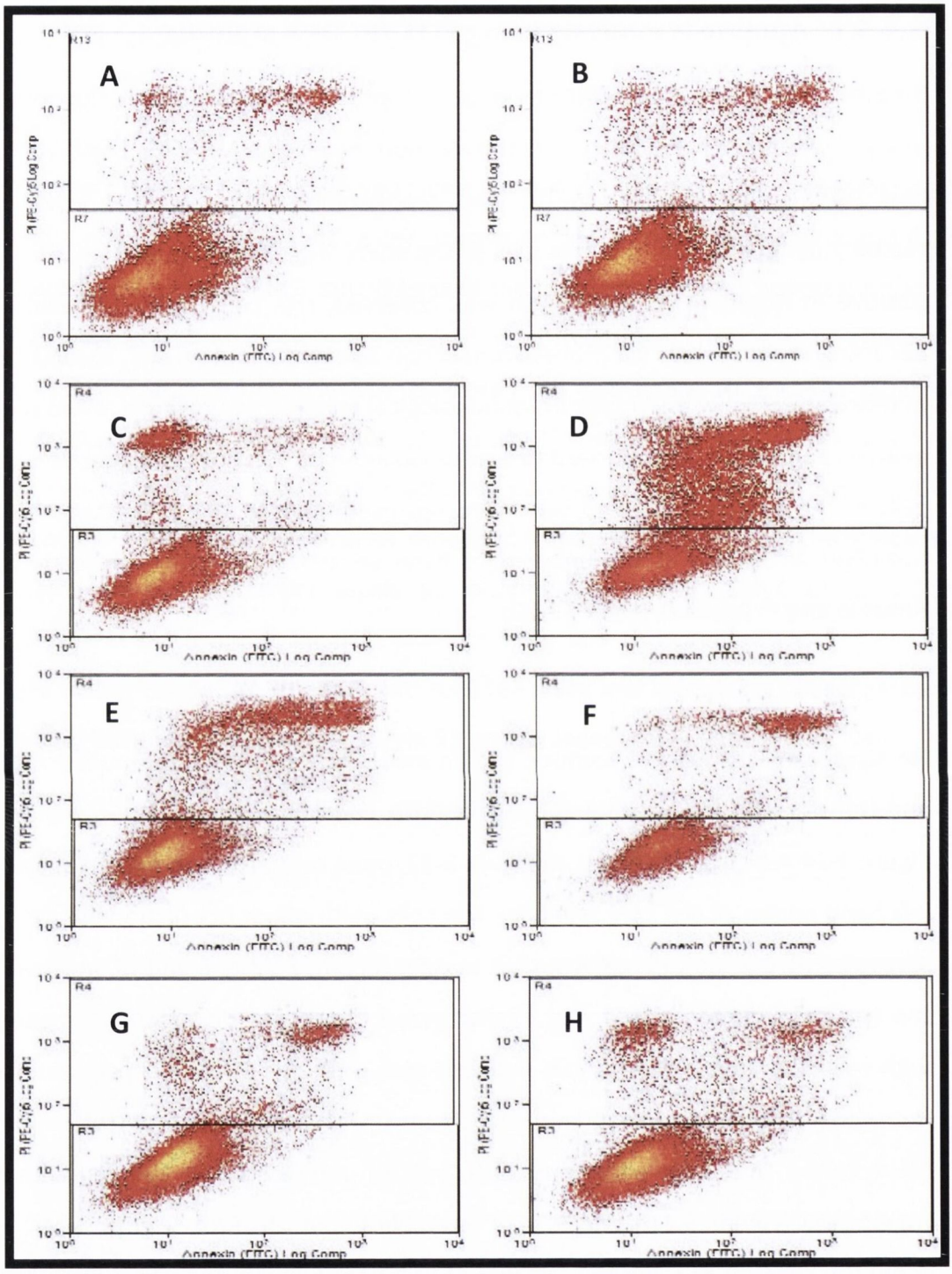

Figure 3-22: Dot Plot fluorocytograms of apoptosis analysis on SiHa cells 72hours post E6 siRNA transfection. SiHa cells seeded at $1.5x10^5$ cells were left (A) untreated, (B) mock transfected, (C) transfected with scrambled controll siRNA (10nM) or E6 targeting siRNAs; E6#1 (D), E6#2 (E), E6#3 (F), E6#4 (G) and E6#5 (H). 72 hours post transfection, all cells were collected (adherent and non-adherent), stained with FITC Annexin V and PI and analysed by flow cytometry. The dot plots show the movement of cells form lower left corner to upper right hand corner indicative of cells undergoing apoptosis. The data presented is representative of three biological replicates.

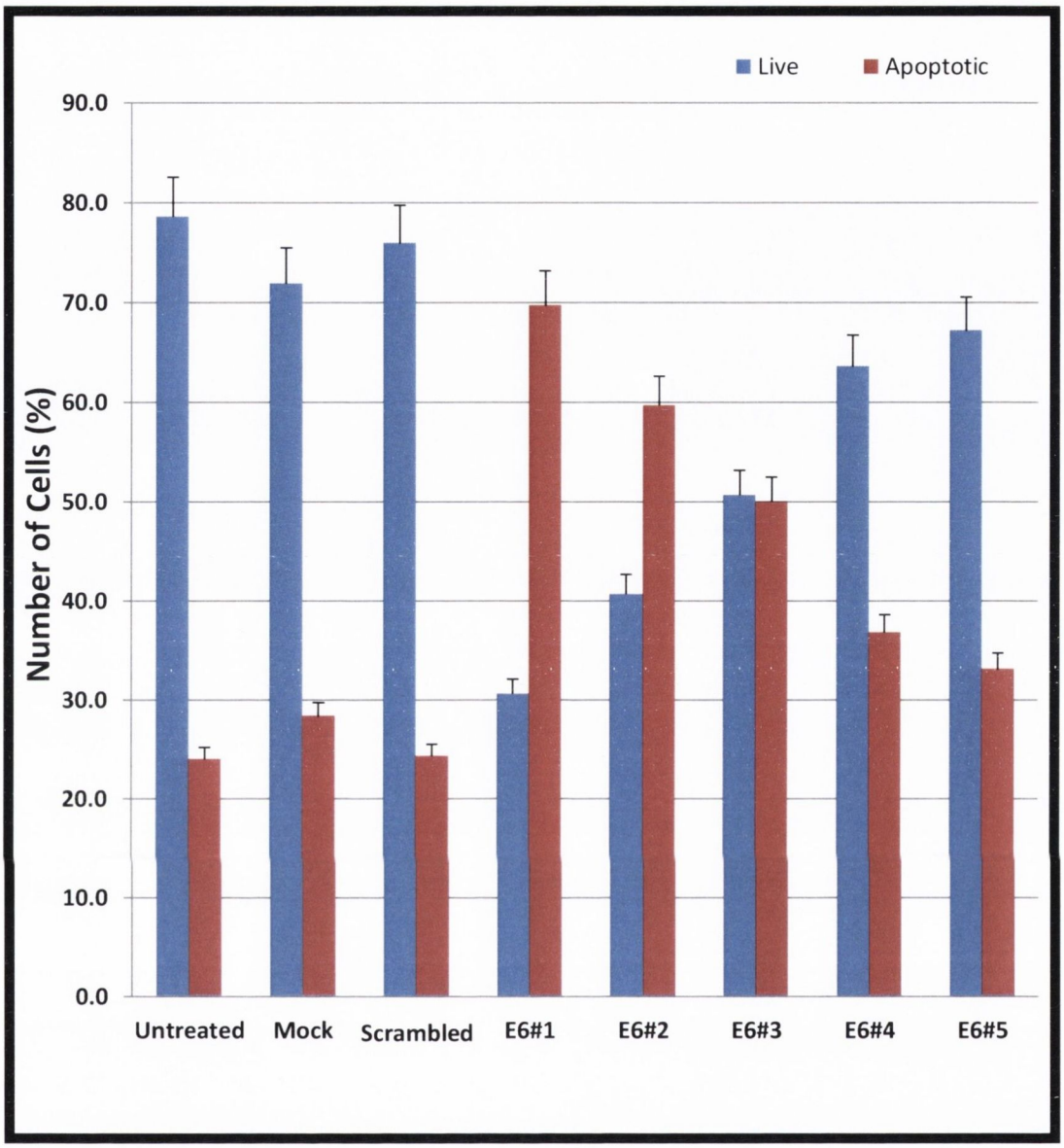

Figure 3-23: Bar chart of apoptosis analysis on SiHa cells 72 hours post E6 siRNA transfection. SiHa cells seeded at $1.5x10^5$ cells were left untreated, transfected with scrambled control siRNA (10nM) or E6 targeting siRNAs E6#1, E6#2, E6#3, E6#4 and E6#5 siRNA. 72 hours post transfection, all cells were collected (adherent and non-adherent), stained with FITC Annexin V and PI and analysed by flow cytometry. The bar chart depicts the percentage of live and dead cells for each condition. The data presented is representative of three technical replicates.

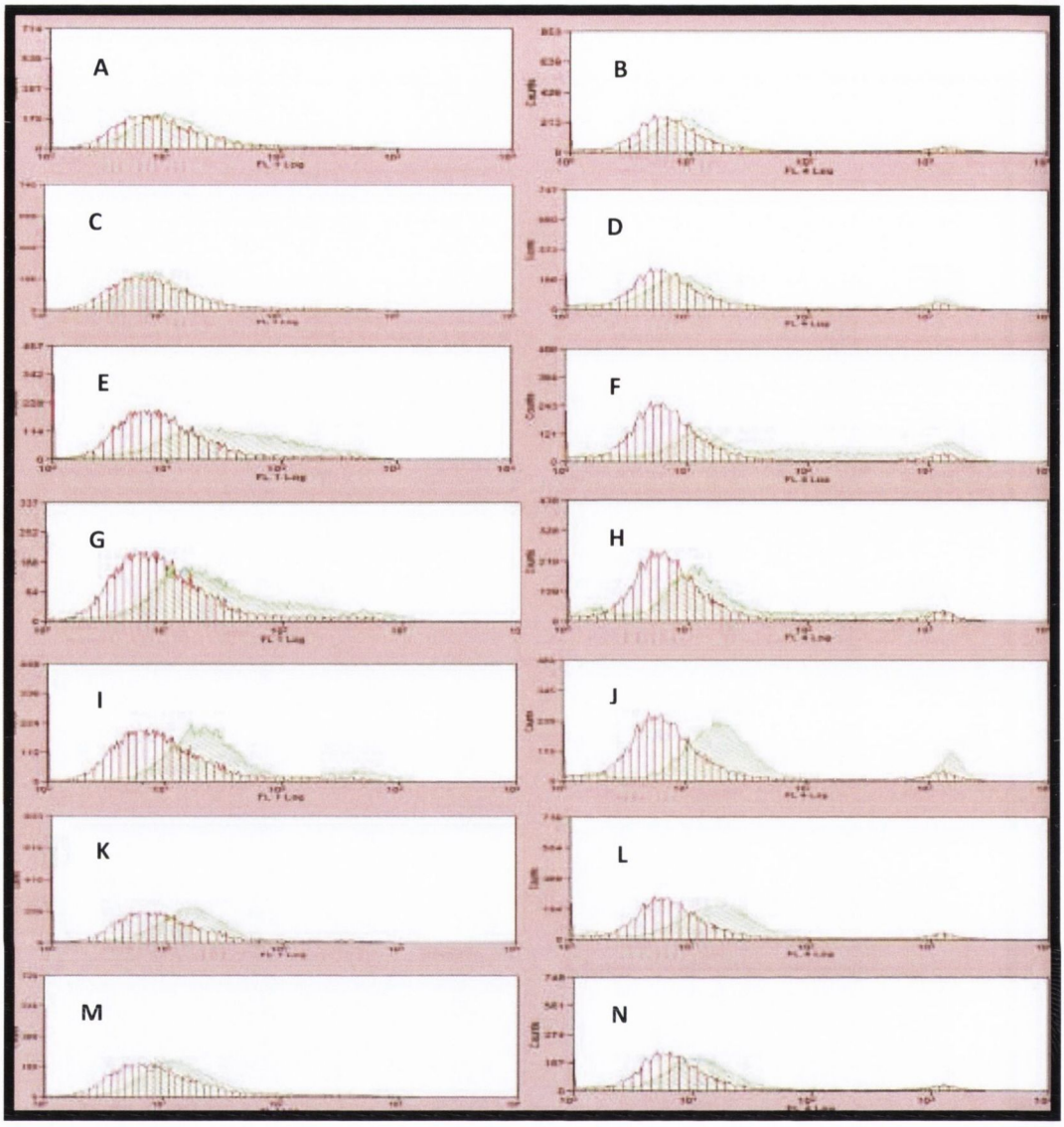

Figure 3-24: Overlay histograms fluorocytograms of apoptosis analysis on SiHa cells 72 hours post E6 siRNA transfection. SiHa cells seeded at $1.5x10^5$ cells were left untreated, mock transfected, transfected with scrambled control siRNA (10nM) or E6 targeting siRNAs (E6#1, E6#2, E6#3, E6#4 and E6#5 siRNA). 72 hours post transfection, all cells were collected (adherent and non-adherent), stained with FITC Annexin V and PI and analysed by flow cytometry. In the above figure, overlay histograms on the left hand side depict untreated (highlighted in red) versus mock (highlighted in green) and denoted A, untreated (highlighted in red) versus scrambled control (highlighted in green) and denoted C, untreated (highlighted in red) versus E6#1 (highlighted in green) and denoted E, untreated (highlighted in red) versus E6#2 (highlighted in green) and denoted G, untreated (highlighted in red) versus E6#3 (highlighted in green) and denoted I, untreated (highlighted in red) versus E6#4 (highlighted in green) and denoted K, untreated (highlighted in red) versus E6#5 (highlighted in green) and denoted M. While the overlay histograms on the right hand side depict scrambled control (highlighted in red) versus mock (highlighted in green) and denoted B, scrambled control (highlighted in red) versus scrambled control (highlighted in green) and denoted D, scrambled control (highlighted in red) versus E6#1 (highlighted in green) and denoted F, scrambled control (highlighted in red) versus E6#2 (highlighted in green) and denoted H, scrambled control (highlighted in red) versus E6#3 (highlighted in green) and denoted J, scrambled control (highlighted in red) versus E6#4 (highlighted in green) and denoted L, scrambled control (highlighted in red) versus E6#5 (highlighted in green) and denoted N. For this dual staining, peaks on the left hand side represent a normal dataset (live population of cells) and any shift in the peaks to the right represents the presence of a positive dataset (population of dead apoptotic cells).

E6#1 siRNA demonstrated the most significant change, with a sizeable population of cells midway and the in upper right hand side of the fluorocytogram, representing a population of dead cells (Figure 3-22D). This movement of cells was mirrored in Figure 3-24E and F; single parameter histogram overlay with untreated cells which reveal the presence of a positive dataset (broad positively skewed histogram) of cells stained with Annexin V-FITC (Figure 3-24E) and PI (Figure 3-24F)compared to the controls. This substantial change in profile of cells was also reflected in the bar chat whereby, E6#1 siRNA had the highest population of dead cells compared to the controls and any other siRNA (Figure 3-23). E6#2 siRNA also displayed a significant change in fluorocytograms with a sizeable smear of cells leading form the lower left live cell population to the dead cell population (Figure 3-22E). This transfer of cells was reflected in Figure 3-24G and H single parameter histogram overlay with untreated cells which show the presence of a positive dataset (similar to E6#1 but less broadly skewed) of cells stained with Annexin V-FITC (Figure 3-24G) and PI (Figure 3-24H) compared to the controls. The bar chart revealed E6#2 as having the second highest population of dead cells compare to the controls and other siRNAs (Figure 3-23).

E6#3 siRNA revealed a slight change in fluorocytograms with a population cells on the lower left hand side (live cells) of the plot and dead cell population at the upper right hand side of the plot (Figure 3-22F). The single parameter histogram overlay with untreated cells however, show a very small population of cells representative of a positive dataset stained with Annexin V-FITC (Figure 3-24I) and as well as a distinct peak of positive dataset stained with PI (Figure 3-24J) compared to the controls. These peaks were also observed in the bar chart as E6#3 siRNA having almost an equal number of dead and live cells (Figure 3-23). E6#4 and E6#5 siRNAs had very similar profiles to each other (Figure 3-22G and H respectively) and also the controls, indicating that these siRNAs do not induce any form of apoptosis or cell death. Their single parameter histogram overlay with untreated cells also reveal the absence of a positive dataset stained with Annexin V-FITC (Figure 3-24K and M respectively) and cells stained with PI (Figure 3-24L and M respectively) compared to the controls, confirming the above result.

3.4.5.2. Apoptosis analysis using FITC/PI DNA staining on E6#1 and E6#2 siRNAs

From the flow cytometry analysis in Section 3.3.5.1, E6#1 appears to have a subpopulation of cells between its live cell population and dead cell population. Hence, a further apoptotic analysis was carried out to determine if this sub population was missing the early apoptotic point, where cells would be PI negative and Annexin positive at earlier transfection time points. SiHa cells were transfected independently with E6#1 and E6#2 siRNAs at 24hrs and 48hrs post transfection. All adherent and non-adherent cells were harvested and stained using Annexin V-FITC and PI dual staining. There were no substantial changes in the apoptotic profile dot plot of the untreated and transfected with scrambled control siRNA controls at 24hrs (Figure 3-25A) and at 48hrs (Figure 3-26A), neither were there significant changes in bar chart representation of the number of live cells and dead cells at 24hrs (Figure 3-25B) and at 48hrs (Figure 3-26B).

At 24hrs, E6#1 and E6#2 siRNA dot plots show a very similar profile to the scrambled control siRNA plot where most cells congregated at the lower left hand corner of the plot signifying live cells and an upward movement of cells across the plot towards the upper right hand corner without an obvious significant increase in the number of dead cells (Figure 3-25A). However, the increase in the number of dead cells is more obvious in the bar chart representation of the plot where E6#1 siRNA has twice as many dead cells as the negative (21% to 11% respectively) while E6#2 siRNA has a slightly smaller number of cells (17%) as depicted in Figure 3-25B. The light scattering plot at 24hrs (Figure 3-27A) shows a slightly diminished forward scatter for E6#1 and E6#2 siRNAs and unchanged side scatter compared to the untreated and scrambled control siRNA.

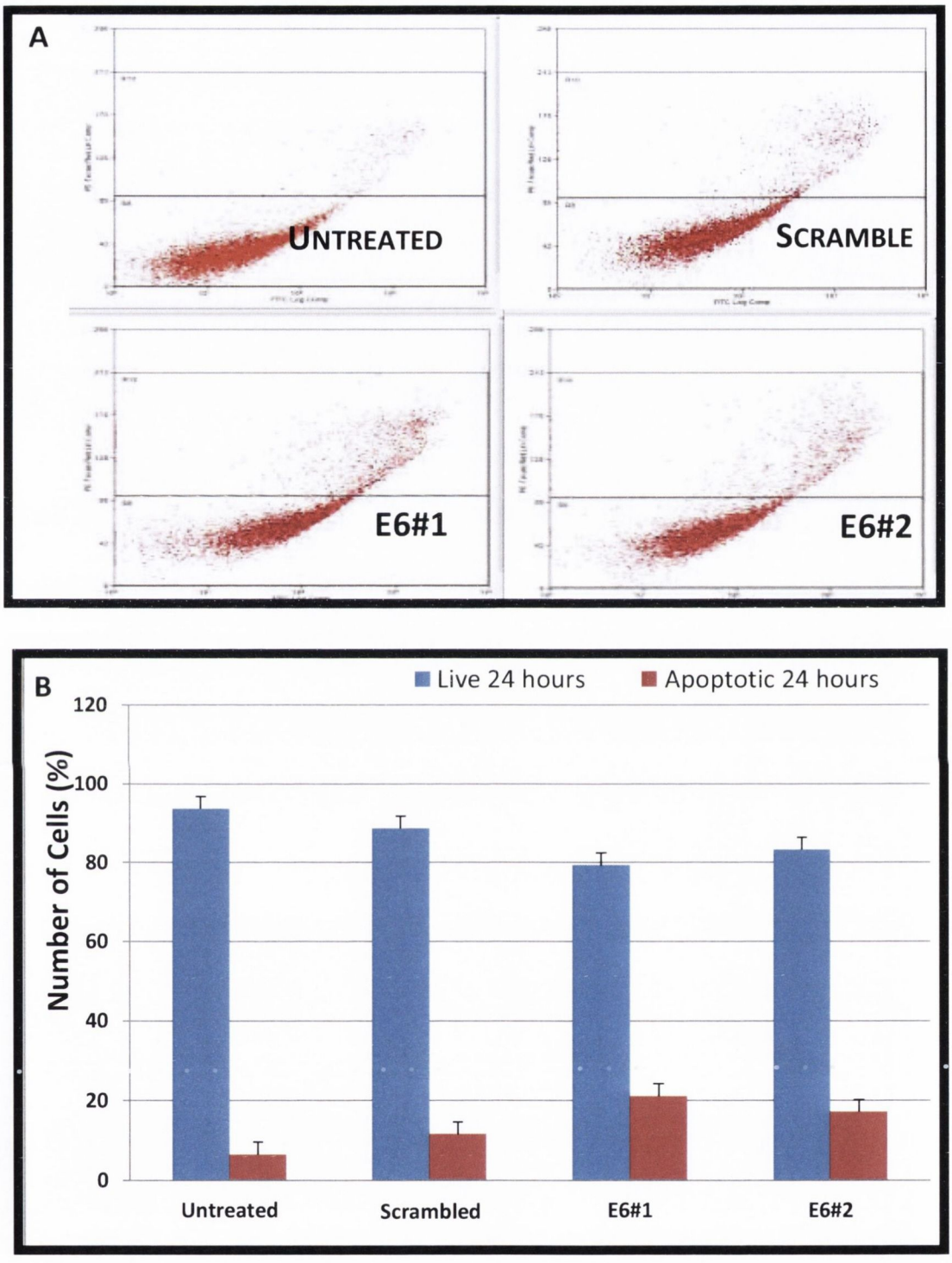

Figure 3-25: Dot Plot and bar chart of apoptosis analysis on SiHa cells 24hours post E6 siRNA transfection. SiHa cells seeded at $1.5x10^5$ cells were left untreated, transfected with scrambled control siRNA (10nM) or E6 targeting siRNAs E6 targeting siRNAs (E6#1, E6#2, E6#3, E6#4 and E6#5 siRNA). 72 hours post transfection, all cells were collected (adherent and non-adherent), stained with FITC Annexin V and PI and analysed by flow cytometry. The dot plots show the movement of cells from the lower left corner to the upper right hand corner indicative of cells undergoing apoptosis (panel A). The bar chart shows the percentage of live and apoptotic cells at 24 hours (panel (B). The data presented is representative of three biological replicates.

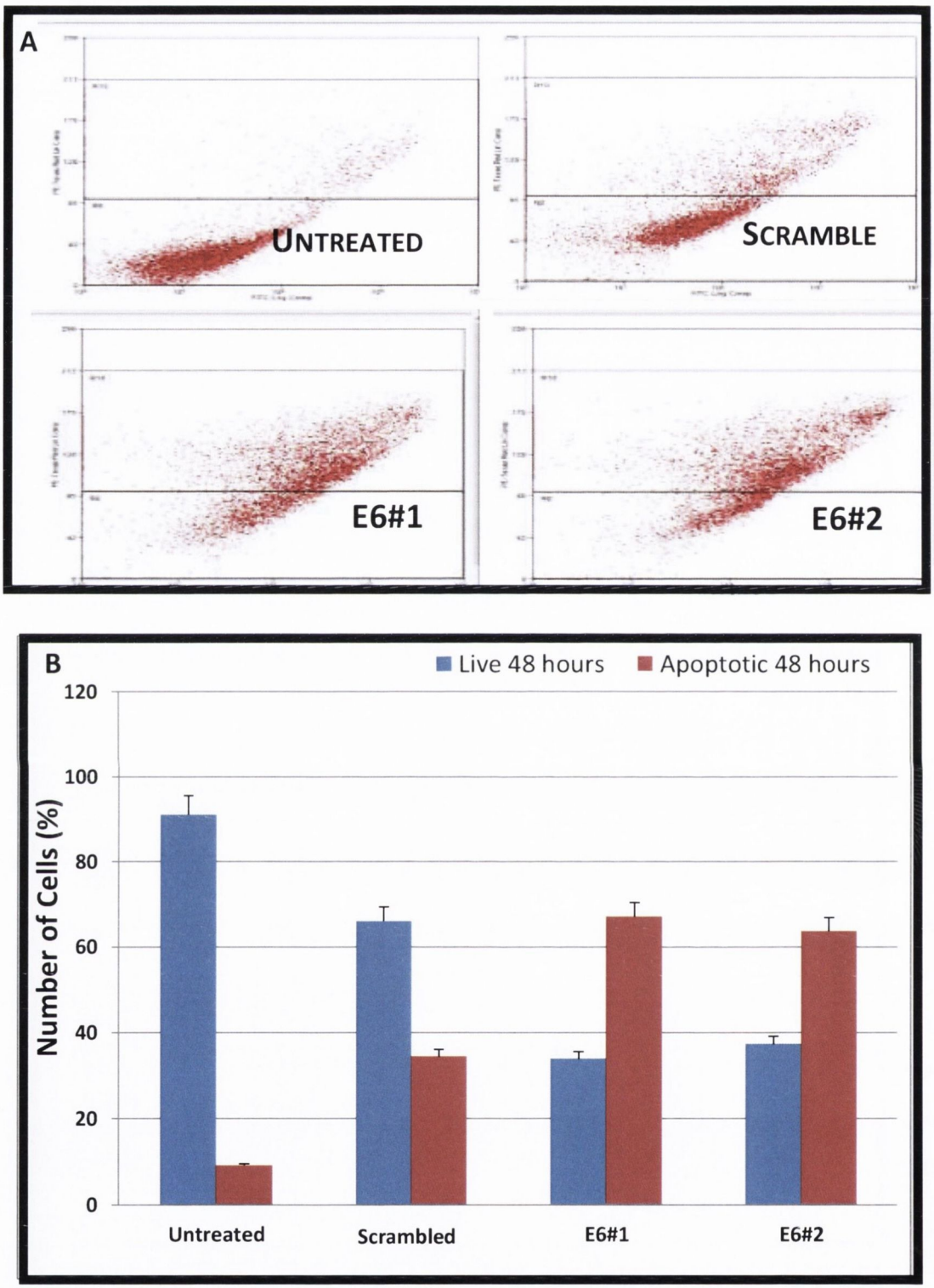

Figure 3-26: Dot Plot and bar chart of apoptosis analysis on SiHa cells 48hours post E6 siRNA transfection. . SiHa cells seeded at $1.5x10^5$ cells were left untreated, transfected with scrambled control siRNA (10nM) or E6 targeting siRNAs E6 targeting siRNAs (E6#1, E6#2, E6#3, E6#4 and E6#5 siRNA). 72 hours post transfection, all cells were collected (adherent and non-adherent), stained with FITC Annexin V and PI and analysed by flow cytometry. The dot plots show the movement of cells from the lower left corner to the upper right hand corner indicative of cells undergoing apoptosis (panel A). The bar chart shows the percentage of live and apoptotic cells at 48 hours (panel (B). The data presented is representative of three biological replicates.

At 48hrs, a greater shift toward the upper right hand side of the plot (dead cells) is observed in E6#1 siRNA (Figure 3-26 A) which is represented in the bar chart as an increase to 67% apoptotic cells (Figure 3-26B) while E6#2 siRNA has a similar increase of 64% dead cells (Figure 3-26B). The light scattering profile at 48hrs also reveal a greatly diminished forward and side scattering in E6#1 and E6#2 (Figure 3-27B) compared to the untreated and scrambled control siRNA (Figure 3-27B) which is characteristic of the diminished ability of dead cells to scatter light in both forward and side scatter directions and hence confirming cell death.

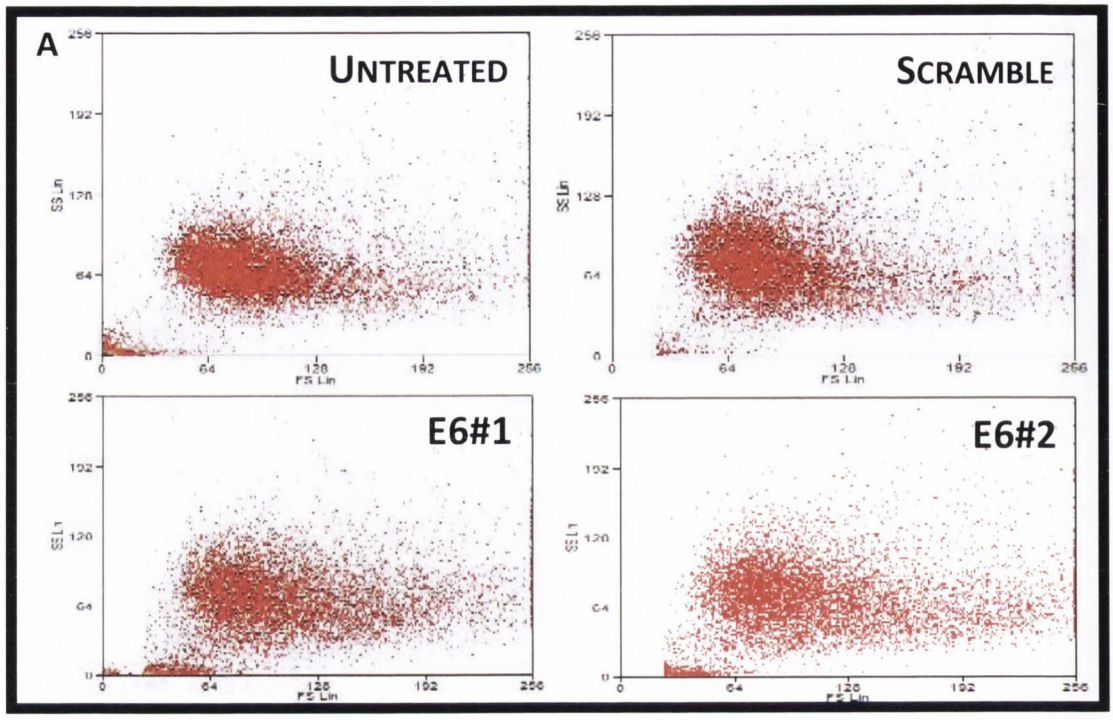

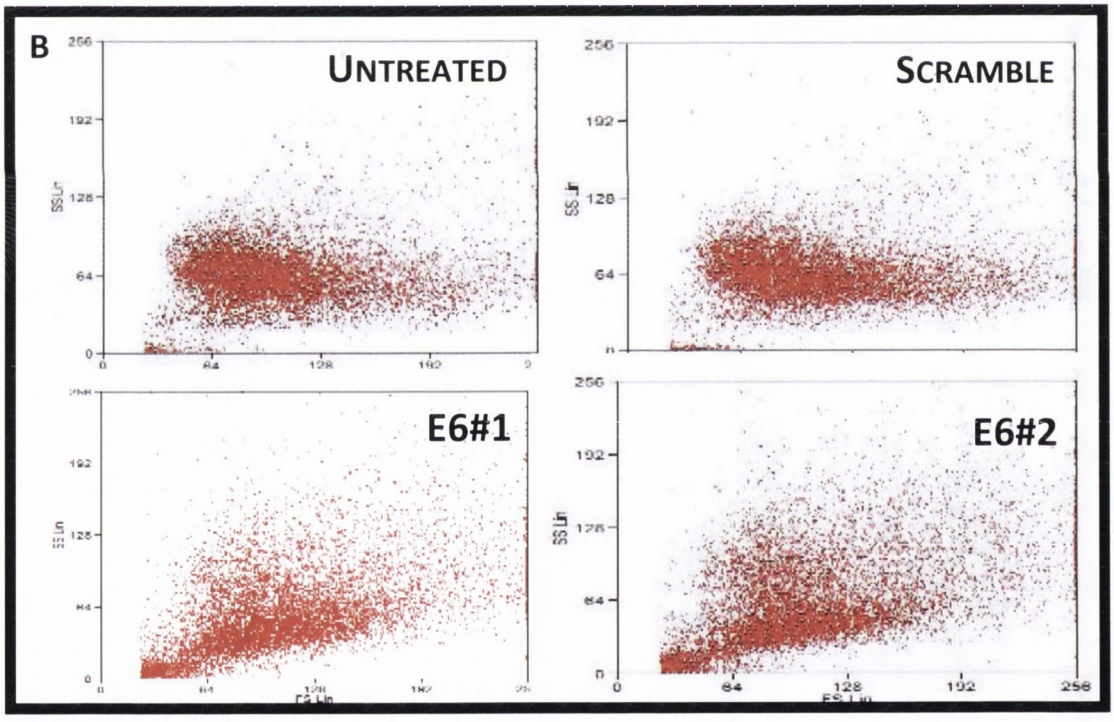

Figure 3-27: Light scatter plot of SiHa cell line 24 and 48 hours post forward transfection technique. SiHa cells seeded at 1.5x105 cells were left untreated, transfected with scrambled control siRNA (10nM), E6#1 siRNA or E6#2 siRNA. At 24 and 48 hours post transfection, all cells were collected (adherent and non-adherent), stained with PI and analysed by flow cytometry. The dual parametric dot plots combine side and forward scatter profiles of the cells. The side scatter on the vertical axis is proportional to cellular granularity that is the more granular a cell, the greater the lights scatter and the higher the signal detected. The forward scatter on horizontal axis is proportional to cell size that is the larger the cell the greater the light scatter and the higher the signal detected. The data presented is from one complete experiment and representative of three biological replicates.

3.5. Discussion

The aim of this work was to develop an *in vitro* system in which HPV oncogene E6 and/or its splice forms could be supressed separately from HPV oncogene E7. This system was proposed to elucidate E6 specific functions in cervical carcinogenesis, and to correlate with previous work carried out in this lab by Dr Spillane wherein the expression of HPV oncogenes, E6 and E7 were simultaneously silenced via E7 targeting siRNAs and thereby to provide a better overall understanding of the mechanism of tumourigenesis by each oncogene in high risk HPV. It was also anticipated that the established system would then become the foundation for future studies to identify novel and distinct intracellular functions of E6 and E7. RNAi technology is of exceptional reproducibility and specificity and was employed during this study due to its use in the previous work by Dr Spillane. It was expected to present a delineated overview of E6 and E7 specific functions in cervical cancer.

The objective behind the design of these siRNAs was to delineate E6 oncogene from E7 by targeting varying regions within full length E6 and/or its splice forms. Several papers have been published on the targeting of E6 and/or E7 in HPV18 or HPV16 cell lines using siRNA since the first report of the silencing of HPV infected cervical cancer cells using siRNA in 2002. In this study, E6 siRNAs were demonstrated to specifically hinder the expression E6 and/or E6 splice form to which they were targeted without any crossover effect. Five siRNAs were designed that is in-house E6#1 to target full length E6 only, E6#2 to target full length E6 and E6*I, E6#3 to target full length E6, E6*I and E6*II and Ambion designed E6#4 to target full length E6 and E6*I and E6#5 to target full length E6 and partially target E6*I and E6*II. In-house siRNAs were designed by multiple online predictive tools in combination with literature criteria while Ambion designed siRNAs were based on their silencer select design protocol. The decision to use multiple design siRNAs strategies meant that at least two siRNAs would be functional and could be used to implement a multiplicity control (Multiplicity controls boost confidence in RNAi data by establishing two or more siRNAs targeted to different sites of the same mRNA exhibit similar effects).

A crucial aspect of this study was the selection of a suitable transfection protocol technique and appropriate endogenous control. This was to done to ensure the elimination of any probability of non-specific, off-target effects of the siRNAs employed. The relationship between transfection efficiency and cell density is an established factor in the selection of a suitable transfection technique. The forward and reverse transfection technique protocols were initially assessed using a GAPDH positive control from Ambion which had been extensively validated as an ideal control of siRNA experiments. This control siRNA targets GAPDH mRNA and its effects can be measured using TaqMan® RT-PCR. The reverse transfection technique protocol was carried out using previously optimised conditions by this lab and these conditions were also replicated using the forward transfection technique protocol. GADPH siRNA sufficiently enforced the suppression of GAPDH mRNA (98%) in SiHa cells using the identical conditions for both protocols with minimal toxicity and cell death (Figure 3-3).

Having established optimal basic requirements for forward and reverse transfection technique protocols, it was decided to perform a reverse transfection technique protocol using two of the five designed siRNAs; in-house designed E6#1 which targets full length E6 only and Ambion designed E6#5 which targets full length E6 and partially target E6*I and E6*II in a HPV16 infected cervical cancer cell model due to HPV16 being identified as one of two predominant high risk HPVs in cervical neoplasia (Goldie, et al., 2008). The reverse transfection technique protocol using these two siRNA failed to provide a consistent suppression of HPV E6 (Figure 3-6) or E7 mRNAs using the designed primers and probes targeting these mRNAs respectively. Hence, the adoption of the forward transfection technique protocol whereby only an actively dividing cell population was present at the time of transfection was employed. As no previous optimisations had been made in this lab for the forward transfection technique protocol, an initial assessment was performed by varying seeding concentrations and transfection durations. A seeding concentration of $1x10^5$ and an extended duration of 72hrs resulted in a gradual, consistent but unsubstantial suppression of E6 and E7 mRNAs (Figure 3-7) in spite of distinct, significant morphological phenotypes observed

in both siRNAs compared to the controls (Figure 3-8, Figure 3-9 and Figure 3-10). This therefore led to the evaluation of the endogenous control employed (B2M).

As no single control can serve as a universal endogenous control for all experimental conditions, certain qualities are of crucial importance in the selection of an appropriate control for an experiment. In this study, as siRNA silencing effects at mRNA level was to be measured using TaqMan® RT-PCR qualities such as consistency and non-variability in expression levels to generate accurate and reproducible data was essential. A panel of endogenous controls of different origins were selected and examined; 18S rRNA, ACTB_AB, and GAPDH in addition to B2M to assess the suitability of B2M as a control in this study. These controls were evaluated for significant variations between the control samples and within biological replicates using the same cDNA via Ct values (representative of their level of abundance in the cells), Ct standard deviations (representative of their variability and consistency in expression levels) and amplification plots. 18S rRNA is an abundant RNA as it makes up 85-90% of total cellular RNA and has been shown to be consistent in rat and liver cells, human and mouse malignant cell lines (Vilches-Flores, et al., 2010) (Wiebe & Lewis, 2003). Its high level of abundance in most cells can however, become a disadvantage to its use as an endogenous control when examining low-medium expression targets as observed in the amplification curves in Figure 3-11 (Wei, et al., 2013). Although Ct values obtained for 18S rRNA were the lowest of all four controls which suggests its abundance in SiHa cells, it had the second highest Ct standard deviations amongst all four controls (> 0.3) as depicted in (Table 3-5). High Ct standard deviations were indicative of increased variability which offers uncertainty as to the true Ct value for the target amplicons. Another observation was the initial cycles being too close to the start of the PCR run on the amplification plot and therefore resulting in short or narrow baseline in this control (Figure 3-11A and B). These results therefore points to the difficulty of determining the RNA concentration at which 18S rRNA would provide a wide enough baseline, generate target gene Cts with 40 cycles and hence points to its unsuitability for this study.

In the case of ACTB_AB however, it is a moderately expressed gene in most cells and cell lines though its consistency has been questioned in blastomeres, canine myocardium, breast epithelial cells (Albershardt, et al., 2012). Its amplification plots show that initial cycles are at a sufficient distance from the start of the PCR run with a wide enough baseline and normal Ct values (Figure 3-11C and D). ACTB_AB nevertheless, had the highest Ct standard deviations of all four controls (>0.3) Table 3-2 which is representative of its increased variability and obscurity of its true Ct value for the target amplicons, which lowers confidence in distinguishing between small differences in target concentrations as is required in this study's analysis. GAPDH is a common normaliser in qPCR experiments and maybe consistent in many cases, yet it has been shown to be up-regulated in some cancerous cells, cells treated with tumour suppressor genes, under hypoxia and manganese or insulin treated samples. (Everaert, et al., 2011) (Jacob, et al., 2013). GAPDH displayed good Ct standard deviations values of <0.3 and its amplification plots show that initial cycles were at a sufficient distance from the start of the PCR run with a wide enough baseline (Figure 3-11G and F), (Table 3-5). However, these plots also reveal its curves are plateauing beyond 40 cycles (too close to the end of the PCR run) which is the reaction limit in qPCR, due to the depletion in one of the reaction components. Thus owing to statistical distribution, a high level of Ct variation is present in these samples as high Cts usually occurs when target quantities approach a single copy (Ct values of 35 to 40) hence these samples possess poor precision and thus make low-fold changes difficult to accurately quantify.

B2M displayed best Ct standard deviations values of <0.3 and its amplification plots show that initial cycles were at a sufficient distance from the start of the PCR run with a wide enough baseline and within 40 cycles (Table 3-2) (Figure 3-13E and F). These suggest B2M had most consistent expression levels with the least degree of variability amongst the controls. Therefore, the analysis of these endogenous controls reveal a high level of Ct variation amongst untreated cells, mock-transfected and scrambled control siRNA transfected cells which would inevitably give rise to poorer precision and subsequently less control to detect low-fold changes hence none was found to be better suited for these experiments than B2M, consequently B2M remained the most

appropriate control for this study. The suitability of B2M for this study was further assessed by using primers and probe set selective for an indirect biomarker of HPV E6 expression, p21, where highly significant fold changes ($p<0.001$) were observed in E6#5 siRNA and less significant changes in E6#1 siRNA (Figure 3-12).

All five siRNAs E6#1, E6#2, E6#3, E6#4 and E6#5 were then forward transfected for 72hrs using previously optimised protocols for E6#1 and E6#5 for 72hrs. In-house designed E6#2 E6#3 and Ambion designed E6#4 demonstrated an equivalent, highly substantial, simultaneous reduction in both E6 and E7 expression at the RNA level of more than 70% while Ambion designed E6#5 demonstrated an equivalent, considerable simultaneous reduction in both E6 and E7 expression at the RNA level of less than 70% and more than 70% respectively (Figure 3-13). However, in-house designed E6#1 demonstrated no reduction in both E6 and E7 expression at the RNA level as it was designed to target full length E6 only (Figure 3-13). The concomitant silencing of HPV E6 and E7mRNAs in this study correlates with similar work in literature demonstrating that the application of RNAi using siRNAs to HPV16 or HPV18 infected cervical cell lines resulted in similar suppressions (Sima, et al., 2007) (Yamato, et al., 2008) (Yoshinouchi, et al., 2003) (Zhou, et al., 2012) .

It has been established that bicistronic E6/E7 premRNA consists of 3 exons and 2 introns which generate E6 and E7 via the retention of the first codon, a pre-requisite for full length E6 production or the splicing of this intron leading to the generation of spliced transcripts denoted as E6*I and E6*II (Stacey, et al., 2000) (Stacey, et al., 1995). It has also been demonstrated that E6*I mRNA is the most predominant transcript in high risk HPVs *in vivo* and *in vitro* and is primarily responsible for E7 production though E7 can also be efficiently translated from E6 (Tang, et al., 2006) (Zheng & Baker, 2006). As a result, it is expected that a reduction in the expression levels of E6 should be to the same degree as E7 which was observed in this study in correlation with previous findings (Figure 3-13). To confirm the dissociation of the above silencing from full length E6 silencing, primers and probe selective for full length E6 only were designed

and used to evaluate all siRNAs. E6#2 E6#3 and E6#4 also demonstrated a highly substantial reduction in full E6 expression at the RNA level while E6#1 also demonstrated a highly substantial reduction of more than 70%. E6#5 however, demonstrated no reduction in full E6 expression at the RNA level (Figure 3-13) The degree of suppression of full length E6 mRNA in all siRNAs correlates with previous finding that E6*I is the most dominant transcript (Tang, et al., 2006) as the level of full length E6 suppression detected is not to the same degree as the level of suppression of E6/E7 and though an increase in full length E6 expression was observed in E6#5, the majority of the E6 amplicons detected were E6*I (Tang, et al., 2006).

The cellular stabilisation of the p53 protein was used to indicate siRNA-mediated suppression of E6 as high risk HPV E6 induces p53 degradation. Therefore, the degree of full length E6 mRNA suppression was expected to correlate with the amount of p53 protein stabilised. The expression of p21, a downstream target of p53, was assessed also at the RNA and protein levels to reaffirm p53 stabilisation. E6#1 displayed no stabilisation of p53 protein or transactivation of p21 transcript at RNA or protein levels (Figure 3-17) while the remaining four siRNAs employed induced an accumulation of p53 protein with substantial variations amongst them (Figure 3-17). The lack of any protein accumulation in E6#1 was anticipated due to the difficulty in obtaining sufficient RNA and protein quantities 72hrs post transfection as a result of the dramatic loss of adherent cells which were required for TaqMan® RT-PCR and western blot analysis. The quality of the RNA obtained from this siRNA was further assessed using Agilent's 2100 Bioanalyser and its integrity found to be degraded (not shown). Ambion® designed siRNAs E6#4 and E6#5 had the greatest and most demonstrable accumulation of p53, which was translated by the transactivation of the p21 transcript and observed as p21 accumulation at the RNA and protein levels. E6#4 was shown to be more effective than E6#5 at both the RNA and protein levels in p21 and the protein level in p53. E6#2 and E6#3 also induced reasonable p53 protein stabilisation which generated a corresponding transactivation of p21 transcript in both siRNAs and observed in p21 RNA levels. The levels of p53 protein accumulation of E6#3, however, did not equal its silencing effectiveness despite inducing the largest reduction in E7

and E6 mRNA expression levels amongst all five siRNAs, p21 transactivation in this siRNA was only observed at the RNA level. In other words, although E6#3 and E6#2 displayed similar p21 transcript levels, p21 protein accumulation was only observed in E6#2.

In response to cellular stress such as DNA damage, oncogene activation and hypoxia, p53 accumulates and regulates the transcription of specific target genes (Shieh, et al., 1997) (Sakaguchi, et al., 1998) (Serrano, et al., 1997) (Palmero, et al., 1998) (An, et al., 1998). Activated p53 is also known to induce or repress the transcription of genes involved in cell cycle arrest, DNA repair, apoptosis, and senescence (Rahman, et al., 2005) (Rahman-Roblick, et al., 2007). As p21 is an effector of cell cycle arrest, a downstream senescent marker was employed for additional analysis of the siRNAs and the levels of β-galactosidase activity at pH6 was used to further assess the lack of p21 protein accumulation and validity of p53 stabilisation observed in E6#3. E6#1 and E6#2 displayed no statistically significant level of β-galactosidase activity at pH6 (Figure 3-18). The absence of β-galactosidase activity in E6#1 is as expected but the absence of β-galactosidase activity in E6#2, which displayed distinct morphological phenotypes with over 70% reduction in E6 and E7 RNA levels, stabilisation of p53 protein in addition to transactivation of p21 transcript at RNA or protein levels, indicated the absence of the senescence process in these cells.

Studies using DNA damaging agents to activate p53 have shown that in response, the p53 protein is stabilised and can mediate either apoptosis or cell cycle arrest and that although the exact mechanism of p53-dependent apoptosis is yet to be full elucidated, p53-dependent cell cycle arrest has been established to be mediated by p21 (Yoshinouchi, et al., 2003) (Gartel & Tyner, 2002) (Zhang, et al., 2013). In these studies, p21 has also been shown to be a major inhibitor of p53-dependent and p53-independent apoptosis. However, in a study whereby the non-genotoxic activation of p53 was employed has shown the stabilisation of p53 which also induces p21 transactivation has resulted in an apoptotic outcome regardless of the presence of

p53-dependent and p53-independent inhibitor of apoptosis, p21 (Xia, et al., 2011). Furthermore, similar observations have been made in studies using cells that frequently undergo cell cycling (for example myelogenic and lymphatic leukemic cells) as is the case with HPV16^{+} SiHa cells, wherein oncogenic E7 dysregulates cell cycle regulator Rb. These cells were reported to be induced to undergo apoptosis via proteasome inhibition, accompanied by the accumulation of cyclin-dependent kinase inhibitors p21$^{WAF1/Cip1}$, p27^{Kip1} and tumour suppressor protein p53 (Lopes, et al., 1997) (An, et al., 1998) (Maki, et al., 1996) (Blagosklonny, et al., 1996) (Naujokat, et al., 2000).

HPV oncogenes E6 and E7 mechanism of instigating cervical dysplasia is via disruption of the tumour suppressor proteins p53 and Rb. It is therefore possible that the reversal of HPV's oncogenesis via E6 and E7 silencing by E6#2, may have instigated a non-genotoxic activation of p53, causing its accumulation and transactivation of p21 at RNA and protein level. This activation may have also possibly triggered proteasomal inhibition which would result in the accumulation of cellular proteins with the induction of cell death via apoptosis. This was further evaluated by apoptotic Annexin V-FITC/PI staining and cell cycle PI staining (Figure 3-22 Figure 3-23 and Figure 3-24). E6#3, E6#4 and E6#5 conversely, demonstrated an extremely statistically significant increase in the level of β-galactosidase activity at pH6 with p values of <0.0001 and with E6#4 displaying the highest levels of activity as expected. From these results, it became more evident that E6#4 and E6#5 were possibly inducing senescence and this was further evaluated by Annexin V-FITC/PI staining and cell cycle PI staining.

E6#3 portrayed substantially reduced E6 mRNA expression signifying p53 stabilisation, p21 transactivation, significant β-galactosidase activity and distinct morphological phenotype with minor cell death. However, the absence of the p21 protein could be explained as E6#3 may not have attained its maximum activity whereby the transactivation of p21 at RNA level has not been translated to the protein level. This was further substantiated by Annexin V-FITC/PI staining and cell cycle PI staining.

Studies using siRNAs have shown that silencing of E6 and E7 expression is adequate to cause growth suppression of HPV-mediated cancer cells (Yoshinouchi, et al., 2003) (Jiang & Milner, 2005). Three of the five siRNAs employed, induced a reduction in cellular proliferation which was associated with an increase in cell numbers in the G1 phase of the cell cycle and a decrease in the S phase. Ambion® designed siRNA, E6#4 and E6#5 had highly pronounced effects with S phase being almost entirely annihilated. This was similarly reflected by an increase in G1 arrest mirrored by the changes in cellular morphology in these cells. E6#4 and E6#5 transfected cells displayed morphologies of large flattened cells. The forward and side scatter profiles of E6#4 and E6#5 transfected cells also indicated increased size and granularity respectively, further confirming the induction of senescence in these cells. In addition, the annexin V-FITC and PI analysis performed revealed the absence of a significant apoptotic profile of cells and demonstrated a shift in the fluorescent profile of both E6#4 and E6#5. This shift in fluorescence was ascribed to the higher fluorescent nature of senescing cells, in other words, autofluorescence of E6#4 and E6#5 transfected cells.

E6#3 siRNA displayed the most distinctive profile in cellular proliferation. It was characterised by a double peak in G1 arrest (Figure 3-20) with a subset of apoptotic cells which was also reflected in its morphological phenotype of rounded refractile cells. This phenotype although different from normal senescent cells has been reported in the literature as oncogene-induced senescence (OIS) *in vitro,* though OIS mechanisms do not seem to be universal across cell types and genetic contexts (Serrano, et al., 1997) (Palmero, et al., 1998) (Vredeveld, 2009) (Seoane, et al., 2008) (Kuliman, et al., 2010). Normally in these cell types, oncogenic signals result in OIS to protect against cancer development, safeguard genome integrity and activate DNA damage response (DDR). Therefore the induction of senescence acts as a barrier against tumour progression (Seoane, et al., 2008). Theories that explain the impact of senescence can be broadly categorised into programmed and stochastic theories whereby, each theory attributes a different cause to changes in gene expression that affect biological systems. Programmed theories suggest biological clocks; that is systems responsible for maintenance, repair and defence responses as the basis for

aging (hormonal signalling) while stochastic theories suggest cumulative damage of environmental factors such as free radicals (Rattan, 2006) (Gavrilova, et al., 2012) (Lawler, 2011). These cells display classical senescent characteristics of loss of proliferation, morphological changes, increased SA-β-GAL activity, rise in the levels of DDR markers (Myc, Ras, Cdc, E2F, cyclin E) and rise in cell cycle inhibitors ($p16^{INK4A}$, $p15^{INK4B}$, $p21^{CIP1}$ and p53 (Kuliman, et al., 2010). However, E6#3 cells become small and refractile instead of adopting large and flat morphology and they do not arrest strictly in G1, but also in G2/M. (Vredeveld, 2009). It is therefore probable that E6#3 is inducing similar responses in these cells. Similarly, E6#3 displayed the shift in fluorescence, observed in E6#4 and E6#5 transfected cells.

No significant changes in cell proliferation were observed for E6#1 and E#2. However, these siRNAs displayed the most dramatic apoptotic profile using Annexin V-FITC/PI staining. As initially surmised, E6#1 transfected cells were undergoing highly significant cell death, although the normal progression sequence observed in cell death via apoptosis was not witnessed. E6#2 also displayed significant cell death with a less clear progression of cell death via apoptosis. 24 and 48hour post transfection profiles however, confirm a progression into apoptosis by these siRNA with gradual increase in the number of dead cells from 24 to 48hrs. A clear shift of the major high forward scatter/low side scatter population to the low forward scatter / high side scatter population characteristic of apoptotic cells was also observed in E6#1 and E6#2.

The results of this chapter establish that targeting of the HPV E6 viral oncogenes induces cell cycle arrest and potentially cellular senescence as well as apoptosis as reported by (Bartlett & Davis, 2006) (Jiang & Milner, 2005) (Zhou, et al., 2012). Furthermore, these findings advocate the model of RNAi therapy and support its potential application in the treatment of HPV mediated cervical cancers over traditional non-HPV therapies.

Chapter Four

Differential gene expression analysis

4. Differential gene expression analysis

4.1.Introduction

HPV is the most important factor in the disease pathogenesis of cervical cancer. Cervical cancer remains an avoidable, increasingly common cause of death in women worldwide, preceded by a long pre-invasive disease phase known as cervical intraepithelial neoplasia (CIN) (Behtash & Mehrdad, 2006). Efforts to reduce cervical cancer incidence have involved the adoption of screening and vaccination programmes by some mid to high income countries (Lynge, et al., 2009). However, poor accesses to such in especially low and some mid income countries that make up a significant proportion of disease burden has resulted in observed increasing rates observed worldwide in 2012 reported by IARC (Ferlay, et al., 2013).

Although a step in the right direction, a number of issues still convey that vaccination is not the silver bullet. Age caps for vaccination due to decline in cost-effectiveness for HPV vaccination above 26 years means it is not offered to older women who still fall within the highest risk group (18-30 years). These women could benefit from being vaccinated as well as potentially prevent a significant burden of disease. Also, despite reports from clinical trials, the exact duration of vaccine protection is unknown. Hence, potential risks still exist for the vaccinated population.

Hence, vaccination does not negate the need for pap smears and is still encouraged at regular intervals in vaccinated women (same guidelines as women who have not been vaccinated). The emergence of other possibly cancer causing high-risk HPV types (HPV 31, 33, 35, 39, 45, 51, 52, 56, 58 and 66) for which both vaccines have no cross protection is also a cause for concern. Finally, vaccination is a preventative measure hence it is of no benefit to women with pre-existing conditions or infected women with cervical cancer. Therefore, despite the availability and the benefits of prophylactic vaccines, it is still necessary to the elucidate mechanisms involved in HPV-induced carcinogenesis due to the widespread nature of HPV infections and to develop effective intervention options in these women.

Other issues such as competing health priorities, inadequate numbers of trained providers, insufficient financial resources and weak health systems are just some of the issues compounding cervical cancer in these countries (Poljak, 2012).

Therefore, the development of novel technologies potentially offers a comprehensive approach to tackling cervical cancer. This approach however, must act across the life course of HPV via its natural history to identify opportunistic instances, in the relevant age groups to deliver effective treatments (Ault, 2006). In spite of the promise of prophylactic vaccines in addition to current screening methods, no effective means of HPV transmission prevention or cures for clinical manifestation are available. The current method of clinical sequelae involving the removal of abnormal cells and subsequent surveillance for reoccurrence has reaffirmed the evident need for novel biomarkers (Ault, 2006). This nevertheless, can only be achieved by a better understanding of the molecular activities of oncogenes (HPV E6 and E7) whose overexpression drive malignancy (Morrison, et al., 2011). These oncogenes work synergistically to inhibit apoptosis and induce genomic instabilities via the abrogation of cell cycle checkpoints and chromosomal rearrangements (Park, et al., 1995) (Plug-DeMaggio, et al., 2004).

DNA microarray technology offers large scale gene expression analysis that enables the examination of thousands of genes at a given time while reverse genetics involves the assessment of a gene's function via the assessment of downstream effects of its disruption (Tseng, et al., 2012). When combined, reverse genetics facilitates a comprehensive approach to the examination of the downstream effects due to gene modifications and thereby enables the elucidation of the function of such genes. The reliance of HPV on overexpression of E6 and E7 which abrogate tumour suppressor proteins without damaging cellular machinery facilitates the use of RNAi (Tan, et al., 2012). This technology has been employed to examine E6 and E7 activities via RNAi and ectopic expression of E2 (Jiang & Milner, 2005) (Morrison, et al., 2011) (Sima, et al., 2007) (Yamato, et al., 2008) (Zhou, et al., 2012) (Smith, et al., 2010) (Jeong, et al., 2004) (Demeret, et al., 2003). Hence, the combination of these approaches and functional taxonomy of differentially expressed genes aids the elucidation of the role

of these oncogenes in disease carcinogenesis, in addition to potentially delivering biomarkers to assist in diagnosis and treatment of cervical cancer.

4.2.Chapter aim

The aim of this chapter was to detect cellular targets influenced by the activity of HPV16 E6 at the transcriptome level via genome wide expression analysis. This analysis was achieved via evaluation of concomitantly silenced E6 and E7 oncogenes 72hrs post forward transfection protocol using E6 targeting siRNA in a SiHa cervical cell line model. The application of these quality control validated knockdown samples to Affymetrix GeneChip® microarrays, enabled a comprehensive analysis of gene expression changes that arise on silencing E6 and E7.

4.3.Materials and Methods

4.3.1. Sample and RNA preparation

Total RNA from the HPV16 positive SiHa cervical cell line was employed for part of this study. Samples employed were from the validated 72hrs post forward transfection protocol (described in section 3.4.2 to section 3.4.5) using four biological replicates with E6#2 siRNA and three biological replicates transfected with scrambled control siRNA and E6#4 siRNAs. The forward transfection protocol was utilised as RNA of better quality was obtained. E6#2 and E6#4 siRNAs target similar regions of the E6 mRNA transcript (3'end of both E6 and E6*I) and induced very different phenotype changes of cell death and senescence respectively. Total RNA was isolated using Ambion MirVana isolation kit (section 2.3.3.1); DNase digested (section 2.3.3.2) and purified using the Qiagen RNeasy mini kit (as per the manufacturer's instructions). The quantity and purity of RNA was determined using the NanoDrop® ND-2000 spectrophotometer (section 2.3.3.3.1) and the integrity verified using the Agilent 2100 bioanalyser (section 2.3.3.3.2)

4.3.2. Affymetrix GeneChip® Gene 1.0 ST microarray

For this analysis, 150ng of RNA from each sample was reverse transcribed, fragmented and biotin labelled following manufacturer's instructions. Single stranded fragmented, biotin labelled DNA was then hybridised to GeneChip® Human Gene 1.0 ST Arrays (Affymetrix, CA, USA) and scanned on an Affymetrix GeneChip® Scanner 3000 7G (Affymetrix, CA, USA). A total of nine microarray experiments were performed consisting of three biological replicates of transfected with scrambled control siRNA, E6#2 and E6#4 siRNAs.

4.3.3. Quality control

Quality controls were assessed using the Expression Console ™ (EC) software (Affymetrix, CA, USA) to identify outlying microarrays. This involved the visual inspection of array images for hybridisation artefacts and for the performance of the positive hybridisation control, B2 oligo. Subsequent analysis was then based on quality control metrics generated by the EC software via its calculation of various quality assessment metrics. Probe intensities were summarised into probeset intensities using the Robust Multiplechip Analysis (RMA) summarisation method and both were used for quality assessment metrics. A brief outline of the different quality control metrics, their meanings and functions are given below.

I. **Probe Level Metrics**: This quality assessment metric is based on the probe signal level data.
    a. **pm_mean** is the mean of the raw intensity for all of the perfect match (PM) probes on the array prior to any intensity transformations (for example quantile normalisation, RMW style background correction). pm_mean value can be used to determine whether certain arrays are unusually dim or bright. Dim or bright arrays may not be a problem per se but give an indication for a closer inspection of the probeset based metrics is required to ensure no further irregularities are not present such as unusually high median absolute deviation of residuals and unusually high mean absolute relative log expression values when looking within replicates.

II. **Probeset Summarisation Based Metrics**: This set of metrics is based on the summarised probeset intensities. The majority of these metrics are performed for different categories of probesets; for example the hybridisation or "bac spike" controls.
    a. **pos_vs_neg_auc** is the area under the curve (AUC) for a plot comparing signal values for the positive controls to the scrambled control siRNAs. The ROC curve is generated by assessing how well the signals separate the positive controls from the scrambled control siRNAs, with the postulation that the scrambled control siRNAs are a measure of false positives and the positive controls are a measure of true positives. An AUC of 1 reflects perfect

separation, whereas, as an AUC value of 0.5 would reflect no separation. Expected value for this metric is tissue type specific and may be sensitive to the quality of the RNA sample as values between 0.80 and 0.90 are typical.

b. **X_probesets** is the number of probesets analysed from category "X and can be useful in identifying those metrics based on a very limited number of probesets (for example, bacterial spikes) versus those based on a large number of probesets (for example All or positive controls).

c. **X_mean** is the mean signal value for all the probesets analysed from category "X".

d. **X_mad_residual_mean** is the mean of the absolute deviation of the residuals from the median, for all probesets analysed from category "X". Different probes return to different intensities when hybridised to a common target. To account for these relative differences in intensity, the RMA and PILER algorithms creates a model for individual probe responses. The difference between the actual signal intensity value and the predicted value is the residual. If the residual for a probe on any given array is very different from the median, it means that it is a poorer fit to the model. Hence, calculating the mean of the absolute value of all the deviations yields a measure of how well or poor all of the probes on a given array fit the model. An unusually high mean absolute deviation of the residuals from the median is suggestive of problematic data for that array.

e. **X_rle_mean** is the mean absolute relative log expression (RLE) for all the probesets analysed from category "X". This metric is generated by taking the signal estimate for a given probeset on a given array and calculating the difference in log base 2 from the median signal value of that probeset over all the chips. This mean is then computed from the absolute RLE for all the probe sets analysed from category "X". When only replicates from a cell line are analysed together, the mean absolute RLE should be consistently low, reflecting the low biological variability of the replicates.

III. **Probeset signals as quality metrics**: These sets of quality assessment metrics are individual probe set signal values for various controls. These include the bacterial spike and polyA spike probesets. The main use in looking at specific probeset values is to determine if expected behaviours for these probesets are observed, that is constant expression levels for housekeeping genes, rank order of signal values between spike probe sets.

IV. **Probeset Categories:** From the above descriptions, many of the quality assessment metrics, values are reported not just for the entire probe sets analysed, but also for particular subsets of probesets. Hence, this can be useful when troubleshooting a poorer performing sample as described below.

a. **all_probeset** is all the probe sets analysed. In most cases, this category is the bulk of probesets that will be carried into downstream statistical analysis. Thus the metrics reported for this category will be the most representative of the quality of the data being used downstream.

b. **bac_spike** is the set of probesets which hybridise to the pre-labelled bacterial spike controls (BioB, BioC, BioD, and Cre). This category is useful in identifying problems with the hybridisation and/or array. Metrics in this category have more variability than other categories (that is, positive controls, all probesets) due to the limited number of spikes and probesets for this category.

c. **polya_spike** is the set of polyadenylated RNA spikes (Lys, Phe, Thr, and Dap). This category is useful in identifying problems with the target preparation. As with the bacterial spike controls, metrics in this category have more variability than other categories due to the limited number of spikes and probesets for this category.

d. **neg_control** is the set of putative intron-based probesets from putative housekeeping genes. Several species-specific probesets were selected against putative intronic regions in genes that were previously shown to have constitutive expression over a large number of samples. Thus in any given sample, some (or many) of these putative intronic regions may be transcribed and retained. These probesets form a reasonably large collection

which generally has very low signal values and are used to estimate the false positive rate for the pos_vs_neg_auc metric.

e. pos_control is the set of putative exon-based probe sets from putative housekeeping genes. Several species-specific probesets were selected against the putative exonic regions in these genes as they were previously shown to have constitutive expression over a large number of samples. These probesets form a reasonably large collection of probesets with target present which generally have moderate to high signal values. These probesets are used to estimate the true positive rate for the pos_vs_neg_auc metric.

4.3.4. Microarray data analysis

Microarray data analyses and comparisons were executed using Bioconductor software libraries (www.bioconductor.org). The oligo package (Carvalho & Irizarry, 2010) was used to import data from CEL files and compute RMA expression values (Irizarry, et al., 2003) (Bolstad, et al., 2003) (Irizarry, et al., 2003). The overview box plot of the RMA expression values was plotted using made4 (Culhane, et al., 2005). Differential expression analysis of the RMA expression values was performed using RankProd (Breitling, et al., 2004), a non-parametric statistical method for identifying significantly de-regulated genes based on the estimated percentage of false predictions or False Discovery Rate (FDR). The RankProd method has been shown to perform well in cases where datasets had low numbers of samples or high levels of noise (Jeffery, et al., 2006). De-regulated genes were identified as those with a log-based fold-change in expression value of 1.0 or more, using a significance threshold p-value of 0.05, adjusted for multiple testing. Gene annotation was provided by annaffy (Smith, 2010). Heatmaps were drawn using gplots (Warnes, et al., 2014).

4.3.5. Target gene list analysis

The online database DAVID 6.7 (Database for Annotation, Visualisation and Integrated Discovery 2013) (Huang, et al., 2009) (Huang, et al., 2009) was used to categorise genes according to their functions and pathways. This database methodically maps a large number of genes of interest in a list to the associated biological annotation (gene ontology terms) and statistically points out the most overrepresented (abundant or enriched) biological annotation out of thousands of linked terms and contents. The unique feature of DAVID is its knowledgebase, which is based on more than 20 gene identifier types and more than 40 functional annotation categories from dozens of heterogeneous public databases, including Kyoto encyclopaedia of genes and genomes (KEGG) and PANTHER which simplifies ontology of protein function by biological functions. DAVID's annotation data is comprehensively integrated by a distinctive single linkage method. These 40 annotation categories include GO terms, protein-protein interactions, protein functional domains, disease associations, bio-pathways, sequence general features, homologies, gene functional summaries, gene tissue expressions and literatures.

4.4.Results

4.4.1. Microarray quality control

4.4.1.1. Quality control for RNA utilised in microarray gene expression analysis.

The quality of extracted RNA is highly important in whole genome gene expression analysis, as RNA of low or even moderate quality can result in variable or un-interpretable data. Hence, to avoid these issues, the purity and quality (integrity) of extracted RNA was established using NanoDrop®ND-100 and the Agilent 2100 Bioanalyser, respectively. Purity was determined by the 260/280 ratio of extracted RNA samples, where values between 1.9 and 2.1 were considered pure from contaminants, such as phenol and chloroform (Table 4-1). All samples employed in this study fell within this range and hence were considered to be of high quality. The RNA integrity of these samples was evaluated via visual assessment of their 18S and 28S RNA bands on a gel image (Figure 4-1) and review of the calculated RIN numbers (Table 4-1), as outlined in section 2.3.3.3.2. For this study, Figure 4-1 depicts the high quality and minimal degradation of each sample employed. In addition, the RIN numbers of all samples were all above 7. Therefore, as all samples met both the purity and quality criteria they were judged of satisfactory quality for use in the resultant microarray experiments.

Table 4-1: Table of 260/280 ratios and RIN numbers. This table shows the 260/280 ratios and RIN numbers of RNA samples demonstrating suitability for microarray analysis. As a result of dry patches observed in one of the E6#2 replicates during the hybridisation and washing steps of the microarray experiment, a fourth replicate was employed.

Sample	260/280	RIN
E6#2 Rep1	2.12	8.3
E6#2 Rep2	2.02	9.8
E6#2 Rep3	2.05	9.3
E6#2 Rep4	2.02	7.1
E6#4 Rep1	2.06	8.1
E6#4 Rep2	2.05	10
E6#4 Rep3	2.01	9
Scrambled control siRNA Rep 1	2.06	8
Scrambled control siRNA Rep 2	2.07	10
Scrambled control siRNA Rep 3	1.98	10

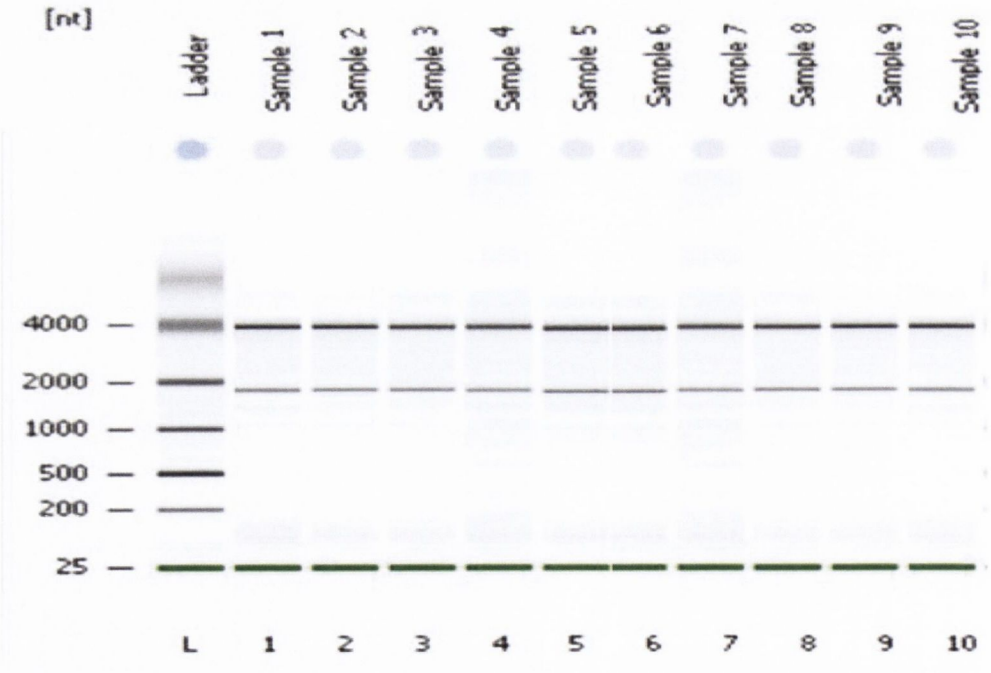

Figure 4-1: Output gel-like image of RNA samples from Agilent 2100 Bioanalyser depicting RNA quality assessment. Lanes 1-4 represent RNA samples from four biological replicates of E6#2, lanes 5-7 represents three biological replicates of E6#4 RNA samples and lanes 8-10 represent three biological replicates of scrambled control RNA extracts. 18S and 28S RNA bands in each sample clearly mark RNA of good quality.

4.4.1.2. Quality control valuation of microarrays

Preliminary quality checks were carried out via visual inspection of the microarray images. These included initially checking for image artefacts on arrays that is regions of high or low intensity spots, scratches and high regional or overall background. Then the performance of the positive hybridisation control, B2 oligo, was evaluated. Hybridisation of the B2 oligo control was assessed by examining specific regions of the array image (checkerboard corners and alternating borders). This control is of particular importance as it is essential for grid alignment over the microarray image. If the intensity of the oligo B2 controls is too high or low or skewed due to image artefacts, grid alignment will not automatically occur. All arrays passed these preliminary quality controls, that is no artefacts were present and the B2 oligo control appeared correctly on all images.

4.4.1.3. Quality control valuation of microarrays via calculated quality metrics

The quality of the arrays was further assessed to certify the absence of outliers or defective arrays that could bias downstream analysis. These procedures were carried out using Affymetrix EC software, which calculated the quality assessment metrics and generated graphs in order to facilitate data quality assessment. This is achieved by calculating summary statistics for each array and then comparing the level of the summary statistics across all the arrays.

The critical quality control metrics assessed are shown in Figure 4-2. A low level of variation was observed in all of the quality control metrics as projected when microarrays using RNA from the same cell line are assessed together. The pos_control and all_probeset categories were used to evaluate the overall quality of the data from each array (Figure 4-2 A and B).

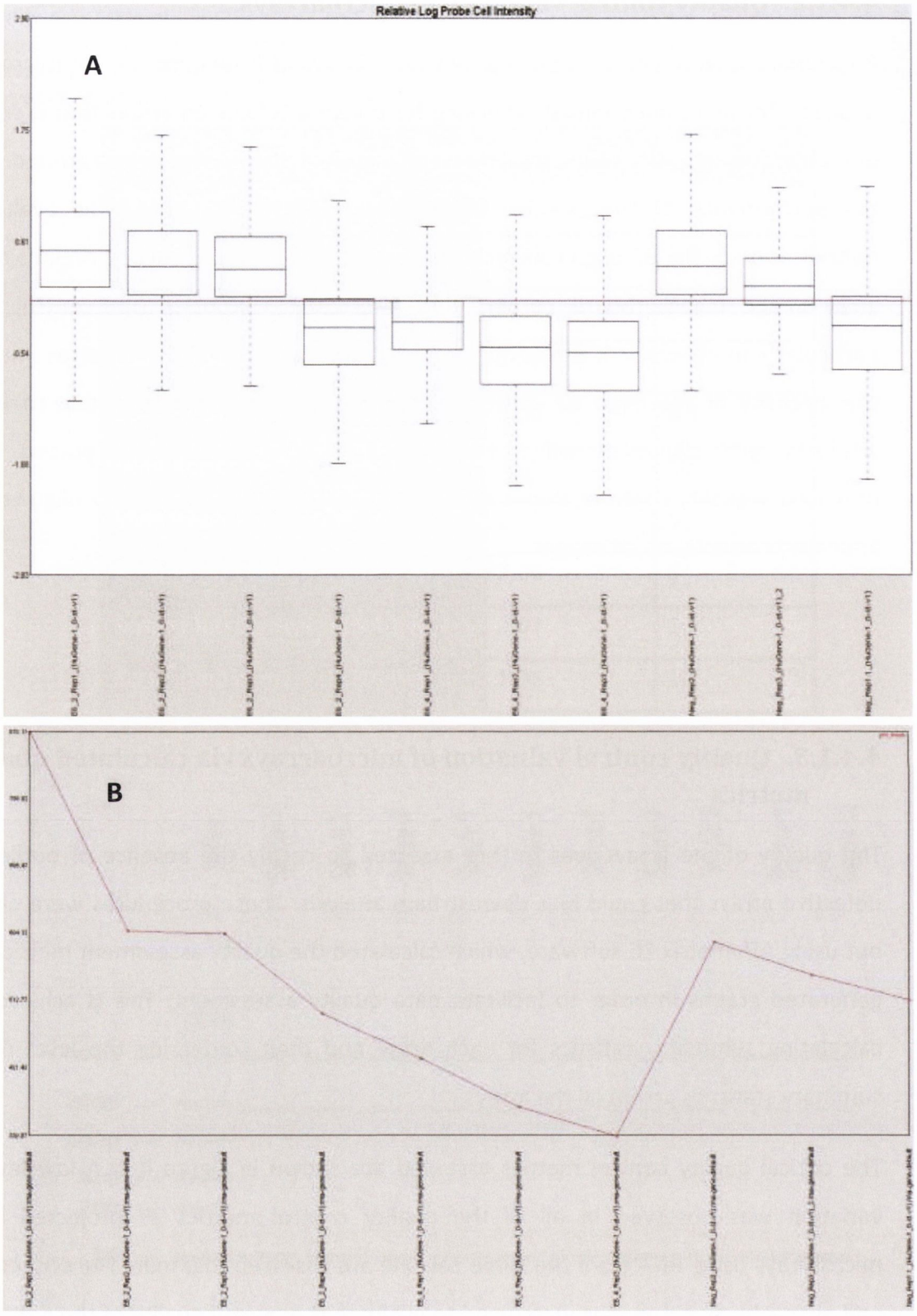

Figure 4-2: Quality control metrics of microarrays performed on siRNA transfected SiHa cells. The value of a metric for a particular microarray is represented by each point in the diagrams, whereby for each point the sample name on the x-axis has a corresponding arbitrary value on the y-axis. (A) Box plots of the RLE for all the probesets analysed. The mean absolute RLE is proportional to the width of the box plots, or the inter quartile range of RLE values. The middle bar in each box is the median RLE. (B) Illustrates the mean probe level intensity prior to normalisation or background correction.

Metrics based on these classifications reflect the quality of the whole experiment including RNA quality, target preparation, chip, hybridisation, scanning, and griding. Hence, they enabled the assessment of the type of data utilised in downstream statistical analysis. The signal discrimination of the positive and scrambled control siRNAs was above 0.75 for all arrays and indicated a low amount of variation between samples (not shown). This infers that there is a good separation between the positive and scrambled control siRNAs, which is a measure of true and false positives, and therefore, indicates the success of the entire microarray experiment.

A second example of the similarity of the samples is the box plot of the relative log expression (RLE) of the probe sets (Figure 4-2A). The middle bar in each box is the median RLE and should be zero. Deviations from zero usually signify skewness in the raw intensities of an array that was not properly corrected by normalisation. Any skewness observed in this quality control metric would also be reflected on visual inspection of the array, where dense areas of unusually bright or unusually dim intensities would be observed. All samples employed a zero median RLE, with their RLEs ranging between 1.85 and -1.85, reflecting the similarity (lack of skewness) amongst them. The absence of any image artefacts on visual inspection also supports no bias in the computed expression values. This lack of variability in expression values is consistent with the mean absolute relative log expression value and other metrics. The pm_mean of an array (prior to normalisation or background correction) also gives an indication as to unusually dim or bright chips. In this study, the pm_mean appears to vary a lot between microarrays, but when the range of the signal intensity of this metric is viewed, it is low (879 - 330) and therefore reiterates the low levels of inter-array variation (Figure 4-2B).

The mean absolute deviation of residuals (not shown) revealed the consistency between the positive controls (green), bacterial spikes (red), and the polyA spikes (blue). It demonstrated that there are problems with the chips, hybridisation or sample preparation. The metrics for bac_spike controls used to evaluate the efficiency of the

hydrisation of the samples to the microarray chips displayed expected rank order of BioB < BioC < BioD < Cre) signifying that no problem occurred at the hybridisation phase (not shown). The quality control metrics discussed above reflect that the microarray experiments were successful and no outlier was present.

4.4.2. Differential gene expression analysis

A whole-genome transcriptional profiling was performed to define gene expression modifications brought on due to siRNA silencing of the viral oncogenes E6 and E7 in $HPV16^{+}$ SiHa cervical cells. The design, validation and selected functional analysis of these siRNAs targeting the HPV16 E6 only or and its splice forms coding region was outlined in chapter 3. All five siRNAs designed indicated functionality of varying degrees but four only precisely generated sufficient, good quality RNA extracts for analysis (E6#2, E6#3, E6#4 and E6#5). Of these four, only three resulted in similar levels of highly significant knockdown in E6 and E7 RNA expression, two in-house designed siRNAs (E6#2 and E63) and Silencer® Select Ambion designed E6#4. It was decided to investigate the transcriptional response induced by E6#2 and E6#4 siRNAs in SiHa cells as both target similar regions of the E6 mRNA transcript, the 3' end of both E6 and E6*I, but provoked very different phenotype changes. E6#4 induces a senescent phenotype, while E6#2 appears to induce cell death.

Changes in gene pattern expression were identified by comparing these experimental E6 and E7 knocked down siRNA samples with samples transfected with scrambled control siRNA. The RNA samples used in this study originated from three independent experiments in which SiHa cells were forward transfected for 72hrs with E6#2, E6#4 or scrambled control siRNA and where E6/E7 RNA knockdown was validated by TaqMan® RT-PCR (section 2.3.4 and section 4.4.4). The Affymetrix Human GeneChip® Gene ST 1.0 microarrays, which consist of 818,005 probes that correspond to 28,869 gene transcripts, were used to hybridise biotinylated DNA. Data analysis was carried out using Bioconductor software libraries and probe intensities were transformed and

summarised using the oligo package as described in section 4.3.4 The relative change in abundance for each transcript between the baseline sample (scrambled control siRNA) and the experimental samples (E6#2 and E6#4) was determined using RankProd. A false discovery rate (FDR) was also calculated using the method outlined by (Benjamini & Hochberg, 1995) to adjust for multiple comparisons. An FDR of ≤ 0.05 and fold change ≥2 were used to define differentially expressed genes. Table 4-2 shows the number of differentially regulated genes upon silencing of the E6/E7 oncogenes in SiHa cells by E6#2 and E6#4 siRNAs.

Table 4-2: Table of the number of differentially expressed genes in E6#2 and E6#4 siRNAs forward transfected into SiHa cells.

siRNA	Significant* differentially regulated genes	Significant* down-regulated genes	Significant* up-regulated genes
E6#2	171	29	142
E6#4	399	346	53

*FDR≤0.05, Fold change≥2

4.4.3. Relative analysis of differentially expressed genes

From the previous morphological changes observed, an apoptotic profile in E6#2 and G1 arrest cell cycle in E6#4, it was anticipated that there would be differences between these siRNAs. The number of significantly differentially regulated genes varied substantially between the two experimental groups (Table 4-2), as E6#2 induced more of an up-regulation of genes and E6#4 a down-regulation of genes. This was further investigated using a hierarchical clustering and heat map representing all possible pair-wise combinations of samples used in the microarray analysis. The heat map was used to visualise the probe data of all differentially expressed genes (Figure 4-3 and Figure 4-4). The hierarchal clustering of normalised, background corrected data from the E6#2, E6#4 and scrambled control siRNA correlated with the heat map groups. They also reveal a great diversity in differential gene expression between E6#2 and E6#4. Despite the distinction in differential gene expression between E6#2 and E6#4 siRNAs, associations between their significantly differentially expressed genes and their observed transcriptional profiles was assessed using a cross comparison analysis of the differentially expressed gene lists. This revealed there were 171 and 399 genes differentially expressed at ≥2 fold and with a FDR ≤0.05 in the E6#2 and E6#4 groups respectively compared to the scrambled control siRNA group, of which 16 of these were represented in both array groups (Table 4-3). Some of the up-regulated and down regulated genes for E6#2 and E6#4 are shown in Table 4-4 and Table 4-5 respectively.

Keratin 34 and Stearoyl-CoA Desaturase (Delta-9-Desaturase) were the most significantly up-regulated and down regulated genes in E6#2 with fold change of 12 and 3 respectively, while Sulphatase 2 and Kinesin Family Member 20A were the most significantly up-regulated and down regulated genes in E6#4 with fold changes of 6.3 and 18 respectively. This result is in good correlation with the heat maps and reflects a good differentiation between the two groups of differentially expressed genes. Amongst the 16 genes, 5 were up-regulated (CDKN1A, SERPINE1, GLIPR1, PSG2, ITGA2) (highlighted red in Table 4-3) and 8 were down regulated (highlighted green in Table 4-3). However, 3 genes were shown to be up-regulated in E6#2 and down regulated in

E6#4 (Table 4-3). Cyclin-dependent kinase inhibitor 1A (p21, Cip1) and family with sequence similarity 111, member B were the most significantly up-regulated and down regulated genes represented in both array groups. Most of the other significantly up-regulated and down regulated genes in both had a fold change of between 2 and 3.

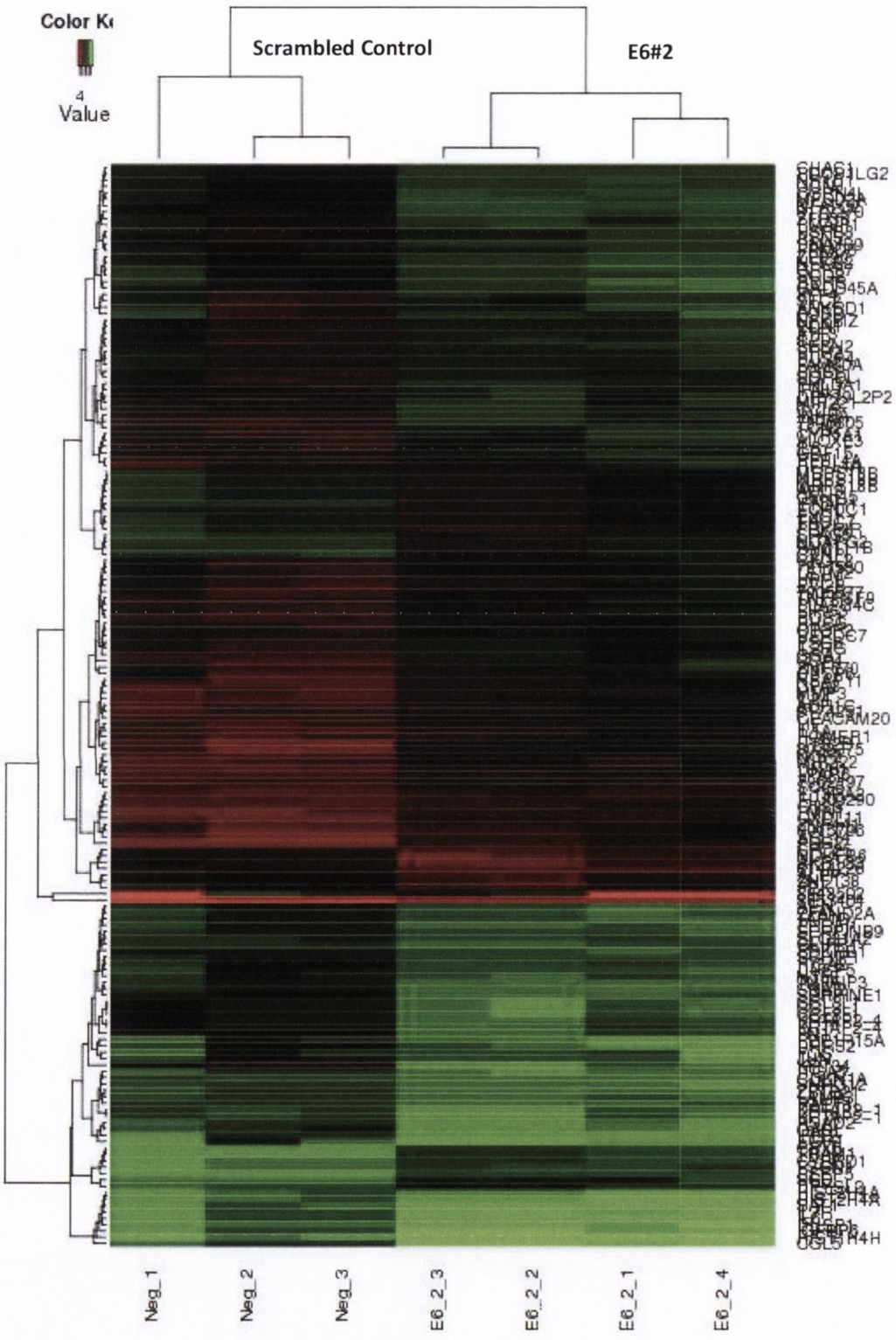

Figure 4-3: Heat map of significantly differentially regulated genes in E6#2 compared with scrambled control siRNA cells (FDR ≤ 0.05 and fold change ≥ 2). Red indicates up-regulated genes and green indicates down-regulated genes. Heat map demonstrates a clear distinction or separation differentially regulated genes between both siRNAs from those of the scrambled control treated samples. The hierarchical clustering depicted at the top of the graph also reflects the similarity between biological replicates.

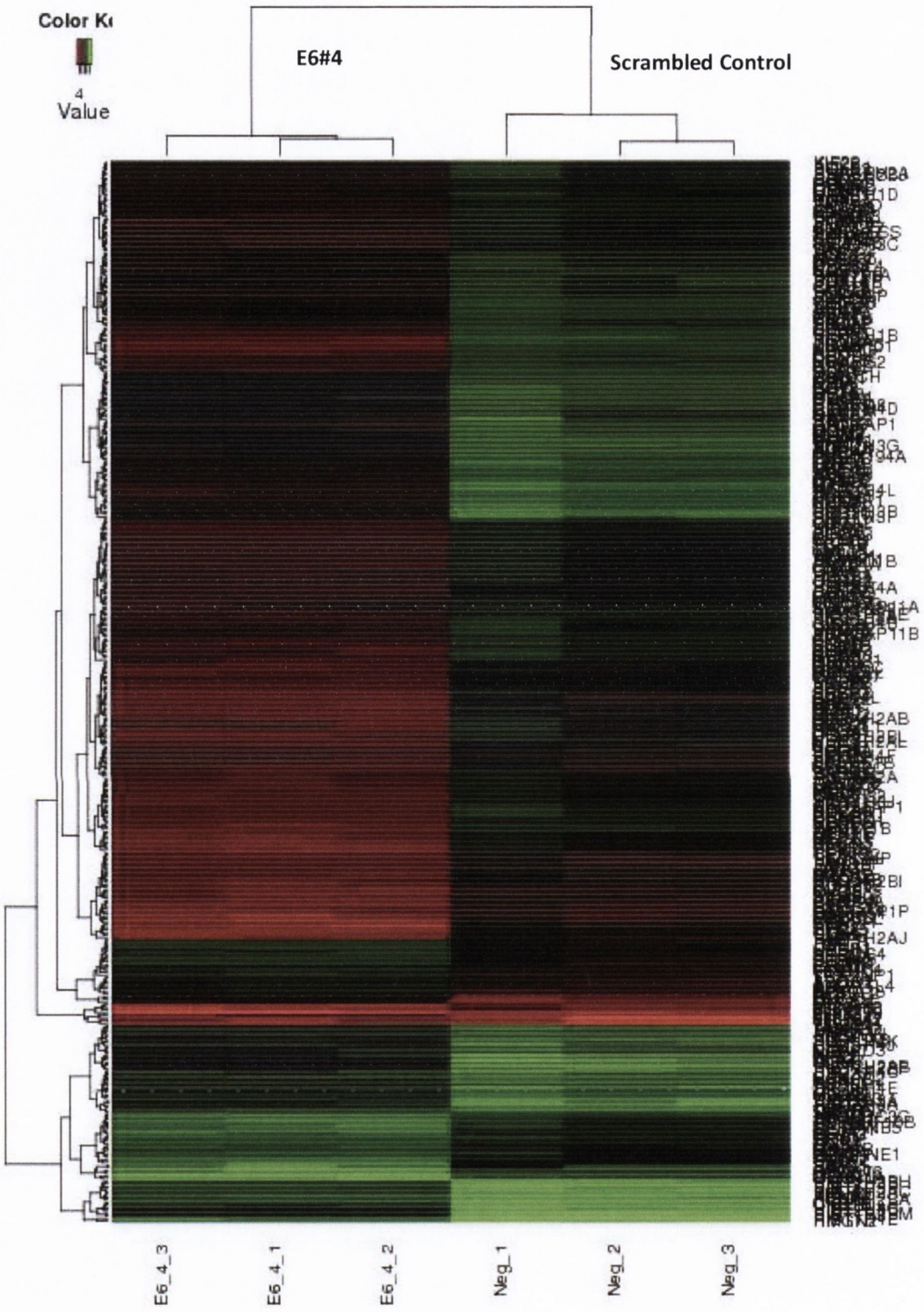

Figure 4-4: Heat map of significantly differentially regulated genes in E6#4 compared with scrambled control siRNA cells (FDR ≤ 0.05 and fold change ≥ 2). Red indicates up-regulated genes and green indicates down-regulated genes. Heat map demonstrates a clear distinction or separation differentially regulated genes between both siRNAs from those of the scrambled control treated samples. The hierarchical clustering depicted at the top of the graph also reflects the similarity between biological replicates.

Table 4-3: Table of all common differentially expressed genes (16 genes) in E6#2 and E6#4 siRNAs. Cells highlighted in red and blue represent up regulated and down regulated genes respectively. This table shows gene names, gene IDs, fold changes and false discovery rates.

Symbol	Gene Name	E6#2		E6#4	
		Fold-Change	FDR	Fold-Change	FDR
CDKN1A	Cyclin-dependent kinase inhibitor 1A (p21, Cip1)	2.12	0.0300	5.21	0.0000
SERPINE1	Serpin peptidase inhibitor, clade E (nexin, plasminogen activator inhibitor type 1), member 1	4.58	>0.0001	3.89	0.0043
GLIPR1	GLI pathogenesis-related 1	2.23	0.0190	3.36	0.0111
PSG2	pregnancy specific beta-1-glycoprotein 2	4.72	>0.0001	3.16	0.0163
ITGA2	integrin, alpha 2 (CD49B, alpha 2 subunit of VLA-2 receptor)	2.40	0.0085	2.75	0.0286
DHRS2	dehydrogenase/reductase (SDR family) member 2	4.90	0.0000	3.48	0.0039
OASL	2'-5'-oligoadenylate synthetase-like	3.49	>0.0001	2.85	0.0130
RSAD2	radical S-adenosyl methionine domain containing 2	2.73	0.0043	2.71	0.0214
FAM111B	family with sequence similarity 111, member B	2.53	0.0327	14.42	>0.0001
PBK	PDZ binding kinase	2.47	0.0271	9.81	>0.0001
SPC25	SPC25, NDC80 kinetochore complex component	2.42	0.0397	8.07	>0.0001
SPAG5	sperm associated antigen 5	2.61	0.0308	6.90	0.0002
CENPI	centromere protein I	2.40	0.0394	6.76	0.0002
NCAPG2	non-SMC condensin II complex, subunit G2	2.47	0.0315	6.23	0.0002
EXO1	exonuclease 1	2.71	0.0250	5.95	0.0003
POSPLDRAFT_92938	hypothetical protein [Postia placenta Mad-698-R]	2.67	0.0043	2.87	0.0087

Table 4-4: Table of top 10 differentially expressed genes in E6#2 siRNA. This table shows up regulated genes (red) and top ten down regulated genes (blue), gene names, gene IDs, fold changes and false discovery rates. (See Table 8-1 in the appendix for full list).

Symbol	Gene Name	Entrez GeneID	Fold-Change	FDR
KRT34	keratin 34	3885	12.18	>0.0001
CCL5	chemokine (C-C motif) ligand 5	6352	7.91	>0.0001
CCR4	chemokine (C-C motif) receptor 4	1233	5.82	>0.0001
INHBA	inhibin, beta A	3624	5.80	>0.0001
DHRS2	dehydrogenase/reductase (SDR family) member 2	10202	4.90	>0.0001
PSG2	pregnancy specific beta-1-glycoprotein 2	5670	4.72	>0.0001
SERPINE1	serpin peptidase inhibitor, clade E (nexin, plasminogen activator inhibitor type 1), member 1	5054	4.58	>0.0001
UTS2B	urotensin 2B	257313	4.57	>0.0001
FN1	fibronectin 1	2335	4.54	>0.0001
TCN2	transcobalamin II	6948	4.33	>0.0001
SCD	stearoyl-CoA desaturase (delta-9-desaturase)	6319	3.61	>0.0001
IFNAR1	interferon (alpha, beta and omega) receptor 1	3454	3.28	0.0133
ALPP	alkaline phosphatase, placental	250	3.22	0.0100
NDUFB6	NADH dehydrogenase (ubiquinone) 1 beta subcomplex, 6, 17kDa	4712	3.06	0.0100
AKR1C3	aldo-keto reductase family 1, member C3	8644	2.87	0.0117
CYBRD1	cytochrome b reductase 1	79901	2.86	0.0157
CBX5	chromobox homolog 5	23468	2.78	0.0233
EXO1	exonuclease 1	9156	2.71	0.0250
TRAM1	translocation associated membrane protein 1	23471	2.73	0.0236
SPAG5	sperm associated antigen 5	10615	2.61	0.0308
PBK	PDZ binding kinase	55872	2.47	0.0271

Table 4-5: Table of top 10 differentially expressed in E6#4 siRNA. This table shows up regulated genes (red) and top ten down regulated genes (blue), gene names, gene IDs, fold changes and false discovery rates (See Table 8-2 in the appendix for full list).

Symbol	Gene Name	Entrez GeneID	Fold-Change	FDR
SULF2	sulfatase 2	55959	6.39	>0.0001
SPATA18	spermatogenesis associated 18	132671	5.88	>0.0001
BTG2	BTG family, member 2	7832	5.75	>0.0001
TP53INP1	tumor protein p53 inducible nuclear protein 1	94241	5.74	>0.0001
CDKN1A	cyclin-dependent kinase inhibitor 1A (p21, Cip1)	1026	5.21	>0.0001
MIR224	microRNA 224	407009	4.74	0.0012
ZMAT3	zinc finger, matrin-type 3	64393	4.41	0.0011
SESN1	sestrin 1	27244	4.48	0.0010
ACTBL2	actin, beta-like 2	345651	4.18	0.0025
SERPINE1	serpin peptidase inhibitor, clade E (nexin, plasminogen activator inhibitor type 1), member 1	5054	3.89	0.0043
KIF20A	kinesin family member 20A	10112	18.12	>0.0001
RRM2	ribonucleotide reductase M2	6241	17.70	>0.0001
HIST1H2BM	histone cluster 1, H2bm	8342	16.95	>0.0001
HIST1H3I	histone cluster 1, H3i	8354	14.77	>0.0001
ANLN	anillin, actin binding protein	54443	14.13	>0.0001
DTL	denticleless E3 ubiquitin protein ligase homolog (Drosophila)	51514	14.13	>0.0001
MKI67	antigen identified by monoclonal antibody Ki-67	4288	13.79	>0.0001
HIST1H1B	histone cluster 1, H1b	3009	14.04	0.0250
FAM111B	family with sequence similarity 111, member B	374393	14.42	0.0236
HIST1H3F	histone cluster 1, H3f	8968	12.34	0.0308

4.4.4. p21, an investigative control

As p21 was employed as a surrogate marker in chapter 3, it was decided to investigate the expression profile of p21 as a quality control measure. The microarray data supports the differential expression of p21 gene between E6#2 and E6#4 siRNAs. The p21 gene had an average fold change expression value of 5.2 in E6#4 and 2.1 in E6#2, this was reflected in TaqMan® RT-PCR analysis (Figure 4-5) which also showed that though p21 was expressed in both siRNAs, E6#4 had a significantly greater fold change of p21 expression.

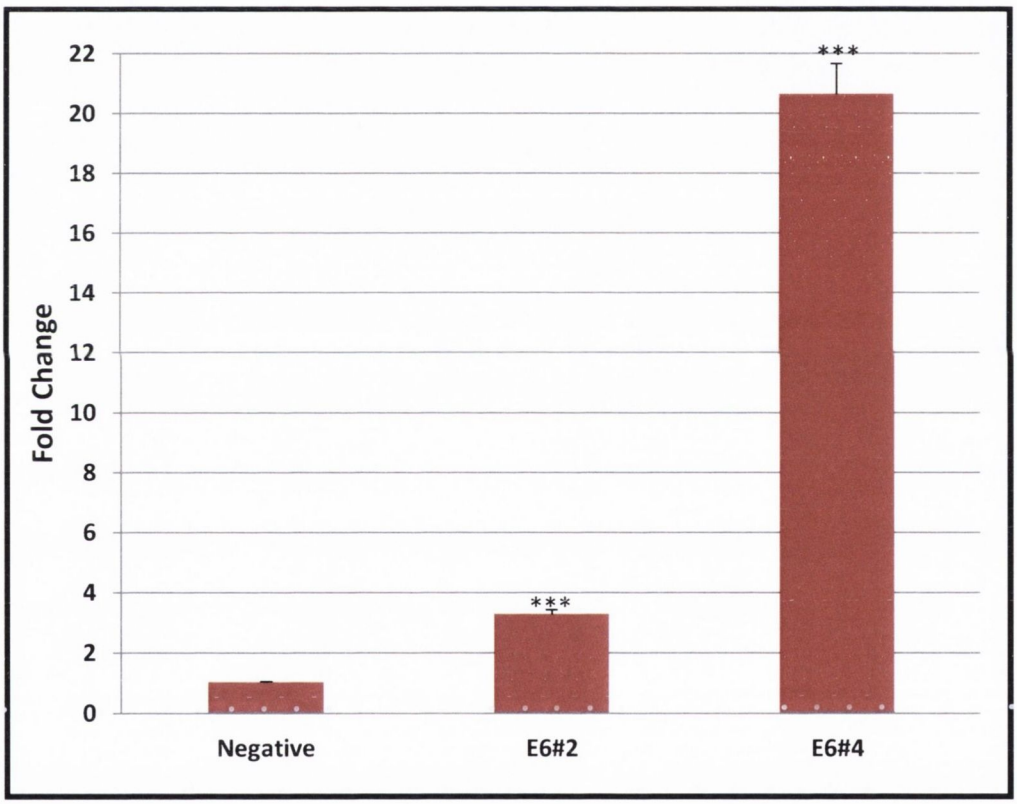

Figure 4-5: TaqMan® RT-PCR validation: TaqMan® RT-PCR validation of E6/E7 RNA knockdown using primers and probes selective for p21 mRNA from the same RNA used in microarray analysis. p21 mRNA expression was normalised to B2M and calibrated to cells transfected with scrambled control to establish the relative level of mRNA expression. A paired T-test via graph pad prism was carried out and values calculated were compared to scrambled control; ***$p<0.05$.

4.4.5. Gene ontology analysis

In order to explore significantly modified genes and processes due to E6 and E7 silencing, the group gene lists of E6#2 and E6#4 were uploaded and analysed in the web-based gene ontology database DAVID. DAVID is a functional annotation tool for gene-enrichment analysis that systematically summarises the relevant biological patterns from user-classified gene lists by comparing input list to a reference list to identify under and over-represented molecular functions and biological processes. A total of 357 of 399 differentially expressed genes in E6#4 were present in the DAVID database while 158 of the 171 differentially expressed genes in E6#2 were present in the DAVID database. With FDR at ≤ 0.05 in DAVID, a measure of overrepresentation of a functional category compared to its representation in the Homo sapiens proteome was determined. Table 4-6 and Table 4-7 show an abundance of up-regulated genes in E6#2 were associated with immune response and down-regulated genes with homeostasis while an abundance of up-regulated genes in E6#4 were associated with cell cycle arrest and homeostasis and down-regulated genes with cell cycling DNA replication. DAVID also determined overrepresented cellular pathways in both siRNAs from KEGG and Biocarta publically available databases, although featured pathways were more from the KEGG database.

In E6#2, differentially expressed pathways in context of biological pathways using KEGG and Biocarta resource revealed pathways involved in inflammatory response and signal transduction in up-regulated genes and pathways involved in metabolism in down regulated genes. A high number of up-regulated E6#2 genes were in the gene ontology categories of inflammatory response and signal transduction, with a high number of down-regulated genes in metabolism. In E6#4, a high number of up-regulated genes were in the gene ontology category of p53 signalling, with a high number of down-regulated genes in DNA replication and nucleotide metabolism (Table 4-7).

Table 4-6: Table of differentially expressed gene associations in E6#2. Representative table of 40 differentially expressed gene associations in E6#2. 20 up-regulated genes highlighted in red and 20 down regulated genes highlighted in blue.

Term	Count	%	p value	FDR
Response to wounding	19	14.50	5.49E-08	8.94E-05
Immune response	21	16.03	1.23E-07	2.00E-04
Defence response	19	14.50	5.03E-07	8.18E-04
Inflammatory response	14	10.69	7.59E-07	1.24E-03
Behaviour	14	10.69	4.02E-05	6.54E-02
Chemotaxis	8	6.11	1.81E-04	2.94E-01
Taxis	8	6.11	1.81E-04	2.94E-01
Locomotory behaviour	9	6.87	9.52E-04	1.54E+00
Regulation of viral genome replication	3	2.29	4.65E-03	7.30E+00
Regulation of viral reproduction	3	2.29	1.04E-02	1.56E+01
Response to extracellular stimulus	11	8.40	5.09E-06	8.29E-03
Response to nutrient levels	9	6.87	1.04E-04	1.69E-01
Response to oxidative stress	8	6.11	2.11E-04	3.42E-01
Response to reactive oxygen species	6	4.58	2.29E-04	3.71E-01
Response to inorganic substance	8	6.11	8.06E-04	1.30E+00
Response to drug	8	6.11	1.09E-03	1.77E+00
Senescence	6	4.58	1.32E-03	2.13E+00
Response to hydrogen peroxide	4	3.05	8.18E-03	1.25E+01
Response to cAMP	3	2.29	3.85E-02	4.72E+01
Response to extracellular stimulus	11	8.40	5.09E-06	8.29E-03
M phase	5	18.52	6.36E-04	7.71E-01
Cell cycle phase	5	18.52	1.50E-03	1.81E+00
Nuclear division	4	14.81	2.44E-03	2.93E+00
Mitosis	4	14.81	2.44E-03	2.93E+00
M phase of mitotic cell cycle	4	14.81	2.57E-03	3.08E+00
Organelle fission	4	14.81	2.73E-03	3.27E+00
Cell cycle process	5	18.52	4.64E-03	5.50E+00
Mitotic cell cycle	4	14.81	1.04E-02	1.19E+01
Cell cycle	5	18.52	1.40E-02	1.58E+01
Cell division	3	11.11	5.20E-02	4.77E+01
Chromosome, centromeric region	4	14.81	5.49E-04	6.07E-01
Chromosome	5	18.52	2.71E-03	2.97E+00
Kinetochore	3	11.11	4.59E-03	4.98E+00
Non-membrane-bounded organelle	9	33.33	1.20E-02	1.25E+01
Intracellular non-membrane bounded organelle	9	33.33	1.20E-02	1.25E+01
Chromosomal part	4	14.81	1.36E-02	1.41E+01

Table 4-7: Table of differentially expressed gene associations in E6#4. Representative table of 40 differentially expressed gene associations in E6#4. 20 up-regulated genes highlighted in red and 20 down regulated genes highlighted in green.

Term	Count	%	p value	FDR
Cell cycle arrest	4	7.84	2.76E-03	4.18E+00
Cell cycle process	5	9.80	6.71E-02	6.58E+01
Cell cycle	5	9.80	1.60E-01	9.33E+01
Wound healing	5	9.80	1.77E-03	2.69E+00
Coagulation	4	7.84	2.68E-03	4.06E+00
Blood coagulation	4	7.84	2.68E-03	4.06E+00
Response to wounding	7	13.73	2.90E-03	4.39E+00
Haemostasis	4	7.84	3.16E-03	4.76E+00
Regulation of body fluid levels	4	7.84	6.65E-03	9.78E+00
Regulation of response to external stimulus	4	7.84	9.24E-03	1.33E+01
Homeostatic process	5	9.80	1.47E-01	9.15E+01
Positive regulation of anti-apoptosis	4	7.84	7.27E-05	1.12E-01
Regulation of anti-apoptosis	4	7.84	1.49E-04	2.29E-01
Response to oxygen levels	5	9.80	5.72E-04	8.79E-01
Regulation of apoptosis	9	17.65	1.24E-03	1.90E+00
Regulation of programmed cell death	9	17.65	1.32E-03	2.02E+00
Regulation of cell death	9	17.65	1.36E-03	2.07E+00
Response to organic substance	8	15.69	3.01E-03	4.54E+00
Response to hormone stimulus	6	11.76	3.05E-03	4.61E+00
Response to organic cyclic substance	4	7.84	4.35E-03	6.50E+00
Cell cycle	139	45.42	2.24E-106	3.52E-103
Cell cycle phase	106	34.64	9.89E-95	1.55E-91
Cell cycle process	115	37.58	1.48E-91	2.32E-88
M phase	96	31.37	7.56E-91	1.19E-87
Mitotic cell cycle	89	29.08	2.14E-75	3.36E-72
Nuclear division	73	23.86	4.48E-72	7.04E-69
Mitosis	73	23.86	4.48E-72	7.04E-69
M phase of mitotic cell cycle	73	23.86	2.03E-71	3.19E-68
Organelle fission	73	23.86	1.28E-70	2.01E-67
Cell division	75	24.51	1.61E-64	2.53E-61
DNA replication	54	17.65	2.36E-48	3.70E-45
DNA-dependent DNA replication	24	7.84	2.37E-25	3.73E-22
DNA metabolic process	82	26.80	2.06E-54	3.23E-51
Response to DNA damage stimulus	52	16.99	3.68E-30	5.78E-27
DNA repair	44	14.38	2.84E-27	4.46E-24
Cellular response to stress	53	17.32	1.79E-22	2.81E-19

Table 4-8: Significantly over-represented pathways in E6#2. These pathways are as defined by DAVID databases. Up-regulated genes highlighted in red and down regulated genes highlighted in blue. *Values for count, FDR and P value were not supplied by DAVID database for down regulated genes.

Source	Pathway	Count	PValue	FDR
BIOCARTA	Regulation of MAP Kinase Pathways Through Dual Specificity Phosphatases	3.00	1.39E-02	1.42E+01
BIOCARTA	Cells and Molecules involved in local acute inflammatory response	3.00	3.47E-02	3.19E+01
BIOCARTA	Cytokine Pathway: Cytokine Network	3.00	5.25E-02	4.44E+01
BIOCARTA	Cytokines and Inflammatory Response	3.00	8.38E-02	6.14E+01
KEGG	Cytokine-cytokine receptor interaction	17.00	1.35E-08	1.41E-05
KEGG	Toll-like receptor signalling pathway	7.00	8.46E-04	8.79E-01
KEGG	Chemokine signalling pathway	7.00	1.75E-02	1.68E+01
KEGG	MAPK signalling pathway	11.00	6.48E-04	6.74E-01
KEGG	NOD-like receptor signalling pathway	6.00	5.89E-04	6.13E-01
KEGG	Toll-like receptor signalling pathway	7.00	8.46E-04	8.79E-01
KEGG	Prion diseases	4.00	6.78E-03	6.85E+00
KEGG	Jak-STAT signalling pathway	8.00	1.57E-03	1.63E+00
KEGG	Hematopoietic cell lineage	5.00	1.53E-02	1.48E+01
KEGG	Hypertrophic cardiomyopathy (HCM)	3.00	2.47E-01	9.48E+01
KEGG	Pathways in cancer	10.00	9.93E-03	9.90E+00
KEGG	Small cell lung cancer	4.00	6.73E-02	5.17E+01
KEGG	ECM-receptor interaction	4.00	6.73E-02	5.17E+01
KEGG	Focal adhesion	6.00	7.33E-02	5.48E+01
KEGG	Regulation of actin cytoskeleton	4.00	4.36E-01	9.97E+01
KEGG	B cell receptor signalling pathway		2.05E-01	9.09E+01
KEGG	T cell receptor signalling pathway		3.42E-01	9.87E+01
KEGG	Regulation of actin cytoskeleton		4.36E-01	9.97E+01
BIOCARTA	Regulation of MAP Kinase Pathways Through Dual Specificity Phosphatases		1.39E-02	1.42E+01
BIOCARTA	Cells and Molecules involved in local acute inflammatory response		3.47E-02	3.19E+01
BIOCARTA	Cytokine Network		5.25E-02	4.44E+01
BIOCARTA	Cytokines and Inflammatory Response		8.38E-02	6.14E+01
KEGG	Oxidative phosphorylation, Alzheimer's disease, Parkinson's disease, Huntington's disease,			
KEGG	Steroid hormone biosynthesis, Arachidonic acid metabolism, Metabolism of xenobiotics by cytochrome P450,			
KEGG	Folate biosynthesis, Axon guidance, Mismatch repair			

KEGG	Cytokine-cytokine receptor interaction, Toll-like receptor signalling pathway, Jak-STAT signalling pathway, Natural killer cell mediated cytotoxicity,
KEGG	Biosynthesis of unsaturated fatty acids, PPAR signalling pathway,
BIOCARTA	IFN alpha signalling pathway, Bone Remodelling,

Table 4-9: Significantly over-represented pathways in E6#4. These pathways are as defined by DAVID databases. Up-regulated genes highlighted in red and down regulated genes highlighted in blue.

Source	Pathway	Count	PValue	FDR
KEGG	Complement and coagulation cascades	4.00	3.49E-03	3.16E+00
KEGG	p53 signalling pathway	8.00	1.16E-08	1.06E-05
KEGG	Complement and coagulation cascades	4.00	3.49E-03	3.16E+00
KEGG	Pathways in cancer	3.00	4.42E-01	9.95E+01
BIOCARTA	Role of BRCA1, BRCA2 and ATR in Cancer Susceptibility	7.00	4.75E-06	**0.004264**
BIOCARTA	Cell Cycle: G2/M Checkpoint	5.00	1.18E-03	**1.054797**
BIOCARTA	Regulation of p27 Phosphorylation during Cell Cycle Progression	3.00	3.03E-02	**24.14546**
KEGG	DNA replication	21.00	1.16E-26	**1.05E-23**
KEGG	Systemic lupus erythematosus	15.00	1.85E-09	**1.66E-06**
KEGG	Homologous recombination	9.00	2.13E-08	**1.91E-05**
KEGG	Mismatch repair	7.00	2.50E-06	**0.002245**
KEGG	Nucleotide excision repair	8.00	1.20E-05	**0.010809**
KEGG	Pyrimidine metabolism	12.00	9.29E-07	**0.000835**
KEGG	Nucleotide excision repair	8.00	1.20E-05	**0.010809**
KEGG	Base excision repair	6.00	3.86E-04	**0.346405**
KEGG	Purine metabolism	10.00	1.77E-03	**1.581943**
KEGG	Small cell lung cancer	4.00	1.98E-01	**86.23732**
KEGG	Prostate cancer	3.00	4.88E-01	**99.75296**
KEGG	Pathways in cancer	7.00	5.61E-01	**99.93831**
KEGG	Ubiquitin mediated proteolysis	4.00	4.61E-01	**99.60805**

4.5. Discussion

HPV infection is the established etiological factor of cervical cancer, a devastating disease that affects women in their prime. Despite advances in our knowledge of its molecular biology and implementation of prevention programmes for this disease, a better understanding of its subversive actions that lead to cervical carcinogenesis is still required. Microarray analysis was used to quantify the mRNA concentration of all genes present in the genome of HPV16 positive SiHa cells forward transfected with E6#2 and E6#4 siRNA. This experimental approach had advantages of being unbiased and revealing potential effects due to uncharacterised E6 functions. In addition, in this approach we employed p21, a cyclin dependent kinase inhibitor, as an internal control whose differential gene expression is accompanied by the activation of p53. The disadvantage of this approach was the inability to assess some of the E6 functions that are not exhibited at the level of gene expression modification. For example, the role of the E6/E6AP complex which functions as ubiquitin ligase can only be assessed in terms of alterations in global protein levels. Therefore, until the development of a protein array technology that enables the investigation of a significant fraction of the proteome, gene expression analysis provides the most inclusive and balanced method for analysing the response of HPV-positive cells to silencing by siRNAs. In accordance with the validation data, the silencing effects of these siRNAs were reflected in the array data, by an up-regulation in p21 gene with a fold change of 2.1 in E6#2 and 5.2 in E6#4. This suggests that p21 is accumulating and complexing with cell cycle division stimulating protein cdk2 thereby halting cellular division.

An overall up-regulation of significantly expressed genes in E6#2 (142 of 171 genes) and down-regulation in E6#4 (346 of 399 genes) was observed in the SiHa cell line. This result, though unanticipated, is not surprising due to the differences in cell morphologies post transfection, the induction of a G1 arrest in E6#4 and the induction of cell death by E6#2, as discussed above. A total of 357 of 399 differentially expressed genes in E6#4 were present in the DAVID database while 158 of the 171 differentially

expressed genes in E6#2 were present in the DAVID database. A cross comparison of differentially expressed genes in E6#2 with E6#4 revealed the presence of only 16 genes in common (Table 4-3). Of these genes, five were up-regulated, eight were down-regulated and three were shown to be up-regulated in E6#2 and down-regulated in E6#4. All up-regulated genes (CDKN1A, SERPINE1, GLIPR1, PSG2, ITGA2) except CDKN1A related to the cellular components of extracellular signalling peptides, eight were linked to the biological process of inhibiting of cycle progression and division (FAM111B, PBK, SPC25, SPAG5, CENPI, NCAPG2, EXO1, POSPLDRAFT_92938) while the last three were linked to biological process of immune response (OASL, DHRS2 and RSAD2). Remarkably, the classification of these 16 genes is representative of the overall gene ontology overrepresentation in both siRNAs.

The CDKN1A (p21Cip1/Waf1) protein is a dual functioning protein which act either as a tumour suppressor or an oncogene (prevent apoptosis). It plays a regulatory role in S phase DNA replication and DNA damage repair (p53 mediator of inhibition of cellular proliferation). Following DNA damage, CDKN1A becomes localised in the nucleus, binds and inhibit cyclin dependent kinases (Cdk1-4), thus blocking G1 to S phase transition or G2 to mitosis to facilitate DNA repair or induce senescence (Xia, et al., 2011). However, in the cytoplasm, CDKN1A binds and inhibit caspase 3, apoptotic kinases such as ASK1 and JNK (anti-apoptotic effect). Therefore, CDKN1A function is possibly largely determined by the scale of DNA damage wherein low-level damage instigates cell cycle arrest and severe DNA damage results in apoptosis (Ćmielová & Řezáčová, 2011). In this study, the rise in CDKN1A/p21 levels observed at both RNA and protein level for E6#2 and E6#4 was shown to be instigated by its up-regulation at gene level.

Similarly, PDZ binding kinase (PBK), differentially down-regulated in E6#2 and E6#4 is also known as T-LAK-cell-originated protein kinase (TOPK). PBK is a mitotic kinase often up-regulated in malignancies and mitotically active neoplastic cell lines and tissues that requires mitotic phosphorylation for its kinase catalytic activity. PBK phosphorylates

p38 MAPK resulting in its complex with p53, causing p53 destabilization and attenuation of G2/M checkpoint during DNA damage (Nandi, et al., 2004) (Nandi, et al., 2007) (Hu, et al., 2010). Therefore, PBK down-regulation could be one of the mechanisms by which p53 stabilisation observed at protein level in E6#2 and E6#4 is occurring.

Interestingly, PBK is linked OASL gene via intracellular pathways involved in the processing of dsRNA in mammalian cells (Figure 4-6). The OASL gene is a relatively novel gene related to the 2'-5'-oligoadenylate synthetase family. This family of genes consist of three genes encoding active OAS enzymes (OAS1-3) and an OAS-Like (OASL) gene encoding an inactive protein which binds dsRNA. The main difference between OASL and the other member of this family is the lack of 2',5'-oligoadenylate synthetase activity (Melchjorsen, et al., 2009). OAS proteins are pathogen recognition receptors (PRRs) that exist at different basal levels in different cell types and are induced by interferons in response to viral infection. On induction by pathogen-associated molecular pattern (PAMPs) that is viral dsRNA, the synthetase (OAS)/RNase L pathway is activated whereby, OAS proteins synthesize 2',5'-oligoadenylate from ATP, which binds antiviral enzyme RNase L causing its dimerization and activation (Silverman & Weiss, 2014). OASL has been shown to displays antiviral activity against encephalomyocarditis virus and hepatitis C virus via an alternative antiviral pathway independent of RNase L (Figure 4-6) (Marques & Williams, 2005) (Zhu, et al., 2014).

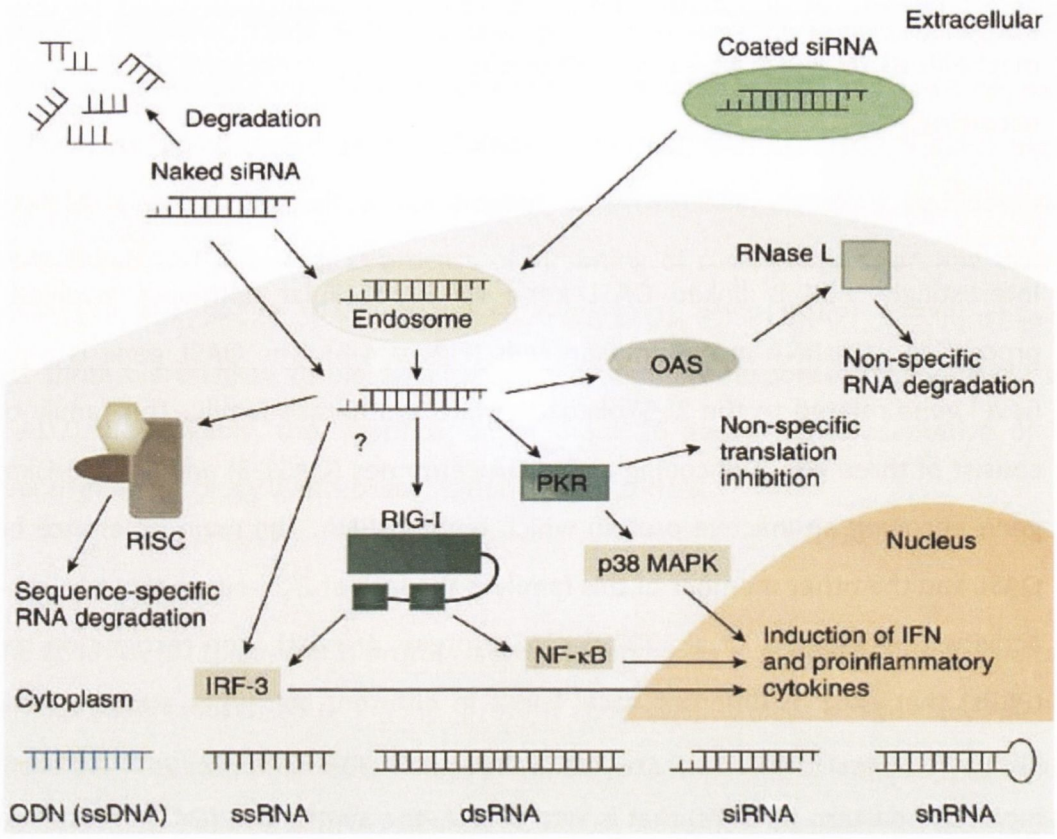

Figure 4-6: Intracellular pathways involved in the processing of dsRNA in mammalian cells. These pathways include RNA-induced silencing complex (RISC), Interferon regulatory factor (IRF-3), Retinoic acid inducible protein (RIG-I), dsRNA-activated protein kinase (PKR) and 2'5'-oligoadenylate synthetases (OAS) (Marques & Williams, 2005). IFN, Interferon; ODN, Oligodeoxynucleotide; ssRNA, single stranded RNA; shRNA, short hairpin RNA;

The DHRS2 gene belongs to a family of NADPH-dependent reductase enzymes responsible for quenching cytotoxic xenobiotics generated during metabolic processes and oxidative stress. The non-enzymatic activity of this gene however, involves the binding of MDM2 protein in the nucleus, thereby attenuating MDM2-mediated p53 degradation. This leads to p53 stabilization and increased transcription activity, resulting in the accumulation of MDM2 and CDKN1A/p21. Hence, the nuclear concentration of DHRS2 can control the initiation of cell cycle arrest and apoptosis as is observed in E6#4 and E6#2 respectively (Shafqat, et al., 2006) (Deisenroth, et al., 2010) (Thorner, et al., 2010). The RSAD2 also known as Cytomegalovirus-Induced Gene 5 Protein (CIG) and Virus Inhibitory Protein Endoplasmic Reticulum-Associated (vig

1/Viperin) is an antiviral effector induced in response to lipopolysaccharide and dsRNA viruses that inhibits virus production. RSAD2 plays an important role in regulation of Golgi trafficking of secretary molecules such as TNF-α (Chung, et al., 2011). RSAD2 has been shown to be redistributed, on infection with human cytomegalovirus (HCMV), which results in its redistribution from the cytosolic face of the endoplasmic reticulum to the Golgi apparatus and cytoplasmic vacuoles containing HCMV structural proteins (glycoprotein B and phospho-protein 28) essential for production and assembly of infectious virions. This redistribution aids viral evasion as RSAD2 could interfere with transport of critical viral components (Chin & Cresswell, 2001) (Helbig, et al., 2005).

Conversely, E6#2 exhibited an abundance of up-regulated genes associated with biological processes of innate immune response and down-regulated genes with homeostasis (Table 4-6). In addition, up-regulated gene ontology categories of inflammatory response and signal transduction pathways and down-regulated metabolism were also identified (Table 4-8). Genes included were: inflammatory stimulators such as cytokines and chemokines, toll like receptors, MAPK phosphatases, JAK-STAT signalling pathways, regulators of apoptosis and lymphocyte activators. Innate immunity is the first line evolutionarily conserved defence against potential hosts that involves the use of a range of pattern recognition receptors (PRRs) to identify specific pathogen-associated molecular patterns (PAMPs) solely present on microbes such as viruses etc. The recognition of PAMPs by the PRRs initiates an inflammatory response causing the secretion of cytokines and chemokines, stimulation of antimicrobial peptides, pyroptotic cell death and recruitment of phagocytic cells (Broz, et al., 2012)

A recently published paper by Karim, et al. examined the link between the up-regulation of cellular protein ubiquitin carboxyl-terminal hydrolase L1 (UCHL1) by HPV and the suppression of innate immune response in keratinocytes (Karim, et al., 2013). It reported that UCHL1 carried out this suppression via inhibition of PRR- signalling pathway adaptor molecules such as tumour necrosis factor receptor-associated factor

3 (TRAF3) and TRAF6 to suppress production of the type-I interferon pathway and pro-inflammatory NF-kappa-B (NF-κB) pathway respectively (Karim, et al., 2013). Two signalling pathways lead to the activation of NF-κB; the classical/canonical and the non-canonical/alternative pathway. The NF-κB signalling pathway supressed by UCHL1 was the classical/canonical NF-κB pathway which involved ligand binding to cell surface receptors (Toll-like receptor superfamily), recruiting adaptors such as TRAF and IKK complex, leading to phosphorylation and degradation of the IkB inhibitor.

However, in this study, a non-canonical activator of NF-κB signalling pathway, nuclear factor of kappa light polypeptide gene enhancer in B-cells 2 (NF-κB /p49/p100), was identified from the significantly differentiated up-regulated genes. This gene had a fold change value of 2.1, FDR of 0.0235 and a p value of 0.0001. p100 complexes with RelB to form p100/RelB which is a central activator of genes involved in immune function and inflammation. This complex usually only occurs during the development of lymphoid organs to generate B and T lymphocytes. In this pathway, ligand receptor binding induces activation resulting in NFkB-inducing kinase (NIK) which phosphorylates and activates an IKK alpha complex that in turn phosphorylates the IkB domain of p100 leading to the liberation of p52/RelB. This heterodimer is subsequently translocated to the nucleus to activate target genes regulated by kB sites. Interestingly, only a small number of stimuli, (lymphotoxin B and B cell activating factor; a membrane protein and a cytokine of tumour necrosis factor family) have been identified to activate NFkB via this pathway.

Furthermore, a downstream effector of NFkB signalling and p100 regulation also identified from our significantly differentiated up-regulated genes was interleukin-6 (IL-6) (Figure 4-7). IL-6 is a cytokine released by activated monocytes that plays a crucial role in the immune response. The activation of its gene expression by NFkB in Hela cells has also been reported (Libermann & Baltimore, 1990). Similarly, another study by Niebler M, et al. has shown HPV16 E6 oncoprotein to escape innate immune surveillance via post-translational control of IL-1β. E6 abrogates iL-1β processing and

secretion in a NACHT-, leucine-rich repeat (LRR)-and PYD-containing protein 3] (NALP3) inflammasome-independent manner (Niebler, et al., 2013). Hasan U A, et al. has also shown the ability of high-risk HPV16 to interfere with innate immunity by affecting the expression of TLRs in an in vivo context and also inability of low-risk HPV type 6 to down-regulate the TLR9 promoter. (Hasan U A, et al., 2007).

Conversely, most E6#2 down-regulated genes were associated with cell cycling and gene ontology pathways of metabolism such as oxidative phosphorylation, folate biosynthesis and steroid hormone biosynthesis (Table 4-8). These metabolic pathways are particularly important in production of cellular energy ATP via the transfer of electrons from donor atoms to electron acceptors such as oxygen. Therefore the down-regulation of components such metabolic processes results in the generation of reactive oxygen species such as super oxides and hydrogen peroxides which led to the propagation of free radicals within the cell and cell damage. Therefore overrepresented down-regulated and up-regulated genes in E6#2 are driving towards the initiation of an innate immune response with the secretion of chemokine, cytokines and interferons in addition to the generation of reactive oxygen species thereby stimulating apoptosis.

These results are therefore in line with previously published data that HPV16 evades innate host immunity and also reveals the mechanism of suppression to be PRR-induced production of interferons, cytokines and chemokines, which normally results in the attraction and activation of an adaptive immune response. Likewise, an abundance of down-regulated genes associated with disruption in metabolism via generation of reactive oxygen species and radicals which also propagate the role of apoptosis complements this notion. Therefore, E6#2 siRNA is potentially activating PRR-induced immune response and consequently silencing viral subversion.

The differential gene expression in E6#4 revealed entirely different patterns and associations. A bulk of its genes were down-regulated with an abundance of genes associated with replication and cell cycling and gene ontologies categories of nucleotide metabolism (purines and pyrimidines) and regulation of p27 phosphorylation during cell cycle progression (Table 4-7). DNA replication is a basis of biological inheritance which involves the unwinding of the double helix such that one strand serves as a template for the synthesis of a complementary strand by the addition of nucleotides matched to the template. Similarly, p27 regulates the cell cycle by binding cyclin dependent kinase/cyclin E and blocking G1 to S phase transition. It is regulated by phosphorylation, synthesis and degradation. The phosphorylation of p27 results in its association with an SCF complex that targets p27 for proteolytic degradation. E6#4 exhibited an abundance of down-regulated genes associated with biological processes of cell cycling and DNA replication while up-regulated genes with cell cycle arrest and homeostasis In addition, down-regulated gene ontology categories of DNA replication and nucleotide metabolism pathways and up-regulated category of p53 signalling were also identified (Table 4-9). Included genes associated with chromosomal stability and DNA repair were BRCA1, BRCA2, cell division cycle protein (CDC25C, CDC45, CDC6, CDC7, CDCA2, CDCA3, CDCA4, CDCA5), CENPA, FANCA, FANCB, FANCD2, FANCG, histone cluster genes (HIST1H1E), kinesin family member genes (KIF22), MCM and ORC. A similar pattern of genes was also reporter by Kuner et al. study whereby RNAi was used to silence HPV E6 and E7 in HeLa cells and differentially expressed genes were compared with published microarray data from HPV-positive cervical cancer biopsies (Kuner, et al., 2007). On comparison, 18% of differentially regulated genes in E6#4 were represented in Kuner et al. paper.

Breast cancer, early onset genes (BRCA1 and BRCA2) generate tumour suppressor proteins to aid DNA damage repair and ensure stability of the cell's genetic material (Brose, et al., 2002) (Chen & Parmigiani, 2007). The Fanconi anemia complementation group (FANCA, FANCB, FANCD2, FANCG), is linked to a homozygous recessive disorder characterised by chromosomal instability, hypersensitivity to DNA crosslinking agents, increased chromosomal breakage, and defective DNA repair (Narayan, et al., 2004).

Cell division cycle proteins (CDC25C, CDC45, CDC6, CDC7, CDCA2, CDCA3, CDCA4, CDCA5) form part of the pre-replicative complex required for loading mini chromosome maintenance (MCM) proteins onto the DNA at origin recognition complex (ORC), an essential step in the commencement of DNA synthesis (Maiorano, et al., 2000) (Lei, 2005). Other proteins like Centromere proteins (CENPA), histone cluster genes, (HIST1H1E) and kinesin family member genes (KIF22) are required by the cell for targeting the centromere, nucleosome structure and movement during mitosis.

The overrepresentation of p53 pathway induction by E6#4 was expected due to the expression of its biomarker, p21 and its expression at protein level. A number of p53 responsive genes such as BTG family member 2 (BTG2), MDM2, p21 and p27 were also up-regulated. These results strongly suggest that the viral oncogene influences the G1/S phase transition of the cell cycle and is in agreement with previous in-house studies (Spillane et al, 2009). Garner-Hamrick et al reported a microarray analysis of organotypic cultures of human primary keratinocytes retrovirally transduced with the HPV18 E6 and E7 under the control of the native differentiation-dependent HPV enhancer-promoter. Their results showed up-regulated transcripts of MCM proteins, ORC6, cdc6, and cdc45 and DNA metabolism transcripts similar to this study (Garner-Hamrick, et al., 2004). Similarly, an over-representation of mitotic checkpoint proteins observed in our study has also been shown in (Amato, et al., 2009).

Previously, the 'role of BRCA1, BRCA2 and ATR in Cancer Susceptibility' pathway was identified following knockdown of E6/E7 using E7 siRNA in this lab. This pathway was also identified using the E6#4 siRNA at a lower p value of 4.75E-06 compared to (p-value ≤ 1.0E-5 (Table 4-8) These genes are members of the Fanconi Anaemia (FA) - breast cancer associated gene (BRCA) pathway involved in a rare autosomal recessive chromosomal instability disorder, known as Fanconi anaemia.

In summary, the inactivation of cellular oncogenes in SiHa cells by E6#2 and E6#4 siRNAs result in differential genes patterns. In E6#2, there is an induction of the innate immune response via a non-canonical NFkB signalling pathway that results in secretion of chemokine, cytokines, interferons and the generation of reactive oxygen species promotes apoptosis. However, E6#4 drives an up-regulation of p53 signalling pathway via stabilisation of its regulatory response proteins such as BTG, p21 and p27 in addition to the down-regulation of DNA replication resulting in cell cycle arrest.

Chapter Five

Raman Spectroscopy

5. Raman Spectroscopy

5.1.Introduction

Cervical cancer is a treatable yet predominant cause of cancer mortality amongst women worldwide. HPV is the primary risk factor in disease development and despite remarkable advances in our understanding of its natural history; early detection remains a crucially defining element in the prevention of disease progression. Prevention programs targeted against the disease comprises of two stages, primary prevention programs which involve the implementation of vaccination programs and secondary prevention programs which involve cervical screening programs (conventional Pap smear tests, liquid based cytology (LBC), visual inspection with acetic acid, HPV testing for high risk types and colposcopy) which are directed towards the detection and treatment of precancerous lesions amongst asymptomatic women aged 25 to 60 years.

The use of conventional microscopy with numerous dyes, fluorophore and labels to "stain" target sample features can bring about limitations in observing or studying certain properties and structures without chemical damage or preferential solvent washing. For instance, the detection of low-grade squamous intraepithelial lesions (LSIL) is particularly limited due to the broad sensitivity range, high levels of inaccuracy and equivocal diagnoses using the Pap smear test. However, the use of LBC as a more efficient method of cervical sampling for laboratory examination has resulted in a 47% to 65% increase in the diagnosis of LSIL (using SurePath Pap test and ThinPrep Pap test respectively) compared with the conventional Pap test (Gibb & Martens, 2011). Yet, the ability of up to 80% of low grade abnormalities to spontaneously regress (Matsumoto, et al., 2010), results in an increased likelihood of over referrals, overtreatments and inappropriate follow ups. This therefore, demonstrates a need for the development of new screening technologies to compliment this high LSIL detection rate by discriminating between regressive and progressive LSILs as well as high-grade squamous intraepithelial lesions and those difficult to diagnose cases.

Raman spectroscopy is an inelastic scattering phenomenon used to investigate the biochemistry of biological molecules and in recent times has emerged as an attractive molecular optical imaging strategy tool in biomedical applications such as cancer diagnosis over other optical imaging techniques such as flow cytometry. Raman spectroscopy involves the interaction of electromagnetic radiation with matter and the spectrum of vibrational energies produced can be used to characterise a molecular structure or changes to it (Brauchle & Schenke-Layland, 2013). Its use includes ultrasensitive detection of several biomolecules and investigation their various characteristics *in vivo* and *ex vivo* to provide a 'molecular fingerprint' via Raman scattering of monochromatic laser light. Tissues and cells are composed of nucleic acids, proteins, water, lipids and carbohydrates which are further made up of amino acids (purines and pyrimidines) which can be probed and identified using spectroscopy. The amount of energy lost or gained by a photon due to its interaction with a molecule is characteristic of the nature of each vibrational bond present within that molecule and though not all vibrations are observed, adequate information is revealed to enable a very detailed characterisation of its molecular structure (Figure 5-1). An excited molecule may relax back to its initial vibrational energy level results in release of photons of the same energy and wavelength (Rayleigh scattering) or de-excite to a different vibrational state in a very tiny proportion of molecules (Raman scattering). However, a Stokes shift may occur if the final vibrational state is more energetic (longer wavelength) than the initial state that is the emitted photon will be shifted to a lower frequency in order to balance the total energy of the system and vice versa in an anti-Stokes shift.

In Raman scattering, energy transitions are exclusively based on vibrational transitions and perturbations of a molecule due to excitation via photon interaction induces vibrational transitions. The change in wavelength of the scattered photon provides chemical and structural information on the molecule and the difference in energy of the incident photon and the Raman scattered photon is equal to the vibrational energy of the scattering molecule (Brauchle & Schenke-Layland, 2013). This information is presented as a Raman spectrum plot of scattered light versus energy difference which

gives a precise spectral fingerprint of various wavelengths of scattered light whereby wavelengths associated with the different bonds and vibrations can be inferred from a table of Raman band positions for example the amount of energy shift for a C-H bond is different to that seen with a C-O bond or a Group 1 Metal element-O bond.

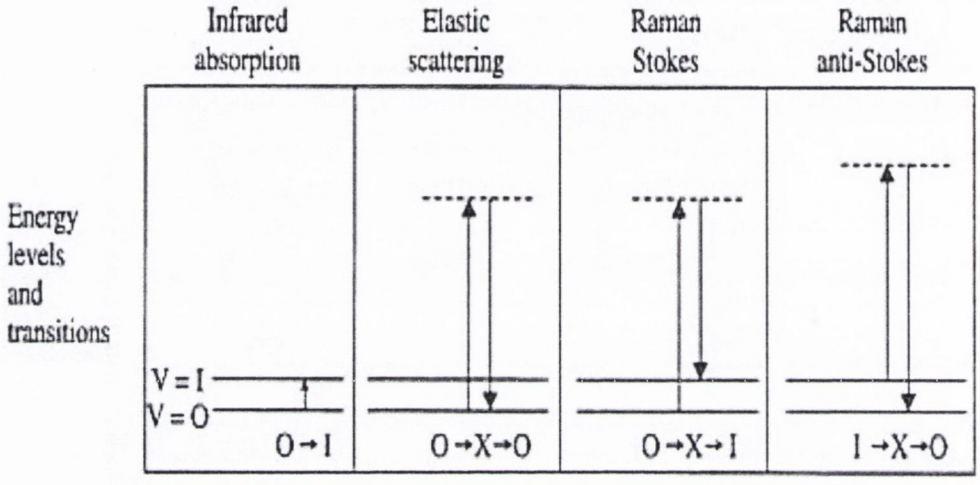

Figure 5-1: Schematic energy-level diagram showing the different states involved in Raman signalling: Infrared absorption, Elastic scattering and inelastic scattering; Raman Stokes, Raman Anti-stokes by a molecule with two vibrational quantum states (ground state v=0 and v=1 energy level. In infrared absorption, incident light has the same frequency as the molecular vibration. In elastic and in elastic scattering, incident light/photon has a much higher frequency (7 times more in this diagram). Scattered photons of lower frequency are Stokes and scattered photons of higher frequency are anti-Stokes. **(Colthup, et al., 1990)**

Despite its advantages (such as adaptability to *in vivo/in situ* measurements, easily extractable data from spectra, almost no sample preparation, no dependence on wavelengths and no exposure to harmful radiations or chemical) over other optical imaging techniques, Raman spectroscopy is an inherently weak process. This is due to the small number of Raman scattered photons produced hence improvisations such as resonance Raman, surface-enhanced Raman scattering (SERS) (Dinish, et al., 2014), and Raman micro spectroscopy have been made. Spectroscopic analysis has however, improved the prospects of understanding and detecting disease at a cellular level as biochemical changes to cellular constituents at a molecular level is the basis for cancer. (Pudlas, et al., 2011)

Mahadevan et al. were the first group to record the Raman spectrum of cervical tissues. They described the possibility of using Raman spectroscopy to distinguish cervical pre-cancers from other conditions and developed a fibre-optic probe to measure the spectra of cervical tissue in vivo (Mahadevan-Jansen, et al., 1998). Since, Raman spectroscopy has been used to detect HPV infection in cervical cells that is, in multivariate analysis to discriminate between normal and abnormal cells, in cervical biopsy samples, cervical cytology samples and also amongst cervical cancer cell lines (Jess, et al., 2007) (Jess, et al., 2008) (Ostrowska, et al., 2010) (Kelly, et al., 2010). Jess et al. revealed the ability of Raman spectroscopy to discriminate between normal keratinocytes and the transformed cervical carcinoma-derived cell line CaSki, to identify cells expressing the HPV16 E7 gene and suggested the use of Raman in the identification and discrimination of the different stages of HPV-associated neoplasia (Jess, et al., 2007). Ostrowska et. al investigated four cervical cancer cell lines including HPV negative C33A cells, HPV-16 positive SiHa (low copy HPV), HPV-18 HeLa (moderate copy number) and HPV-16 CaSki (high copy number) cells using Raman and Fourier Transform Infra Red absorption techniques. Using Principal Component Analysis (PCA), they demonstrated the ability to discriminate between the cell lines on the basis of their biochemical composition (cellular differences originating from proteins, nucleic acids and lipids) where by the most significant discrimination was between the C33A-SiHa group and HeLa and CaSki cell lines indicative of the effect of HPV presence in these cells (Ostrowska, et al., 2010).

5.2.Chapter aim

The aim of this chapter was to identify changes in the biochemical compositions due to the effect of silencing HPV16 E6 and E7 oncogenes. This was accomplished by examining spectra discriminations induced in cellular components of HPV16 infected cervical cells by the concomitant silencing of E6 and E7. The viral oncogenes were repressed using E6 targeting siRNAs as described in chapter 3 and validated to ensure unprejudiced analysis of spectra discrimination attributed to silencing of E6 and E7.

5.3. Materials and Methods

5.3.1. Cell culture

HPV16^{+} SiHa cervical cancer cell line were grown and cultured at 37°C in a humidified 5% CO_2 atmosphere. SiHa cells were then independently forward transfected with scrambled control siRNA and E6#2 siRNA for 72hrs as described in Section 2.5 and Section 2.10. E6#2 was selected for spectra discrimination analysis as a result of its distinct dramatic morphological phenotype and the induction of a cell death immunological response. The suppression of HPV E6 and E7 was confirmed visually based on previously confirmed experiments.

5.3.2. Raman spectroscopy

72hrs following forward transfection, CaF_2 chips were fixed in 10% filtered formalin solution at -20°C for 15mins and moved to the Focas Research Institute at Dublin Institute of Technology (DIT), where Raman analysis was performed using a HORIBA Jobin Yvon XploRA^{TM} system (Villeneuve d'Ascq, France) which incorporates an Olympus microscope BX41 equipped with a 100X objective (MPlanN, Olympus). The laser source used throughout this study was a 532nm diode which produces a high level of long-term output power of <5mW to 20 W and was set at 100% at the objective. The confocal hole was set at the specified setting for confocal operation (100µm) for all measurements. The system was pre-calibrated to the 520.7 cm^{-1} spectral line of Silicon. The confocal spectrometer of the XploRA^{TM} system contains 4 interchangeable gratings of 600, 1200, 1800 and 2400 lines/mm. The 1200 lines/mm grating which gave a spectral dispersion of ~3 cm^{-1} per pixel and an acquisition time of 30secs without compromising or decreasing the signal to noise ratio in the spectra collected was used in this study. Higher resolution grating such as 2400 gr/mm which although may give a better spectral resolution of <1 cm^{-1}, would tremendously increase acquisition time to a matter of minutes and hence was not considered. The backscattered light was measured using an air-cooled charge-coupled device (CCD)

detector (Andor, 1024 x 256 pixels) and the spectrometer controlled by Labspec Version 5.0 software.

5.3.3. Spectral analysis

Following the collection of raw Raman spectra, spectral analysis was carried out by Dr. Luke O'Neill and Padraig Kearney of the Focas Research Institute at Dublin Institute of Technology. In total, single spectra and backgrounds were acquired from 40 fixed scrambled control siRNA cells and 40 fixed E6#2 siRNA cells. For each cell, 3 spectra were recorded (nucleus, nucleolus, and cytoplasm), each of them corresponding to the average of two accumulations of 30secs in the spectral range 400-1800 cm^{-1}. For each sample, 25 cells were selected for recording and Raman spectra were collected in the region of 400cm^{-1} to 1900cm^{-1}. After acquisitions, each cell had its individual background subtracted and the laser line, also recorded on the CCD camera, was used to convert the spectra into relative wavenumbers and subsequent Raman spectra were analysed using multivariate techniques of unsupervised, supervised and clustering using Matlab 7.9.0.

Raw Raman spectra were initially subject to a pre-processing protocol which entails spectra overlay, baseline correction and vector normalisation as depicted in section 5.4. Spectra overlay involves the overlay of all spectra from the control and knockdown on a plot of intensity against wave number (cm^{-1}). In a baseline correction, both ends of all spectra are adjusted down to the x-axis that is each spectra begins on the axis and ends on the x-axis) while preserving the differences in intensities. Vector normalisation is the alignment of all spectra such that all spectra are brought to the same intensity. Following pre-processing, the mean spectra of the pre-processed data were calculated for every sample which allowed for an initial assessment of the recorded spectra results (section 5.4). This procedure enables a rapid visual assessment for any differences in spectra between the controls and knockdown before more a detailed further analysis is carried out.

5.3.4. Principle component analysis (PCA)

In order to further analyse the data, initially pre-processed spectra were subjected to PCA, in order to identify any possible differentiation of the samples. PCA is a statistical method used in exploratory analysis and establishing predictive models and mathematically consists of numerous steps. Therefore based on the PCA calculations, statistically significant differences between spectral profiles of the scrambled control and E6#2 could be determined and verified. The first step in PCA involves mean data centring which entails the subtraction of the mean (average across each dimension) from the data for each data dimension which results in a data set with mean equal zero. Subsequently, the covariance matrix calculation is carried out, which is a measure of the linear relationships between the variables for the data set and finally, calculations of eigenvectors and eigenvalues for the covariance matrix are carried out.

Eigenvectors (also known as characteristic vectors, proper vectors, or latent vectors) are a special set of vectors associated with a linear system of equations or a matrix equation while eigenvalues (characteristic roots, characteristic values, proper values, or latent roots) are a special set of scalars also associated with a linear system of equations or a matrix equation (Teukolsky, et al., 2007). Mathematically, there are two different kinds of eigenvectors which are distinguished as left eigenvectors and right eigenvectors, however, for many problems in physics and engineering, it is sufficient to consider only right eigenvectors hence the "eigenvector" term is used without qualification in such applications but can therefore be understood to refer to a right eigenvector. Eigenvectors are perpendicular to each other, every eigenvector has a corresponding right eigenvector and a corresponding left eigenvector; there is no analogous distinction between left and right for eigenvalues. In this study, the determination of the eigenvectors and eigenvalues of a system is equivalent to matrix diagonalisation of small oscillations of vibrating systems (Teukolsky, et al., 2007). The eigenvector with the highest eigenvalue explains the most variance in a data set and is called the first principal component *pc1* or *p1*. The second principal component, *pc2* or *p2* is the eigenvector with the second highest eigenvalue and holds information about the remaining variances and subsequent principal components are named in this

manner. In general, eigenvectors organised according their eigenvalues, from highest to lowest, give the components in order of significance (Teukolsky, et al., 2007).

5.4. Results

5.4.1. Raman spectra of silenced HPV16 E6 and E7 SiHa cells

Raman spectra were recorded from the nucleus, nucleolus, and cytoplasm of 10% formalin fixed CaF_2 chips SiHa cells 72hrs post transfection (Figure 5-2) and analysed using multivariate analysis techniques as described in Section 4.3.3 and 4.3.4 above. HPV E6/E7 silenced cells were visually confirmed as per similarity in features (cell shrinkage, nuclear fragmentation, chromatin condensation, blebbing and death) to previously validated experiments in TaqMan RT-PCR analysis (Section 3.3.2) and apoptosis analysis using FITC/PI DNA staining (Section 3.3.5.1).

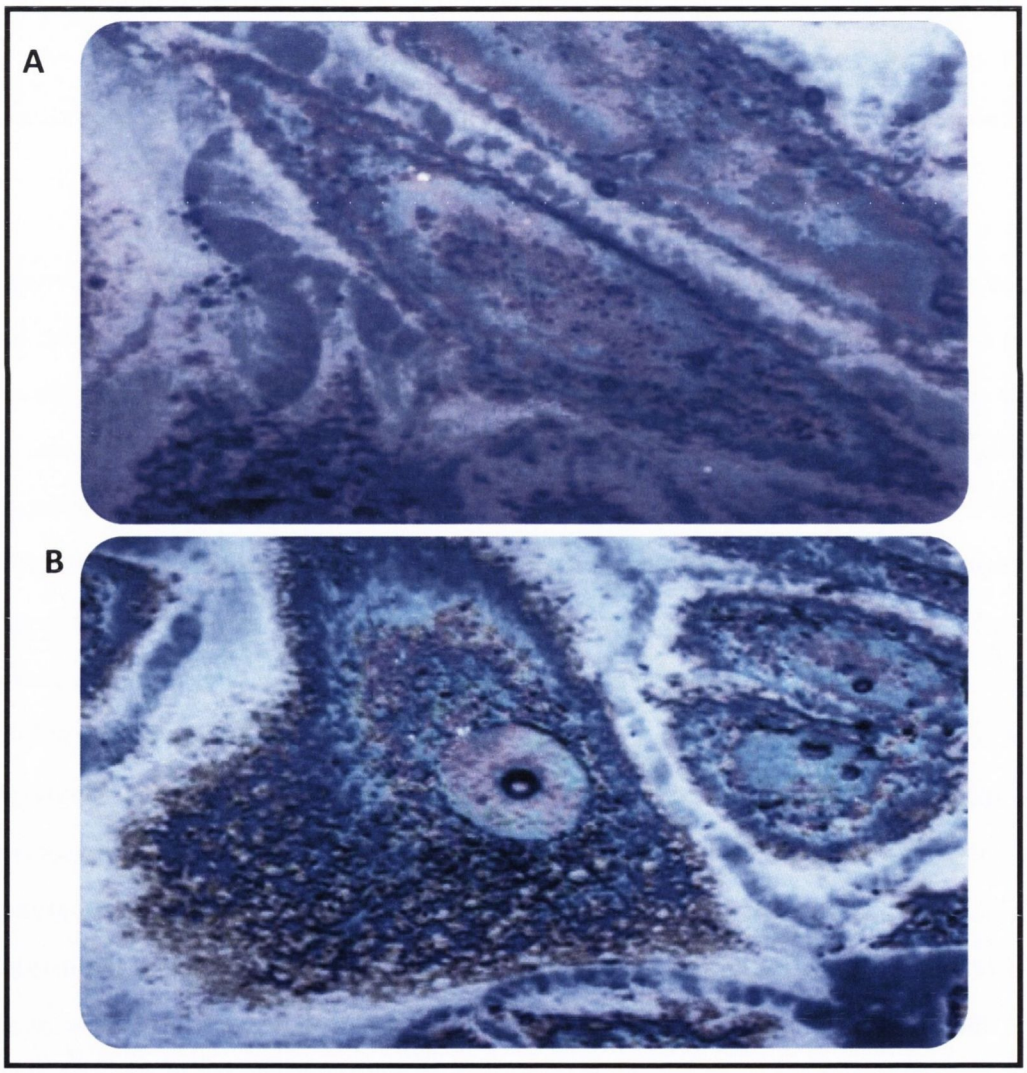

Figure 5-2: Confocal microscopy of SiHa cells 72hrs post forward transfection technique. SiHa cells seeded at $1.5x10^5$ cells were left transfected with scramble control siRNA (A), E6#2 siRNA (B) in biological duplicates. The confocal image shows the dramatic morphological phenotype in E6#2(B) compared to the scrambled control (A) (Magnification 100X).

The Raman spectra overlay (Figure 5-3A, Figure 5-4A, Figure 5-5A), baseline corrections (Figure 5-3B, Figure 5-4B, Figure 5-5B) and vector normalisation (Figure 5-3C, Figure 5-4C, Figure 5-5C) for the nucleus, nucleolus, and cytoplasm of the scrambled control siRNA and E6#2 siRNA cells show no significant discriminations. The Raman spectra showed no significant discriminations between the principal components *pc1* and *pc3* of the scrambled control siRNA and E6#2 siRNA cells for the nucleus, nucleolus, and cytoplasm (not shown). There were also no significant discriminations between the principal component *pc1* and *pc3* in the scrambled control siRNA and E6#2 siRNA cells for the nucleus, and the nucleolus (Figure 5-3D, Figure 5-4D). There were however, significant discriminations between the principal component *pc1* and *pc3* in the cytoplasm for the scrambled control siRNA and E6#2 siRNA cells (Figure 5-5C). This biochemical distinction was better observed on rotating the coordinates (Figure 5-5C) to (Figure 5-6) whereby there is a major right hand side clustering of scrambled control siRNA cells (green) and a leftward dispersion or movement of E6#2 siRNA cells (blue) with a few scrambled control siRNA cells (green) cross overs which are attributed to our spectra data being from a population size of 25 cells each. Increasing this number to 40 cells would make our spectra a little more consistent and hence the PCA separation analysis more evident.

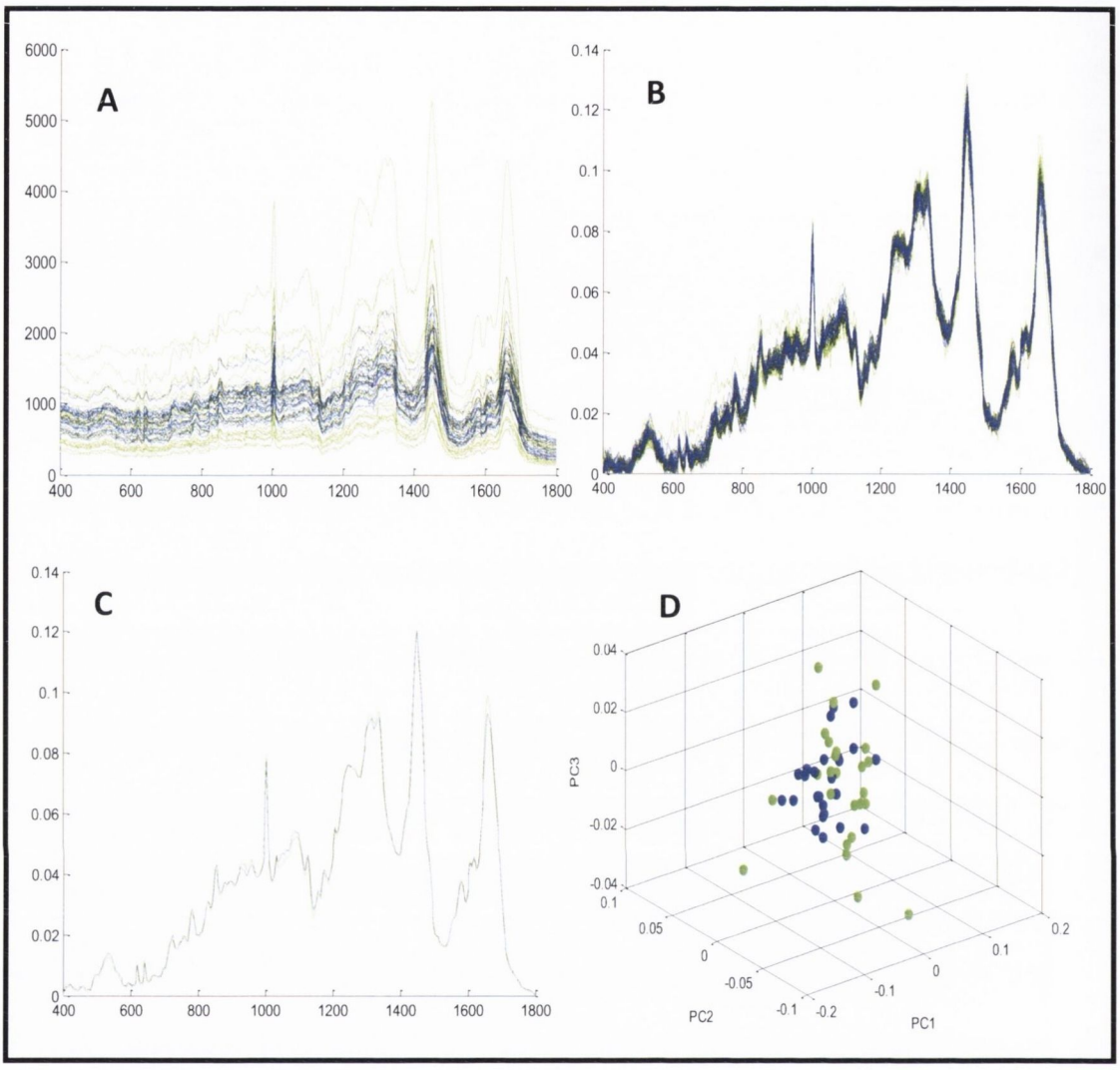

Figure 5-3: Nuclei spectra comparisons of HPV16 E6 silenced cells 72 hours post transfection. Cells transfected with negative siRNA a are depicted in green and knockdown cells are depicted in blue. Initial spectra overlay taken from nuclei (A), spectra taken post normalisation and baseline correction (B), mean spectra taken post pre-processing (C), Principal component analysis three dimensional scatter plot of spectra (D), all showing no significant discrimination between green coloured scrambled control siRNA and the blue coloured E6#2 siRNA cells . Spectra obtained from 25 cells were used for this analysis.

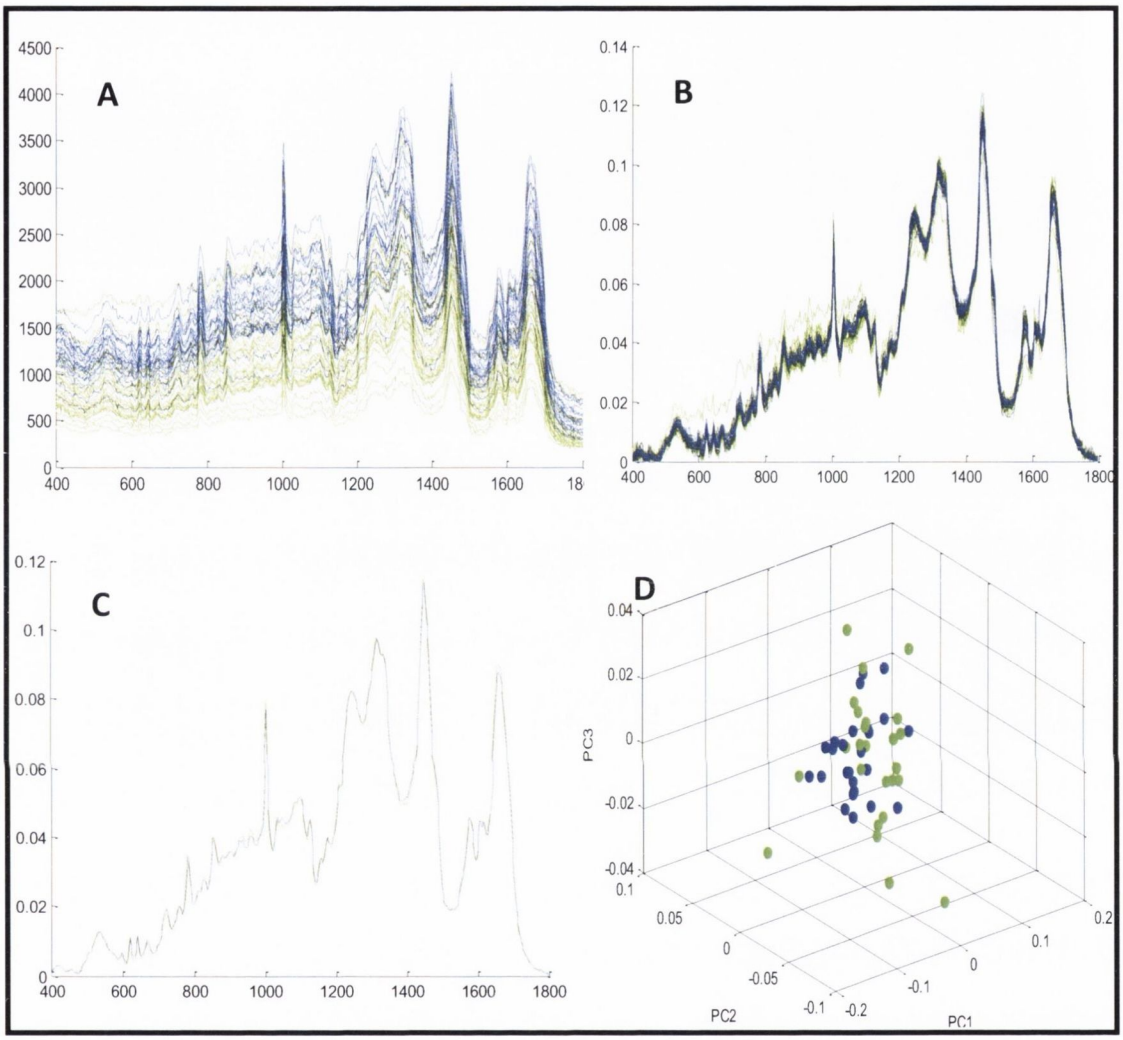

Figure 5-4: Nucleoli spectra comparisons of HPV16 E6 silenced cells 72 hours post transfection. Cells transfected with negative siRNA are depicted in green and knockdown cells are depicted in blue. Initial spectra overlay taken from nucleoli (A), spectra taken post normalisation and baseline correction (B), mean spectra taken post pre-processing (C), Principal component analysis three dimensional scatter plot of spectra (D), all showing no significant discrimination between green coloured scrambled control siRNA and the blue coloured E6#2 siRNA cells. Spectra obtained from 25 cells were used for this analysis.

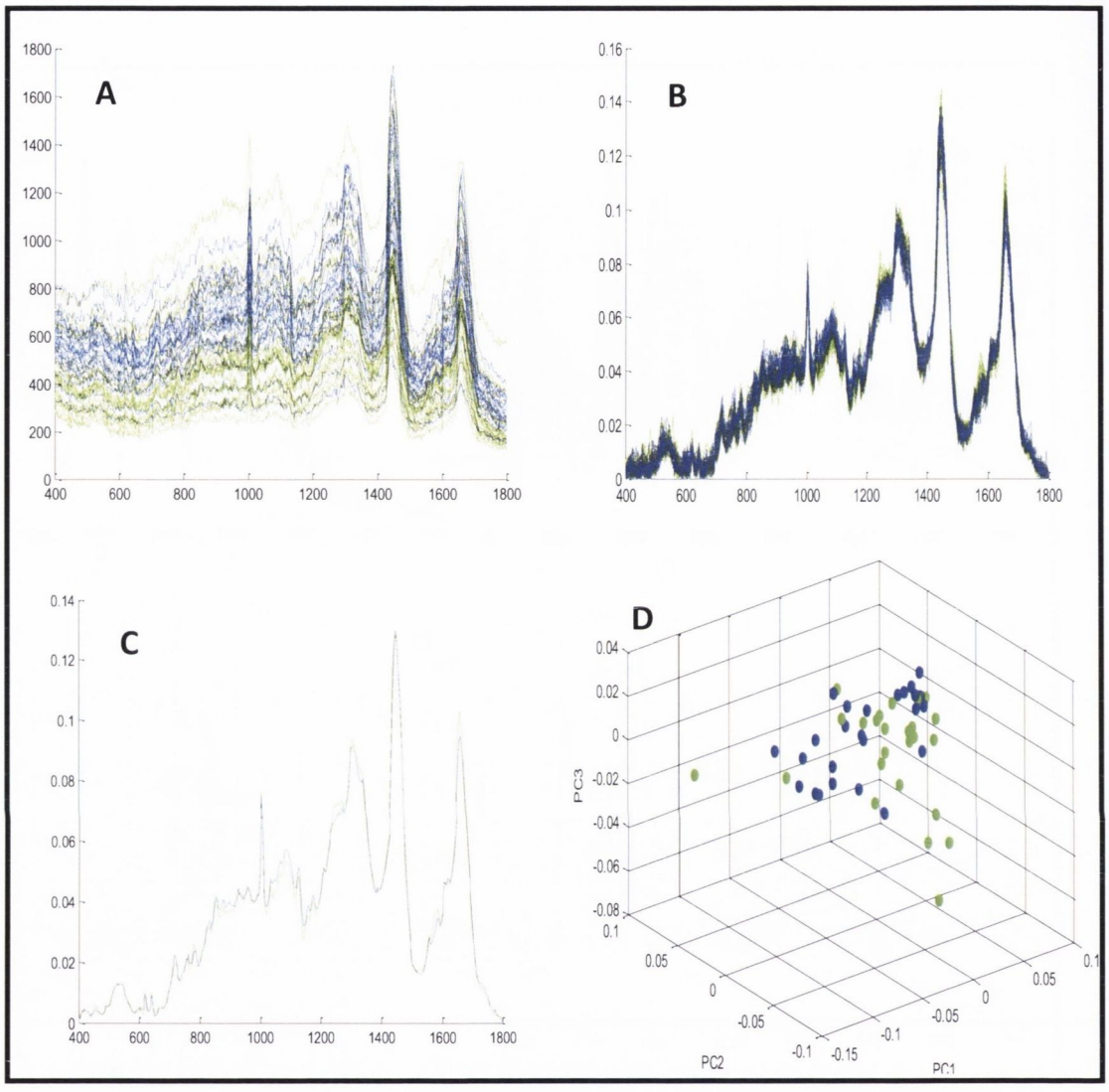

Figure 5-5: Cytoplasmic spectra comparisons of HPV16 E6 silenced cells 72 hours post transfection. Cells transfected with negative siRNA are depicted in green and knockdown cells are depicted in blue. Initial spectra taken from cytoplasm (A), spectra taken post normalisation and baseline correction (B), mean spectra taken post pre-processing (C), Principal component analysis three dimensional scatter plot of spectra (D), all showing a significant discrimination between green coloured scrambled control siRNA and the blue coloured E6#2 siRNA cells. This discrimination can be better observed on rotation of the coordinates in Figure5-8. Spectra obtained from 25 cells were used for this analysis.

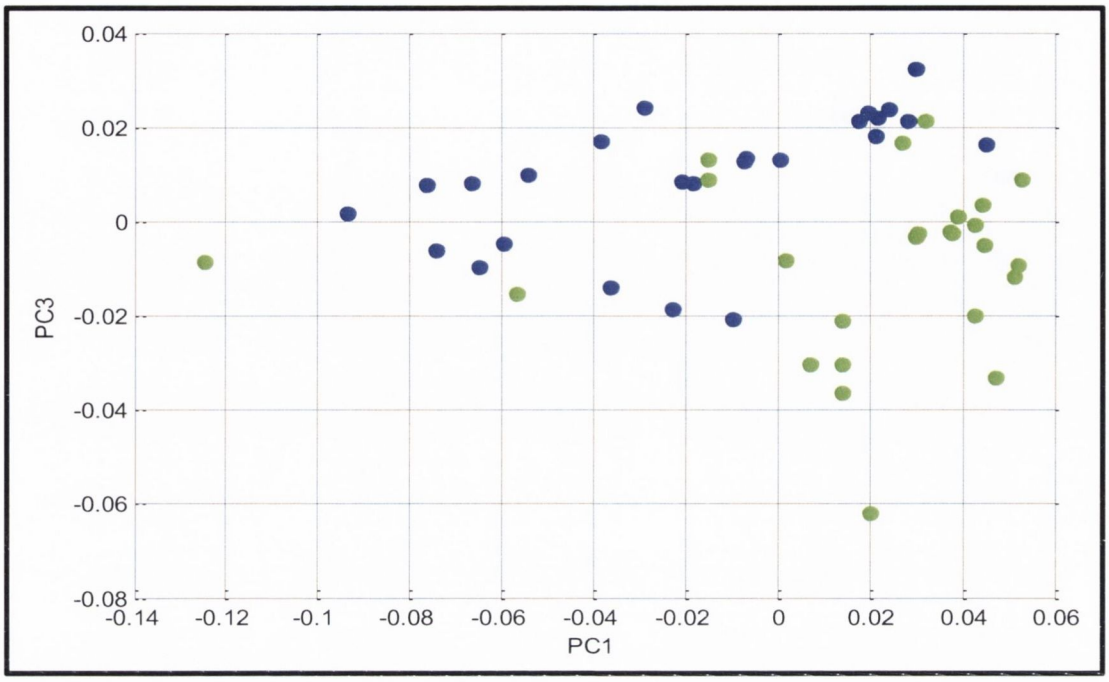

Figure 5-6: Principal component analysis plot of cytoplasm spectra comparisons of HPV16 E6 silenced cells 72 hours post transfection. Negative siRNA cells are depicted in green and knockdown cells are depicted in blue. The above plot provides a better illustration of the significant discrimination between green coloured scramble control siRNA and the blue coloured E6#2 siRNA cells in figure5-6, whereby a rotation of the coordinates produces a 2D plot of *PC3* against *PC1* with a leftward dispersion of blue cells (E6#2 siRNA) away from the clustering of green cells (scrambled control). Spectra obtained from 25 cells were used for this analysis.

Figure 5-7 illustrates the principal component loadings plot of main peaks contributing to discrimination spectra between scrambled control siRNA and E6#2 siRNA cells 72hrs post transfection with PC1 highlighted in blue and PC3 highlighted in red. Tentative band assignments to PC loading for the Raman peaks are displayed in Table 5-1. These band assignments contribute to discrimination spectra between scrambled control siRNA and E6#2. Each peak is higher in the control in comparison to the knockdown, meaning that there were more of these biomolecules prior to the SiHa cells being knocked down. This analysis of the loadings correlates with the visual analysis of the mean spectrum comparing the cytoplasm of the control and knockdown cells.

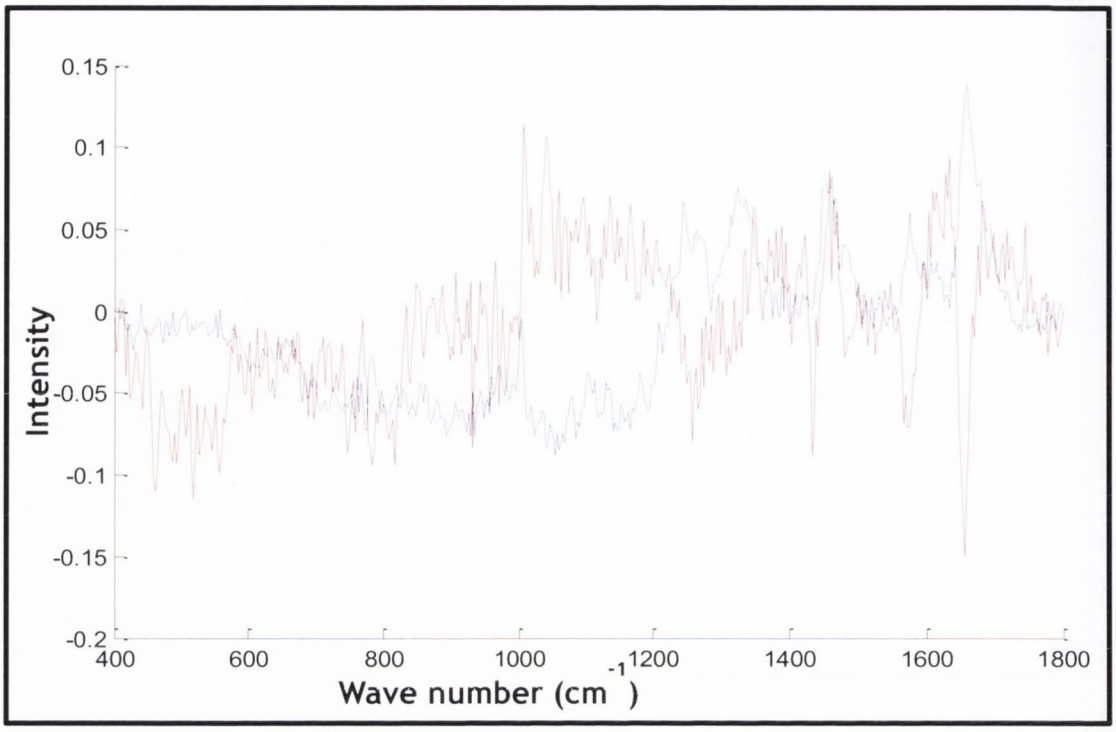

Figure 5-7: Principal component loadings plot of main peaks contributing to discrimination spectra between scrambled control siRNA and E6#2 siRNA **cells 72 hours post transfection**. *PC1* highlighted in blue and *PC3* highlighted in red. Spectra obtained from 25 cells were used for this analysis.

Table 5-1: Tentative band assignments for the Raman peaks. These assignments are for peaks displayed in Figure 5-7 (above). Band assignments contribute to discrimination spectra between scrambled control siRNA and E6#2 siRNA cells 72 hours post transfection. Each of these peaks is higher in the control in comparison to the knockdown (there were more of these biomolecules before the cells were silenced). The analyses of these loadings correlate with the visual analysis of the mean spectrum comparing the cytoplasm of the control and knockdown cells. Therefore, the decrease in peak variations (protein and nucleic acid levels) infer as to the reprogramming of protein expression in cells due to silenced HPV oncogenes.

Peak positions (cm^{-1})	Assignment
1007	C–C aromatic ring stretching in Phenylalanine (Phe)
1245	Amide III (C-N stretching, N-H bending), Phosphate asymmetric stretching (DNA/RNA)
1575	A,G (DNA/RNA); C=C bending mode of Phenylalanine (Phe)
1657	Proteins, amide I, α helix, phospholipids

5.5. Discussion

Raman spectroscopy was used to further characterise the effect of knocking down E6 and E7 oncogenes in a HPV positive cervical cancer cell line. From affymetrix microarray gene analysis of E6#2 siRNA which revealed the induction of an innate immune response accompanied by the generation of cytokines and chemokines (chapter 4), a spectroscopic protein analysis was performed to further assess biochemical changes. E6#2 siRNA transfected cells displayed distinct morphological changes, highly significant reductions in E6 and E7 mRNA expression levels which was further confirmed by increased levels of p53 and p21 via western blot analysis. Flow cytometry analysis also revealed E6#2 siRNA cells to be undergoing substantial cell death though not as extensive as E6#1 siRNA cells. This spectroscopic protein analysis was to further elucidate the mechanism and processes undergone in these cells during cell death. This study demonstrated that Raman spectroscopy can discriminate objectively between HPV-16 positive SiHa cells (with 1-2 integrated HPV strands per cell) control expressing E6/E7 and knockdowns with supressed E6 and E7 expression. This discrimination was more effectively observed by the increase in variance observed in scrambled control siRNA compared to E6#2 siRNA cells using PCA.

The mean of 25 spectra recorded from $HPV16^{+}$ SiHa cells forward transfected with scrambled control siRNA and E6#2 siRNA (25 spectra each) were derived from raw spectra via the pre-processing procedures and are represented in Figure 5-3, Figure 5-4 and Figure 5-5. In the mean Raman spectra of the nucleoli and nuclei, no significant differences between scrambled control siRNA and E6#2siRNA are discernible. However, subtle changes and variations were observed in the cytoplasmic peak comparisons and the tentative band assignments of these peaks observed in Figure 5-7 are shown in Table 5-1. Prominent Raman peak variations were located at around 1007 cm^{-1}, 1245 cm^{-1}, 1575 cm^{-1} and 1657 cm^{-1} and were tentatively assigned to C–C aromatic ring stretching in Phenylalanine (Phe), Amide III (C-N stretching, N-H bending), Phosphate asymmetric stretching (DNA/RNA) A,G (DNA/RNA); C=C bending mode of Phe respectively. These peak variations were all shown to be decreased in E6#2 compared to scrambled control siRNA.

A highly significant peak variation observed between these cells affected by none to low HPV E6 and E7 oncogene expression (E6#2) to high HPV oncogene expression (scrambled control siRNA) was in the Amide III region (1245 cm^{-1}). The decrease in variation in this region with normal Raman spectra compared to LGSIL Raman spectra in cervical dysplasia has been reported by (Kanter, et al., 2009) and (Kanter, et al., 2009). This decrease has also been shown by (Kanter, et al., 2011) when comparing Raman spectra from true normal ecto-cervix with previously diseased normal ecto-cervix and (Duraipandian, et al., 2011) when *in vivo* Raman spectra from 29 patients with cervical abnormalities (ranging from normal, benign, precancerous lesions, low-grade and high-grade CIN) were examined. In these papers, differences were attributed to a variety of biochemical changes and hence optical changes occurring in these cervical tissues as a result of increased dysplasia. Therefore, the cellular transformation by HPV oncogenes ultimately effect an increase in the ratio of nucleus to cytoplasm due to increased DNA content in dysplastic cells and changes in levels of proteins such as elastin and collagen. These changes are also reflected in our study, as following the reduction in mRNA levels of E6 and E7 and the stabilisation of p53 confirmed via TaqMan® RT-PCR and western blot analysis, E6#2 cells were more likely to display Raman signatures of previously diseased normal ecto-cervix. Hence, despite the silencing of HPV oncogenes in E6#2, permanent changes in the amount and arrangement of DNA, collagen and glycogen within these cells is most probably associated with HPV.

Another peak variations observed at 1575 cm^{-1} wavelength assigned to DNA/RNA and Phe (Table 5-1) was similarly reported by (Ostrowska, et al., 2010). In their report, this peak was found to be the only significantly variable peak between HPV negative C33As with HPV positive SiHa cells and demonstrated the effect of the presence of HPV in a cell. In our study, a reduction in this peak was observed in E6#2 which is in line with Ostrowska, et al and our previous data and as to the effect of silencing of HPV oncogenes by E6#2.

Further differences exhibited in protein vibrations between scrambled control cells and E6#2 were observed in the Amide I region (1657cm^{-1}) and protein constituent amino acids; Phe (1007cm^{-1}) while variations associated with nucleic acid constituents: PO_2 group (1245cm^{-1}), A and G (1575cm^{-1}) were also observed. These results are consistent with (Vargis, et al., 2012) who examined patient samples tested for the presence of high-risk HPV strands and (Ostrowska, et al., 2010) who examined HPV negative C33A, HPV18 HeLa, HPV-16 SiHa and HPV-16 CaSki. They are also in good agreement with observations made by (Lyng, et al., 2007), who examined histological patient samples of normal, CIN and invasive carcinoma tissue and (Duraipandian, et al., 2011) . The differences in protein and nucleic acid composition support the molecular data which demonstrates the silencing of HPV E6 and E7 oncogenes and the subsequent downstream effects of their oncoproteins on host cell proteins such as p53.

The principal component analysis scatterplot for the Raman spectroscopic results presented in Figure 5-5 was used to reduce the number of parameters needed to represent the variance in the spectral data set and then principal components identified were used to further generate a linear discriminant model (Figure 5-6). This plot shows a distinctive separation between scrambled control siRNA and E6#2 cells, and is very similar to that noted by Ostrowska, et al, in their cell line comparisons (Ostrowska, et al., 2010), suggesting the concentration HPV oncogene as a dependence factor. In (Ostrowska, et al., 2010), greater separations based on mean spectra analysis were observed between cell lines with increasing HPV concentration. Principal component loadings are presented in Figure 5-7. Peak numbers correspond to assignments presented. The first principal component is dominated by the protein contribution of the Amide I vibrations (α-helix) exhibited at 1657 cm^{-1}. While the third principal component contains a lot of biological information with mainly nucleic acid and protein contributions corresponding to distinctive peaks vibrations. DNA and RNA contributions are observed in PC3 are at 1245 cm^{-1}and 1575 cm^{-1} in addition to strong influence of variation arising from protein vibrations of Amide I (1657 cm^{-1}), C=C Phe at 1575cm^{-1}, C-C Phe at (1007 cm^{-1}) and Amide III (1245 cm^{-1}). The source of variations

shown in the principal component loadings is also consistent with those observed in the analysis of the mean spectra for the investigated cell lines by (Ostrowska, et al., 2010) with main peak loadings arising from protein and nucleic acid component vibrations. Each principal component is dominated by different cellular components; proteins in PC1, and nucleic acids and proteins in PC3. Amide I contributions are present in both principal component loadings and are indicative of differences in structural conformation of the protein in α-helix PC1 and PC3. As mentioned previously, variations in protein and nucleic acid levels arise from the fact that the silencing of HPV oncogenes causes the reprogramming of protein expression in the cell.

This chapter for the first time describes the application of Raman spectroscopy to demonstrate simultaneous silenced E6 and E7 oncogenes by RNAi in a HPV16 cervical cancer model. Our preliminary result suggests that Raman spectroscopy can differentiate between cells with functional E6/E7 (unsilenced) and those with silenced E6/E7 expression via significant spectra discrimination between their biochemical compositions. This approach has previously been used to discriminate between the HPV positive and negative cell lines to elucidate cellular differences due to proteins, nucleic acids and lipids (Ostrowska, et al., 2010). This chapter also affirms the diagnostic potential of Raman spectroscopy in conjunction with cervical cancer screening methods of pap smears and liquid-based cytology to discriminate between HPV-mediated dysplasia and cervical cancer using PCA spectral analysis thereby reducing the number false positive and negative results as well as colposcopy referrals particularly in women with borderline or mild cytological abnormalities. This study has therefore, revealed the potential application of this approach in improving our understanding of HPV-induced carcinogenesis *in vitro* and as non-invasive real-time diagnostic tool to support current methods for cervical cancer screening.

Chapter Six

General Discussion

6. General Discussion

The premise of this project was that high-risk HPV16 E6 is necessary, but not sufficient to induce malignant transformation to cervical carcinoma. The objective of this project was to examine the effects of silencing the expression of HPV E6 oncogene in a cervical cancer cell line model in order to gain a better understanding of the role of HPV E6 in cervical carcinogenesis, assess the downstream effects of silencing HPV E6 expression by gene expression analysis and Raman spectroscopy. These techniques were employed with the expectations of identifying possible pharmacological targets in the oncogenic pathway and evaluating a novel potential screening technology. This was accomplished by silencing the endogenous expression of the viral oncogene at the RNA level using RNAi technology whereby E6 and E7 expression was simultaneously silenced.

In chapter 3 of this study, five siRNAs (E6#1, E6#2 E6#3, E6#4 and E6#5) targeted towards the coding region of HPV16 E6 and its splice variant forms were designed and validated. These siRNAs demonstrated variations in their efficiency at silencing E6 and E7. E6#2 E6#3 and E6#4 induced a simultaneous reduction in mRNA expression levels of E6 and E7 expression of >70%, while E6#5 induced a considerable simultaneous reduction in mRNA expression levels of less than 70% in E6 and more than 70% in E7 expression.

E6#1 targeting just full length E6 only, induced no reduction in mRNA expression levels of both E6 and E7 expression. The bicistronic nature of HPV E6 and E7 transcript predicates the concomitant silencing of E6 and E7mRNAs (Stacey, et al., 2000) (Stacey, et al., 1995), and has previously been reported by studies that examined the effect siRNAs in HPV16 or HPV18 infected cervical cell lines: resulting in similar suppressions (Sima, et al., 2007) (Yamato, et al., 2008) (Yoshinouchi, et al., 2003) (Zhou, et al., 2012).

An evaluation of full length E6 only mRNA expression levels indicated E6#2 E6#3 and E6#4 induced about 65% reduction while E6#5 had no effect on full length E6 only

mRNA expression levels, whereas E6#1 induced a 70% reduction in full length E6 only mRNA expression levels. The level of suppression of full length E6 mRNA in all siRNAs correlates with previous findings that majority of the E6 amplicons detected were E6*I (Tang, et al., 2006).

A further examination of the proficiency of these siRNAs at protein level also indicated variations in their efficiencies. The assessment of siRNA-mediated suppression of E6 using p53 and p21 biomarkers (Rahman-Roblick, et al., 2007) (Rahman-Roblick, et al., 2008) revealed that E6#4 and E6#5 induced significant stabilisation of p53 protein similar to the knockdowns at RNA level. This effect was also translated downstream as an increase in p21 mRNA expression and an accumulation in protein levels, with E6#4 being the more potent of the two. Similarly, E6#2 and E6#3 induced the stabilisation of p53 protein and p21 transcript transactivation but to a lesser degree than E6#4 or E6#5. E6#2 also induced p21 protein accumulation equivalent to its transcript transactivation while E6#3 did not induce any p21 protein accumulation. In addition, the levels of p53 protein stabilisation and p21 protein observed in E6#3 did not correlate with the knockdown at RNA level. E6#1, however, induced no stabilisation p53 or p21 protein, similarly GAPDH loading control band was also absent. The absence of any protein and bioanalyser assessment of its mRNA (See Figure 8-2 in the appendix) demonstrated the degradation occurring within this sample.

Activated p53 and p21 regulate the transcription of genes involved in cell cycle arrest (Kim & Zhao, 2005). Hence, the effects of silencing the oncogenes activity on downstream targets via western blot analysis were further assessed by levels of β-galactosidase activity (Shlush, et al., 2011) (Gary & Kindell, 2005). Three siRNAs (E6#3, E6#4 and E6#5) demonstrated an extremely significant level of β-galactosidase activity ($p<0.001$) suggesting the induction of the senescence process in these knockdowns. Similarly, flow cytometry analysis of E6#3, E6#4 and E6#5 siRNAs revealed a G1 arrest profile in cellular proliferation and autofluorescence in the siRNA knockdowns, further supporting an induction of senescence. The observed mediation of p53-dependent cell

cycle arrest by p21 in E6#4 and E6#5 is in line with previously reported studies on p21 inhibiting p53-dependent and p53-independent apoptosis (Yoshinouchi, et al., 2003) (Gartel & Tyner, 2002) (Zhang, et al., 2013).

The demonstration of a G1 arrest, autofluorescence, and p21 transactivation in spite of the absence of p21 protein in E6#3 supported an induction in senescence. The distinct rounded refractile morphology observed in this siRNA knockdown compared to an enlarged flat morphology observed in normal senescent cells indicates elicitation of an oncogene-induced senescence (OIS). OIS is a form of senescence has been reported with certain cell types and genetic contexts, with a similar display of characteristics and particular morphology (Serrano, et al., 1997) (Palmero, et al., 1998) (Vredeveld, 2009) (Seoane, et al., 2008) (Kuliman, et al., 2010). However, these reports all confirm an increase in cell cycle inhibitors such as p21. It is therefore possible that E6#3 may not have achieved its maximum silencing ability whereby the transactivation of p21 at RNA level had been translated to the protein level or that despite its stabilisation, p53 might be impaired by E6#3 siRNA via an inhibition of DNA synthesis which could prevent one or more critical kinases from phosphorylating p53 as E6#3 siRNA does not reflect the double banding normally observed in p53 and present in other siRNA knockdowns described by Gottifredi, et al. (Gottifredi, et al., 2001).

While flow cytometry analysis of E6#1 and E6#2 demonstrated they had no influence on cellular proliferation, an induction in cell death was reflected in both siRNAs. The induction of cell death demonstrated in E6#2 in addition to p53 stabilisation and p21 accumulation has been reported in a number of studies (Butz, et al., 2003) (Xia, et al., 2011) (Lopes, et al., 1997) (An, et al., 1998) (Maki, et al., 1996) (Blagosklonny, et al., 1996) (Naujokat, et al., 2000). A study by Xia et al 2011, revealed that a non-genotoxic activation of p53 could instigate p53 stabilisation, p21 transactivation and apoptosis induction. However, the phenotypic morphology and degradation observed at RNA and protein levels in E6#1, in addition to issues with B2M endogenous control reflected the induction of cell death by this siRNA. Studies reporting, the role of B2M in

apoptosis provided an indication as to initial consistency and reproducibility TaqMan® RT-PCR issues with E6#1 (Wu, et al., 2002) (Mori, et al., 1999) (Yang, et al., 2009) (Hyafil & Strominger, 1979) (Sugita & Brenner, 1994). Various studies demonstrate that B2M is widely involved in the functional regulation of survival, proliferation, multi-drug resistance, apoptosis and even metastasis in cancer cells as depicted in Figure 6-1 (Klein, et al., 1996) (Molica, et al., 1999) (Morabito, et al., 2009) (Li, et al., 2012) (Nomura, et al., 2014) (Shi, et al., 2009). B2M is the non-transmembrane light-chain protein that is covalently associated to the transmembrane heavy chain protein which makes up the MHC class I antigens. MHC class I molecules play a role in central and peripheral tolerance by displaying primarily endogenous or exogenous protein fragments to T cells to perturb or illicit an immune response. The fate of the infected cell is usually apoptosis induction via cell-mediated immunity to prevent risk of spreading the infection to neighbouring cells. Tumour cells can however, circumvent immune responses by down-regulating MHC class I expression although the molecular basis for reduced MHC class I expression is incompletely understood. It then follows to state that "healthy" tumor cells have low B2M expression due to immune evasion and apoptotic tumor cells will have a greater B2M expression that is the higher the number of presenting MHC class I molecules on a cancer of which B2M is non covalently linked, the greater the chance of that cell undergoing apoptosis. Therefore, it is resonable to infer that the induction of apoptosis by E6#1 siRNA in HPV16 SiHa cells, is triggering or overcoming a down-regulation pathway and causing the inconsistencies in RNA levels in B2M reflected in TaqMan® RT-PCR analysis.

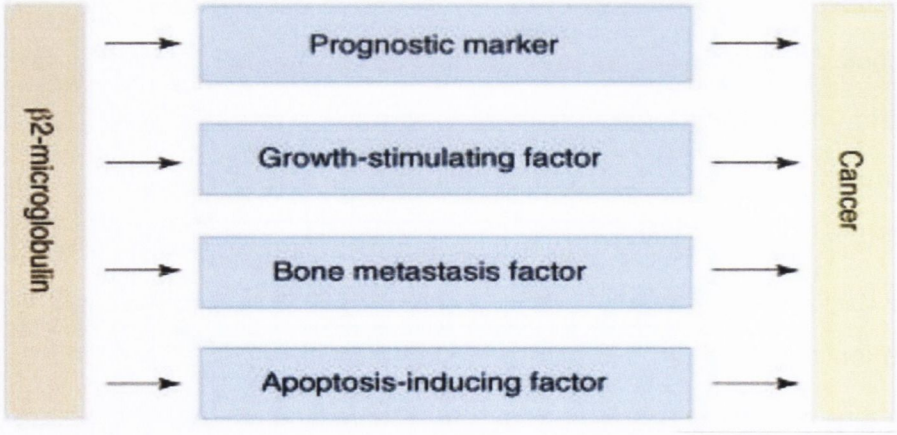

Figure 6-1: Schematic diagram showing the complicated effects of β2-microglobulin in cancer (Shi, et al., 2009)

In order to obtain a complete and balanced assessment of the response to the reduction of E6/E7 expression gene expression, a microarray analysis was performed using E6#2 and E6#4 in Chapter 4. These siRNAs were selected due to similar levels of reduction in E6 and E7 mRNA expression levels, p53 stabilisation, p21 transcript transactivation and p21 protein accumulation resulting in the induction of a G1 arrest in E6#4 and the induction of apoptosis in E6#2 despite targeting of the same regions in the E6 transcripts (3'end of E6 and E6*I). Microarray analysis demonstrated an overall up-regulation in E6#2 (142 of 171 genes) and down-regulation in E6#4 (346 of 399 genes) of significantly expressed genes in SiHa cells post transfection. Array analysis also identified 16 significantly differentially expressed genes common to both E6#2 and E6#4, and the classification of these were representative of the overall gene ontology of overrepresented genes in both siRNAs. Five of the up-regulated genes in this group except CDKN1A, were related to the cellular components of extracellular signalling peptides, eight of the down-regulated genes were linked to the biological process of inhibiting of cycle progression and division while the last three genes which were up-regulated in E6#2 and down-regulated in E6#4 were linked to biological process of immune response. These three differentially regulated biological immune response genes to viral infection offer an insight into the possible mechanisms of immune subversion by HPV via inhibition OASL antiviral activity, attenuating p53 function (DHRS2) and manipulating Golgi trafficking (RSAD2) (Honegger, et al., 2013).

E6#4 however, demonstrated an over-representation of down-regulated genes associated with biological processes and pathways of DNA replication and nucleotide metabolism and up-regulated genes associated with p53 signalling. These over-represented genes suggest an indication to E6#4 suppression of HPV oncogenes causing p53 pathway signalling via $p14^{ARF}$-MDM2-p53 pathway in collaboration with an inhibition in DNA replication. Over-represented down-regulated genes such as BRCA1 and BRCA2 linked to increase risks of breast, prostate, ovarian and pancreatic cancer (Chen & Parmigiani, 2007) (Brose, et al., 2002) (Kersemaekers, et al., 1998), and Fanconi anaemia genes FANCB, FANCD2 and FANCG (Juko-Pecirep, et al., 2011) (Narayan, et al., 2004) (Park, et al., 2014) (Wang, et al., 2009) have similarly been

reported to increase risks of HPV-mediated cervical cancer and have also been identified in this lab when effect of HPV E7siRNA on SiHa cells were examined. Another group of over-represented downregulated genes are histone cluster genes (42 genes) which encode members of the histone family responsible for formation of higher order chromatin structures. These genes may be sub grouped according to their temporal expression into replication-dependent histones (mainly expressed during S phase) or replication-independent histones (expressed throughout the cell cycle).

E6#2 demonstrated an over-representation of up-regulated genes associated with biological processes and pathways of innate immune inflammatory response and down-regulated genes associated with metabolism. Over-represented genes suggest E6#2's mechanism of suppression to be PRR-induced non-canonical/alternative NF-κB signalling pathway via p100 which ensued the generation of interferons, cytokines and chemokines, in addition to generation of reactive oxygen species: both of which contribute to cellular damage and the attraction and activation of the adaptive immune response. Similar findings have been reported in studies (Libermann & Baltimore, 1990) (Niebler, et al., 2013) (Hasan, et al., 2007) (Aguilar-Lemarroy, et al., 2002), which show that the up-regulation of similar genes played a role in the immune response. In addition, TaqMan® RT-PCR analysis of E6#2 and E6#4 using a surrogate biomarker, p21 as an investigative quality control substantiated the observed differences between E6#2 and E6#4 siRNA in SiHa cells post transfection as valid responses and not off target effects.

A spectroscopic protein analysis was performed on E6#2 siRNA using Raman spectroscopy to further investigate the induction of an immune response and biochemical changes to cellular constituents at a molecular level. Discriminations in Raman spectra between E6#2 to scrambled control siRNA were only observed in cytoplasmic spectra. These discriminations were observed as a decrease in peak variations and depicted as a leftward dispersion of E6#2 transfected cells from transfected with scrambled control siRNA cells in the PCA plot. Biochemical variations

in the Amide III region (1245 cm^{-1}), DNA/RNA and Phenylalanine region (1575 cm^{-1}), Amide I region (1657cm^{-1}), protein constituent amino acids; Phe (1007cm^{-1}), nucleic acid constituents: PO_2 group (1245cm^{-1}), A and G (1575cm^{-1}) were observed. The variations observed in protein and nucleic acid levels arise from the fact that silencing HPV oncogenes is causing a reprogramming of protein expression in the cell. Cell death can be achieved through signal transduction via death domain receptors and adaptor proteins or release of cytochrome C from the mitochondria, which all involve the activation of a cascade of various enzymes and proteins.

In summary, E6#4 siRNA is most probably inducing the silencing of HPV E6 and E7, the loss of which is resulting in the observed senescent profile. This senescent profile and associated genes have also been observed in this lab when HPV E7 siRNAs were employed to silence HPV E6 and E7 oncogenes. A study by Park et.al better explains the role of HPV oncogenes, as they reported that the disruption of the Fanconi anemia DNA damage repair pathway increases the incidence of HPV-associated cancers in the female lower reproductive tract via induction of DNA damage by E7, reduction in p53 activity by E6 which lead to a further accumulation of HPV-induced DNA damage which, increases the propensity for tumours to arise (Park, et al., 2014). However, HPV16 E6 augments E7-induced DNA damage. Therefore, the selective targeting of E6 by E6#2 leads to E7 becoming a cellular stressor, causing the erratic response of the cellular machinery observed in the an up-regulation of effectors of an inflammatory response and the cytoplasmic spectra of the Raman spectroscopy and therefore instigating cell death in this knockdown which correlates with the synergistic role of HPV oncogenes in HPV-associated carcinogenesis.

6.1. Study Limitations

A major limitation of RNAi (siRNA) is the potential for the misinterpretation of data due to non-specific or off-target effects. However, the use of multiplicity controls in this study eliminated such a limitation. A multiplicity control is the use of several siRNAs against the same target since it is unlikely that all would have similar sequence-dependent off-target effects. Another limitation of this study was the use of genome wide expression analysis on silenced HPV16 infected cervical cells. This is due to the inability to assess some of the E6 functions that were not exhibited at the level of gene expression modification. For example, the role of the E6/E6AP complex which functions as ubiquitin ligase can only be assessed in terms of alterations in global protein levels. Hence, changes to biochemical compositions (molecular level) due to the silencing of HPV16 E6 and E7 oncogenes were assessed using Raman Spectroscopy. Raman Spectroscopy provided a more cost effective method of unprejudiced analysis via spectra discriminations induced in cellular components of silenced HPV16 infected cervical cells. However, the collection of raw Raman spectra and its analysis was quiet tedious due to the requirement of an expert in this field and the novelty of this technique.

6.2. Future Directions

This study demonstrated that RNAi using HPV E6 targeting siRNAs in HPV16 positive cervical cancer cell model results in a reduction in the mRNA expression levels of E6 and E7 which could induce either a senescent or apoptotic phenotype. To further validate this apoptotic finding, a protein array analysis assessment of this knockdown will be carried out to elucidate global protein alterations occurring in this apoptotic and reaffirm the effect of this siRNA as a valid response and not an off target effect (as validated by p21 quality control expression). A mitochondrial function assay will also be carried out to assess key biomarkers of mitochondrial function and cellular toxicity. These assessments would full validate the apoptotic profile observed in differential gene expression pathways involving innate immune response and metabolic pathways

of oxidative phosphorylation and steroid biosynthesis. This approach will provide an unbiased assessment of PPARs regulation by HPV oncogenes in cervical cancer.

As a result of the importance of p21 as the main surrogate biomarker for this study, a Confocal Microscopy antibody staining of this protein would reveal its localisation in each knockdown and further support the proposed roles of p21 in senescence and apoptosis. In addition, to further elucidate the cellular death mechanism taking place in E6#1 silenced HPV16 SiHa cells, post transfection downstream analysis maybe carried out at earlier time points of 10-24 hours to obtain better quality RNA and protein. Furthermore, potential application of Raman Spectroscopy as a diagnostic tool to support current methods for cervical cancer screening maybe investigated via biochemical analysis of siRNA targeted E6 splice forms.

7. References

Aguilar-Lemarroy, A. et al., 2002. Restoration of p53 expression sensitizes human papillomavirus type 16 immortalized human keratinocytes to CD95-mediated apoptosis. *Oncogene,* 21(2), pp. 165-175.

Albershardt, T. C., Iritani, B. M. & Ruddell, A., 2012. Evaluation of reference genes for quantitative PCR analysis of mouse lymphocytes. *Journal of Immunological Methods,* 31 October, 384(1-2), pp. 196-199.

Allerton, R. & Butler-Manuel, S., 2014. *Cancer Research UK.* [Online] Available at: http://www.cancerresearchuk.org/cancer-help/type/cervical-cancer/treatment/chemotherapy/about-chemotherapy-for-cervical-cancer [Accessed 2 August 2014].

Allshire, R., 2002. Molecular biology. RNAi and heterochromatin--a hushed-up affair. *Science,* 13 September, 297(5588), pp. 1818-1819.

Alvarez-Salas, L. M., Benítez-Hess, M. L. & DiPaolo, J. A., 2003. Advances in the development of ribozymes and antisense oligodeoxynucleotides as antiviral agents for human papillomaviruses. *Antiviral Therapy,* August, 8(4), pp. 265-278.

Alvarez-Salas, L. M. & DiPaolo, J. A., 2007. Molecular approaches to cervical cancer therapy. *Current Drug Discovery Technologies,* October, 4(3), pp. 209-219.

Amato, A. et al., 2009. RNAi mediated acute depletion of retinoblastoma protein (pRb) promotes aneuploidy in human primary cells via micronuclei formation. *BMC Cell Biolology,* November, Volume 10, p. 79.

An, B., Goldfarb, R., Siman, R. & Dou, Q., 1998. Novel dipeptidyl proteasome inhibitors overcome Bcl-2 protective function and selectively accumulate the cyclin-dependent kinase inhibitor p27 and induce apoptosis in transformed but not normal human fibroblasts. *Cell death and Differentiation,* December, 5(12), pp. 1062-1075.

Andersson-Ellstrom, A. et al., 1996. Comparison of Development of Serum Antibodies to HPV16 and HPV33 and Acquisition of Cervical HPV DNA Among Sexually Experienced and Virginal Young Girls: A Longitudinal Cohort Study. *Sexually Transmitted Diseases,* May, 23(3), p. 234–238.

An, W. et al., 1998. Stabilization of wild-type p53 by hypoxia-inducible factor 1alpha. *Nature,* 26 March, 392(6674), pp. 405-408.

Apple, R. J., Becker, T. M., Wheeler, C. M. & Erlich, H. A., 1995. Comparison of Human Leukocyte Antigen DR-DQ Disease Associations Found With Cervical Dysplasia and Invasive Cervical Carcinoma. *Journal of the National Cancer Institute,* 15 March, 87(6), pp. 427-436.

Ault, K. A., 2006. Epidemiology and Natural History of Human Papillomavirus Infections in the Female Genital Tract. *Infectious Diseases in Obstetrics and Gynecology,* 2006(Suppl 40470).

Baker, T. et al., 1991. Structures of bovine and human papillomaviruses. Analysis by cryoelectron microscopy and three-dimensional image reconstruction. *Biophysical Journal,* December, 60(6), pp. 1445-1456.

Bartlett, D. & Davis, M., 2006. Insights into the kinetics of siRNA-mediated gene silencing from live-cell and live-animal bioluminescent imaging. *Nucleic Acids Research,* 12 January, 34(1), pp. 322-333.

Baseman, J. & Kotsky, L., 2005. The epidemiology of human papillomavirus infections. *Journal of Clinical Virology : the official publication of the Pan American Society for Clinical Virology,* 32(Suppl 1), p. S16–24.

Bedell, M. et al., 1991. Amplification of human papillomavirus genomes in vitro is dependent on epithelial differentiation. *Journal of Virology,* May, 65(5), pp. 2254-2260.

Behtash, N. & Mehrdad, N., 2006. Cervical cancer: screening and prevention. *Asian Pacific Journal of Cancer Prevention : APJCP,* 7(4), pp. 683-686.

Benjamini, Y. & Hochberg, Y., 1995. Controlling the False Discovery Rate: A Practical and Powerful Approach to Multiple Testing. *Journal of the Royal Statistical Society. Series B (Methodological),* 57(1), pp. 289-300.

Bennett, C. et al., 1998. Structural requirements for cationic lipid mediated phosphorothioate oligonucleotides delivery to cells in culture. *Jornal of Drug Targeting,* 5(3), pp. 149-162.

Bernard, H., 2005. The clinical importance of the nomenclature, evolution and taxonomy of human papillomaviruses. *Journal of Clinical Virology,* Issue Suppl 32, p. S1–6.

Bernstein, E., Caudy, A., Hammond, S. & Hannon, G., 2001. Role for a bidentate ribonuclease in the initiation step of RNA interference. *Nature,* 18 January, 409(6818), pp. 363-366.

Blagosklonny, M., W. G., Omura, S. & El-Deiry, W., 1996. Proteasome-dependent regulation of p21WAF1/CIP1 expression. *Biochemical and Biophysical Research Communications,* 14 October , 227(2), pp. 564-569.

Blow, N., 2009. Journeys across the membrane. *Nature Methods,* Volume 6, pp. 305-309.

Bolstad, B., Irizarry, R., Astrand, M. & Speed, T., 2003. A comparison of normalization methods for high density oligonucleotide array data based on variance and bias. *Bioinformatics,* 19(2), pp. 185-193.

Bonanni, P., Boccalini, S. & Bechini, A., 2009. Efficacy, duration of immunity and cross protection after HPV vaccination: a review of the evidence. *Vaccine,* 29 May, 27(Suppl1), pp. A46-53.

Bonelli, M. et al., 1999. Attenuated expression of 70-kDa heat shock protein in WI-38 human fibroblasts during aging in-vitro. *Experimental Cell Research,* 10 October, 251(1), pp. 20-32.

Bosch, F. & de Sanjosé, S., 2003. Human papillomavirus and cervical cancer--burden and assessment of causality. *Journal of the National Cancer Institute. Monographs,* Volume 31, pp. 3-13.

Bosch, F. et al., 2002. The causal relation between human papillomavirus and cervical cancer. *Journal of Clinical Pathology,* April, 55(4), pp. 244-265.

Bosch, X. & de Sanjosé, S., 2003. Chapter 1: Human Papillomavirus and Cervical Cancer - Burden and Assessment of Causality. *Journal of the National Cancer Institute,* 2003(31), pp. 3-13.

Bosch, X., Qiao, Y. & Castellsagué, X., 2006. The epidemiology of human papillomavirus infection and its association with cervical cancer. *International Journal of Gynecology and Obstetrics,* 94(Suppl1), pp. s8-21.

Bousarghin, L., Touzé, A., Sizaret, P. & Coursaget, P., 2003. Human papillomavirus types 16, 31, and 58 use different endocytosis pathways to enter cells. *Journal of Virology,* 77(6), pp. 3846-3850.

Boxman, I. et al., 2000. Case-control study in a subtropical Australian population to assess the relation between non-melanoma skin cancer and epidermodysplasia verruciformis human papillomavirus DNA in plucked eyebrow hairs. The Nambour Skin Cancer Prevention Study Group. *International Journal of Cancer,* 1 April, 86(1), pp. 118-121.

Boxman, I. et al., 2001. Association between epidermodysplasia verruciformis-associated human papillomavirus DNA in plucked eyebrow hair and solar keratoses.. *The Journal of Investigative Dermatology,* November, 117(15), pp. 1108-1012.

Brauchle, E. & Schenke-Layland, K., 2013. Raman spectroscopy in biomedicine - non-invasive in vitro analysis of cells and extracellular matrix components in tissues. *Biotechnology Journal,* 8(3), pp. 288-297.

Bray, F., Ren, J., Masuyer, E. & Ferlay, J., 2013. Global estimates of cancer prevalence for 27 sites in the adult population in 2008. *International Journal of Cancer,* 1 March, 132(5), pp. 1133-1145.

Breitling, R., Armengaud, P., Amtmann, A. & Herzyk, P., 2004. Rank products: a simple, yet powerful, new method to detect differentially regulated genes in replicated microarray experiments. *Federation of European Biochemical Societies Letters (FEBS letters)* , 573(1-3), pp. 83-92.

Brentjens, M., Yeung-Yue, K., Lee, P. & Tyring, S., 2002. Human papillomavirus: a review. *Dermatologic Clinics,* April, 20(2), pp. 315-331.

Brose, M. et al., 2002. Cancer risk estimates for BRCA1 mutation carriers identified in a risk evaluation program. *Journal of the National Cancer Institute,* 94(18), pp. 1365-1372.

Broz, P., Ohlson, M. & Monack, D., 2012. Innate immune response to Salmonella typhimurium, a model enteric pathogen. *Gut Microbes,* 3(2), pp. 62-70.

Burchell, A., de Sanjosé, S., Franco, E. & Winer, R., 2006. Epidemiology and transmission dynamics of genital HPV infection. *Vaccine,* 31 Aug, 24(Suppl 3), pp. 52-61.

Burd, E., 2003. Human Papillomavirus and Cervical Cancer. *Clinical Microbiology Reviews,* 16(1), pp. 1-17.

Butz, K. et al., 2003. siRNA targeting of the viral E6 oncogene efficiently kills human papillomavirus-positive cancer cells. *Oncogene,* 4 September, 22(38), p. 5938–5945.

Carter, J., Mandeleine, M. & Shera, K., 2001. Human papilloma virus 16 & 18 L1 serology compared across anogenital cancer sites. *Cancer Research,* 1 March, 61(5), pp. 1934-1940.

Carvalho, B. & Irizarry, R., 2010. A Framework for Oligonucleotide Microarray Preprocessing. *Bioinformatics,* 26(19), pp. 2363-2367.

Castellsagué, X., 2008. Natural history and epidemiology of HPV infection and cervical cancer. *Gynecologic Oncology,* September , 110(3), pp. S4-S7.

Castellsagué, X. & Muñoz, N., 2003. Chapter 3: Cofactors in human papillomavirus carcinogenesis--role of parity, oral contraceptives and tobacco smoking. *Journal of the National Cancer Institute. Monographs,* Volume 31, pp. 20-28.

Castle, P. et al., 2002. A prospective study of high-grade cervical neoplasia risk among human papillomavirus-infected women. *Journal of the National Cancer Institute,* 18 Sep, 94(18), pp. 1406-1414.

Cattani, P. et al., 2009. Clinical performance of human papillomavirus E6 and E7 mRNA testing for high-grade lesions of the cervix. *Journal of Clinical Microbiology,* 47(12), pp. 3895-3901.

Central Statistics Office (CSO), 2004. *Population and Labour Force Projections 2006-2036.* Dublin: The Stationery Office Dublin Ireland.

CervicalCheck-National Cancer Screening Service, 2012. *CervicalCheck Programme Report; Overview of cervical screening and update on the CervicalCheck Programme,* Dublin: National Cancer Screening Service.

Chaiwongkot, A. et al., 2013. Differential methylation of E2 binding sites in episomal and integrated HPV16 genomes in pre-invasive and invasive cervical lesions. *International Journal of Cancer,* 132(9), pp. 2087-2094.

Chakrabarti, O. & Krishna, S., 2003. Molecular interactions of 'high risk' human papillomaviruses E6 and E7 oncoproteins: implications for tumour progression. *Journal of Biosciences,* April, 28(3), p. 337–348.

Chen, S. & Parmigiani, G., 2007. Meta-analysis of BRCA1 and BRCA2 penetrance. *Journal of clinical oncology,* 25(11), pp. 1329-1333.

Chin, K. & Cresswell, P., 2001. Viperin (cig5), an IFN-inducible antiviral protein directly induced by human cytomegalovirus. *Proceedings of the National Academy of Sciences of the United States of America (PNAS),* 98(26), pp. 15125-15130.

Chung, E., Chung, H. & Bae, H., 2011. RSAD2 is a key requirement for Golgi trafficking of TNF-α in activated microglia. *The Journal of Immunology,* 186(Supplement 117.26).

Ćmielová, J. & Řezáčová, M., 2011. Protein and its function based on a subcellular localization. *Journal of Cellular Biochemistry,* 112(12), pp. 3502-3506.

Colthup, N., Daly, L. & Wibberly, S., 1990. *Introduction to Infrared and Raman Spectroscopy.* 3rd ed. San Diego: Academic Press.

Comber, H. & Gavin, A., 2004. Recent trends in cervical cancer mortality in Britain and Ireland:the case for population-based cervical cancer screening. *British Journal of Cancer,* 16 November, 91(11), pp. 1902-1904.

Conrad, M., Bubb, V. & Schlegel, R., 1993. The Human Papillomavirus Type6 and 16 E5 proteins are membrane associated proteins which associate with the 16Kda pore forming protein. *Journal of Virology,* October, 67(10), pp. 6170-6178.

Coste, J. et al., 2003. Cross sectional study of conventional cervical smear, monolayer cytology, and human papillomavirus DNA testing for cervical cancer screening. *British Medical Journal,* 5 April, 326(7392), p. 733.

Crow, J., 2012. HPV: The global burden. *Nature,* 30 Aug, 488(7413), pp. S2-3.

Culhane, A., Thioulouse, J., Perrière, G. & Higgins, D., 2005. MADE4: an R package for multivariate analysis of gene expression data. *Bioinformatics,* 21(11), pp. 2789-2790.

Culp, T. & Christensen, N., 2004. Kinetics of in-vitro adsorption and entry of papillomavirus virions. *Virology,* Febuary, 319(1), pp. 152-161.

Cuzick, J. et al., 2003. Management of women who test positive for high-risk types of human papillomavirus: the HART study. *Lancet,* 6 December, 362(9399), pp. 1871-1876.

Dall, K. et al., 2008. Characterization of naturally occurring HPV16 integration sites isolated from cervical keratinocytes under non-competitive conditions. *Cancer Research,* 15 October , 68(20), pp. 8249-8259.

Day, P., Lowy, D. & Schiller, J., 2003. Papillomaviruses infect cells via a clathrin-dependent pathway. *Virology,* 1 March, 307(1), pp. 1-11.

de Boer, M. et al., 2007. Circulating human papillomavirus type 16 specific T cells are associated with HLA Class I expression on tumor cells but not related to the amount of viral oncogene transcripts. *International Journal of Cancer,* 15 Dec, 121(12), pp. 2711-2715.

De Geest, K. et al., 1993. Growth and differentiation of human papillomavirus type 31b positive human cervical cell lines. *Gynecologic Oncology,* June, 49(3), pp. 303-310.

de Magalhaes, J. et al., 2004. Gene expression and regulation in H2O2-induced premature senescence of human foreskin fibroblasts expressing or not telomerase. *Experimental Gerontology,* September, 39(9), pp. 1379-89.

De Schutter, T. et al., 2013. Cidofovir selectivity is based on the different response of normal and cancer cells to DNA damage. *BMC Medical Genomics,* 6(18).

de Villiers, E. et al., 2004. Classification of papillomaviruses. *Virology,* 20 Jun, 324(1), pp. 17-27.

de Villiers, E., Gissman, L. & zur Hausen, H., 1981. Molecular cloning of viral DNA from human genital warts. *Journal of Virology,* December, 40(3), pp. 932-935.

Deacon, J. et al., 2000. Sexual behaviour and smoking as determinants of cervical HPV infection and of CIN3 among those infected: a case-control study nested within the Manchester cohort. *British Journal of Cancer,* Dec, 83(11), pp. 1565-1572.

Deisenroth, C. et al., 2010. Mitochondrial Hep27 is a c-Myb target gene that inhibits Mdm2 and stabilizes p53. *Molecular and Cellular Biology,* 30(16), pp. 39881-3993.

Delmas, M. et al., 2000. Cervical squamous intraepithelial lesions in HIV-infected women: Prevalence, incidence and regression. European Study Group on Natural History of HIV Infection in Women. *AIDS,* 14(12), pp. 1775-1784.

Demeret, C., Garcia-Carranca, A. & Thierry, F., 2003. Transcription-independent triggering of the extrinsic pathway of apoptosis by human papillomavirus 18 E2 protein. *Oncogene,* 22(2), pp. 168-175.

DiMaio, D. & Mattoon, D., 2001. Mechanisms of cell transformation by papillomavirus E5 proteins. *Oncogene,* 26 November, 20(54), pp. 7866-7873.

Dinish, U., Balasundaram, G., Chang, Y. & Olivo, M., 2014. Actively Targeted In Vivo Multiplex Detection of Intrinsic Cancer Biomarkers Using Biocompatible SERS Nanotags. *Scientific Reports,* Volume 4, p. 4075.

DiPaolo, J. & Alvarez-Salas, L., 2004. Advances in the development of therapeutic nucleic acids against cervical cancer. *Expert Opinion on Biological Therapy,* August, 4(8), pp. 1251-1264.

Doorbar, J., 2006. Molecular biology of human papillomavirus infection and cervical cancer. *Clinical Science (London),* 110(5), pp. 525-541.

Doorbar, J., 2006. Molecular biology of human papillomavirus infection and cervical cancer. *Clinical Science (London),* 110(5), p. 525–541.

Doudna, J. & Cech, T., 2002. The chemical repertoire of natural ribozymes. *Nature,* 11 July, 418(6894), pp. 222-228.

Duraipandian, S. et al., 2011. In vivo diagnosis of cervical precancer using Raman spectroscopy and genetic algorithm techniques. *Analyst,* 21 October, 136(20), pp. 4328-4336.

Dürst, M., Gissmann, L., Ikenberg, H. & zur Hausen, H., 1983. A papillomavirus DNA from a cervical carcinoma and its prevalence in cancer biopsy samples from different geographic regions. *Proceedings of the National Academy of Sciences of the United States of America (PNAS),* 15 June, 80(12), pp. 3812-3815.

Elbashir, S. et al., 2001. Duplexes of 21-nucleotide RNAs mediate RNA interference in cultured mammalian cells. *Nature,* 24 May, 411(6836), pp. 494-498.

Elbashir, S., Lendeckel, W. & Tuschl, T., 2001. RNA interference is mediated by 21- and 22-nucleotide RNAs. *Genes & Developement,* 15 Janurary , 15(2), pp. 188-200.

Elson, D. et al., 2000. Sensitivity of the cervical transformation zone to estrogen-induced squamous carcinogenesis. *Cancer Research,* 1 Mar, 60(5), pp. 1267-1275.

Engelmark, M., Beskow, A., Magnusson, J. & Gyllensten, U., 2004. Affected sib-pair analysis of the contribution of HLA class I and class II loci to development of cervical cancer. *Human Molecular Genetics,* 13(7), pp. 1951-1958.

Engelmark, M. et al., 2006. Identification of susceptibility loci for cervical carcinoma by genome scan of affected sib-pairs. *Human Molecular Genetics,* 15(22), pp. 3351-3360.

Etscheid, B., Foster, S. & Galloway, D., 1994. The E6 protein of human papillomavirus type 16 functions as a transcriptional repressor in a mechanism independent of the tumor suppressor protein, p53. *Virology,* December , 205(2), pp. 583-585.

Everaert, B., Boulet, G., Timmermans, J. & Vrints, C., 2011. Importance of suitable reference gene selection for quantitative real-time PCR: special reference to mouse myocardial infarction studies. *Public Library of Science one (PLoS),* 6(8), p. e23793.

Fehrman, F., Klumpp, D. & Laimins, L., 2003. Human papillomavirus type 31 E5 protein supports cell cycle progression and activates late viral functions upon epithelial differentiation. *Journal of Virology,* March , 77(5), pp. 2819-2831.

Felgner, J., Bennett, F. & Felgner, P., 1993. Cationic lipid-mediated delivery of polynucleotides. *Methods,* April, 5(1), pp. 67-75.

Felgner, J. et al., 1994. Enhanced gene delivery and mechanism studies with a novel series of cationic lipid formulations. *Journal of biological chemistry,* 28 Jan, 269(4), pp. 2550-2561.

Ferlay, J. et al., 2013. *Cancer Incidence and Mortality Worldwide,* Lyon: International Agency for Research on Cancer.

Filippova, M. et al., 2007. The large and small isoforms of human papillomavirus type 16 E6 bind to and differentially affect procaspase 8 stability and activity. *Journal of Virology,* 81(8), p. 4116–4129.

Filippova, M., Parkhurst, L. & Duerksen-Hughes, P., 2004. The human papillomavirus 16 E6 protein binds to Fas-associated death domain and protects cells from Fas-triggered apoptosis. *Journal of Biological Chemistry,* 11 June, 279(24), pp. 25729-25744.

Fire, A. & Mello, C., 2006. *Advanced Information: The 2006 Nobel Prize in Physiology or Medicine.* [Online]
Available at: http://nobelprize.org/nobel_prizes/medicine/laureates/2006/adv.html
[Accessed 14 July 2011].

Fire, A. et al., 1998. Potent and specific genetic interference by double-stranded RNA in Caenorhabditis elegans. *Nature,* 19 Feburary, 391(6669), pp. 806-811.

Frattini, M., Lim, H. & Laimins, L., 1996. In-vitro synthesis of oncogenic human papillomaviruses requires episomal genomes for differentiation-dependent late expression. *Proceedings of the National Academy of Sciences of the United States of America (PNAS),* 2 April, 93(7), pp. 3062-3067.

Ganguly, N. & Parihar, S., 2009. Human papillomavirus E6 and E7 oncoproteins as risk factors for tumorigenesis. *Journal of Biosciences,* March, 34(1), pp. 113-123.

Gao, X. & Huang, L., 1995. Cationic liposome-mediated gene transfer. *Gene Therapy,* December, 2(10), pp. 710-722.

Garcıa-Closas, R., Castellsague, X., Bosch, X. & Gonzalez, C., 2005. The role of diet and nutrition in cervical carcinogenesis: A review of recent evidence. *International Journal of Cancer,* 117(4), p. 629–637.

Garner-Hamrick, P. et al., 2004. Global effects of human papillomavirus type 18 E6/E7 in an organotypic keratinocyte culture system. *Journal of Virology,* September, 78(17), pp. 9041-9050.

Gartel, A. & Tyner, A., 2002. The role of the cyclin-dependent kinase inhibitor p21 in apoptosis. *Molecular Cancer Therapeutics,* 1(8), pp. 639-649.

Gary, R. & Kindell, S., 2005. Quantitative assay of senescence-associated beta-galactosidase activity in mammalian cell extracts. *Analytical Biochemistry,* 342(2), pp. 329-334.

Gavrilova, N., Gavrilov, L., Severin, F. & Skulachev, V., 2012. Testing predictions of the programmed and stochastic theories of aging: comparison of variation in age at death, menopause and sexual maturation. *Biochemistry,* July, 77(7), p. 754–760.

Ghittoni, R. et al., 2009. The biological properties of E6 and E7 oncoproteins from human papillomaviruses. *Virus Genes,* 17 October, 40(1), pp. 1-13.

Giacinti, C. & Giordano, A., 2006. Rb and Cell cycle progression. *Oncogene,* August, 25(8), pp. 5220-5227.

Gibb, R. & Martens, G., 2011. The Impact of Liquid-Based Cytology in Decreasing the Incidence of Cervical Cancer. *Reviews in Obstetrics and Gynecology,* 4(Supplement 1), pp. S2-11.

Giroglou, T. et al., 2001. Human papillomavirus infection requires cell surface heparan sulfate. *Journal of Virology,* February, 75(3), p. 1565–1570.

Gissmann, L. & zur Hausen, H., 1980. Partial characterization of viral DNA from human genital warts (Condylomata acuminata). *International Journal of Cancer,* 15 May , 25(5), pp. 605-609.

Goldie, S., O'Shea, M., Diaz, M. & Kim, S. Y., 2008. Benefits, cost requirements and cost-effectiveness of the HPV16,18 vaccine for cervical cancer prevention in developing countries: policy implications. *Reproductive Health Matter,* 16(32), pp. 86-96.

Gonçalves, M. et al., 2008. Classical and non-classical HLA molecules and p16INK4a expression in precursors lesions and invasive cervical cancer. *European Journal of Obstetrics & Gynecology and Reproductive Biology,* November, 141(1), pp. 70-74.

González, C. et al., 2011. Dietary factors and in situ and invasive cervical cancer risk in the European prospective investigation into cancer and nutrition study. *International Journal of Cancer,* 15 July, 129(2), pp. 449-459.

Gopinath, S. et al., 2006. An RNA aptamer that distinguishes between closely related human influenza viruses and inhibits haemagglutinin-mediated membrane fusion. *Journal of General Virology,* March , 87(3), pp. 479-487.

Gottifredi, V., Shieh, S., Taya, Y. & Prives, C., 2001. p53 accumulates but is functionally impaired when DNA synthesis is blocked. *Proceedings of the National Academy of Sciences of the United States of America (PNAS),* 98(3), pp. 1036-1041.

Gravitt, P., 2011. The known unknowns of HPV natural history. *Journal of Clinical Investigation,* 1 December, 121(12), pp. 4593-4599.

Groskreutz, D. & Schenborn, E., 1997. Reporter systems. *Methods in Molecular Biology,* Volume 63, pp. 11-30.

Hammond, S., Bernstein, E., Beach, D. & Hannon, G., 2000. An RNA-directed nuclease mediates post-transcriptional gene silencing in Drosophila cells. *Nature,* 16 March, 404(6775), pp. 293-296.

Harley, C., Futcher, A. & Greider, C., 1990. Telomeres shorten during ageing of human fibroblasts. *Nature,* 31 May, 345(6274), pp. 458-460.

Harris, J., 1996. Cigarette Smoke Components and Disease: Cigarette Smoke is more than a triad of Tar, Nicotine and Carbon monoxide. In: J. Harris, ed. *The FTC Cigarette Test Method for Detemining Tar, Nicotine, and Carbon Monoxide Yields of U.S. Cigarettes.* Cambridge(Massachusetts): National Institutes of Health National Cancer Institute, pp. 59-77.

Hasan, U. et al., 2007. TLR9 expression and function is abolished by the cervical cancer-associated human papillomavirus type 16. *Journal of Immunology,* 178(5), pp. 186-197.

Helbig, K. et al., 2005. Analysis of ISG expression in chronic hepatitis C identifies viperin as a potential antiviral effector. *Hepatology,* 42(3), pp. 702-710.

Herrington, C. et al., 1992. Detection of high risk human papillomavirus in routine cervical smears: strategy for screening. *Journal of Clinical Pathology,* 45(5), pp. 385-390.

Hildesheim, A. et al., 2001. HPV co-factors related to the development of cervical cancer: results from a population-based study in Costa Rica. *British Journal of Cancer,* 4 May, 84(9), pp. 1219-1226.

Hildesheim, A. et al., 1998. Human leukocyte antigen class I/II alleles and development of human papillomavirus-related cervical neoplasia: results from a case-control study conducted in the United States. *Cancer Epidemiol Biomarkers Prev 1,* 1 November, 7(11), pp. 1035-1041.

Hildesheim, A. & Wang, S., 2002. Host and viral genetics and risk of cervical cancer: a review. *Virus Research,* November , 89(2), pp. 229-240.

Hinkula, M. et al., 2004. A population-based study on the risk of cervical cancer and cervical intraepithelial neoplasia among grand multiparous women in Finland. *British Journal of Cancer,* 8 Mar, 90(5), pp. 1025-1029.

Ho, J. & Benchimol, S., 2003. Transcriptional repression mediated by the p53 tumour suppressor. *Cell Death and Differentiation,* April, 10(4), pp. 404-408.

Honegger, A. et al., 2013. Silencing of human papillomavirus (HPV) E6/E7 oncogene expression affects both the contents and the amounts of extracellular microvesicles released from HPV-positive cancer cells. *International Journal of Cancer,* 133(7), pp. 1631-1642.

Horner, S., DeFilippis, R., Manuelidis, L. & DiMaio, D., 2004. Repression of the human papillomavirus E6 gene initiates p53-dependent, telomerase-independent senescence and apoptosis in HeLa cervical carcinoma cells. *Journal of Virology,* April, 78(8), pp. 4063-4073.

Horvitz, H., 1999. Genetic control of programmed cell death in the nematode Caenorhabditis elegans. *Cancer Research,* 1 April, 59(Suppl 7), pp. 1701s-1706s.

Howie, H., Katzenellenbogen, R. & Galloway, D., 2009. Papillomavirus E6 proteins. *Virology,* 20 February, 384(2), pp. 324-334.

Huang, D., Sherman, B. & Lempicki, R., 2009. Bioinformatics enrichment tools: paths toward the comprehensive functional analysis of large gene lists. *Nucleic Acids Research,* 37(1), pp. 1-13.

Huang, D., Sherman, B. & Lempicki, R., 2009. Systematic and integrative analysis of large gene lists using DAVID Bioinformatics Resources. *Nature Protocols,* 4(1), pp. 44-57.

Huang, L., Chao, S. & Lee, B., 2008. Integration of human papillomavirus type-16 and type-18 is a very early event in cervical carcinogenesis. *Journal of Clinical Pathology,* May, 61(5), pp. 627-31.

Huang, S. & McCance, D., 2002. Down regulation of the interleukin-8 promoter by human papillomavirus type 16 E6 and E7 through effects on CREB binding protein/p300 and P/CAF. *Journal of Viroogy,* September, 76(17), p. 8710–8721.

Hu, F. et al., 2010. PBK/TOPK interacts with the DBD domain of tumor suppressor p53 and modulates expression of transcriptional targets including p21. *Oncogene,* 29(40), pp. 5464-5474.

Hummel, M., Hudson, J. & LAimins, L. A., 1992. Differentiation-induced and constitutive transcription of human papillomavirus type 31b in cell lines containing viral episomes. *Jounal of Virology,* October, 66(10), pp. 6070-6080.

Hyafil, F. & Strominger, J., 1979. Dissociation and exchange of the beta 2-microglobulin subunit of HLA-A and HLA-B antigens. *Proceedings of the National Academy of Sciences of the United States of America (PNAS),* November, 76(11), pp. 5834-5838.

International Agency for Research on Cancer IARC, 2007. *Monograph on the evaluation of carcinogenic risks to humans - Human papillomaviruses,* Lyon: International Agency for Research on Cancer IARC.

Irizarry, R. et al., 2003. Summaries of Affymetrix GeneChip probe level data. *Nucleic Acids Research,* 31(4), p. e15.

Irizarry, R. et al., 2003. Exploration, normalization, and summaries of high density oligonucleotide array probe level data. *Biostatistics,* 4(2), pp. 249-264.

Jacob, F. et al., 2013. Careful selection of reference genes is required for reliable performance of RT-qPCR in human normal and cancer cell lines. *Public Library of Science one (PLoS),* 8(3), p. e59180.

James, H. & Gibson, I., 1998. The therapeutic potential of ribozymes. *Blood,* 15 January, 91(2), pp. 371-382.

Jeffery, I., Higgins, D. & Culhane, A., 2006. Comparison and evaluation of methods for generating differentially expressed gene lists from microarray data. *BMC Bioinformatics,* 26 July, Volume 7, p. 359.

Jeong, S. et al., 2004. The role of HPV oncoproteins and cellular factors in maintenance of hTERT expression in cervical carcinoma cells. *Gyneocologic Oncology,* 94(1), pp. 40-47.

Jess, P. et al., 2008. Early identification of cervical neoplasia with Raman spectroscopy and advanced methods for biomedical applications. *Biomedical Optical Spectroscopy,* 8 February .Volume 6853.

Jess, P. et al., 2007. Early detection of cervical neoplasia by Raman spectroscopy. *International Journal of Cancer,* 15 December, 121(12), pp. 2723-2728.

Jiang, M. & Milner, J., 2005. Selective silencing of viral gene E6 and E7 expression in HPV-positive human cervical carcinoma cells using small interfering RNAs. *Methods in Molecular Biology,* Volume 292, pp. 401-420.

Jimenez-Wences, H., Peralta-Zaragoza, O. & Fernandez-Tilapa, G., 2014. Human papilloma virus, DNA methylation and microRNA expression in cervical cancer (Review). *Oncology Reports,* 31(6), pp. 2467-2476.

Johnson, K. et al., 2009. Role of heparan sulfate in attachment to and infection of the murine female genital tract by human papillomavirus. *Journal of Virology,* Volume 83, pp. 2067-2074.

Jones, P., Simons, B. & Watt, F., 2007. Sic transit gloria: farewell to the epidermal transit amplifying cell?. *Cell Stem Cell,* 11 Oct , 1(4), pp. 371-381.

Juko-Pecirep, I., Ivansson, E. & Gyllensten, U., 2011. Evaluation of Fanconi anaemia genes FANCA, FANCC and FANCL in cervical cancer susceptibility. *Gynecologic Oncology,* 122(2), pp. 377-381.

Kanter, E. et al., 2009. Effect of hormonal variation on Raman spectra for cervical disease detection. *American Journal of Obsterics and Gynecology,* Volume 200, pp. 512.e1-512.e5..

Kanter, E. et al., 2011. Effect of normal variations on disease classification of Raman spectra from cervical tissue. *Analyst,* Volume 136, pp. 2981-2987.

Kanter, E. et al., 2009. Application of Raman Spectroscopy for cervical dysplasia diagnosis. *Journal of Biophotonics,* 2(1-2), pp. 81-90.

Karim, R. et al., 2013. Human papillomavirus (HPV) upregulates the cellular deubiquitinase UCHL1 to suppress the keratinocyte's innate immune response. *Public Library of Science Pathogen (PLoS Pathog.),* 9(5), p. e1003384.

Katzenellenbogen, R., Vliet-Gregg, P., Xu, M. & Galloway, D., 2009. NFX1-123 increases hTERT expression and telomerase activity posttranscriptionally in human papillomavirus type 16 E6 keratinocytes. *Journal of Virology,* July, 83(13), p. 6446–6456.

Kelly, J. et al., 2010. A spectral phenotype of oncogeneic human papillomavirus-infected exfoliated cervical cytology distinguishes women based on age. *Clinica Chimica Acta,* 5 August, 411(15-16), pp. 1027-1033.

Kersemaekers, A., Hermans, J., Fleuren, G. & van de Vijver, M., 1998. Loss of heterozygosity for defined regions on chromosomes 3, 11 and 17 in carcinomas of the uterine cervix. *British Journal of Cancer,* 77(2), pp. 192-200.

Kim, Y. & Zhao, M., 2005. Aberrant cell cycle regulation in cervical carcinoma. *Yonsei Medical Journal,* 46(5), pp. 597-613.

Kingerey, L., 1921. The aetiology of common warts—their production in the third generation. *Journal of the American Medical Association,* Volume 76, pp. 440-442.

Klein, T. et al., 1996. Correlation between tumour and serum beta 2m expression in patients with breast cancer. *European journal of immunogenetics : official journal of the British Society for Histocompatibility and Immunogenetics,* December, 23(6), pp. 417-423.

Kruger, K. et al., 1982. Self-splicing RNA: autoexcision and autocyclization of the ribosomal RNA intervening sequence of Tetrahymena. *Cell,* November, 31(1), pp. 147-157.

Kulasingam, S. et al., 2002. Evaluation of human papillomavirus testing in primary screening for cervical abnormalities: comparison of sensitivity, specificity, and frequency of referral. *Journal of the American Medical Association (JAMA),* 9 October, 288(14), pp. 1749-1757.

Kuliman, T., Michaloglou, C., Mooi, W. & Peeper, D., 2010. The essence of senescence. *Genes and Development,* 15 November, 24(22), pp. 2463-2479.

Kumar, A. et al., 2002. Human papillomavirus oncoprotein E6 inactivates the transcriptional coactivator human ADA3. *Molecular Cell Biology,* 22(16), p. 5801–5812.

Kuner, R. et al., 2007. Identification of cellular targets for the human papillomavirus E6 and E7 oncogenes by RNA interference and transcriptome analyses. *Journal of Molecular Medicine (Berlin, Germany),* 85(11), pp. 1253-1262.

Kurreck, J., 2003. Antisense technologies: Improvement through novel chemical modifications. *European Journal of Biochemistry,* April, 270(8), pp. 1628-1644.

Lacey, J. et al., 2001. Associations between smoking and adenocarcinomas and squamous cell carcinomas of the uterine cervix (United States). *Cancer Causes Control,* Feb, 12(2), pp. 153-161.

Lawler, D., 2011. The changing understanding of ageing. Part 1: Evaluating ageing theories and studies. *Veterinaria italiana,* July-September, 47(3), pp. 229-240.

Lei, M., 2005. The MCM complex: its role in DNA replication and implications for cancer therapy. *Current Cancer Drug Targets,* 5(5), pp. 365-380.

Leonard, S. et al., 2012. Oncogenic human papillomavirus imposes an instructive pattern of DNA methylation changes which parallel the natural history of cervical HPV infection in young women. *Carcinogenesis,* 33(7), pp. 1286-1293.

Libermann, T. & Baltimore, D., 1990. Activation of Interleukin-6 Gene Expression through the NF-KB Transcription Factor. *Molecular and cellular biology,* 10(5), pp. 2327-2334.

Liu, X., Clements, A., Zhao, K. & Marmorstein, R., 2006. Structure of the human Papillomavirus E7 oncoprotein and its mechanism for inactivation of the retinoblastoma tumor suppressor. *Journal of Biological Chemistry,* 6 January, 281(1), pp. 578-86.

Liu, Y. et al., 2009. Determinants of Stability for the E6 Protein of Papillomavirus Type 16. *Journal of Molecular Biology,* 6 March, 386(4), pp. 1123-1137.

Li, Z. et al., 2012. Serum beta2-microglobin is a predictor of prognosis in patients with upper aerodigestive tract NK/T-cell lymphoma. *Annals of Haematology,* August, 91(8), pp. 1265-1270.

Lopes, U., Erhardt, P., Yao, R. & Cooper, G., 1997. p53-dependent induction of apoptosis by proteasome inhibitors. *Journal of Biological Chemistry,* 16 May, 272(20), pp. 12893-12896.

Lowe, J. et al., 2008. Evolutionary and structural analyses of alpha-papillomavirus capsid proteins yields novel insights into L2 structure and interaction with L1. *Virology Journal,* 17 December, Volume 5, p. 150.

Loyter, A., Scangos, G. & Ruddle, F., 1982. Mechanisms of DNA uptake by mammalian cells: fate of exogenously added DNA monitored by the use of fluorescent dyes. *Proceedings of the National Academy of Sciences of the United States of America (PNAS),* Jan, 79(2), pp. 422-426.

Luque, A., Demeter, L. & Reichman, R., 1999. Association of human papillomavirus infection and disease with magnitude of human immunodeficiency virus type 1 (HIV-1) RNA plasma level among women with HIV-1 infection. *Journal of Infectious Diseases,* 179(6), pp. 1405-1409.

Lyngea, E. et al., 2009. What's next? Perspectives and future needs of cervical screening in Europe in the era of molecular testing and vaccination. *European Journal of Cancer,* 45(15), p. 2714–2721.

Lynge, E., Antilla, A., Arbyn, M. & Segnan, N., 2009. What's next? Perspectives and future needs of cervical screening in Europe in the era of molecular testing and vaccination. *European Journal of Cancer,* 45(15), pp. 2714-2721.

Lyng, F. et al., 2007. Vibrational spectroscopy for cervical cancer pathology from biochemical analysis to diagnostic tool. *Experimental and Molecular Pathology,* April, 82(2), pp. 121-129.

Macrae, I. et al., 2006. Structure of Dicer and mechanistic implications for RNAi. *Cold Spring Harbor symposia on quantitative biology,* Volume 71, pp. 73-80.

Madeleine, M. et al., 2008. Comprehensive analysis of HLA-A, HLA-B, HLA-C, HLA-DRB1, and HLA-DQB1 loci and squamous cell cervical cancer risk. *Cancer Research 2008,* 1 May 1, 68(9), pp. 3532-3539.

Madison, K., 2003. Barrier function of the skin: "la raison d'etre" of the epidermis. *Journal of Investigative Dermatology,* August, 121(2), pp. 231-241.

Maiorano, D., Moreau, J. & Mechali, M., 2000. XCDT1 is required for the assembly of pre-replicative complexes in Xenopus laevis. *Letters to Nature,* 6 April, 404(6778), pp. 622-625.

Maki, C., Huibregtse, J. & Howley, P., 1996. In vivo ubiquitination and proteasome-mediated degradation of p53. *Cancer Research,* 1 June, 56(11), pp. 2649-2654.

Malanchi, et al., 2002. Identification of a novel activity of human papillomavirus type 16 E6 protein in deregulating the G1/S transition. *Oncogene,* 21(37), pp. 5665-572.

Marques, J. & Williams, R., 2005. Activation of the mammalian immune system by siRNAs. *Nature Biotechnology,* 23(11), pp. 1399-1405.

Martin, S. & Caplen, N., 2007. Applications of RNA interference in mammalian systems. *Annual Review of Genomics and Human Genetics,* Volume 8, pp. 81-108.

Massad, L. et al., 1999. Prevalence and predictors of squamous cell abnormalities in Papanicolaou smears from women infected with HIV-1. Women's Interagency HIV Study Group. *Journal of Acquired Immune Deficiency Syndromes,* 21(1), pp. 33-41.

Massimi, P. et al., 1999. Interaction between the HPV-16 E2 transcriptional activator and p53. *Oncogene,* 16 December , 18(54), pp. 7748-7754.

Matsumoto, K. et al., 2010. Tobacco smoking and regression of low-grade cervical abnormalities. *Cancer Science,* 101(9), pp. 2065-2073.

Matsumoto, K. et al., 2003. Are smoking and chlamydial infection risk factors for CIN? Different results after adjustment for HPV DNA and antibodies. *British Journal of Cancer,* 1 Sept, 89(5), pp. 831-833.

McBride, A., Oliveira, J. & McPhillips, M., 2006. Partitioning viral genomes in mitosis: same idea, different targets. *Cell Cycle,* July, 5(14), pp. 1499-1502.

McCutchan, J. & Pagano, J., 1968. Enchancement of the infectivity of simian virus 40 deoxyribonucleic acid with diethylaminoethyl-dextran. *Journal of the National Cancer Institute,* August, 41(2), pp. 351-357.

McLaughlin-Drubin, M. & Münger, K., 2009. The human papillomavirus E7 oncoprotein. *Virology,* 20 February, 384(20), pp. 335-344.

Melchjorsen, J. et al., 2009. Differential regulation of the OASL and OAS1 genes in response to viral infections. *Journal of Interferon & Cytokine Research : the official Journal of the International Society for Interferon and Cytokine Research (J. Interferon Cytokine Res.),* 29(4), pp. 199-207.

Michalovitz, D., Eliyahu, D. & Oren, M., 0986. Overproduction of protein p53 contributes to simian virus 40-mediated transformation. *Molecular and Cellular Biology,* 6 October, 6(10), pp. 3531-3536.

Middleton, K. et al., 2003. Organisation of the human papillomavirus productive cycle during neoplastic progression provides a basis for the selection of diagnostic marker. *Journal of Virology,* October, 77(19), pp. 10186-10201.

Middleton, K. et al., 2003. Organization of human papillomavirus productive cycle during neoplastic progression provides a basis for selection of diagnostic markers. *Journal of Virology,* Oct, 77(19), pp. 10186-10201.

Mitrani-Rosenbaum, S., Tsvieli, R. & Tur-Kaspa, R., 1989. Oestrogen Stimulates Differential Transcription of Human Papillomavirus Type 16 in SiHa Cervical Carcinoma Cells. *Journal of General Virology,* Aug, 70(8), pp. 2227-32.

Modis, Y., Trus, B. & Harrison, S., 2002. Atomic model of the papillomavirus capsid. *European Molecular Biology Organization Journal,* 16 September, 21(18), pp. 4754-4762.

Molica, S. et al., 1999. Clinico-prognostic implications of simultaneous increased serum levels of soluble CD23 and beta2-microglobulin in B-cell chronic lymphocytic leukemia. *European Journal of Haematology,* February, 62(2), pp. 117-122.

Monreno, V. et al., 2002. Effect of oral contraceptives on risk of cervical cancer in women with human papillomavirus infection: the IARC multicentric case-control study. *The Lancet,* 30 Mar, 359(9312), pp. 1085-1092.

Moody, C. & Laimins, L., 2010. Human papillomavirus oncoproteins: pathways to transformation. *Nature Reviews Cancer,* 10(8), pp. 550-560.

Moody, C. & Laimins, L., 2010. Human papillomavirus oncoproteins: pathways to transformation. *Nature Reviews Cancer,* August, 10(8), pp. 550-560.

Morabito, A. et al., 2009. Analysis and clinical relevance of human leukocyte antigen class I, heavy chain, and beta2-microglobulin downregulation in breast cancer. *Human Immunology,* 70(7), pp. 492-495.

Mori, M. et al., 1999. β2Microglobulin identified as an apoptosis-inducing factor and its characterization. *Blood,* 15 October, 94(8), pp. 2744-2753.

Morrison, M. et al., 2011. Targeting the Human Papillomavirus E6 and E7 oncogenes through expression of the bovine papillomavirus type 1 E2 protein stimulates cellular motility. *Journal of Virology,* 85(20), pp. 10487-10498.

Moscicki, A. et al., 2001. Risks for incident human papillomavirus infection and low-grade squamous intraepithelial lesion development in young females. *Journal of the American Medical Association,* 285(23), pp. 2995-3002.

Moxfyre, 2009. *Wikipedia.org.* [Online]
Available at:
http://en.wikipedia.org/wiki/Raman_spectroscopy#mediaviewer/File:Raman_energy_levels.svg
[Accessed August 2014].

Munger, K. et al., 2004. Mechanisms of human papillomavirus-induced oncogenesis. *Journal of Virology,* 78(21), p. 11451–11460.

Muñoz, N. et al., 2002. Role of parity and human papillomavirus in cervical cancer: the IARC multicentric case control study. *The Lancet,* 259(9312), pp. 1093-1101.

Nakahara, T. et al., 2002. Modulation of the cell division cycle by Human Papillomavirus type 18 E4. *Journal of Virology,* November, 76(21), p. 10914–10920.

Nandi, A. et al., 2007. Attenuation of DNA damage checkpoint by PBK, a novel mitotic kinase, involves protein-protein interaction with tumor suppressor p53. *Biochemical and Biophysical Research Communications,* 358(1), pp. 181-188.

Nandi, A., Tidwell, M., Karp, J. & Rapoport, A., 2004. Protein expression of PDZ-binding kinase is up-regulated in hematologic malignancies and strongly down-regulated during terminal differentiation of HL-60 leukemic cells. *Blood Cells, Molecules & Diseases,* 32(1), pp. 240-245.

Napoli, C., Lemieux, C. & Jorgensen, R., 1990. Introduction of a Chimeric Chalcone Synthase Gene into Petunia Results in Reversible Co-Suppression of Homologous Genes in trans. *Plant Cell,* April, 2(4), pp. 279-289.

Nappi, L. et al., 2005. Cervical squamous intraepithelial lesions of low-grade in HIV-infected women: recurrence, persistence, and progression, in treated and untreated women. *European Journal of Obstetrics & Gynecology and Reproductive Biology,* 121(2), pp. 226-232.

Narayan, G. et al., 2004. Promoter hypermethylation of FANCF: disruption of Fanconi Anemia-BRCA pathway in cervical cancer. *Cancer Research,* 64(9), pp. 2994-2997.

Narisawa-Saito, M. & Tohru, K., 2007. Basic mechanisms of high-risk human papillomavirusinduced carcinogenesis: Roles of E6 and E7 proteins. *Cancer Science* , October , 98(10), p. 1505–1511.

National Cancer Screening Service, 2008. *Cervicalcheck.* [Online]
Available at: http://www.cervicalcheck.ie/news/national-cancer-screening-service-publishes-first-annual-report.118.html
[Accessed 16 Oct 2012].

National Immunisation Advisory Committee of the Royal College of Physicians of Ireland, 2011. *Immunisation Guidelines for Ireland, 2008 Edition (with updated corrections and amendments).* [Online]
Available at:
http://www.immunisation.ie/en/Downloads/NIACGuidelines/PDFFile_16868_en.pdf
[Accessed 16 October 2012].

Naujokat, C. et al., 2000. Proteasome inhibitors induce caspase-dependent apoptosis and accumulationof p21WAF1/Cip1 in human immatureleukemic cells. *European Journal of Haematology,* October, 65(4), pp. 221-236.

Niebler, M. et al., 2013. Post-translational control of IL-1β via the human papillomavirus type 16 E6 oncoprotein: a novel mechanism of innate immune escape mediated by the E3-ubiquitin ligase E6-AP and p53. *Public Library of Science Pathogens (PLoS Pathog),* 9(8), p. e1003536.

Niebler, M. et al., 2013. Post-translational control of IL-1β via the human papillomavirus type 16 E6 oncoprotein: a novel mechanism of innate immune escape mediated by the E3-ubiquitin ligase E6-AP and p53. *Public Library of Science Pathogens (PLoS Pathog),* 9(8), p. e1003536.

Nomine, Y. et al., 2006. Structural and functional analysis of E6 oncoprotein: insights in the molecular pathways of human papillomavirus-mediated pathogenesis. *Molecular Cell,* 3 March, 21(5), p. 665–678.

Nominé, Y. et al., 2006. Structural and functional analysis of E6 oncoprotein: insights in the molecular pathways of human papillomavirus-mediated pathogenesis. *Molecular Cell,* 3 March, 21(5), pp. 665-678.

Nomura, T. et al., 2014. β2-Microglobulin-mediated Signaling as a Target for Cancer Therapy. *Anti-cancer agents in Medicinal Chemistry,* 11 March, 14(3), pp. 343-352.

Odunsi, K. et al., 1996. Susceptibility to human papillomavirus-associated cervical intra-epithelial neoplasia is determined by specific HLA DR-DQ alleles. *International Journal of Cancer,* 4 September, 67(5), pp. 595-602.

Olsen, A., Dillner, J., Skrondal, A. & Magnus, P., 1998. Combined effect of smoking and human papillomavirus type 16 infection in cervical carcinogenesis. *Epidemiology,* May, 9(3), pp. 346-349.

Ostrowska, K. et al., 2010. Investigation of the influence of high-risk human papillomavirus on the biochemical composition of cervical cancer cells using vibrational spectroscopy. *Analyst,* December, 135(12), pp. 3087-3093.

Ozubun, M. & Meyers, C., 1997. Characterization of late gene transcripts expressed during vegetative replication of human papillomavirus type 31b. *Journal of Virology,* July, 71(7), pp. 5161-5172.

Palanichamy, J. et al., 2010. Silencing of integrated human papillomavirus-16 oncogenes by small interfering RNA-mediated heterochromatization. *Molecular Cancer Therapeutics,* July, 9(7), pp. 2114-2122.

Palefsky, J., 1999. Anal squamous intraepithelial lesions: relation to HIV and human papillomavirus infection. *Journal of acquired immune deficiency syndromes,* 1 Aug, 21(Suppl 1), pp. S42-48.

Palmero, I., Pantoja, C. & Serrano, M., 1998. p19ARF links the tumour suppressor p53 to Ras. *Nature,* 10 September, 395(6698), pp. 125-126.

Park, J., Shin, M. & Lambet, P., 2014. High incidence of female reproductive tract cancers in FA-deficient HPV16-transgenic mice correlates with E7's induction of DNA damage response, an activity mediated by E7's inactivation of pocket proteins. *Oncogene,* 26 June, 33(26), pp. 3383-3391.

Park, T., Fujiwara, H. & Wright, T., 1995. Molecular biology of cervical cancer and its precursors. *Cancer,* 76(suppl 10), pp. 1902-1913.

Parry, J., 2007. *Vaccinating against cervical cancer,* Hong Kong: World Health Organization,

Patil, S., Rhodes, D. & Burgess, D., 2005. DNA-based therapeutics and DNA delivery systems: A comprehensive review. *The American Association of Pharmaceutical Scientists,* March, 7(1), pp. E61-E77.

Peh, W. et al., 2002. Life cycle heterogeneity in animal models of human papillomavirus-associated disease. *Journal of Virology,* October, 76(20), pp. 10401-10416.

Plug-DeMaggio, A. et al., 2004. Telomere erosion and chromosomal instability in cells expressing the HPV oncogene 16 E6. *Oncogne,* 29 April, 23(20), pp. 3561-3571.

Poletti, P., Halfon, A. & Marti, M., 1998. Papillomavirus and anal carcinoma. *International Journal of Colorectal Disease,* 13(2), pp. 108-111.

Poljak, M., 2012. Prophylactic human papillomavirus vaccination and primary prevention of cervical cancer: issues and challenges. *Clinical Microbiology and Infection,* 18(Suppl 5), pp. 64-69.

Popa, L. et al., 1996. Specific targeting of human papillomavirus type 16 E7 oncogene with triple-helix forming purine oligodeoxyribonucleotides. *Biochemistry and Molecular Biology International,* Feburary, 38(2), pp. 285-295.

Pudlas, M. et al., 2011. Raman spectroscopy: a non-invasive analysis tool for the discrimination of human skin cells. *Tissue engineering Part C, methods,* 17(10), pp. 1027-1040.

Rahman, R., Latonen, L. & Wiman, K., 2005. hTERT antagonizes p53-induced apoptosis independently of telomerase activity. *Oncogene,* 17 February, 24(8), pp. 1320-1327.

Rahman-Roblick, R. et al., 2008. Proteomic identification of p53-dependent protein phosphorylation. *Oncogene,* 27(35), pp. 4854-4859.

Rahman-Roblick, R. et al., 2007. p53 targets identified by protein expression profiling. *Proceedings of the National Academy of Sciences of the USA (PNAS),* 104(13), pp. 5401-5406.

Ramalingam, D. et al., 2011. RNA aptamers directed to human immunodeficiency virus type 1 Gag polyprotein bind to the matrix and nucleocapsid domains and inhibit virus production. *Journal of Virology,* January, 85(1), pp. 305-314.

Rattan, S., 2006. Theories of biological aging: genes, proteins, and free radicals. *Free Radical Research,* 40(12), pp. 1230-1238.

Reyes-Gutiérrez, P. & Alvarez-Salas, L., 2009. Cleavage of HPV-16 E6/E7 mRNA mediated by modified 10-23 deoxyribozymes. *Oligonucleotides,* September, 19(3), pp. 233-242.

Reynolds, A. et al., 2004. Rational siRNA design for RNA interference. *Nature Biotechnology,* March, 22(3), pp. 326-330.

Reynolds, A. et al., 2004. Rational siRNA design for RNA interference. *Nature Biotechnology,* March, 22(3), pp. 326-330.

Rho, H. et al., 2010. Identification of valid reference genes for gene expression studies of human stomach cancer by reverse transcription-qPCR. *BioMed Central,* Volume 10, p. 240.

Roberts, S., Ashmole, I., Rookes, S. & Gallimore, P., 1997. Mutational analysis of the human papillomavirus type 16 E1^E4 protein shows that the C terminus is dispensable for keratin cytoskeleton association but is involved in inducing disruption of the keratin filaments. *Journal of Virology,* 71(5), pp. 3354-3562.

Ronco, L., Karpova, A., Vidal, M. & Howley, P., 1998. Human papillomavirus 16 E6 oncoprotein binds to interferon regulatory factor-3 and inhibits its transcriptional activity. *Genes Development,* 1 July, 12(13), p. 2061–2072.

Roque, D., Wysham, W. & Sope, J., 2014. The surgical management of cervical cancer: an overview and literature review. *Obstetrical & Gynecological Survey,* 69(7), pp. 426-441.

Rositch, A. et al., 2013. Patterns of persistent genital human papillomavirus infection among women worldwide: A literature review and meta-analysis. *International Journal of Cancer,* 15 September, 133(6), pp. 1271-1285.

Rous, P., 1911. A sarcoma of the fowl transmissible by an agent separable from the tumor cells. *Journal of Experimental Medicine,* 1 April, 13(4), pp. 397-411.

Rous, P. & Beard, J., 1935. The progression to carcinoma of virus-induced rabbit papillomas (Shope). *Journal of Experimental Medicine,* 30 September , 62(4), pp. 523-548.

Rous, P., Kidd, J. & Beard, J., 1936. Observations on the relation of the virus causing rabbit papillomas to the cancers deriving therefrom: I. The influence of the host species and of the pathogenic activity and concentration of the virus. *Journal of Experimental Medicine,* 31 August, 64(3), pp. 385-400.

Saavedra, K., Brebi, P. & Roa, J., 2012. Epigenetic alterations in preneoplastic and neoplastic lesions of the cervix. *Clinical Epigenetics,* 4(1), pp. 4-13.

Sakaguchi, K. et al., 1998. DNA damage activates p53 through a phosphorylation - acetylation cascade. *Genes and Development,* 15 September, 12(18), pp. 2931-2841.

Sanjeevi, C. et al., 1996. Different HLA-Dr-DQ haplotypes are associated with cervical intraepithelial neoplasia among human papillomavirus type 16 seropositive and seronegative Swedish women. *International Journal of Cancer,* 15 November, 68(4), pp. 409-414.

Schiffman, M. & Kjaer, S., 2003. Chapter 2: Natural History of Anogenital Human Papillomavirus Infection and Neoplasia. *Journal of the National Cancer Institute Monographs,* Issue 31, pp. 14-19.

Schmitt, A. et al., 1994. Comparison of the properties of the E6 and E7 genes of low- and high-risk cutaneous papillomaviruses reveals strongly transforming and high Rb-binding activity for the E7 protein of the low-risk human papillomavirus type 1. *Journal of Virology,* November, 68(11), pp. 7051-7059.

Sellors, J. et al., 2003. Incidence, clearance and predictors of human papillomavirus infection in women. *Canadian Medical Association Journal (CMAJ),* 18 February, 168(4), pp. 421-425.

Seoane, M. et al., 2008. Retinoblastoma loss modulates DNA damage response favoring tumor progression. *Public Library of Science One,* November, 3(11), p. e3632.

Serrano, M. et al., 1997. Oncogenic ras provokes premature cell senescence associated with accumulation of p53 and p16INK4a. *Cell,* March, 88(5), pp. 593-602.

Shafqat, N. et al., 2006. Hep27 a member of the short-chain dehydrogenase/reductase family is an NADPH-dependent dicarbonyl reductase expressed in vascular endothelial tissue. *Cellular and Molecular Life Sciences (CMLS),* 63(10), pp. 1205-1213.

Shi, C. et al., 2009. Beta2-microglobulin: emerging as a promising cancer therapeutic target. *Drug DiscoveryToday,* January, 14(1-2), pp. 25-30.

Shieh, S., Ikeda, M., Taya, Y. & Prives, C., 1997. DNA damage-induced phosphorylation of p53 alleviates inhibition by MDM2. *Cell,* 31 October , 91(3), pp. 325-334.

Shlush, L. et al., 2011. Quantitative digital in situ senescence-associated β-galactosidase assay. *BioMed Central Cell Biology,* 15 April, Volume 12, p. 16.

Silverman, R. & Weiss, S., 2014. Viral phosphodiesterases that antagonize double-stranded RNA signaling to RNase L by degrading 2-5A. *Journal of Interferon & Cytokine Release,* 34(6), pp. 455-463.

Sima, N. et al., 2007. Antisense targeting human papillomavirus type 16 E6 and E7 genes contributes to apoptosis and senescence in SiHa cervical carcinoma cells. *Gynecologic Oncology,* August, 106(2), pp. 299-304.

Smith, C., 2010. *annaffy: Annotation tools for Affymetrix biological metadata.* s.l.:Colin A. Smith (2010). annaffy: Annotation tools for Affymetrix biological metadata. R package version 1.30.0..

Smith, J., Campos, S. & Ozbun, M., 2007. Human papillomavirus type 31 uses a caveolin 1- and dynamin 2-mediated entry pathway for infection of human keratinocytes. *Journal of Virology,* September, 81(18), pp. 9922-9931.

Smith, J. et al., 2002. Herpes simplex virus-2 as a human papillomavirus cofactor in the etiology of invasive cervical cancer. *Journal of the National Cancer Institute,* 6 November, 94(21), pp. 1604-1613.

Smith, J. et al., 2002. Evidence for Chlamydia trachomatis as a human papillomavirus cofactor in the etiology of invasive cervical cancer in Brazil and the Philippines. *Journal of Infectious Diseases,* 1 February, 185(3), p. 324–331.

Smith, J. et al., 2010. Genome-wide siRNA screen identifies SMCX, EP400 and Brd4 as E2-dependent regulators of human papillomavirus oncogene expression. *Proceedings of the National Academy of Sciences of the United States of America (PNAS),* 23 February, 107(8), pp. 3752-3757.

Somsubhra, D. & Sachchithanantham, K., 2010. Human Papilloma Virus Vaccine – An update. *European Journal of Scientific Research,* 43(2), pp. 256-264.

Sørensen, J., Nielsen, J. & Petersen, M., 2004. Solution structure of a dsDNA:LNA triplex. *Nucleic Acids Research,* 18 November, 32(20), pp. 6078-6085.

Stacey, S. et al., 1995. Translation of the human papillomavirus type 16 E7 oncoprotein from bicistronic mRNA is independent of splicing events within the E6 open reading frame. *Journal of Virology,* November, 69(11), pp. 7023-7031.

Stacey, S. et al., 2000. Leaky scanning is the predominant mechanism for translation of human papillomavirus type 16 E7 oncoprotein from E6/E7 bicistronic mRNA. *Journal of Virology,* August, 74(16), pp. 7284-7297.

Stanley, M., 2010. Pathology and epidemiology of HPV infection in females. *Gynecologic Oncology,* May, 117(Suppl 2), pp. S5-10.

Stanley, M., Browne, H., Appleby, M. & Minson, A., 1989. Properties of a non-tumorigenic human cervical keratinocyte cell line. *International Journal of Cancer,* 15 April, 43(4), p. 672–676.

Stern, P. et al., 2012. Therapy of Human Papillomavirus-Related Disease. *Vaccine,* Issue Suppl 30, p. F71– F82.

Stone, K. et al., 2002. Seroprevalence of human papillomavirus type 16 infection in the United States. *The Journal of Infectious Diseases,* 15 Nov, 186(10), pp. 1396-402.

Sugita, M. & Brenner, M., 1994. An unstable beta 2-microglobulin: major histocompatibility complex class I heavy chain intermediate dissociates from calnexin and then is stabilized by binding peptide. *Journal of Experimental Medicine,* 1 December, 180(6), pp. 2163-2167.

Sundarama, P., Kurniawan, H., Byrne, M. & Wower, J., 2013. Therapeutic RNA aptamers in clinical trials. *European Journal of Pharmaceutical Sciences,* 23 January , 48(1–2), p. 259–271.

Tang, S., Tao, M., McCoy, J. J. & Zheng, Z., 2006. The E7 oncoprotein is translated from spliced E6*I transcripts in high-risk human papillomavirus type 16- or type 18-positive cervical cancer cell lines via translation reinitiation. *Journal of virology,* May, 80(9), pp. 4249-4263.

Tan, S., de Vries, E., van der Zee, A. & de Jong, S., 2012. Anticancer drugs aimed at E6 and E7 activity in HPV-positive cervical cancer. *Current Cancer Drug Targets,* 12(2), pp. 170-184.

Tan, S. et al., 2012. Human papilloma virus 16 E6 RNA interference enhances cisplatin and death receptor-mediated apoptosis in human cervical carcinoma cells. *Molecular Pharmacology,* May, 81(5), pp. 701-709.

Teukolsky, S., Vetterling, W. & Flannery, B., 2007. *Numerical Recipes: The art of scientific computing.* 3rd ed. s.l.:William H. Press.

Thomas, M. et al., 2002. Oncogenic human papillomavirus E6 proteins target the MAGI-2 and MAGI-3 proteins for degradation. *Oncogene,* 1 August, 21(33), pp. 5088-5096.

Thorner, A., Parker, J., Hoadley, K. & Perou, C., 2010. Potential tumor suppressor role for the c-Myb oncogene in luminal breast cancer. *Public Library of Science one (PLoS 1),* 5(10), p. e13073.

Tomita, L. et al., 2009. Dietary predictors of serum total carotene in low-income women living in São Paulo, south-east Brazil. *Public Health Nutrition,* November, 12(11), pp. 2133-2142.

Tomita, L. et al., 2010. Diet and serum micronutrients in relation to cervical neoplasia and cancer among low-income Brazilian women. *International Journal of Cancer,* 1 February, 126(3), p. 703–714.

Towbin, H., Staehelin, T. & Gordon, J., 1979. Electrophoretic transfer of proteins from polyacrylamide gels to nitrocellulose sheets: procedure and some applications. *Proceedings of the National Academy of Sciences of the United States of America (PNAS),* September, 76(9), pp. 4350-4354.

Tseng, G., Ghosh, D. & Feingold, E., 2012. Comprehensive literature review and statistical considerations for microarray meta-analysis. *Nucleic Acid Research,* 40(9), pp. 3785-3799.

Tungteakkhun, S., Filippova, M., Fodor, N. & Duerksen-Hughes, P., 2010. The full-length isoform of human papillomavirus 16 E6 and its splice variant E6* bind to different sites on the procaspase 8 death effector domain. *Journal of Virology,* Feburary, 84(3), pp. 1453-1463.

Ui-Tei, K. et al., 2004. Guidelines for the selection of highly effective siRNA sequences for mammalian and chick RNA interference. *Nucleic Acids Research,* 32(3), pp. 936-948.

Ullmann, E., 1923. On the aetiology of the laryngeal papilloma. *Acta Oto-Laryngologica,* Volume 5, pp. 317-338.

Vaccarella, S. et al., 2008. Smoking and human papillomavirus infection: pooled analysis of the International Agency for Research on Cancer HPV Prevalence Surveys. *International Journal of Epidemiology,* June, 37(3), pp. 536-546.

Vargis, E., Tang, Y., Khabele, D. & Mahadevan-Jansen, A., 2012. Near-infrared Raman microspectroscopy detects high-risk Human Papillomaviruses 1. *Translational Oncology,* June, 5(3), pp. 172-179.

Venturini, F. et al., 1999. Kinetic selection of HPV 16 E6/E7-directed antisense nucleic acids: anti-proliferative effects on HPV 16-transformed cells. *Nucleic Acids Research,* 27(7), p. 1585–1592.

Vilches-Flores, A. et al., 2010. Biotin increases glucokinase expression via soluble guanylate cyclase/protein kinase G, adenosine triphosphate production and autocrine action of insulin in pancreatic rat islets. *Journal of Nutritional Biochemistry,* July, 21(7), pp. 606-612.

Vinokurova, S. et al., 2008. Type-dependent integration frequency of human papillomavirus genomes in cervical lesions. *Cancer Research,* 1 January, 68(1), pp. 307-313.

Volpe, T. et al., 2002. Regulation of heterochromatic silencing and histone H3 lysine-9 methylation by RNAi. *Science,* 13 September, 297(5588), pp. 1833-1837.

Vredeveld, L., 2009. *Oncogene-induced senescence: from in vitro tool to in vivo tumour suppression.* Netherlands: Het Nederlands Kanker Instituut - Antoni van Leeuwenhoek Ziekenhuis.

Walboomers, J. et al., 1999. Human Papillomavirus is a necessary cause of invasive cervical cancer worldwide. *Journal of Pathology,* September, 189(1), pp. 12-19.

Wang, S. et al., 2009. Common variants in immune and DNA repair genes and risk for human papillomavirus persistence and progression to cervical cancer. *Journal of Infectious Disease,* 199(1), pp. 20-30.

Wang, S. et al., 2003. Seroprevalence of human papillomavirus-16, -18, -31, and -45 in a population-based cohort of 10,000 women in Costa Rica. *British Journal of Cancer,* 6 Oct, 89(7), pp. 1248-1254.

Wang, X. et al., 1994. Hepatitis B virus X protein inhibits p53 sequence-specific DNA binding, transcriptional activity, and association with transcription factor ERCC3. *Proceedings of the National Academy of Sciences (PNAS),* 15 March, 91(6), pp. 2230-2234.

Warnes, G. et al., 2014. *gplots: Various R programming tools for plotting data.* US: CRAN.

Wei, R., Stewart, E. & Amoaku, W., 2013. Suitability of endogenous reference genes for gene expression studies with human intraocular endothelial cells. *BioMed Central Research Notes,* 4 February, Volume 6, p. 46.

Whiteside, M., Siegel, E. & Unger, E., 2008. Human papillomavirus and molecular considerations for cancer risk. *Cancer,* 15 November, 113(Suppl 10), pp. 2981-2994.

WHO/FAO, 2003. *Diet, Nutrition and the Prevention of Chronic Diseases,* Geneva: World Health Organisation/Food and Agriculture Organisation of the united nations.

Wiebe, J. & Lewis, M., 2003. Activity and expression of progesterone metabolizing 5alpha-reductase, 20alpha-hydroxysteroid oxidoreductase and 3alpha(beta)-hydroxysteroid oxidoreductases in tumorigenic (MCF-7, MDA-MB-231, T-47D) and nontumorigenic (MCF-10A) human breast cancer cells. *BioMed Central cancer Cancer,* 22 March, Volume 3, p. 9.

Wilson, V., West, M., Woytek, K. & Rangasamy, D., 2002. Papillomavirus E1 Proteins: Form, Function and Features. *Virus Genes,* 24(3), pp. 275-290.

Winer, R. et al., 2012. Prevalence and risk factors for oncogenic human papillomavirus infections in high-risk mid-adult women. *Sexually Transmitted Diseases,* Nov, 39(11), pp. 848-56.

Winer, R. et al., 2003. Genital Human Papillomavirus infection: Incidence and risk factors in a cohort of female university students. *American Journal of Epidemiology,* 1 Feb, 157(3), pp. 218-226.

Woodman, C., Collins, S. & Young, L., 2007. The natural history of cervical HPV infection: unresolved issues. *Nature Reviews Cancer,* January, 7(1), pp. 11-22.

World Health Organisation, 2012. *Report of the HPV Vaccine Delivery Meeting,* Geneva: Expanded Programme on Immunization (EPI) of the Department of Immunization, Vaccines and Biologicals.

Wu, C., Gordon, J., Zhong, X. & Safa, A., 2002. Mechanism of beta 2-microglobulin-induced apoptosis in the K562 leukemia cell line defective in major histocompatibility class 1. *Anticancer Research,* 22(5), pp. 2613-2621.

Wu, K. et al., 1999. Direct activation of TERT transcription by c-MYC. *Nature Genetics,* 21(2), pp. 220-224.

Xia, M., Knezevic, D. & Vassilev, L., 2011. p21 does not protect cancer cells from apoptosis induced by nongenotoxic p53 activation. *Oncogene,* 20 January, 30(3), pp. 346-355.

Yamato, K. et al., 2008. New highly potent and specific E6 and E7 siRNAs for treatment of HPV16 positive cervical cancer. *Cancer Gene Therapy,* March, 15(3), pp. 140-153.

Yang, H., Li, Y., Deng, H. & Peng, F., 2009. Identification of beta2-microglobulin as a potential target for ovarian cancer. *Cancer Biology & Therapy,* December, 8(24), pp. 2323-2328.

Yizhuo, Y. et al., 209. Effects of Cidofovir on Human Papillomavirus-positive cervical cancer cells xenografts in nude mice. *Oncology Research,* 18(11-12), pp. 519-527.

Yoshinouchi, M. et al., 2003. In-vitro and in-vivo growth suppression of human papillomavirus16 positive cervical cancer cells by E6 siRNA. *Molecular Therapy,* November, 8(5), pp. 762-768.

Zanier, K. et al., 2007. Formation of well-defined soluble aggregates upon fusion to MBP is a generic property of E6 proteins from various human papillomavirus species. *Protein Expression and Purification,* JAnuary, 51(1), pp. 59-70.

Zhang, Z. et al., 2013. Genistein induces G2/M cell cycle arrest and apoptosis via ATM/p53-dependent pathway in human colon cancer cells. *International Journal of Oncology,* July, 43(1), pp. 289-296.

Zheng, Z., 2010. Viral oncogenes, non-coding RNAs and RNA splicing in human tumor viruses. *International Journal of Biological Sciences,* December, 6(7), pp. 730-755.

Zheng, Z. & Baker, C., 2006. Papillomavirus genome structure, expression and post-transcriptional regulation. *Frontiers in Biosciences,* 1 September, Volume 11, pp. 2286-2302.

Zhou, J. et al., 2012. Transcriptional gene silencing of HPV16 E6/E7 induces growth inhibition via apoptosis in-vitro and in-vivo. *Gyneocologic Oncology,* 124(2), pp. 296-302.

Zhou, J., Sun, X., Louis, K. & Frazer, I., 1994. Interaction of human papillomavirus (HPV) type 16 capsid proteins with HPV DNA requires an intact L2 N-terminal sequence. *Journal of Virology,* February, 68(2), pp. 619-625.

Zhu, J. et al., 2014. Antiviral activity of human OASL protein is mediated by enhancing signaling of the RIG-I RNA sensor. *Immunity,* 19 June, 40(6), pp. 936-948.

Zimmermann, H., Degenkolbe, R., Bernard, H. & O'Connor, M., 1999. The human papillomavirus type16 E6 oncoprotein can down-regulate p53 activity by targeting the transcriptional coactivator CBP/p300. *Journal of Virology,* August, 73(8), p. 6209–6219.

Zoodsma, M. et al., 2005. Analysis of the entire HLA region in susceptibility for cervical cancer: a comprehensive study. *Journal of Medical Genetics,* 42(8), p. e49.

Appendix

Table 8-1: Table of all differentially expressed gene associations in E6#2. Up-regulated genes highlighted in red and down regulated genes highlighted in blue.

Symbol	GeneName	Entrez GeneID	Fold-Change	FDR
KRT34	keratin 34	3885	12.18	>0.0001
CCL5	chemokine (C-C motif) ligand 5	6352	7.91	>0.0001
CCR4	chemokine (C-C motif) receptor 4	1233	5.82	>0.0001
INHBA	inhibin, beta A	3624	5.80	>0.0001
DHRS2	dehydrogenase/reductase (SDR family) member 2	10202	4.90	>0.0001
PSG2	pregnancy specific beta-1-glycoprotein 2	5670	4.72	>0.0001
SERPINE1	serpin peptidase inhibitor, clade E (nexin, plasminogen activator inhibitor type 1), member 1	5054	4.58	>0.0001
UTS2B	urotensin 2B	257313	4.57	>0.0001
FN1	fibronectin 1	2335	4.54	>0.0001
TCN2	transcobalamin II	6948	4.33	>0.0001
IL24	interleukin 24	11009	4.30	>0.0001
TNFAIP3	tumor necrosis factor, alpha-induced protein 3	7128	3.93	>0.0001
PMAIP1	phorbol-12-myristate-13-acetate-induced protein 1	5366	3.74	>0.0001
CCL3L1	chemokine (C-C motif) ligand 3-like 1	6349	3.88	0.0006
GADD45A	growth arrest and DNA-damage-inducible, alpha	1647	3.42	>0.0001
KLF4	Kruppel-like factor 4 (gut)	9314	3.51	>0.0001
OASL	2'-5'-oligoadenylate synthetase-like	8638	3.49	>0.0001
IL20	interleukin 20	50604	3.43	>0.0001
ANKRD1	ankyrin repeat domain 1 (cardiac muscle)	27063	3.21	>0.0001
SNAI2	snail family zinc finger 2	6591	3.49	>0.0001
ARL14	ADP-ribosylation factor-like 14	80117	3.37	>0.0001
CYP1A1	cytochrome P450, family 1, subfamily A, polypeptide 1	1543	3.30	>0.0001
ALOXE3	arachidonate lipoxygenase 3	59344	3.27	>0.0001
JUN	jun proto-oncogene	3725	3.26	>0.0001
KRTAP2-4	keratin associated protein 2-4	85294	3.52	0.0002
NFATC2	nuclear factor of activated T-cells, cytoplasmic, calcineurin-dependent 2	4773	3.28	0.0003

Symbol	GeneName	Entrez GeneID	Fold-Change	FDR
NCF2	neutrophil cytosolic factor 2	4688	3.25	0.0006
CGA	glycoprotein hormones, alpha polypeptide	1081	3.04	0.0011
BIRC3	baculoviral IAP repeat containing 3	330	2.91	0.0011
PPP1R15A	protein phosphatase 1, regulatory subunit 15A	23645	2.88	0.0014
CXCL11	chemokine (C-X-C motif) ligand 11	6373	3.04	0.0013
LPAR6	lysophosphatidic acid receptor 6	10161	3.03	0.0013
IGFBP6	insulin-like growth factor binding protein 6	3489	3.03	0.0012
SESN2	sestrin 2	83667	2.77	0.0017
ADH1C	alcohol dehydrogenase 1C (class I), gamma polypeptide	126	2.89	0.0017
HIST1H4H	histone cluster 1, H4h	8365	2.79	0.0019
RFPL4A	ret finger protein-like 4A	342931	3.00	0.0020
PDCD1LG2	programmed cell death 1 ligand 2	80380	2.81	0.0020
DNAI1	dynein, axonemal, intermediate chain 1	27019	2.79	0.0020
NR1D1	nuclear receptor subfamily 1, group D, member 1	9572	2.71	0.0031
DDIT3	DNA-damage-inducible transcript 3	1649	2.68	0.0031
NSAP11	nervous system abundant protein 11	100131275	2.71	0.0032
IL6	interleukin 6 (interferon, beta 2)	3569	2.75	0.0031
ROS1	c-ros oncogene 1 , receptor tyrosine kinase	6098	2.69	0.0033
ATF3	activating transcription factor 3	467	2.68	0.0034
TAF1D	TATA box binding protein (TBP)-associated factor, RNA polymerase I, D, 41kDa	79101	2.66	0.0039
EGR1	early growth response 1	1958	2.83	0.0038
GDF15	growth differentiation factor 15	9518	2.73	0.0041
CCRN4L	CCR4 carbon catabolite repression 4-like (S. cerevisiae)	25819	2.64	0.0040
FOSB	FBJ murine osteosarcoma viral oncogene homolog B	2354	2.45	0.0043
EDN1	endothelin 1	1906	2.62	0.0044
RSAD2	radical S-adenosyl methionine domain containing 2	91543	2.73	0.0043
IFIT2	interferon-induced protein with tetratricopeptide repeats 2	3433	2.62	0.0043

Symbol	GeneName	Entrez GeneID	Fold-Change	FDR
CPA2	carboxypeptidase A2 (pancreatic)	1358	2.65	0.0042
STC2	stanniocalcin 2	8614	2.47	0.0041
IL1A	interleukin 1, alpha	3552	2.60	0.0042
CEACAM20	carcinoembryonic antigen-related cell adhesion molecule 20	125931	2.66	0.0042
ZNF670	zinc finger protein 670	93474	2.37	0.0055
IL8	interleukin 8	3576	2.55	0.0055
TNFRSF9	tumor necrosis factor receptor superfamily, member 9	3604	2.55	0.0059
PSG6	pregnancy specific beta-1-glycoprotein 6	5675	2.57	0.0062
MMP3	matrix metallopeptidase 3 (stromelysin 1, progelatinase)	4314	2.59	0.0063
SNHG12	small nucleolar RNA host gene 12 (non-protein coding)	85028	2.48	0.0062
RFPL4A	ret finger protein-like 4A	342931	2.69	0.0062
MIR221	microRNA 221	407006	2.69	0.0062
CHAC1	ChaC, cation transport regulator homolog 1 (E. coli)	79094	2.47	0.0061
ERRFI1	ERBB receptor feedback inhibitor 1	54206	2.52	0.0060
NT5E	5'-nucleotidase, ecto (CD73)	4907	2.59	0.0059
GPR87	G protein-coupled receptor 87	53836	2.42	0.0058
IL7R	interleukin 7 receptor	3575	2.50	0.0065
DNAJB9	DnaJ (Hsp40) homolog, subfamily B, member 9	4189	2.45	0.0065
NFKBIZ	nuclear factor of kappa light polypeptide gene enhancer in B-cells inhibitor, zeta	64332	2.42	0.0072
IL2RG	interleukin 2 receptor, gamma	3561	2.48	0.0072
BDKRB1	bradykinin receptor B1	623	2.47	0.0073
PHLDA1	pleckstrin homology-like domain, family A, member 1	22822	2.51	0.0073
MIR222	microRNA 222	407007	2.59	0.0073
MFSD2A	major facilitator superfamily domain containing 2A	84879	2.40	0.0079
HSPB8	heat shock 22kDa protein 8	26353	2.33	0.0083
OTOP2	otopetrin 2	92736	2.40	0.0084

Symbol	GeneName	Entrez GeneID	Fold-Change	FDR
ITGA2	integrin, alpha 2 (CD49B, alpha 2 subunit of VLA-2 receptor)	3673	2.40	0.0085
IFNL1	interferon, lambda 1	282618	2.41	0.0091
DUSP6	dual specificity phosphatase 6	1848	2.20	0.0091
RGS2	regulator of G-protein signaling 2, 24kDa	5997	2.43	0.0090
ZNF441	zinc finger protein 441	126068	2.32	0.0091
LIF	leukemia inhibitory factor	3976	2.33	0.0094
SQRDL	sulfide quinone reductase-like (yeast)	58472	2.33	0.0099
CTSS	cathepsin S	1520	2.35	0.0108
ASNS	asparagine synthetase (glutamine-hydrolyzing)	440	2.26	0.0113
UPP1	uridine phosphorylase 1	7378	2.19	0.0113
SERPINB9	serpin peptidase inhibitor, clade B (ovalbumin), member 9	5272	2.30	0.0115
HIST2H4A	histone cluster 2, H4a	8370	2.26	0.0120
HIST2H4A	histone cluster 2, H4a	8370	2.26	0.0120
CXCL2	chemokine (C-X-C motif) ligand 2	2920	2.26	0.0129
DUSP4	dual specificity phosphatase 4	1846	2.23	0.0128
PLA2G4C	phospholipase A2, group IVC (cytosolic, calcium-independent)	8605	2.24	0.0129
SOD2	superoxide dismutase 2, mitochondrial	6648	2.17	0.0148
RAET1L	retinoic acid early transcript 1L	154064	2.28	0.0154
SAT1	spermidine/spermine N1-acetyltransferase 1	6303	2.20	0.0156
FRMD6	FERM domain containing 6	122786	2.17	0.0162
ZFAND2A	zinc finger, AN1-type domain 2A	90637	2.18	0.0176
ZFP36	ZFP36 ring finger protein	7538	2.26	0.0176
EVI2B	ecotropic viral integration site 2B	2124	2.15	0.0179
GLIPR1	GLI pathogenesis-related 1	11010	2.23	0.0190
DUSP5	dual specificity phosphatase 5	1847	2.15	0.0200
FOS	FBJ murine osteosarcoma viral oncogene homolog	2353	2.05	0.0207
ZFP90	ZFP90 zinc finger protein	146198	2.13	0.0208

Symbol	GeneName	Entrez GeneID	Fold-Change	FDR
HOMER1	homer homolog 1 (Drosophila)	9456	2.12	0.0209
AEN	apoptosis enhancing nuclease	64782	2.10	0.0214
DPY19L2P2	dpy-19-like 2 pseudogene 2 (C. elegans)	349152	2.22	0.0213
SCG5	secretogranin V (7B2 protein)	6447	2.19	0.0214
SCHIP1	schwannomin interacting protein 1	29970	2.13	0.0219
NFKB2	nuclear factor of kappa light polypeptide gene enhancer in B-cells 2 (p49/p100)	4791	2.09	0.0235
LETM2	leucine zipper-EF-hand containing transmembrane protein 2	137994	2.11	0.0240
KRTAP2-1	keratin associated protein 2-1	81872	2.21	0.0272
FAM60A	family with sequence similarity 60, member A	58516	2.08	0.0279
DEPDC7	DEP domain containing 7	91614	2.07	0.0282
CCL3	chemokine (C-C motif) ligand 3	6348	2.19	0.0292
RHCG	Rh family, C glycoprotein	51458	2.09	0.0302
CDKN1A	cyclin-dependent kinase inhibitor 1A (p21, Cip1)	1026	2.12	0.0300
LAMB3	laminin, beta 3	3914	2.07	0.0323
DPH2	DPH2 homolog (S. cerevisiae)	1802	2.01	0.0360
ZBTB21	zinc finger and BTB domain containing 21	49854	2.02	0.0366
IL13RA2	interleukin 13 receptor, alpha 2	3598	2.03	0.0396
DUSP1	dual specificity phosphatase 1	1843	2.07	0.0395
CCNJ	cyclin J	54619	2.01	0.0392
FLJ00290	FLJ00290 protein	441310	2.03	0.0399
SLC31A2	solute carrier family 31 (copper transporter), member 2	1318	2.05	0.0405
HOMER1	homer homolog 1 (Drosophila)	9456	2.12	0.0209
AEN	apoptosis enhancing nuclease	64782	2.10	0.0214
DPY19L2P2	dpy-19-like 2 pseudogene 2 (C. elegans)	349152	2.22	0.0213
SCG5	secretogranin V (7B2 protein)	6447	2.19	0.0214
SCHIP1	schwannomin interacting protein 1	29970	2.13	0.0219

Symbol	GeneName	Entrez GeneID	Fold-Change	FDR
ITGA5	integrin, alpha 5 (fibronectin Receptor, alpha polypeptide)	3678	2.04	0.0426
FMN1	formin 1	342184	2.01	0.0498
SCD	stearoyl-CoA desaturase (delta-9-desaturase)	6319	3.61	>0.0001
IFNAR1	interferon (alpha, beta and omega) receptor 1	3454	3.28	0.0133
ALPP	alkaline phosphatase, placental	250	3.22	0.0100
NDUFB6	NADH dehydrogenase (ubiquinone) 1 beta subcomplex, 6, 17kDa	4712	3.06	0.0100
AKR1C3	aldo-keto reductase family 1, member C3	8644	2.87	0.0117
CYBRD1	cytochrome b reductase 1	79901	2.86	0.0157
CBX5	chromobox homolog 5	23468	2.78	0.0233
EXO1	exonuclease 1	9156	2.71	0.0250
TRAM1	translocation associated membrane protein 1	23471	2.73	0.0236
SPAG5	sperm associated antigen 5	10615	2.61	0.0308
PBK	PDZ binding kinase	55872	2.47	0.0271
FAM111B	family with sequence similarity 111, member B	374393	2.53	0.0327
REEP5	receptor accessory protein 5	7905	2.67	0.0318
NCAPG2	non-SMC condensin II complex, subunit G2	54892	2.47	0.0315
C5orf15	chromosome 5 open reading frame 15	56951	2.60	0.0305
THOC7	THO complex 7 homolog (Drosophila)	80145	2.49	0.0305
FSCN1	fascin homolog 1, actin-bundling protein (Strongylocentrotus purpuratus)	6624	2.60	0.0304
MRPS18B	mitochondrial ribosomal protein S18B	28973	2.45	0.0384
PRKRIR	protein-kinase, interferon-inducible double stranded RNA dependent inhibitor, repressor of (P58 repressor)	5612	2.42	0.0389
ECHDC1	enoyl CoA hydratase domain containing 1	55862	2.41	0.0379

Symbol	GeneName	Entrez GeneID	Fold-Change	FDR
DPYSL2	dihydropyrimidinase-like 2	1808	2.41	0.0400
ZNF138	zinc finger protein 138	7697	2.40	0.0403
CENPI	centromere protein I	2491	2.40	0.0394
SPC25	SPC25, NDC80 kinetochore complex component	57405	2.42	0.0397
ADD3	adducin 3 (gamma)	120	2.37	0.0424

Table 8-2: Table of all differentially expressed gene associations in E6#4. Up-regulated genes highlighted in red and down regulated genes highlighted in blue.

Symbol	GeneName	Entrez GeneID	Fold-Change	FDR
SULF2	sulfatase 2	55959	6.39	<0.0001
SPATA18	spermatogenesis associated 18	132671	5.88	<0.0001
BTG2	BTG family, member 2	7832	5.75	<0.0001
TP53INP1	tumor protein p53 inducible nuclear protein 1	94241	5.74	<0.0001
CDKN1A	cyclin-dependent kinase inhibitor 1A (p21, Cip1)	1026	5.21	<0.0001
MIR224	microRNA 224	407009	4.74	0.0012
ZMAT3	zinc finger, matrin-type 3	64393	4.41	0.0011
SESN1	sestrin 1	27244	4.48	0.0010
ACTBL2	actin, beta-like 2	345651	4.18	0.0025
SERPINE1	serpin peptidase inhibitor, clade E (nexin, plasminogen activator inhibitor type 1), member 1	5054	3.89	0.0043
CLCA2	chloride channel accessory 2	9635	4.08	0.0040
C12orf5	chromosome 12 open reading frame 5	57103	3.84	0.0035
ACTA2	actin, alpha 2, smooth muscle, aorta	59	3.74	0.0039
MDM2	MDM2 oncogene, E3 ubiquitin protein ligase	4193	3.67	0.0070
SESN2	sestrin 2	83667	3.46	0.0067
ANGPTL4	angiopoietin-like 4	51129	3.39	0.0087
DGKA	diacylglycerol kinase, alpha 80kDa	1606	3.37	0.0104
GLIPR1	GLI pathogenesis-related 1	11010	3.36	0.0111
F2R	coagulation factor II (thrombin) receptor	2149	3.26	0.0103
FAP	fibroblast activation protein, alpha	2191	3.33	0.0119
PSG2	pregnancy specific beta-1-glycoprotein 2	5670	3.16	0.0163
PAPPA	pregnancy-associated plasma protein A, pappalysin 1	5069	2.99	0.0179
TFPI	tissue factor pathway inhibitor (lipoprotein-associated coagulation inhibitor)	7035	2.96	0.0216
GAS6	growth arrest-specific 6	2621	2.85	0.0250

Symbol	GeneName	Entrez GeneID	Fold-Change	FDR
TNFRSF10B	tumor necrosis factor receptor superfamily, member 10b	8795	2.82	0.0288
ITGA2	integrin, alpha 2 (CD49B, alpha 2 subunit of VLA-2 receptor)	3673	2.75	0.0286
MAP1B	microtubule-associated protein 1B	4131	2.75	0.0326
HMOX1	heme oxygenase (decycling) 1	3162	2.73	0.0336
DRAM1	DNA-damage regulated autophagy modulator 1	55332	2.71	0.0366
A2M	alpha-2-macroglobulin	2	2.87	0.0360
ABCA1	ATP-binding cassette, sub-family A (ABC1), member 1	19	2.69	0.0350
PRDM1	PR domain containing 1, with ZNF domain	639	2.71	0.0354
LIPH	lipase, member H	200879	2.61	0.0345
DSE	dermatan sulfate epimerase	29940	2.65	0.0367
LRP1	low density lipoprotein receptor-related protein 1	4035	2.65	0.0370
GRB7	growth factor receptor-bound protein 7	2886	2.69	0.0383
ABCG2	ATP-binding cassette, sub-family G (WHITE), member 2	9429	2.54	0.0427
SERPINB5	serpin peptidase inhibitor, clade B (ovalbumin), member 5	5268	2.60	0.0445
FUCA1	fucosidase, alpha-L- 1, tissue	2517	2.61	0.0447
FST	follistatin	10468	2.58	0.0464
HYDIN	HYDIN, axonemal central pair apparatus protein	54768	2.57	0.0496
ARRDC4	arrestin domain containing 4	91947	2.56	0.0499
UIMC1	ubiquitin interaction motif containing 1	51720	3.04	0.0495
GPC1	glypican 1	2817	2.54	0.0489
ORAI3	ORAI calcium release-activated calcium modulator 3	93129	2.54	0.0488
APOBEC3C	apolipoprotein B mRNA editing enzyme, catalytic polypeptide-like 3C	27350	2.55	0.0499
CASP1	Caspase 1, apoptosis-related cysteine peptidase	834	2.52	0.0499

Symbol	GeneName	Entrez GeneID	Fold-Change	FDR
KIF20A	kinesin family member 20A	10112	18.12	<0.0001
RRM2	ribonucleotide reductase M2	6241	17.70	<0.0001
HIST1H2BM	histone cluster 1, H2bm	8342	16.95	<0.0001
HIST1H3I	histone cluster 1, H3i	8354	14.77	<0.0001
ANLN	anillin, actin binding protein	54443	14.13	<0.0001
DTL	denticleless E3 ubiquitin protein ligase homolog (Drosophila)	51514	14.13	<0.0001
MKI67	antigen identified by monoclonal antibody Ki-67	4288	13.79	<0.0001
HIST1H1B	histone cluster 1, H1b	3009	14.04	<0.0001
FAM111B	family with sequence similarity 111, member B	374393	14.42	<0.0001
HIST1H3F	histone cluster 1, H3f	8968	12.34	<0.0001
KIAA0101	KIAA0101	9768	12.67	<0.0001
MYBL2	v-myb avian myeloblastosis viral oncogene homolog-like 2	4605	12.60	<0.0001
ESCO2	establishment of sister chromatid cohesion N-acetyltransferase 2	157570	11.98	<0.0001
NCAPG	non-SMC condensin I complex, subunit G	64151	11.79	<0.0001
NCAPH	non-SMC condensin I complex, subunit H	23397	11.48	<0.0001
BUB1	BUB1 mitotic checkpoint serine/threonine kinase	699	11.09	<0.0001
TOP2A	topoisomerase (DNA) II alpha 170kDa	7153	10.50	<0.0001
CDC20	cell division cycle 20	991	10.48	<0.0001
CDK1	cyclin-dependent kinase 1	983	10.27	<0.0001
DLGAP5	discs, large (Drosophila) homolog-associated protein 5	9787	10.32	<0.0001
HIST1H4L	histone cluster 1, H4l	8368	10.23	<0.0001
PBK	PDZ binding kinase	55872	9.81	<0.0001
ASPM	asp (abnormal spindle) homolog, microcephaly associated (Drosophila)	259266	10.27	<0.0001
CEP55	centrosomal protein 55kDa	55165	10.23	<0.0001

Symbol	GeneName	Entrez GeneID	Fold-Change	FDR
CDC6	cell division cycle 6	990	9.86	<0.0001
CENPF	centromere protein F, 350/400kDa	1063	9.97	<0.0001
HIST1H3B	histone cluster 1, H3b	8358	9.65	<0.0001
HIST2H2AB	histone cluster 2, H2ab	317772	9.52	<0.0001
PRC1	protein regulator of cytokinesis 1	9055	9.54	<0.0001
NDC80	NDC80 kinetochore complex component	10403	9.06	<0.0001
HIST2H3D	histone cluster 2, H3d	653604	9.07	<0.0001
HIST1H2AJ	histone cluster 1, H2aj	8331	7.60	<0.0001
CKAP2L	cytoskeleton associated protein 2-like	150468	8.69	<0.0001
CCNE2	cyclin E2	9134	8.64	<0.0001
SHCBP1	SHC SH2-domain binding protein 1	79801	8.35	<0.0001
SGOL1	shugoshin-like 1 (S. pombe)	151648	8.30	<0.0001
TICRR	TOPBP1-interacting checkpoint and replication regulator	90381	8.16	<0.0001
NUSAP1	nucleolar and spindle associated protein 1	51203	8.20	<0.0001
KIF4A	kinesin family member 4A	24137	7.85	<0.0001
SPC25	SPC25, NDC80 kinetochore complex component	57405	8.07	<0.0001
KIF15	kinesin family member 15	56992	7.76	<0.0001
TTK	TTK protein kinase	7272	7.68	<0.0001
CLSPN	Claspin	63967	7.61	<0.0001
RAD51AP1	RAD51 associated protein 1	10635	7.64	<0.0001
CENPK	centromere protein K	64105	7.74	<0.0001
PLK1	polo-like kinase 1	5347	7.84	<0.0001
CASC5	cancer susceptibility candidate 5	57082	7.64	<0.0001
SKA1	spindle and kinetochore associated complex subunit 1	220134	7.58	<0.0001
CCNB2	cyclin B2	9133	7.52	<0.0001
KIF14	kinesin family member 14	9928	7.43	<0.0001
PLK4	polo-like kinase 4	10733	7.40	<0.0001
KIF11	kinesin family member 11	3832	7.36	<0.0001
FOXM1	forkhead box M1	2305	7.40	<0.0001
DEPDC1	DEP domain containing 1	55635	7.25	<0.0001
ASF1B	anti-silencing function 1B histone chaperone	55723	7.21	<0.0001

Symbol	GeneName	Entrez GeneID	Fold-Change	FDR
TK1	thymidine kinase 1, soluble	7083	7.03	0.0002
HIST1H2BF	histone cluster 1, H2bf	8343	6.96	0.0002
GINS2	GINS complex subunit 2 (Psf2 homolog)	51659	6.98	0.0002
SPAG5	sperm associated antigen 5	10615	6.90	0.0002
MCM7	minichromosome maintenance complex component 7	4176	6.79	0.0002
CENPI	centromere protein I	2491	6.76	0.0002
MLF1IP	MLF1 interacting protein	79682	6.59	0.0002
HIST1H4C	histone cluster 1, H4c	8364	6.75	0.0002
ORC1	origin recognition complex, subunit 1	4998	6.72	0.0001
CDKN3	cyclin-dependent kinase inhibitor 3	1033	6.64	0.0001
C11orf82	chromosome 11 open reading frame 82	220042	6.67	0.0001
CCNA2	cyclin A2	890	6.67	0.0001
HMMR	hyaluronan-mediated motility receptor (RHAMM)	3161	6.64	0.0001
MELK	maternal embryonic leucine zipper kinase	9833	6.60	0.0001
SKA3	spindle and kinetochore associated complex subunit 3	221150	6.54	0.0001
BUB1B	BUB1 mitotic checkpoint serine/threonine kinase B	701	6.45	0.0001
CDCA5	cell division cycle associated 5	113130	6.21	0.0001
HIST1H3J	histone cluster 1, H3j	8356	6.23	0.0001
TRIP13	thyroid hormone receptor interactor 13	9319	6.38	0.0001
FANCI	Fanconi anemia, complementation group I	55215	6.40	0.0001
CDCA8	cell division cycle associated 8	55143	6.27	0.0003
CDC45	cell division cycle 45	8318	6.20	0.0002
CENPE	centromere protein E, 312kDa	1062	6.28	0.0002
MASTL	microtubule associated serine/threonine kinase-like	84930	6.26	0.0002
NCAPG2	non-SMC condensin II complex, subunit G2	54892	6.23	0.0002
CCNB1	cyclin B1	891	6.06	0.0002
NEK2	NIMA-related kinase 2	4751	6.10	0.0002

Symbol	GeneName	Entrez GeneID	Fold-Change	FDR
CIT	citron (rho-interacting, serine/threonine kinase 21)	11113	6.14	0.0002
KIF23	kinesin family member 23	9493	6.00	0.0003
EXO1	exonuclease 1	9156	5.95	0.0003
CKS1B	CDC28 protein kinase regulatory subunit 1B	1163	5.89	0.0003
MCM10	minichromosome maintenance complex component 10	55388	5.76	0.0004
TPX2	TPX2, microtubule-associated	22974	5.78	0.0004
BLM	Bloom syndrome, RecQ helicase-like	641	5.70	0.0004
NEIL3	nei endonuclease VIII-like 3 (E. coli)	55247	5.60	0.0005
DLEU2	deleted in lymphocytic leukemia 2 (non-protein coding)	8847	5.38	0.0005
UBE2T	ubiquitin-conjugating enzyme E2T (putative)	29089	5.58	0.0005
CKS1B	CDC28 protein kinase regulatory subunit 1B	1163	5.58	0.0005
DIAPH3	diaphanous-related formin 3	81624	5.49	0.0005
IQGAP3	IQ motif containing GTPase activating protein 3	128239	5.57	0.0005
HIST1H2AE	histone cluster 1, H2ae	3012	5.35	0.0005
HIST1H2BH	histone cluster 1, H2bh	8345	5.34	0.0005
PRIM1	primase, DNA, polypeptide 1 (49kDa)	5557	5.34	0.0005
BRCA2	breast cancer 2, early onset	675	5.23	0.0005
BRIP1	BRCA1 interacting protein C-terminal helicase 1	83990	5.25	0.0005
HJURP	Holliday junction recognition protein	55355	5.10	0.0005
ZWINT	ZW10 interacting kinetochore protein	11130	5.13	0.0005
KIF2C	kinesin family member 2C	11004	4.99	0.0005
PRR11	proline rich 11	55771	5.02	0.0005
AURKB	aurora kinase B	9212	4.95	0.0005
FANCD2	Fanconi anemia, complementation group D2	2177	4.96	0.0005
KIFC1	kinesin family member C1	3833	4.90	0.0005
NUF2	NUF2, NDC80 kinetochore complex component	83540	4.92	0.0005
HIST2H3D	histone cluster 2, H3d	653604	4.92	0.0004
HIST1H2AL	histone cluster 1, H2al	8332	4.94	0.0005
FAM64A	family with sequence similarity 64, member A	54478	4.77	0.0005
HIST2H3A	histone cluster 2, H3a	333932	4.82	0.0006

Symbol	GeneName	Entrez GeneID	Fold-Change	FDR
HIST1H4B	histone cluster 1, H4b	8366	4.79	0.0006
ORC6	origin recognition complex, subunit 6	23594	4.80	0.0006
STIL	SCL/TAL1 interrupting locus	6491	4.79	0.0006
RRM1	ribonucleotide reductase M1	6240	4.77	0.0007
STMN1	stathmin 1	3925	4.79	0.0007
MND1	meiotic nuclear divisions 1 homolog (S. cerevisiae)	84057	4.77	0.0007
HIST1H3A	histone cluster 1, H3a	8350	4.73	0.0007
TROAP	trophinin associated protein	10024	4.68	0.0007
MYBL1	v-myb avian myeloblastosis viral oncogene homolog-like 1	4603	4.69	0.0007
CDCA2	cell division cycle associated 2	157313	4.67	0.0007
RFC3	replication factor C (activator 1) 3, 38kDa	5983	4.60	0.0007
ERCC6L	excision repair cross-complementing rodent repair deficiency, complementation group 6-like	54821	4.66	0.0007
HIST1H3G	histone cluster 1, H3g	8355	4.53	0.0007
UHRF1	ubiquitin-like with PHD and ring finger domains 1	29128	4.51	0.0007
HIST1H1E	histone cluster 1, H1e	3008	4.52	0.0007
KIF18B	kinesin family member 18B	146909	4.47	0.0007
ARHGAP11A	Rho GTPase activating protein 11A	9824	4.51	0.0007
MNS1	meiosis-specific nuclear structural 1	55329	4.40	0.0007
HIST1H2BL	histone cluster 1, H2bl	8340	4.44	0.0007
POLQ	polymerase (DNA directed), theta	10721	4.38	0.0007
PTTG1	pituitary tumor-transforming 1	9232	4.36	0.0008
HIST1H2AB	histone cluster 1, H2ab	8335	4.27	0.0009
OIP5	Opa interacting protein 5	11339	4.28	0.0009
CDC25C	cell division cycle 25C	995	4.23	0.0010
WDHD1	WD repeat and HMG-box DNA binding protein 1	11169	4.19	0.0011
HIST2H2AC	histone cluster 2, H2ac	8338	4.16	0.0011
XRCC2	X-ray repair complementing defective repair in Chinese hamster cells 2	7516	4.09	0.0011
DEPDC1B	DEP domain containing 1B	55789	4.11	0.0011

Symbol	GeneName	Entrez GeneID	Fold-Change	FDR
H2AFZ	H2A histone family, member Z	3015	4.07	0.0011
WDR76	WD repeat domain 76	79968	4.01	0.0012
PKMYT1	protein kinase, membrane associated tyrosine/threonine 1	9088	3.96	0.0012
RFC4	replication factor C (activator 1) 4, 37kDa	5984	3.89	0.0014
FBXO5	F-box protein 5	26271	3.91	0.0015
CDCA3	cell division cycle associated 3	83461	3.87	0.0015
ATAD2	ATPase family, AAA domain containing 2	29028	3.91	0.0015
SLC43A3	solute carrier family 43, member 3	29015	3.88	0.0017
SPC24	SPC24, NDC80 kinetochore complex component	147841	3.85	0.0018
PHGDH	phosphoglycerate dehydrogenase	26227	3.89	0.0017
TMEM194A	transmembrane protein 194A	23306	3.82	0.0017
HIST1H3D	histone cluster 1, H3d	8351	3.86	0.0018
CDT1	chromatin licensing and DNA replication factor 1	81620	3.87	0.0018
KIAA1524	KIAA1524	57650	3.83	0.0018
TCF19	transcription factor 19	6941	3.79	0.0021
POLE2	polymerase (DNA directed), epsilon 2, accessory subunit	5427	3.69	0.0022
H1F0	H1 histone family, member 0	3005	3.74	0.0022
SMC2	structural maintenance of chromosomes 2	10592	3.74	0.0022
TCF19	transcription factor 19	6941	3.70	0.0023
SMC4	structural maintenance of chromosomes 4	10051	3.59	0.0023
KIF20B	kinesin family member 20B	9585	3.59	0.0023
GAS2L3	growth arrest-specific 2 like 3	283431	3.62	0.0023
HELLS	helicase, lymphoid-specific	3070	3.68	0.0023
SCYL3	SCY1-like 3 (S. cerevisiae)	57147	3.60	0.0024
ITGB3BP	integrin beta 3 binding protein (beta3-endonexin)	23421	3.58	0.0024
MCM2	minichromosome maintenance complex component 2	4171	3.65	0.0024
GINS3	GINS complex subunit 3 (Psf3 homolog)	64785	3.68	0.0024

Symbol	GeneName	Entrez GeneID	Fold-Change	FDR
HMGB2	high mobility group box 2	3148	3.67	0.0024
HIST1H4K	histone cluster 1, H4k	8362	3.68	0.0024
AURKA	aurora kinase A	6790	3.51	0.0024
GINS4	GINS complex subunit 4 (Sld5 homolog)	84296	3.61	0.0025
TACC3	transforming, acidic coiled-coil containing protein 3	10460	3.57	0.0026
ATAD5	ATPase family, AAA domain containing 5	79915	3.60	0.0026
MAD2L1	MAD2 mitotic arrest deficient-like 1 (yeast)	4085	3.54	0.0029
CLSPN	claspin	63967	3.50	0.0029
RAD54L	RAD54-like (S. cerevisiae)	8438	3.43	0.0029
UBE2C	ubiquitin-conjugating enzyme E2C	11065	3.51	0.0029
RIBC2	RIB43A domain with coiled-coils 2	26150	3.45	0.0031
ESPL1	extra spindle pole bodies homolog 1 (S. cerevisiae)	9700	3.43	0.0031
KIFC1	kinesin family member C1	3833	3.44	0.0031
RFC5	replication factor C (activator 1) 5,	5985	3.40	0.0031
KNTC1	kinetochore associated 1	9735	3.38	0.0034
DDX12P	DEAD/H (Asp-Glu-Ala-Asp/His) box polypeptide 12, pseudogene	440081	3.40	0.0034
SMC1B	structural maintenance of chromosomes 1B	27127	3.48	0.0034
DDX12P	DEAD/H (Asp-Glu-Ala-Asp/His) box polypeptide 12, pseudogene	440081	3.40	0.0033
E2F1	E2F transcription factor 1	1869	3.41	0.0035
C4orf21	chromosome 4 open reading frame 21	55345	3.41	0.0036
MCM3	minichromosome maintenance complex component 3	4172	3.35	0.0037
CDC7	cell division cycle 7	8317	3.45	0.0036
C5orf34	chromosome 5 open reading frame 34	375444	3.33	0.0037
MCM8	minichromosome maintenance complex component 8	84515	3.27	0.0037
CENPH	centromere protein H	64946	3.38	0.0038
DHRS2	dehydrogenase/reductase (SDR family) member 2	10202	3.48	0.0039

Symbol	GeneName	Entrez GeneID	Fold-Change	FDR
RAD54B	RAD54 homolog B (S. cerevisiae)	25788	3.31	0.0039
BIRC5	baculoviral IAP repeat containing 5	332	3.27	0.0039
CDCA7	cell division cycle associated 7	83879	3.23	0.0039
GINS1	GINS complex subunit 1 (Psf1 homolog)	9837	3.25	0.0038
KIF18B	kinesin family member 18B	146909	3.29	0.0039
GTSE1	G-2 and S-phase expressed 1	51512	3.29	0.0040
DDX11	DEAD/H (Asp-Glu-Ala-Asp/His) box helicase 11	1663	3.19	0.0047
HIST1H2BI	histone cluster 1, H2bi	8346	3.25	0.0047
RNASEH2A	ribonuclease H2, subunit A	10535	3.24	0.0049
CENPA	centromere protein A	1058	3.16	0.0049
TMPO	thymopoietin	7112	3.19	0.0050
TIMELESS	timeless circadian clock	8914	3.20	0.0049
SGOL2	shugoshin-like 2 (S. pombe)	151246	3.22	0.0049
FAM83D	family with sequence similarity 83, member D	81610	3.14	0.0052
CKS1B	CDC28 protein kinase regulatory subunit 1B	1163	3.17	0.0052
OVOS	ovostatin	408186	3.16	0.0052
MTFR2	mitochondrial fission regulator 2	113115	3.20	0.0052
ECT2	epithelial cell transforming sequence 2 oncogene	1894	3.10	0.0054
EZH2	enhancer of zeste homolog 2 (Drosophila)	2146	3.07	0.0055
PHF19	PHD finger protein 19	26147	3.08	0.0057
CHAF1B	chromatin assembly factor 1, subunit B (p60)	8208	3.05	0.0061
CDK2	cyclin-dependent kinase 2	1017	3.01	0.0063
LMNB1	lamin B1	4001	3.26	0.0062
KIF24	kinesin family member 24	347240	3.11	0.0062
C18orf54	chromosome 18 open reading frame 54	162681	3.15	0.0063
POLA2	polymerase (DNA directed), alpha 2, accessory subunit	23649	3.01	0.0065

Symbol	GeneName	Entrez GeneID	Fold-Change	FDR
MMS22L	MMS22-like, DNA repair protein	253714	3.08	0.0065
HIST1H4J	histone cluster 1, H4j	8363	3.11	0.0065
ZWILCH	zwilch kinetochore protein	55055	2.97	0.0066
VRK1	vaccinia related kinase 1	7443	3.03	0.0067
CEP128	centrosomal protein 128kDa	145508	3.00	0.0071
ZNF367	zinc finger protein 367	195828	3.14	0.0073
FANCA	Fanconi anemia, complementation group A	2175	2.91	0.0074
E2F8	E2F transcription factor 8	79733	2.91	0.0074
BARD1	BRCA1 associated RING domain 1	580	3.03	0.0073
NDC1	NDC1 transmembrane nucleoporin	55706	2.93	0.0073
HIST1H4E	histone cluster 1, H4e	8367	2.87	0.0074
NRM	nurim (nuclear envelope membrane protein)	11270	2.89	0.0073
NRM	nurim (nuclear envelope membrane protein)	11270	2.89	0.0073
DSN1	DSN1, MIS12 kinetochore complex component	79980	2.89	0.0074
LRR1	leucine rich repeat protein 1	122769	3.07	0.0074
HIST1H2BJ	histone cluster 1, H2bj	8970	3.06	0.0076
WDR62	WD repeat domain 62	284403	2.84	0.0078
CKS2	CDC28 protein kinase regulatory subunit 2	1164	2.84	0.0084
GSG2	germ cell associated 2 (haspin)	83903	2.96	0.0084
EME1	essential meiotic structure-specific endonuclease 1	146956	2.76	0.0088
CENPO	centromere protein O	79172	2.76	0.0102
RFC2	replication factor C (activator 1) 2, 40kDa	5982	2.80	0.0107
MCM6	minichromosome maintenance complex component 6	4175	2.80	0.0110
KPNA2	karyopherin alpha 2 (RAG cohort 1, importin alpha 1)	3838	2.68	0.0110
LIN9	lin-9 homolog (C. elegans)	286826	2.71	0.0111
CENPW	centromere protein W	387103	2.83	0.0119

Symbol	GeneName	Entrez GeneID	Fold-Change	FDR
PRIM2	primase, DNA, polypeptide 2 (58kDa)	5558	2.67	0.0124
KIF18A	kinesin family member 18A	81930	2.67	0.0127
CENPQ	centromere protein Q	55166	2.62	0.0127
OASL	2'-5'-oligoadenylate synthetase-like	8638	2.85	0.0130
HIST1H4D	histone cluster 1, H4d	8360	2.96	0.0130
NCAPD3	non-SMC condensin II complex, subunit D3	23310	2.65	0.0131
HIST1H4F	histone cluster 1, H4f	8361	2.59	0.0131
DBF4B	DBF4 homolog B (S. cerevisiae)	80174	2.74	0.0130
HIST1H4A	histone cluster 1, H4a	8359	2.63	0.0130
CHEK1	checkpoint kinase 1	1111	2.68	0.0133
FANCG	Fanconi anemia, complementation group G	2189	2.65	0.0133
KPNA2	karyopherin alpha 2 (RAG cohort 1, importin alpha 1)	3838	2.59	0.0133
HAUS8	HAUS augmin-like complex, subunit 8	93323	2.73	0.0132
C19orf48	chromosome 19 open reading frame 48	84798	2.62	0.0133
POLD3	polymerase (DNA-directed), delta 3, accessory subunit	10714	2.82	0.0133
MYO19	myosin XIX	80179	2.63	0.0132
NRM	nurim (nuclear envelope membrane protein)	11270	2.60	0.0132
KIF22	kinesin family member 22	3835	2.66	0.0134
SASS6	spindle assembly 6 homolog (C. elegans)	163786	2.57	0.0145
NCAPD2	non-SMC condensin I complex, subunit D2	9918	2.54	0.0156
KIF22	kinesin family member 22	3835	2.61	0.0157
RBL1	retinoblastoma-like 1 (p107)	5933	2.60	0.0161
DNA2	DNA replication helicase/nuclease 2	1763	2.54	0.0165
RPL39L	ribosomal protein L39-like	116832	2.69	0.0177
CENPJ	centromere protein J	55835	2.50	0.0187
KIF4B	kinesin family member 4B	285643	2.61	0.0186

Symbol	GeneName	Entrez GeneID	Fold-Change	FDR
POLE	polymerase (DNA directed), epsilon, catalytic subunit	5426	2.51	0.0186
HIST3H2A	histone cluster 3, H2a	92815	2.83	0.0190
UBE2S	ubiquitin-conjugating enzyme E2S	27338	2.52	0.0196
KNSTRN	kinetochore-localized astrin/SPAG5 binding protein	90417	2.44	0.0196
RTKN2	rhotekin 2	219790	2.45	0.0206
RECQL4	RecQ protein-like 4	9401	2.47	0.0207
FEN1	flap structure-specific endonuclease 1	2237	2.52	0.0208
RACGAP1P	Rac GTPase activating protein 1 pseudogene	83956	2.55	0.0209
RSAD2	radical S-adenosyl methionine domain containing 2	91543	2.71	0.0214
DNMT1	DNA (cytosine-5-)-methyltransferase 1	1786	2.44	0.0221
GGH	gamma-glutamyl hydrolase (conjugase, folylpolygammaglutamyl hydrolase)	8836	2.64	0.0246
HIST1H1D	histone cluster 1, H1d	3007	2.58	0.0247
POLD1	polymerase (DNA directed), delta 1, catalytic subunit	5424	2.54	0.0257
FANCB	Fanconi anemia, complementation group B	2187	2.34	0.0260
DEK	DEK oncogene	7913	2.33	0.0260
FAM111A	family with sequence similarity 111, member A	63901	2.32	0.0260
PSMC3IP	PSMC3 interacting protein	29893	2.47	0.0259
SPDL1	spindle apparatus coiled-coil protein 1	54908	2.34	0.0263
HIST2H2BA	histone cluster 2, H2ba (pseudogene)	337875	2.31	0.0264
HIST1H3C	histone cluster 1, H3c	8352	2.31	0.0271
USP1	ubiquitin specific peptidase 1	7398	2.37	0.0277
NEFH	neurofilament, heavy polypeptide	4744	2.30	0.0278
DTYMK	deoxythymidylate kinase (thymidylate kinase)	1841	2.40	0.0280
OVOS	ovostatin	408186	2.40	0.0290
CCNF	cyclin F	899	2.32	0.0310
PARPBP	PARP1 binding protein	55010	2.38	0.0312

Symbol	GeneName	Entrez GeneID	Fold-Change	FDR
KLHL35	kelch-like family member 35	283212	2.30	0.0314
GPSM2	G-protein signaling modulator 2	29899	2.46	0.0315
TEX30	testis expressed 30	93081	2.35	0.0324
POC1A	POC1 centriolar protein A	25886	2.30	0.0337
CKAP2	cytoskeleton associated protein 2	26586	2.29	0.0339
LSM5	LSM5 homolog, U6 small nuclear RNA associated (S. cerevisiae)	23658	2.31	0.0347
DBF4B	DBF4 homolog B (S. cerevisiae)	80174	2.23	0.0356
UBE2S	ubiquitin-conjugating enzyme E2S	27338	2.33	0.0355
CCDC77	coiled-coil domain containing 77	84318	2.30	0.0365
CENPN	centromere protein N	55839	2.22	0.0376
NR4A2	nuclear receptor subfamily 4, group A, member 2	4929	2.31	0.0378
CEP152	centrosomal protein 152kDa	22995	2.27	0.0390
DCLRE1B	DNA cross-link repair 1B	64858	2.33	0.0391
BORA	bora, aurora kinase A activator	79866	2.20	0.0392
TOPBP1	topoisomerase (DNA) II binding protein 1	11073	2.27	0.0400
ANP32E	acidic (leucine-rich) nuclear phosphoprotein 32 family, member E	81611	2.30	0.0414
CCDC18	coiled-coil domain containing 18	343099	2.29	0.0417
HMGN2	high mobility group nucleosomal binding domain 2	3151	2.19	0.0416
SYCE2	synaptonemal complex central element protein 2	256126	2.26	0.0424
CDKN2C	cyclin-dependent kinase inhibitor 2C (p18, inhibits CDK4)	1031	2.25	0.0429
TRAIP	TRAF interacting protein	10293	2.31	0.0444
FAM72D	family with sequence similarity 72, member D	728833	2.14	0.0451
TMEM97	transmembrane protein 97	27346	2.16	0.0451
CDCA4	cell division cycle associated 4	55038	2.22	0.0457
POLA1	polymerase (DNA directed), alpha 1, catalytic subunit	5422	2.26	0.0458
CENPM	centromere protein M	79019	2.19	0.0458

Symbol	GeneName	Entrez GeneID	Fold-Change	FDR
GMNN	geminin, DNA replication inhibitor	51053	2.25	0.0463
TIPIN	TIMELESS interacting protein	54962	2.29	0.0466
DBF4	DBF4 homolog (S. cerevisiae)	10926	2.21	0.0475
HIST1H1C	histone cluster 1, H1c	3006	2.19	0.0489

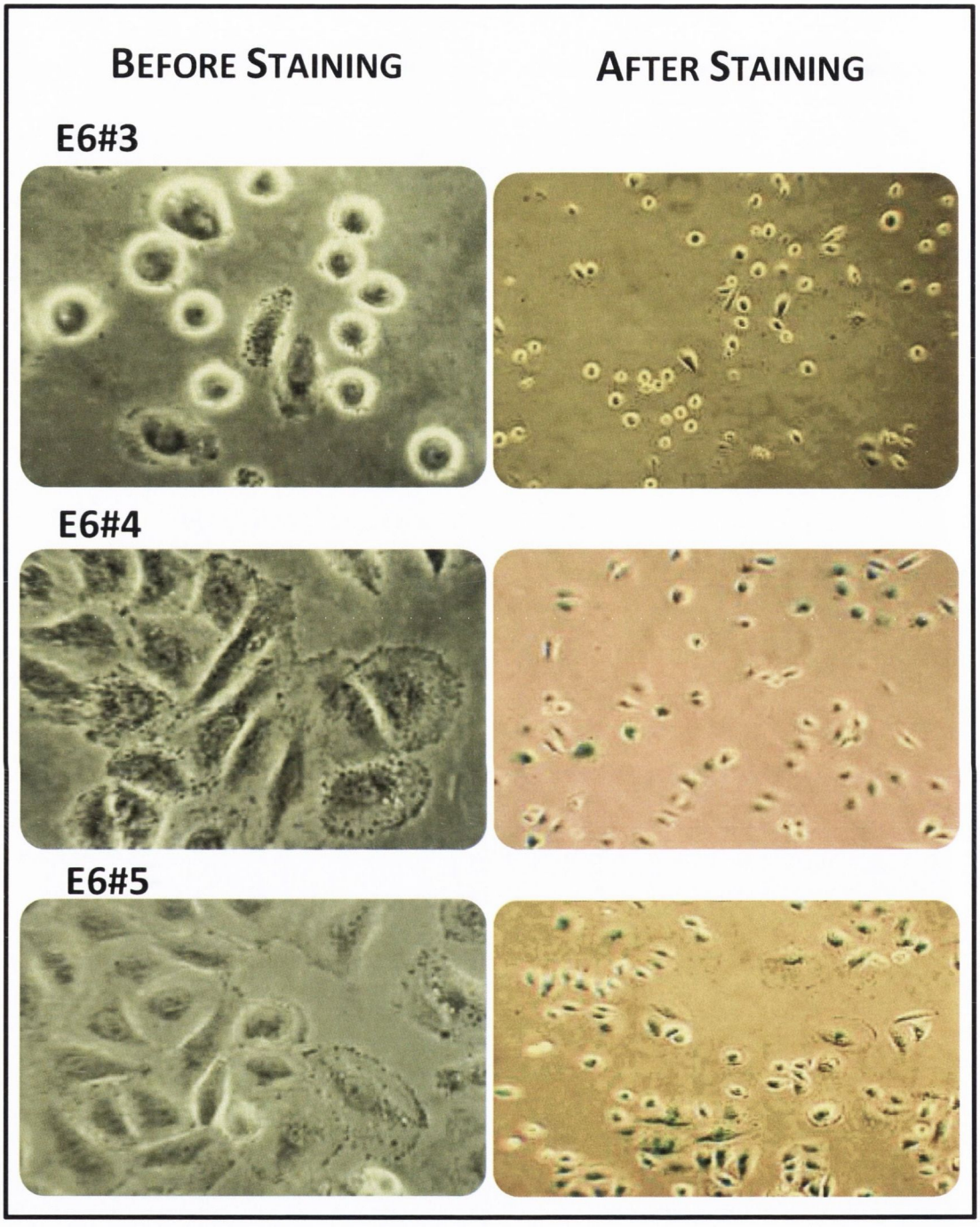

Figure 8-1: Light microscopy of β galactosidase stained SiHa cells using senescence cells histochemical staining kit 72hrs post forward transfection technique. SiHa cells seeded at $1.5x10^5$ cells were left untreated, mock-transfected, transfected with scrambled control siRNA and transfected with GAPDH targeting siRNA or E6 targeting siRNA ((E6#1, E6#2, E6#3, E6#4 and E6#5) in three biological replicates. 72hours post forward transfection; cells were fixed and stained with a mixture containing X-gal solution as substrate and incubated overnight in a CO_2 deprived atmosphere. The following day, the number of blue-stained cells were counted and analysed using a paired T-test via graph pad prism (Magnification 200x).

Table 8-3: Table of HR-HPV E6 target molecules and the effect of E6#2 and E6#4 siRNAs employed in this study. The target molecules are shown to be either up-regulated or down-regulated in differential gene expression.

Target molecules of E6	Implicated biological effect	Differential gene expression 72hrs post forward transfection	
		E6#2	E6#4
E6AP/p53	Degradation of p53/suppression of apoptosis	—	Up-regulated
PDZ-domain-containing proteins	Degradation of PDZ proteins/loss of cell polarity	—	Up-regulated (Fibroblast activation protein alpha, FAP)
GADD34/PP1	Suppression of apoptosis	Up-regulated	—
MCM7	Induction of chromosomal abnormalities	—	Down-regulated (MCM 2,3, 4, 5, 6, 7, 8, 10)
BRCA1	Release the inhibition of ER signalling	—	Down-regulated (BRCA1&2)

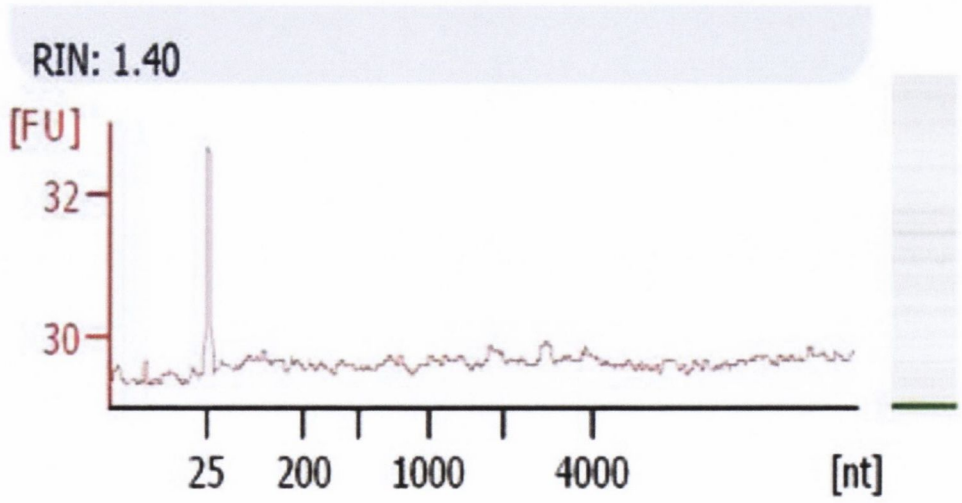

Figure 8-2: Electropherogram showing RNA quality **of E6#1 72hrs post forward transfection technique.** Agilent Bioanalyser electropherogram and gel-like image (right hand side of figure) of RNA integrity depicts completely degraded RNA with no 18s and 28s peaks or bands respectively. RNA Integrity Number (RIN) of 1.4 also confirms this degradation.